JYU DISSERTATIONS 809

Hanna Elomaa

The Roles of Immune Cell Composition and Immunosuppressive Factors in the Colorectal Cancer Microenvironment

UNIVERSITY OF JYVÄSKYLÄ
FACULTY OF MATHEMATICS
AND SCIENCE

JYU DISSERTATIONS 809

Hanna Elomaa

The Roles of Immune Cell Composition and Immunosuppressive Factors in the Colorectal Cancer Microenvironment

Esitetään Jyväskylän yliopiston matemaattis-luonnontieteellisen tiedekunnan suostumuksella
julkisesti tarkastettavaksi yliopiston Ylistönrinteen salissa YAA303
elokuun 30. päivänä 2024 kello 12.

Academic dissertation to be publicly discussed, by permission of
the Faculty of Mathematics and Science of the University of Jyväskylä,
in Ylistönrinne, auditorium YAA303, on August 30, 2024 at 12 o'clock noon.

JYVÄSKYLÄN YLIOPISTO
UNIVERSITY OF JYVÄSKYLÄ

JYVÄSKYLÄ 2024

Editors
Matti Jalasvuori
Department of Biological and Environmental Sciences, University of Jyväskylä
Ville Korkiakangas
Open Science Centre, University of Jyväskylä

ISBN 978-952-86-0244-6 (PDF)
URN:ISBN:978-952-86-0244-6
ISSN 2489-9003

Permanent link to this publication: http://urn.fi/URN:ISBN:978-952-86-0244-6

ABSTRACT

Elomaa, Hanna
The roles of immune cell composition and immunosuppressive factors in the colorectal cancer microenvironment
Jyväskylä: University of Jyväskylä, 2024, 88 p.
(JYU Dissertations
ISSN 2489-9003; 809)
ISBN 978-952-86-0244-6 (PDF)
Yhteenveto: Immuunisolujen ja immuunivastetta hillitsevien tekijöiden merkitys paksu- ja peräsuolisyövän mikroympäristössä
Diss.

Colorectal cancer is among the most prevalent cancers globally. High immune cell density in the tumor microenvironment has been found to be associated with improved colorectal cancer prognosis. However, the role of certain immune cell types remains incompletely understood. Tumor cells can promote their own growth by suppressing immune cell activity, for example, by upregulating the expression of programmed death-1 (PD-1, PDCD1) and programmed death-ligand 1 (PD-L1, CD274) immune checkpoints, or altering amino acid metabolism through increasing the expression of indoleamine 2,3-dioxygenase (IDO) and arginase-1 (ARG1) enzymes. In this study, immunohistochemistry and machine learning-based image analyses were used to assess the prognostic significance of immune cell densities and distribution, along with the expression of immune suppressive molecules, in colorectal cancer. Multimarker analyses enabled detailed phenotyping of immune cell subtypes and examination of the tumor microenvironment. The overall densities of monocytic cells, granulocytes, or mast cells, or their spatial proximity with tumor cells did not independently associate with colorectal cancer patient survival. However, higher density of T cells, particularly within tumor cell proximity was a strong prognostic indicator of favorable outcome. Moreover, despite the immunosuppressive nature of CD274 and IDO, increased infiltration of $CD274^+$ macrophages and IDO^+ monocytic cells was associated with better prognosis in colorectal cancer. These findings enhance the understanding of immune cell infiltration and the spatial interactions between tumor and host immune cells, potentially refining prognostication of colorectal cancer patients and assisting in development of new cancer therapies.

Keywords: Colorectal carcinoma; immunohistochemistry; inflammatory cell; machine-learning; multimarker staining; prognostic factor; spatial analysis.

Hanna Elomaa, University of Jyväskylä, Department of Biological and Environmental Science, P.O. Box 35, FI-40014 University of Jyväskylä, Finland; Wellbeing Services County of Central Finland, Department of Education and Research, Hoitajantie 3, FI-40620 Jyväskylä, Finland.

TIIVISTELMÄ

Elomaa, Hanna
Immuunisolujen ja immuunivastetta hillitsevien tekijöiden merkitys paksu- ja peräsuolisyövän mikroympäristössä
Jyväskylä: Jyväskylän yliopisto, 2024, 88 p.
(JYU Dissertations
ISSN 2489-9003; 809)
ISBN 978-952-86-0244-6 (PDF)
Yhteenveto: Immuunisolujen ja immuunivastetta hillitsevien tekijöiden merkitys paksu- ja peräsuolisyövän mikroympäristössä
Diss.

Paksu- ja peräsuolisyöpä on yksi yleisimmistä syövistä maailmanlaajuisesti. Syövän mikroympäristössä korkean immuunisolumäärän on todettu parantavan paksu- ja peräsuolisyöpäpotilaan ennustetta, mutta joidenkin solutyyppien merkitys tunnetaan vielä huonosti. Syöpäsolut voivat myös edistää omaa kasvuaan heikentämällä immuunisolujen toimintaa esimerkiksi lisäämällä PDCD1 (engl. *programmed death-1*, PD-1) ja CD274 (engl. *programmed death-ligand-1*, PD-L1) immuunivasteen tarkastuspisteproteiinien ilmenemistä tai muuttamalla solujen aminohappoaineenvaihduntaa lisäämällä aminohappoja hajottavien indoleamiini 2,3-dioksigenaasi (IDO) ja arginaasi-1 (ARG1) entsyymien määrää. Tässä tutkimuksessa kartoitettiin useiden eri immuunisolutyyppien tiheyksiä ja spatiaalista järjestäytymistä, immuunivastetta hillitsevien molekyylien ilmenemistä sekä näiden ennustemerkitystä paksu- ja peräsuolisyövässä immunohistokemiallisilla värjäysmenetelmillä ja tietokoneavusteisella kuva-analyysillä. Käytetyt menetelmät mahdollistivat immuunisolutyyppien tarkan tunnistamisen ja immuunivastetta hillitsevien proteiinien ilmenemisen analysoimisen eri solutyypeissä. Monosyyttien, granulosyyttien tai syöttösolujen kokonaistiheyksillä tai spatiaalisella sijainnilla ei ollut itsenäistä ennustemerkitystä, mutta korkealla T-solutiheydellä, etenkin syöpäsolujen läheisyydessä, oli vahva yhteys potilaan parempaan ennusteeseen. Huolimatta CD274 ja IDO proteiinien mahdollisesta immuunisolujen toimintaa hillitsevästä vaikutuksesta, korkeilla $CD274^+$ makrofagien ja IDO^+ monosyyttien tiheyksillä oli potilaan ennustetta parantava vaikutus. Tutkimus lisää tietoa eri immuunisolutyyppien merkityksestä sekä syöpä- ja immuunisolujen välisistä vuorovaikutuksista ja tulokset voisivat edistää paksu- ja peräsuolisyövän ennusteen arviointia sekä uusien syöpähoitojen kehittämistä.

Avainsanat: Ennustetekijä; immunohistokemia; kolorektaalisyöpä; koneoppiminen; monimarkkerivärjäys; spatiaalianalyysi; tulehdussolu.

Hanna Elomaa, Jyväskylän yliopisto, Bio- ja ympäristötieteiden laitos, PL 35, 40014 Jyväskylän yliopisto; Keski-Suomen hyvinvointialue, Tutkimus- ja koulutusyksikkö, Hoitajantie 3, 40620 Jyväskylä.

Author's address Hanna Elomaa
Department of Biological and Environmental Science
P.O. Box 35
FI-40014 University of Jyväskylä
Finland
hanna.k.elomaa@student.jyu.fi

Supervisors Docent Juha Väyrynen
Translational Medicine Research Unit
Aapistie 5A
FI-90220 University of Oulu
Finland

Docent Teijo Kuopio
Department of Biological and Environmental Science
P.O. Box 35
FI-40014 University of Jyväskylä
Finland

Professor Jari Ylänne
Department of Biological and Environmental Science
P.O. Box 35
FI-40014 University of Jyväskylä
Finland

Reviewers Professor Satu Mustjoki
Translational Immunology Research program and
Department of Clinical Chemistry and Hematology
P.O. Box 63
FI-00014 University of Helsinki
Finland

Docent Tuomas Rauramaa
Department of Clinical Pathology and Forensic Medicine
Institute of Clinical Medicine
Puijonlaaksontie 2
FI-70210 School of Medicine University of Eastern Finland
Finland

Opponent Assistant Professor Anniina Färkkilä
Research Program in Systems Oncology, HiLIFE and FIMM
and Department of Oncology and
Obsterics and Gynecology
FI-00014 University of Helsinki and
Helsinki University Hospital
Finland

CONTENTS

LIST OF ORIGINAL PUBLICATIONS

The thesis is based on the following original papers, which will be referred to in the text by their Roman numerals I–III.

I Elomaa H, Ahtiainen M, Väyrynen SA, Ogino S, Nowak JA, Friman M, Helminen O, Wirta EV, Seppälä T, Böhm J, Mäkinen MJ, Mecklin JP, Kuopio T, Väyrynen JP. 2022. Prognostic significance of spatial and density analysis of T lymphocytes in colorectal cancer. *British Journal of Cancer* 127: 514–523.

II Elomaa H, Ahtiainen M, Väyrynen SA, Ogino S, Nowak JA, Lau MC, Helminen O, Wirta EV, Seppälä TT, Böhm J, Mecklin JP, Kuopio T, Väyrynen JP. 2023. Spatially resolved multimarker evaluation of CD274 (PD-L1)/PDCD1 (PD-1) immune checkpoint expression and macrophage polarisation in colorectal cancer. *British Journal of Cancer* 128: 2104–2115.

III Elomaa H, Härkönen J, Väyrynen SA, Ahtiainen M, Ogino S, Nowak JA, Lau MC, Helminen O, Wirta EV, Seppälä TT, Böhm J, Mecklin JP, Kuopio T, Väyrynen JP. 2024. Quantitative multiplexed analysis of indoleamine 2,3-dioxygenase (IDO) and arginase-1 (ARG1) expression and myeloid cell infiltration in colorectal cancer. *Modern Pathology* 37: 100450.

The author's contribution to the original publications:

I The author contributed to the study design, prepared the tissue microarray specimens, and conducted immunohistochemistry. The author also performed image and data analyses and prepared the manuscript under the guidance of J.V.

II The author conducted sample preparation and immunohistochemistry. The author primarily conducted data analysis and prepared the manuscript, with support from J.V. and other coauthors.

III The author contributed to the study design. The author conducted immunohistochemistry, image analyses, and data analyses, except for single-cell data analyses (performed by J.H.). The author prepared the manuscript with assistance from J.V. and J.H. and other coauthors.

ABBREVIATIONS

AEC	3-amino-9-ethylcarbazole
AJCC	The American Joint Committee on Cancer
ARG1	arginase 1
CI	confidence interval
DAB	3,3'-diaminobenzidine
EGFR	epidermal growth factor receptor
HR	hazard ratio
IDO	indoleamine 2,3-dioxygenase
MDSC	myeloid-derived suppressor cell
MHC	major histocompatibility complex
MMR	mismatch repair
MSI	microsatellite instability
NND	Nearest Neighbor Distance
PD-1	programmed death-1
PD-L1	programmed death ligand-1
POLD1	polymerase delta 1
POLE	polymerase epsilon
Th	T helper
TNF	tumor necrosis factor
TNM	tumor, node, metastasis
TRAIL	tumor necrosis factor-related apoptosis-inducing ligand
UICC	The Union for International Cancer Control
VEGF	vascular endothelial growth factor receptor

HUGO (Human Genome Organization)-approved official symbols have been used for genes and gene products, which are described at www.genenames.org

1 INTRODUCTION

Colorectal cancer ranks as the third most prevalent cancer type globally, with over 1.9 million new cases annually (Bray *et al.* 2024). Several risk factors predispose to colorectal cancer, including high age (Miller *et al.* 2022), as well as factors such as obesity and adherence to a Western dietary pattern (Renehan *et al.* 2008, Garcia-Larsen *et al.* 2019). The majority of cases develop sporadically from precursor lesions within colorectal epithelium without specific germline genetic associations (Jasperson *et al.* 2010, Hamilton and Sekine 2019). Most colorectal cancers develop through the chromosomal instability pathway, while others follow the hypermutated pathways, each exhibiting distinct genetic, molecular, and clinical characteristics (Nagtegaal *et al.* 2019).

The cells of innate and adaptive immune systems play a pivotal role in detecting and eliminating pathogens and other aberrant cells (Murphy and Weaver 2017). In cancer, immune cells are crucial in recognizing and targeting tumor cells, although the interaction between tumor and host immune cells is complex (Alexander *et al.* 2020). Immune cell density and composition vary widely within tumors and among different patients (Pagès *et al.* 2008). A strong inflammatory reaction has been found to associate with favorable survival outcomes in colorectal cancer patients (Alexander *et al.* 2020), although certain immune cells may possess anti-inflammatory and tumor growth-promoting effects (Zamarron and Chen 2011). Additionally, tumor cells have the capability to modulate the tumor microenvironment, allowing them to evade immune detection and promote their own proliferation (Vinay *et al.* 2015). For instance, they may upregulate the expression of immune checkpoint proteins or modulate amino acid metabolism (Zhang *et al.* 2023, Chen *et al.* 2024) to potentially decrease immune cell activity (Chen 2004, Vinay *et al.* 2015, Ma *et al.* 2019).

Prognostic assessment and treatment planning for colorectal cancer mainly rely on evaluating the tumor size and extent (Union for International Cancer Control 2017). However, this approach has some limitations and does not consider the immunological state of the tumor (Kannarkatt *et al.* 2017, Cheng *et al.* 2020). Thus, new biomarkers characterizing immune cells in the tumor

microenvironment could complement the existing prognostic parameters in colorectal cancer.

This study characterizes the colorectal cancer microenvironment to provide detailed insights into immune cell infiltration and the expression patterns of immunosuppressive molecules. The objective is to clarify the prognostic role of various immune cell subtypes and analyse interactions between tumor cells and host immune cells.

2 LITERATURE REVIEW

2.1 Large intestine

2.1.1 Anatomy and function

The large intestine, comprising the colon and rectum, has vital roles in the digestive system. The colon is involved in processing and transporting food material, as well as absorbing nutrients and water, while the rectum disposes of unabsorbed waste products (Kierszenbaum and Tres 2020). The large intestine is divided into proximal and distal colon based on their embryological origins. The proximal colon, developed from midgut derivates, extends from the caecum to the splenic flexure, whereas the distal colon develops from hindgut derivates and encompasses the structures from the splenic flexure to the rectum (Fig. 1). These parts differ in their arterial supply and lymphatic drainage patterns (Ponz de Leon and Di Gregorio 2001, Bazira 2023).

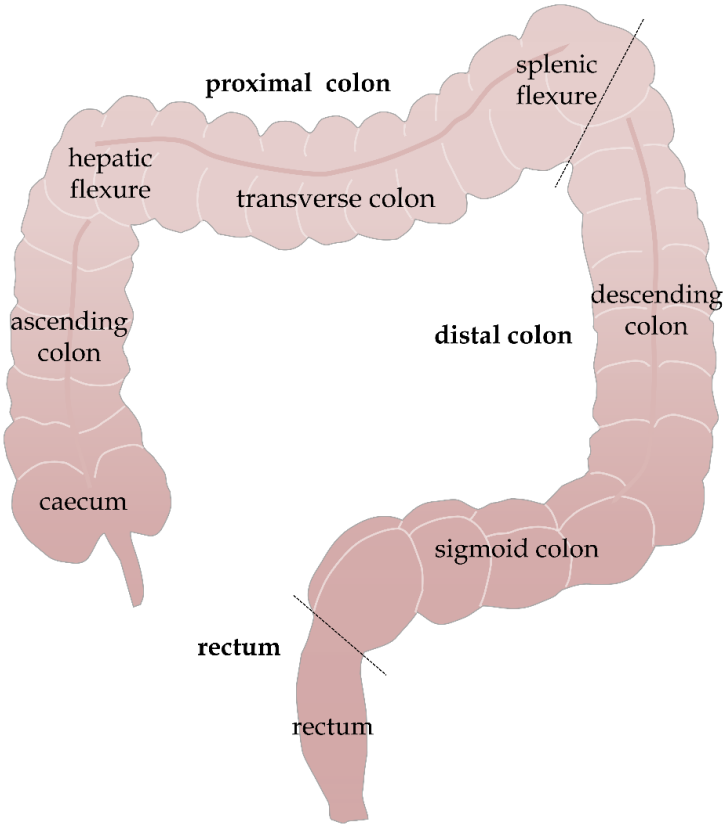

FIGURE 1 The anatomy of the large intestine. Modified from Ponz de Leon and Di Gregorio (2001).

2.1.2 Histology

The large intestine is lined by a mucosal layer, organized as Lieberkühn crypts. The mucosa is composed of epithelium, lamina propria, and muscularis mucosae. The epithelium contains specialized cells, including enterocytes, goblet cells, and immune cells, which maintain the balance of microbial flora, absorb water and nutrients, and provide a protective barrier against harmful microbes and pathogens (Suzuki 2020). The lamina propria is a connective tissue layer with blood and lymphatic vessels and a high variety of cells, including immune cells. The muscularis mucosae is a smooth muscle layer that controls the shape of the mucosa, thereby regulating its physiological properties (Ponz de Leon and Di Gregorio 2001). The histology of colon is represented in Fig. 2.

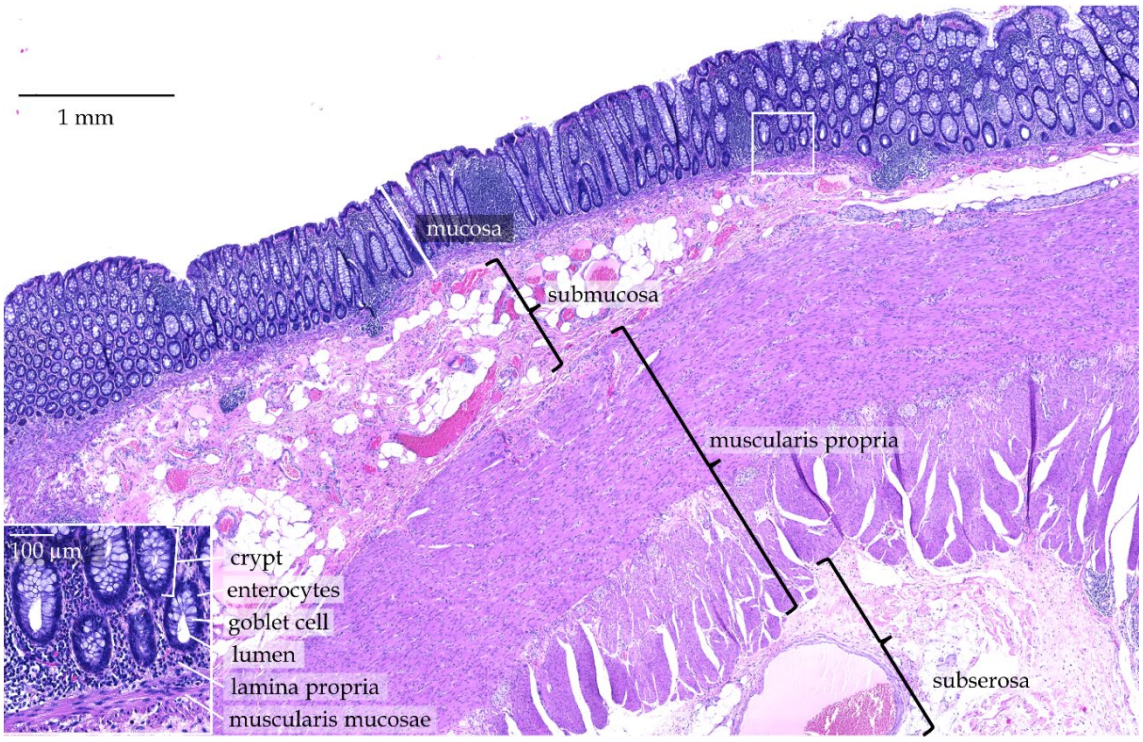

FIGURE 2 The histology of the colon.

2.2 Colorectal cancer epidemiology

Cancer is a disease characterized by uncontrollable proliferation of abnormal cells. It develops through a multistep process known as carcinogenesis, where normal cells transform into malignant cells due to accumulating genetic alterations. Over time, cancer may acquire the potential to spread to other organs through lymphatic vessels or the bloodstream. The hallmarks of cancer, initially introduced by Hanahan and Weinberg (Hanahan and Weinberg 2000), delineate key alterations and typical capabilities shared by most cancers. There are ten core hallmarks, along with four prospective emerging cancer hallmarks and enabling characteristics, which have been proposed as potential hallmarks (Hanahan 2022). The hallmarks are listed in Table 1.

TABLE 1 Cancer hallmarks[1].

Core hallmarks
Sustaining proliferative signaling
Evading growth suppressors
Avoiding immune destruction
Enabling replicative immortality
Tumor-promoting inflammation
Activating invasion and metastasis
Inducing or accessing vasculature
Genome instability and mutation
Resisting cell death
Deregulating cellular metabolism
New emerging hallmarks
Unlocking phenotypic plasticity
Senescent cells
New enabling characteristics
Nonmutational epigenetic reprogramming
Polymorphic microbiomes

[1]Adapted from Hanahan (2022).

Colorectal cancers encompass tumors in both proximal and distal parts of the colon, with rectal cancers typically addressed separately due to their distinct anatomic location, diagnosis, and treatment. Additionally, proximal and distal tumors have shown to differ in molecular, histological, epidemiological, and genetical characteristics (Baran *et al.* 2018). However, rather than being two distinct anatomical sites, the colorectal continuum model suggests that these tumor characteristics evolve gradually and linearly from the proximal colon to the rectum (Yamauchi *et al.* 2012).

2.2.1 Prevalence

Colorectal cancer is globally the third most diagnosed cancer after breast and lung cancers. It comprises over 1.9 million new cases annually and stands as the second leading cause of all cancer deaths after lung cancer. In men, colorectal cancer ranks third in both incidence and mortality. Conversely, among women, it ranks second in incidence and third in mortality worldwide (Bray *et al*. 2024). In Finland, colorectal cancer has the second highest incidence rates for both men and women, while it ranks third in mortality rates for men and fourth in women (Seppä *et al.* 2023). The incidence and mortality rates of colorectal cancer in Finland from 1953 to 2021 are depicted in Fig. 3.

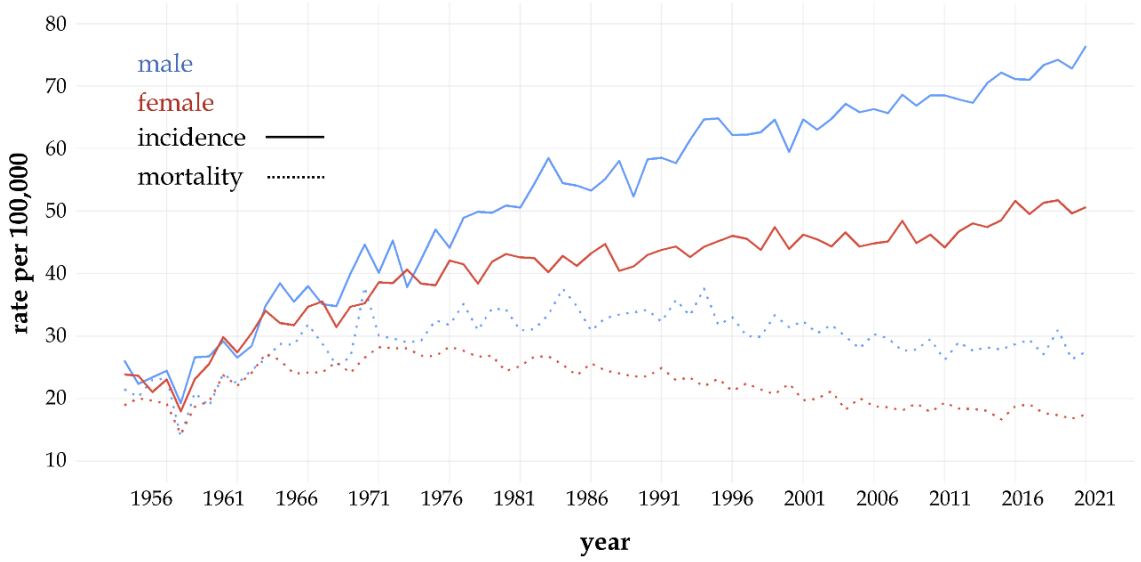

FIGURE 3 Age-standardized (Finland 2014) incidence and mortality rates for colorectal cancer in Finland from 1953 to 2021. Data adapted from the Finnish Cancer Registry (2023).

2.2.2 Risk factors

The primary risk factors for colorectal cancers encompass various lifestyle, environmental, and genetic components. Colorectal cancer incidence notably increases after the age of 50, with the median age at diagnosis for sporadic cases being approximately 67 years (Miller *et al.* 2022). However, there has been a global increase in incidence among individuals under 50 years in recent decades (Saraiva *et al.* 2023). Predominant dietary and lifestyle factors associated with colorectal cancer include obesity (Renehan *et al.* 2008, Clinton *et al.* 2020, Bray *et al.* 2024), adherence to a Western dietary pattern (Garcia-Larsen *et al.* 2019), consumption of red and processed meat (Larsson and Wolk 2006, Clinton *et al.* 2020), excessive alcohol consumption (Fedirko *et al.* 2011, Clinton *et al.* 2020), and smoking (Walter *et al.* 2014). While family history also plays a significant role as a predisposing risk factor, it contributes to a smaller fraction of colorectal cancer cases (Fuchs *et al.* 1994). Several protective factors, such as regular physical activity (Samad *et al.* 2005, Boyle *et al.* 2012, Clinton *et al.* 2020), adherence to a prudent and fibre-rich diet (Garcia-Larsen *et al.* 2019, Bray *et al.* 2024), and consumption of calcium supplements (Bray *et al.* 2024), have also been acknowledged.

Traditionally, the impact of specific risk factors has been evaluated in relation to the overall risk of developing colorectal cancer, without considering interactions between multiple factors or molecular changes. Molecular pathologic epidemiology investigates the interaction of risk factors, somatic molecular changes, and the development of colorectal cancer. It has been suggested that certain factors may facilitate colorectal cancer progression by affecting molecular alterations (Ogino *et al.* 2011). Moreover, it has been demonstrated that smoking, for instance, is associated with microsatellite

instability (Slattery *et al.* 2001), while obesity has been linked to microsatellite stable tumors (Campbell *et al.* 2010).

2.3 Colorectal carcinogenesis

The majority of colorectal cancers are sporadic, indicating that the gene alterations responsible for cancer development occur during the subjects lifetime. Approximately 2–5% of cases result from hereditary cancer syndromes with well-known inherited mutations (Jasperson *et al.* 2010). However, approximately 20–30% of colorectal cancers are associated with some degree of family history, although specific gene alterations have not been identified (Lichtenstein *et al.* 2000).

Colorectal cancer development begins with the accumulation of genetic alterations within the colorectal epithelial cells. The process is influenced by a combination of genetic, environmental, and lifestyle factors. Typically, colorectal cancers originate from precancerous lesions, which are benign, localized growths of abnormal cells within the mucosal layer. These lesions have the potential to evolve into invasive colorectal cancer over time (Simon 2016). A benign tumor becomes colorectal cancer after invasion through the muscularis mucosae (Nagtegaal *et al.* 2019). Tumor cells may acquire the capability to disseminate and spread into lymph nodes or distant organs, such as the liver and lungs, through the lymphatic or blood vessels (Luo *et al.* 2018, Leong *et al.* 2022). Fig. 4 illustrates different stages of colorectal cancer progression.

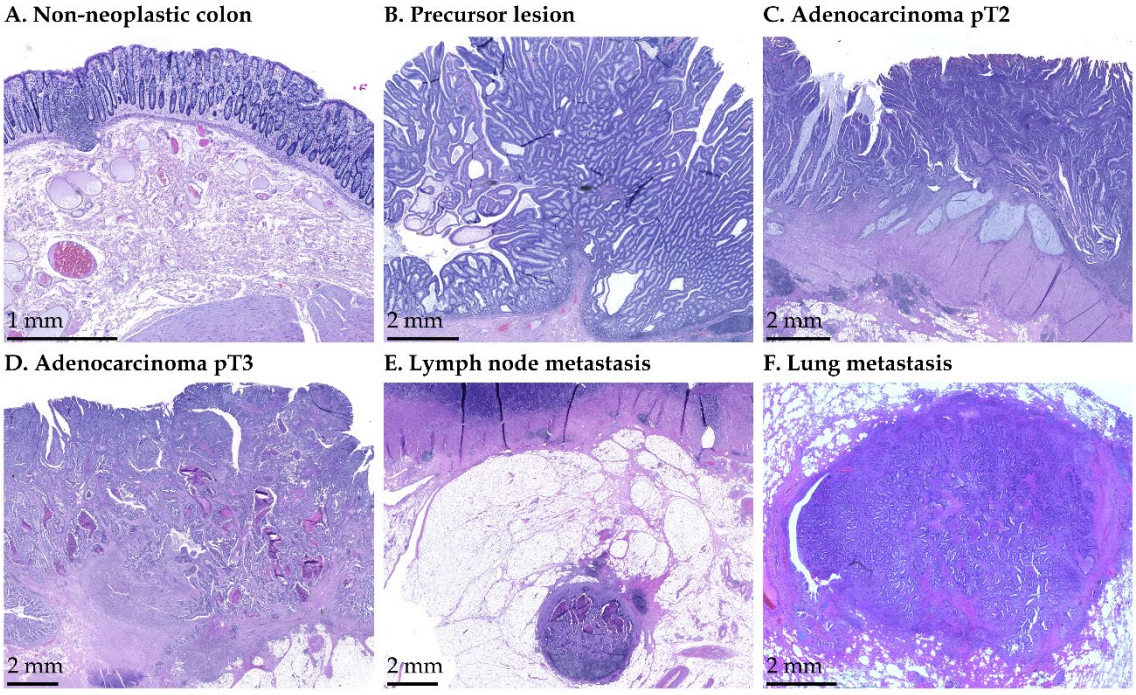

FIGURE 4 Colorectal cancer progression.

2.3.1 Precursor lesions

Colorectal cancers typically originate from benign precursor lesions that develop within the epithelium. However, only a minority of the benign lesions develop into malignant adenocarcinomas. The two main types of precursor lesions are conventional adenomas and serrated lesions and polyps.

Conventional adenomas are characterized by dysplastic epithelium, indicating the presence of abnormal cells. They are further classified based on their villosity into tubular, tubulovillous, and villous adenomas. Tubular adenomas consist mainly of tubular structures, with less than 25% of the adenoma displaying villous structures. Villous adenomas are defined as adenomas displaying more than 75% of villous structures, while tubulovillous adenomas exhibit both tubular and villous structures (Hamilton and Sekine 2019).

The second most common type of precursor lesions is the serrated lesions and polyps, which primarily develop through the sessile serrated neoplasia pathway (Pai *et al.* 2019). Serrated lesions encompass three main subtypes, including hyperplastic polyps, sessile serrated lesions, and traditional serrated adenomas. Hyperplastic polyps are the most prevalent subtype but rarely develop into malignant carcinoma (Nguyen *et al.* 2020).

2.3.2 Pathogenesis

Of colorectal adenocarcinomas, approximately 84% develop via the non-hypermutated conventional adenoma-carcinoma sequence. The pathway is primarily characterized by chromosomal instability, leading to significant chromosomal changes. The remaining cancers arise through the hypermutant pathway, encompassing tumors with microsatellite instability (MSI, 13%) and tumors with defective DNA proofreading polymerases (3%) (Nagtegaal *et al.* 2019).

2.3.2.1 Chromosomal instability pathway

The chromosomal instability pathway results in a high number of structural (*i.e.* translocations, duplications, or deletions) or numeral chromosomal alterations (*i.e.* chromosomal gains or losses) (Pino and Chung 2010). Tumors with the chromosomal instability tend to exhibit a low frequency of mutations but a high frequency of DNA somatic copy number alterations (Noack and Langer 2023). They typically acquire an inactivating mutation in *APC* gene as the first mutation (Powell *et al.* 1992). Other common mutations include loss-of-function mutations in *TP53* and *SMAD4,* as well as activating mutations in *KRAS* and *PIK3CA* (Cancer Genome Atlas Network 2012, Nagtegaal *et al.* 2019).

2.3.2.2 Hypermutated pathway

Hypermutated tumors exhibit a very high frequency of mutations, resulting in increased tumor mutation burden and a high number of neoantigens. Additionally, hypermutated tumors typically display greater intratumoral

heterogeneity compared to tumors with the chromosomal instability (Angelova *et al.* 2015). Most hypermutated tumors are characterized by MSI, where short repeating DNA sequences called microsatellites are accumulated by mutations. MSI is caused by a deficient DNA mismatch repair (MMR) system, which is responsible for correcting errors during DNA replication. A defective MMR system arises from loss-of-function mutations in one or several DNA mismatch repair (MMR) genes (*MLH1*, *MSH2*, *MSH6*, *PMS2*) or from hypermethylation of the *MLH1* promoter (de la Chapelle and Hampel 2010). MSI tumors often exhibit the CpG island methylator phenotype, characterized by abnormal and high-level methylation in CpG sites of gene promoter regions, leading to hypermethylation of *MLH1* (Cancer Genome Atlas Network 2012). MSI tumors are often associated with high tumor grade, mucinous histology, higher infiltration of lymphocytes, a Crohn's like lymphoid reaction, proximal colon location, lower tumor stage, and favorable prognosis (Jenkins *et al.* 2007, Ogino *et al.* 2009).

In some MSI tumors, the *BRAF* mutation is the initiating mutation. These tumors have typically developed from sessile serrated lesions rather than from conventional adenomas and in these cases, the MSI pathway is converged with the sessile serrated pathway (Nagtegaal *et al.* 2019, Nguyen *et al.* 2020). The tumorigenesis in MSI tumors initiated by *BRAF* mutation takes a shorter span of time than that in MSI tumors initiated by *APC* mutation (Nguyen *et al.* 2020).

Approximately 10–15% of MSI colorectal cancers are associated with Lynch syndrome, an inherited syndrome predisposing cancer development (Peltomäki 2014). Unlike most sporadic MSI tumors, Lynch syndrome-related tumors arise from MMR gene mutation rather than *MLH1* hypermethylation (Peltomäki 2014). These tumors do not typically exhibit the CpG island methylator phenotype or harbor the *BRAF* mutation (Deng *et al.* 2004, Bessa *et al.* 2008, Nagasaka *et al.* 2008).

Ultramutated tumors are microsatellite stable, indicating a functional MMR system. They arise from mutations in DNA proofreading polymerases, which replace incorrectly synthetized base pairs during DNA replication. Mutations typically occur in genes encoding the exonuclease domains of DNA polymerase Epsilon (POLE) or Delta 1 (POLD1), leading to errors in DNA replication and accumulation of mutations. In comparison to tumors with chromosomal instability, MSI and ultramutated tumors are strongly enriched for *BRAF* and *TGFBR2* mutations, whereas the frequencies of *APC*, *KRAS* and *TP53* mutations are lower (Rajagopalan *et al.* 2002, Cancer Genome Atlas Network 2012).

2.3.3 Hereditary cancer syndromes

Up to 5% of colorectal cancers are associated with some inherited cancer syndromes, typically leading to cancer development at a relatively young age (Jasperson *et al.* 2010). Lynch syndrome, formerly known as hereditary non-polyposis colorectal cancer, is the most prevalent inherited syndrome, accounting for approximately 1–3% of all colorectal cancer cases (Vasen *et al.* 2013, Peltomäki *et al.* 2023). Lynch syndrome carriers have a significantly increased risk for several gastrointestinal and gynecologic tract cancers, along with a susceptibility to multiple tumors. Lynch syndrome-related colorectal

cancer is primarily caused by a germline MMR mutation combined with an inactivating mutation in the remaining functional allele (Vasen *et al.* 2013).

The second most common hereditary disorder is Familial adenomatous polyposis. It is typically caused by a germline mutation in the *APC* gene, although some cases are related to inherited *MUTYH* mutation. Familial adenomatous polyposis is characterized by the presence of a large number of adenomatous polyps, which almost inevitably progress to colorectal cancer if left untreated (Half *et al.* 2009).

MUTYH-associated polyposis arises from a germline mutation in *MUTYH* and typically presents with an increased number of polyps compared to sporadic colorectal cancers. *MUTYH* is involved in the base excision repair pathway, responsible for repairing oxidative DNA damage resulting from cellular metabolism. A defective base excision repair pathway predisposes to the accumulation of mutations and subsequent cancer development (Ma *et al.* 2018).

Both Lynch syndrome and Familial adenomatous polyposis are dominantly inherited syndromes, whereas *MUTYH*-associated polyposis follows a recessive inheritance pattern (Half *et al.* 2009, Ma *et al.* 2018). Additionally, there are several other polyposis syndromes, such as Peutz-Jeghers syndrome, Juvenile polyposis syndrome, and serrated polyposis syndrome (Ma *et al.* 2018, Arends *et al.* 2019).

2.3.4 Signalling pathways

Colorectal cancer development is a multistep process involving the accumulation of multiple mutations. Mutations contributing to carcinogenesis are typically occurring in tumor-suppressor genes and proto-oncogenes, which are critical regulators of cell growth and differentiation. Tumor-suppressor genes normally restrain cell growth, and mutations in these genes promote uncontrollable cell growth and tumor progression. Proto-oncogenes are genes typically involved in maintaining normal cell growth and division. Mutations in proto-oncogenes may lead to their conversion into oncogenes, which have a potential to drive uncontrollable cell growth and promote carcinogenesis (Fearon and Vogelstein 1990). Many tumor-suppressor genes and oncogenes are key regulators in several signalling pathways, including Wnt/CTNNB1, MAPK, Notch, PI3K/AKT, NF-κB, TGFB, p53, and JAK/STAT pathways (Kandoth *et al.* 2013). Table 2 represents some tumor-suppressor genes and oncogenes implicated in colorectal cancer development.

TABLE 2 Typically mutated tumor-suppressor genes and oncogenes in colorectal cancer[1].

Gene	Pathway	Frequency	Effect of mutation
Tumor-suppressor genes			
APC	WNT	80%	CTNNB1 accumulation leading to activation of proto-oncogene transcription
TP53	P53	60%	Defective response to DNA damages, defects in regulating cell cycle arrest and apoptosis
TGFBR2	TGFB	20%	Defects in regulating cell growth and apoptosis
MLH1, *MSH2*, *MSH6*, *PMS2*	MMR	15%	Defects in DNA repair system, accumulation of oncogenic mutations
SMAD4	TGFB	15–20%	Upregulation of tumor growth
PTEN	PI3K	10–30%	Promoting cell survival and preventing apoptosis
Oncogenes			
KRAS	MAPK	40%	Constant GTP-bound[2] active state, promoting cell survival and preventing apoptosis
BRAF	MAPK	10%	Promoting cancer cell growth
PIK3CA	PI3K	10–20%	Promoting uncontrollable cell growth and survival

[1]Based on Cancer Genome Atlas Network (2012), Kuipers *et al.* (2015), and Nagtegaal *et al.* (2019).
[2]Abbreviations: GTP, guasine triphosphate.

2.4 Immune system

The immune system, divided into the innate and adaptive immune systems, maintains tissue homeostasis by identifying and eliminating abnormal molecules, invading pathogens, and damaged cells. All immune cells develop from multipotent hematopoietic stem cells, first differentiating into common myeloid and lymphoid progenitor cells, and subsequently maturating into innate and adaptive immune cells (Fig. 5) (Murphy and Weaver 2017).

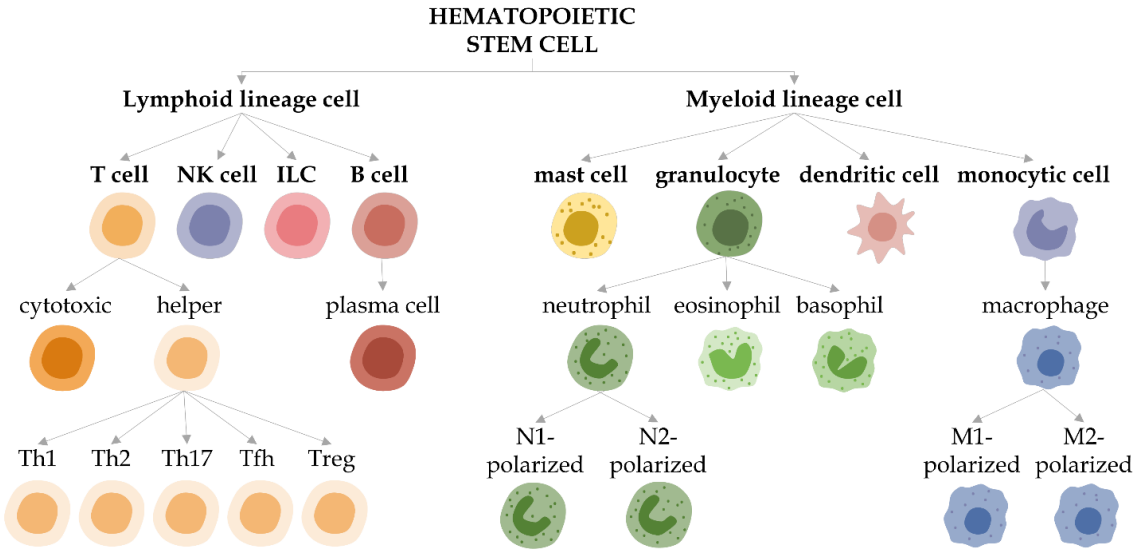

FIGURE 5 Classification of immune cells. Abbreviations: ILC, innate lymphoid cell; NK, natural killer; Tfh, T follicular helper; Th, T helper; Treg, T regulatory. Based on Murphy and Weaver (2017).

2.4.1 Innate immune system

Innate immune cells function as the first-line defence. Some innate immune cells are constantly monitoring tissues for pathogens to prompt a rapid response. In cases where tissue homeostasis is disrupted, macrophages and mast cells activate inflammation by releasing a substantial amount of mediators, which recruit and activate other immune cells, facilitating their migration to the affected tissue (Murphy and Weaver 2017).

2.4.1.1 Macrophages

Macrophages play a pivotal role in maintaining tissue homeostasis, responding to infections, and contributing to overall immune defense. They can perform two functionally different polarization states: classically activated (M1) and alternatively activated (M2) macrophages (Murray 2017). M1 macrophages exhibit a multifaceted role in promoting inflammation. They can directly eliminate pathogens and necrotic host cells. Additionally, they induce T helper (Th) 1 responses by producing proinflammatory cytokines and present antigens to T cells through the major histocompatibility complex (MHC) I and II. Conversely, anti-inflammatory M2 macrophages can promote Th2 responses through anti-inflammatory cytokines and deplete the activity of T cells, B cells, and natural killer cells. In addition, they can contribute to tissue repair and extracellular matrix synthesis (Yadav *et al.* 2022). However, instead of two distinct macrophage subtypes, the M1-M2 polarization is a continuum, and the state can also change in a response to microenvironmental changes (Italiani *et al.* 2014). Macrophages are among the most predominant leukocytes in the tumor microenvironment of solid tumors, including colorectal cancer (Nielsen and Schmid 2017, Li *et al.* 2023). These tumor-associated macrophages are often

influenced by cancer to adopt an M2 polarization. The shift towards M2 polarization results in macrophages that generally support tumor progression and growth (Yahaya *et al.* 2019).

2.4.1.2 Neutrophils

Neutrophils, which are the most abundant immune cell type in blood, play an important role in orchestrating immune responses by promoting inflammation and triggering adaptive immune cells (Jaillon *et al.* 2020). However, like macrophages, neutrophils are plastic and can polarize into two functionally distinct subtypes, N1 and N2 neutrophils, which in cancer can demonstrate anti- and pro-tumorigenic roles, respectively. Tumor cells typically favor the differentiation of neutrophils towards N2 neutrophils through releasing cytokines and other signalling mediators (Fridlender *et al.* 2010).

2.4.1.3 Dendritic cells

Dendritic cells are highly immunogenic and are in a key role in mediating communication between the innate and adaptive immune systems. They can be differentiated into several subtypes, including conventional dendritic cells, plasmacytoid dendritic cells, monocyte-derived dendritic cells, and Langerhans cells. Conventional dendritic cells, which include type 1 and 2 cells, are the predominant subtype capable of capturing and presenting antigens to cytotoxic T cells and helper T cells on MHC I and II, respectively. Dendritic cells can also contribute to the differentiation of helper T cells into effector cells (Hilligan and Ronchese 2020). Under certain circumstances, dendritic cells can exhibit anti-inflammatory effects through various mechanisms, including expressing low levels of MHC molecules and co-stimulatory signals for T cells, promoting helper T cell differentiation into regulatory T cells, or secreting anti-inflammatory cytokines (Ness *et al.* 2021). Cancer may prevent the pro-inflammatory activity of dendritic cells by impeding their maturation (Gabrilovich *et al.* 1996, Michielsen *et al.* 2011).

2.4.1.4 Natural killer cells

Natural killer cells are innate immune cells with T cell-like characteristics. They can detect and directly kill intracellular pathogens and aberrant cells through various cytotoxic mechanisms, including the release of granules and death-receptor-mediated apoptosis. Natural killer cells release granules containing the lytic protein perforin and granzyme proteases. Perforin forms pores in the target cell membrane, allowing granzymes to enter the cell and induce apoptosis. In death-receptor-mediated apoptosis, target cell death is induced when Fas ligand, tumor necrosis factor-related apoptosis-inducing ligand (TRAIL), or tumor necrosis factor (TNF) engage with their specific receptors on the target cell surface (Prager and Watzl 2019). Unlike T cells, natural killer cells lack specific surface antigen receptors and are capable of detecting aberrant cells which have lost MHC I molecules (Kärre *et al.* 1986). Natural killer cells can upregulate inflammation by promoting T cell activity, inducing MHC I expression, or activating dendritic cells (Reid *et al.* 2021). However, they may also restrict

immune activity by eliminating some activated immune cells and releasing immunoregulatory cytokines (Zitti and Bryceson 2018).

2.4.1.5 Mast cells

Mast cells are well-known for their significant role in mediating allergic reactions. When exposed to allergens, activated mast cells release proinflammatory mediators and cytokines, such as histamine, serotonin, and TNFA to contribute to inflammation and trigger physiologic symptoms (Theoharides *et al.* 2012). In inflammatory reactions, mast cells are involved in direct elimination of pathogens and in recruitment of other immune cells to the infection site (De Giovanni *et al.* 2022, Liu *et al.* 2023). Furthermore, mast cells can modulate the function of Th2, regulatory T, and B cells and promote the maturation of Th17 cells (Theoharides *et al.* 2012, Cardamone *et al.* 2016). Conversely, mast cells can also exhibit an anti-inflammatory effect driven by Th2 cytokine secretion (Bischoff *et al.* 2001). In cancer, mast cells have been shown to promote angiogenesis and lymphangiogenesis and to release both pro- and anti-tumor mediators (Liu *et al.* 2023).

2.4.1.6 Myeloid-derived suppressor cells

Myeloid-derived suppressor cells (MDSCs) are a heterogenous population of myeloid cells with immunoregulatory effects. During chronic inflammation and in cancer, myeloid cells may undergo pathological activation, disrupting the maturation process and leading to the development of incompletely maturated MDSCs. MDSCs, comprising polymorphonuclear and monocytic main subsets, share some traits with mature granulocytes and monocytes but exhibit differences in phenotype and function. MDSCs typically lack phagocytotic capability and can secrete immunosuppressive cytokines, reactive oxygen and nitrogen species, and other immunosuppressive molecules, thereby possessing high immunosuppressive and tumor growth-promoting potential (Bronte *et al.* 2016).

2.4.2 Adaptive immune system

The adaptive immune system comprises T and B cells and its activation is slower compared to the innate immune system. Adaptive immunity recognizes aberrant cells or pathogens based on their specific surface antigens and establishes an immunological memory, which enables a faster and more efficient response upon subsequent exposure to the same foreign antigen (Murphy and Weaver 2017).

2.4.2.1 T cells

T cells are adaptive immune cells involved in cell-mediated immunity. T cell activation of naïve T cells into effector cells requires three signals: antigen-dependent, co-stimulatory, and cytokine-dependent signals. The antigen-dependent signal corresponds to the recognition of a specific antigen presented on MHC molecules on antigen presenting cells, including mature dendritic cells, macrophages, and activated B cells. This recognition is mediated by T cell

receptor on T cell (Wilcox 2016). The co-stimulatory signal enhances T cell receptor-mediated activation and prevents T cell anergy, a state in which T cell is unable to respond to the presented antigen and remains inactive. The co-stimulatory signal is formed between the CD28 receptor on T cells and the CD80 (B7.1) or CD86 (B7.2) receptors on antigen presenting cells (Wilcox 2016, Zumerle *et al*. 2017). The cytokine-dependent signal is required to complete the activation process, allowing T cells to differentiate into effector or memory T cells and proliferate (Wilcox 2016). Activated T cells undergo clonal expansion, during which the number of effective antigen-specific T cells is increased, and differentiation, leading to the formation of various specialized T cell subtypes. T cells are categorized into αβ and γδ T cells based on their glycoprotein chains on T cell receptors. αβ T cells encompass helper T cells, cytotoxic T cells, and memory T cells. γδ T cells constitute approximately 5–10% of all T cells, and their role in immune system, as well as their antigen recognition mechanisms, are less well understood compared to αβ T cells (Morath and Schamel 2020).

Helper T cells, activated through MHC II, regulate immune responses by directly interacting with other immune cells and by releasing cytokines. Helper T cells promote the clonal expansion and differentiation of cytotoxic T cells, as well as the activation and antibody production of B cells (Borst *et al.* 2018). Furthermore, a subset of helper T cells can directly work as cytolytic cells and eliminate abnormal cells (Quezada *et al.* 2010, Hashimoto *et al.* 2019). Helper T cells can differentiate into several subsets, including Th1, Th2, Th3, Th9, Th17, Th22, T regulatory 1, follicular Th, and regulatory T cells, each differing in their surface receptors cytokine profiles, and transcription factors (Cenerenti *et al.* 2022). Of the subsets, Th1, Th2, and regulatory T cells are the most well-established. Th1 cells are pro-inflammatory and are involved in the activation of cytotoxic T cells, B cells, and macrophages, particularly in defence against intracellular pathogens and virus-infected cells (Meitei and Lal 2023). Th2 cells are involved especially in promoting the elimination of intracellular pathogens, tissue damage repair, B cell proliferation, and M2 macrophage polarization (Walker and McKenzie 2018). Regulatory T cells downregulate T cell activity and have an important role in preventing autoimmune diseases and the overactivity of cytotoxic T cells (Spence *et al.* 2015). However, they can also suppress the maturation, effector function, or interaction of other immune cells (Vignali *et al.* 2008).

Cytotoxic T cells, activated through MHC I, are considered the primary effectors in the anti-tumor immune response (Schüler *et al.* 1999). Activated cytotoxic T cells can eliminate target cells by inducing apoptosis through the secretion of perforin and granzymes. Alternatively, target cells may also be killed through the interaction between the Fas ligand on cytotoxic T cells and the Fas receptor on the target cell, resulting in target cell DNA fragmentation (Gordy and He 2012, Fu *et al.* 2016, Raskov *et al.* 2021). Some T cells differentiate into memory T cells, which exhibit a long-lasting memory to specific pathogens, enabling the immune system to mount a faster and more efficient response upon re-exposure (Farber *et al.* 2014).

T cells have been extensively studied in the context of colorectal cancer prognosis. Higher densities of cytotoxic T cells and Th1 cells have shown to be associated with prolonged survival and reduced tumor recurrence (Naito *et al.* 1998, Galon *et al.* 2006, Pagès *et al.* 2008, Tosolini *et al.* 2011). In addition, higher infiltration of overall and memory T cell populations has demonstrated a positive prognostic effect (Galon *et al.* 2006, Pagès *et al.* 2008). Regulatory T cells may be associated with worse survival in colorectal cancer patients, although previous studies have reported both positive and negative prognostic associations (Salama *et al.* 2009, Sinicrope *et al.* 2009, Frey *et al.* 2010).

2.4.2.2 B cells

B cells are adaptive immune system cells mediating humoral immunity. Upon activation, they differentiate into antibody-secreting plasma cells and memory cells. B cells directly eliminate pathogens and can amplify inflammation by assisting other immune cells to recognize and eliminate pathogens through antibodies. Additionally, B cells can activate $CD4^+$ and $CD8^+$ T cells and promote their differentiation. In cancer, inactive B cells may deplete T cell responses and potentially promote tumor progression. However, B cells typically become activated in cancer and thus present a high potential for tumor cell elimination (Nelson 2010).

2.5 Interaction between tumor and host

2.5.1 Inflammation

Tumors possess a complex and flexible interaction with the host immune system in colorectal cancer. The immune system induces anti-tumor immunity to efficiently detect and eliminate tumor cells, and a strong immune response is found to be associated with better prognosis in colorectal cancer patients (Alexander *et al.* 2020). However, it is widely acknowledged that inflammation can also predispose to cancer development and certain immune cells may promote cancer progression (Shankaran *et al.* 2001, Hanahan and Weinberg 2011). There exists a balance between pro- and anti-tumor immune responses, in which the composition of immune cells potentially alters in different stages of tumor progression (Bindea *et al.* 2013). Additionally, the densities and localization of immune cells within the colorectal cancer microenvironment and between different patients can be highly heterogenous (Galon *et al.* 2006, Pagès *et al.* 2008, Halama *et al.* 2010, Edin *et al.* 2019).

Acute inflammation is a normal, short-term, and well-coordinated process aiming at restoring tissue homeostasis by eliminating abnormal cells (de Visser *et al.* 2006). However, under certain circumstances, inflammation may persist in a disordered and destructive state and lead to chronic inflammation. Chronic inflammation results in excessive immune activation and disrupted balance between the innate and adaptive systems. In this state, adaptive immunity may

induce constant and excessive activity of innate immunity, while innate immunity may suppress the anti-tumor response of adaptive immunity (de Visser *et al.* 2006). Chronic inflammation is recognized as a significant factor predisposing to cancer progression. Diseases characterized by chronic inflammation, such as Crohn's disease and ulcerative colitis, are notably associated with an increased risk for colorectal cancer development (Eaden *et al.* 2001, Waldner and Neurath 2009).

2.5.2 Tumor microenvironment

Tumor microenvironment is a dynamic ecosystem encompassing tumor cells, immune cells, fibroblasts, epithelial cells, mesenchymal cells, extracellular matrix, blood and lymphatic vessels, and signalling molecules produced by both tumor and host cells (Chen *et al.* 2021b). Cells within the tumor microenvironment interact through direct cell contacts, secreting immunomodulating mediators, or modulating stroma, extracellular matrix, or vascularization (Giraldo *et al.* 2014).

Cytokines serve as signalling molecules regulating numerous cellular processes through autocrine or paracrine signalling, exhibiting either immunostimulatory or tumor growth-preventing, or immunoinhibitory or tumor growth-promoting effects. Additionally, they can modulate angiogenesis and the metastatic potential of tumor cells or influence therapeutic response. Cytokines encompass a high variety of different mediators, including interferons, interleukins, chemokines, mesenchymal growth factors, tumor necrosis factors, and colony-stimulating factors (Conlon *et al.* 2019).

The tumor stroma, consisting of supportive connective tissue and non-neoplastic cells surrounding tumor cells, includes fibroblasts, immune cells, blood vessels, and extracellular matrix. Cancer cells impact the stroma by inducing angiogenesis and upregulating the number of fibroblasts, leading to the synthesis of extracellular matrix and collagen (Bremnes *et al.* 2011). Cancer can also activate fibroblasts into a subset of cancer-associated fibroblasts, which exhibit pro-tumorigenic effects (Sahai *et al.* 2020).

A rapid proliferation rate of tumor cells necessitates an increased oxygen supply within the tumor microenvironment. Consequently, a hypoxic microenvironment induces the production of pro-angiogenic factors resulting in the formation of new, typically functionally and morphologically abnormal blood vessels around the tumor (Carmeliet and Jain 2000). Furthermore, tumor angiogenesis may downregulate immune cell activity by forming a physical barrier, thereby impeding immune infiltration (Hamzah *et al.* 2008).

2.5.3 Cancer immunoediting

The dynamic interplay between a developing tumor and host immunity is described by the three-step cancer immunoediting hypothesis, delineating the key phases of cancer progression: elimination, equilibrium, and escape (Dunn *et al.* 2004). The elimination phase (*i.e.*, immunosurveillance), represents the early

stages of tumor progression, during which the immune system identifies and eliminates transformed tumor cells. Successful tumor elimination significantly depends on the production of pro-inflammatory IFNG and the cytotoxic capabilities of immune cells. However, if some tumor cells manage to evade immune-mediated destruction, cancer progression may undergo a transition into the typically prolonged and dynamic equilibrium phase, sustained by the adaptive immune system. Within the equilibrium, some tumor cells are recognized and destroyed, while novel, unrecognized tumor cell variants emerge and evade immune detection. In the equilibrium phase, the tumor may either be completely eradicated or progress into the escape phase, characterized by immune system failure to restrict tumor growth, leading to the development of invasive cancer (Dunn *et al.* 2004).

2.5.4 Immune evasion

Tumor cells possess the ability to modulate the immune cell composition and exploit host cells to favor their own growth and survival (Vinay *et al.* 2015). Additionally, cancer employs various mechanisms to evade immune destruction. Tumor cells can dampen the expression of tumor antigens or MHC molecules to prevent immune detection and destruction (Beatty and Gladney 2015). Moreover, they typically lack the expression of costimulatory molecules crucial for T cell activation. Instead, they upregulate the expression of inhibitory molecules on both tumor and antigen-presenting cells, thus inducing T cell anergy or tolerance (Driessens *et al.* 2009). Tumor cells also produce immune suppressive cytokines, such as TGFB and IL10, which may contribute to cancer growth, decrease anti-tumor immune responses, or downregulate the antigen-presenting capability of dendritic cells by preventing their maturation (Gabrilovich *et al.* 1996, Vinay *et al.* 2015).

2.5.4.1 PDCD1 and CD274 immune checkpoints

Programmed death-1 (PD-1, PDCD1, CD279) and its ligand, programmed death-ligand-1 (PD-L1, CD274, B7-H1), are immune checkpoint proteins which exert immunoinhibitory effects and have emerged as potential targets for immunotherapy (Pardoll 2012, Marhelava *et al.* 2019). PDCD1 is expressed on various immune cells, including activated T cells, B cells, natural killer cells, and monocytes (Marhelava *et al.* 2019, Chen *et al.* 2024). CD274 is primarily expressed on antigen presenting cells but can also be found on dendritic cells and on some tumor cells (Dong *et al.* 2002, Keir *et al.* 2006, Marhelava *et al.* 2019).

The interaction between PDCD1/CD274 on T cells and antigen presenting cells generates a co-inhibitory signal that prevents T cell activation, resulting in reduced T cell proliferation (Wherry 2011, Chen *et al.* 2024). Under normal conditions, the PDCD1/CD274 interaction serves to prevent immune overactivity. However, during chronic inflammation and in many cancers, including colorectal cancer, the expression levels of PDCD1 and CD274 are typically upregulated. The upregulation contributes to immune evasion and induces T cell exhaustion, characterized by their decreased proliferation, activity,

and effector function (Fig. 6) (Dong *et al.* 2002, Blackburn *et al.* 2009, Chen *et al.* 2024).

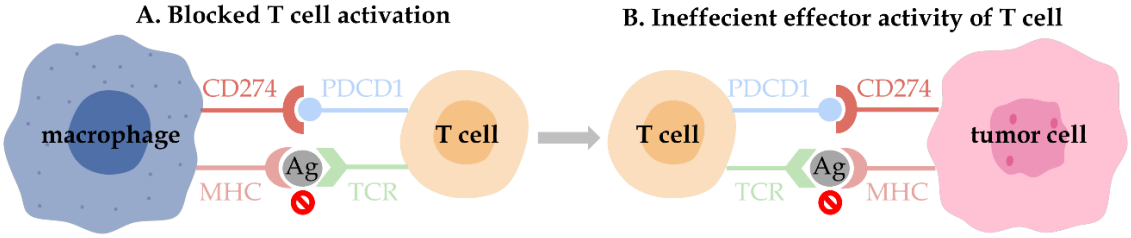

FIGURE 6 Immunosuppressive role of PDCD1/CD274 interaction. The interaction potentially downregulates the activation of T cells (A) or prevent their effector functions (B). Abbreviations: Ag, antigen; MHC, major histocompatibility complex; TCR, T cell receptor. Based on Marhelava *et al.* (2019).

2.5.4.2 IDO and ARG1 metabolic enzymes

Amino acid metabolism is frequently altered in cancer and cancer cells may undergo metabolic reprogramming to facilitate their rapid growth and proliferation (Zhang *et al.* 2023). Indoleamine 2’3’-dioxygenase (IDO) and arginase 1 (ARG1) are amino acid metabolizing enzymes, which frequently show increased expression in colorectal cancer (Leu and Wang 1992, Brandacher *et al.* 2006, Bishnupuri *et al.* 2019, Ma *et al.* 2019). Increased expression of IDO and ARG1 may promote immunosuppression and cancer growth (Vinay *et al.* 2015, Ma *et al.* 2019).

Tryptophan is an essential amino acid involved in kynurenine pathway, which plays a vital role in maintaining cell cycle progression and differentiation of T cells (Lee *et al.* 2002, Ye *et al.* 2019). IDO is a metabolizing enzyme regulating the first and rate-limiting step of tryptophan catabolism (Ye *et al.* 2019). IDO has two isoforms, IDO1 and IDO2, with IDO1 being more prevalent. In addition to IDO, also tryptophan-2,3-dioxygenase contributes to tryptophan catabolism but is primarily expressed in the liver (Hornyák *et al.* 2018). IDO1 promotes the catabolism of tryptophan into toxic kynurenine metabolites, thus having a profound immunoregulatory impact. Specifically, IDO1 downregulates T cell activity, induces T cell apoptosis, promotes the differentiation of regulatory T cells, stimulates the production of immune-inhibiting cytokines, drives M2-like macrophage polarization, and promotes the proliferation while suppressing apoptosis of tumor cells (Fallarino *et al.* 2002, Bishnupuri *et al.* 2019, Yang *et al.* 2019, Ye *et al.* 2019). IDO is primarily expressed in macrophages and dendritic cells, but also in some tumor cells (Meireson *et al.* 2020).

Arginase is a metabolizing enzyme catalysing the conversion of L-arginine into L-ornithine and urea (Caldwell *et al.* 2018). L-Arginine is a semi-essential amino acid that plays a crucial role in the liver, where systemic nitric waste compounds are transformed into less toxic urea in the urea cycle (Caldwell *et al.* 2018). ARG1 is a cytoplasmic isoform of arginase, primarily found in the liver (Jenkinson *et al.* 1996). However, its expression has been found to be increased in various cancers, including colorectal cancer (Niu *et al.* 2022). ARG1 is

predominantly expressed in granulocytes (Zea *et al.* 2005, Munder *et al.* 2005) and on myeloid-derived suppressor cells (Rodriguez *et al.* 2009). L-arginine has an important role in many processes in the immune system. Reduced levels of L-arginine can downregulate T cell activity by preventing the assembly of T cell receptors and by inducing cell cycle arrest (Zea *et al.* 2004, Rodriguez *et al.* 2007). Increased ARG1 expression also leads to elevated levels of L-ornithine, which is further metabolized into polyamines. Polyamines are essential for cell differentiation and proliferation, suggesting that the increased expression of ARG1 may be related to the increased demand of polyamines by cancer cells (Chang *et al.* 2001).

2.6 Colorectal cancer classification

Approximately 90% of colorectal cancers are adenocarcinomas, originating from the glandular epithelial cells of colorectal mucosa. The remaining cancers encompass neuroendocrine and squamous cell carcinomas (Nagtegaal *et al.* 2019). Most colorectal adenocarcinomas are classified as conventional adenocarcinomas, but multiple histopathological subtypes for adenocarcinomas are identified (Table 3). In addition to histology, these variants may differ in other features, including mucin formation, lymphocyte infiltration, site of origin, prognosis, aggressivity, mutation profile, and age at diagnosis (Nagtegaal *et al.* 2019).

TABLE 3 Histological subtypes of colorectal adenocarcinomas[1].

Type	Frequency	Histologic description
Mucinous adenocarcinoma	5–20%	>50% of the tumor lesion composed of extracellular mucins
Micropapillary adenocarcinoma	5–20%	≥5% of the tumor including small tumor cell clusters within stromal spaces
Serrated adenocarcinoma	10–15%	Glandular serrations, low nucleus-to-cytoplasm ratio
Adenoma-like adenocarcinoma	3–9%	≥50% of the invasive areas having an adenoma-like aspect with villous structures and a low-grade differentiation
Medullary carcinoma	2%	Sheets of malignant cells with vesicular nuclei, prominent nucleoli, and abundant eosinophilic cytoplasm with strong immune cell infiltration
Signet-ring cell carcinoma	1%	>50% of the tumor cells with intracytoplasmic mucins
Adenosquamous carcinoma	<0.1%	Features of adenocarcinoma and squamous cell carcinoma
Carcinomas with sarcomatoid component	<0.1%	Partly undifferentiated, sarcomatoid aspects, large tumor size, cells with abundant intra-cytoplasmic, eosinophilic rhabdoid bodies, often dyscohesive and myxoid matrix-embedded cells, pleomorphic giant or spindle cells, areas of glandular differentiation
Undifferentiated carcinoma	<0.1%	No evidence of differentiation, lacking pushing borders, syncytial growth pattern, and prominent lymphoplasmacytic infiltrates

[1]Classification and features adapted from Nagtegaal *et al.* (2019).

Colorectal cancers are classified using a two-tiered grading system based on glandular differentiation within the tumor. The classification is based on the least differentiated component within the tumor, as the invasive margin is excluded. Tumors are categorized into low-grade tumors, characterized by well-differentiated glandular structures, and high-grade tumors, exhibiting poorly differentiated glands (Nagtegaal *et al.* 2019).

2.7 Colorectal cancer diagnosis and treatment

2.7.1 Screening

Cancer screening plays a crucial role in detecting tumors in a localized, early-stage phase, facilitating treatment and reducing cancer-associated mortality (Shaukat and Levin 2022). Colorectal cancer screening tools include faecal occult

blood-based and imaging-based methods from which a faecal immunochemical test and colonoscopy are the most widely used approaches worldwide. The faecal immunochemical test targets haemoglobin with antibodies to detect blood in stool samples, as faecal blood may indicate colorectal cancer or precursor lesions. Colonoscopy is used for detecting and removing polyps or abnormal tissue from the colorectum using a tube-like instrument with a lens. Both the faecal immunochemical test and colonoscopy has shown to be effective in reducing colorectal cancer mortality (Hewitson *et al.* 2008, Brenner *et al.* 2014). Other screening methods include flexible sigmoidoscopy, multitarget stool DNA test, and colonography (Shaukat and Levin 2022). In Finland, nationwide colorectal cancer screening with a faecal immunological test for citizens aged 60–68-year was started in 2022 (Finnish Cancer Registry 2024).

2.7.2 Prognostic and predictive factors

Prognostic factors serve as markers to identify patients at an elevated or reduced risk for cancer-related mortality and to assess the course of the disease. On the other hand, predictive markers are employed in the selection of treatment strategies (Sargent *et al.* 2005). Prognostic and predictive assessment of colorectal cancer primarily relies on histological tumor parameters, supported by some molecular biomarkers (Chen *et al.* 2021a).

2.7.2.1 Histological factors

Tumor, node, metastasis (TNM) staging system, designed by The American Joint Committee on Cancer (AJCC) and The Union for International Cancer Control (UICC), continues to be the primary and most reliable method for evaluating the prognosis of colorectal cancer. TNM staging classifies invasive tumors into four stages (I–IV) based on the extent of the primary tumor, the number of lymph node metastases, and the presence of distant metastases (Table 4) (Union for International Cancer Control 2017). The survival prospects of colorectal cancer patients are closely related on the stage. On average, patients with stage I tumors typically exhibit an average 5-year survival rate of approximately 90%, whereas those with stage IV tumors have a survival rate of only 15% (Cardoso *et al.* 2022). Although TNM staging is a robust prognostic parameter, the prognosis and clinical outcome can vary, particularly in tumors with intermediate stages II or III (Kannarkatt *et al.* 2017).

TABLE 4 TNM staging of colorectal cancer[1].

TNM stage	Classification	Description
Stage 0	Tis N0 M0	No tumor invasion from the lamina propria through the muscularis mucosae, carcinoma in-situ (Tis). No regional lymph node metastases (N0) or distant metastases (M0)
Stage I	T1/T2 N0 M0	Tumor invasion into submucosa (T1) or muscularis propria (T2). No regional lymph node metastases (N0) or distant metastases (M0)
Stage II	T3/T4 N0 M0	Tumor invasion into subserosa or into non-peritonealized pericolic or perirectal tissues (T3) or has invaded into visceral peritoneum and/or into other organs or structures (T4). No regional lymph node metastases (N0) or distant metastases (M0)
Stage III	any T N1/N2 M0	Carcinoma in-situ or tumor invasion into submucosa, muscularis propria, subserosa, non-peritonealized pericolic or perirectal tissues, visceral peritoneum, or other organs/structures (Any T). Metastasis in 1–3 (N1) or in 4 or more (N2) regional lymph nodes. No distant metastases (M0)
Stage IV	any T any N M1	Carcinoma in-situ or tumor invasion into submucosa, muscularis propria, subserosa, non-peritonealized pericolic or perirectal tissues, visceral peritoneum, or other organs/structures (Any T). Metastasis or no metastasis in regional lymph nodes (Any N). Distant metastasis to one or several organs and/or to the peritoneum (M1).

[1]Adapted from Union for International Cancer Control (2017).

Tumor grading is a widely employed histological classification system for prognostication along with TNM staging. High-grade tumors, exhibiting poor glandular differentiation, are typically associated with an advanced TNM stage and poorer survival outcomes compared to low-grade tumors with well-differentiated glandular structures (Nagtegaal *et al.* 2019, Chen *et al.* 2021a). Multiple other histological parameters, such as tumor location and size, lymphovascular and perineural invasion, intramural and extramural vascular invasion, tumor budding, lymph node ratio, circumferential resection margin in rectal cancer, and tumor-infiltrating lymphocytes have demonstrated to be potential additional prognostic markers (Union for International Cancer Control 2017, Nagtegaal *et al.* 2019, Chen *et al.* 2021a).

The characteristics and spatial distribution of tumor-infiltrating lymphocytes in the tumor microenvironment have significant prognostic value in colorectal cancer (Galon *et al.* 2006, Berntsson *et al.* 2017, Glaire *et al.* 2019, Kuwahara *et al.* 2019). Immunoscore® is a method used to assess immune cell infiltration in the colorectal cancer microenvironment. It quantifies $CD3^+$ and $CD8^+$ T cell densities in the tumor center and the invasive margin, resulting in a three-tiered classification categorizing tumors as having low, intermediate, or high Immunoscore (Pagès *et al.* 2018). A high Immunoscore has been shown to

serve as a robust and independent prognostic factor in colorectal cancer patients with stage I–III tumors (Galon *et al.* 2014, Pagès *et al.* 2018).

2.7.2.2 Molecular factors

There are several prognostic and predictive molecular biomarkers, widely used in clinical practice, including *BRAF*, *KRAS/NRAS*, and MSI statuses (Nagtegaal *et al.* 2019, Chen *et al.* 2021a). Moreover, the Colorectal Cancer Subtyping Consortium has defined four consensus molecular subtypes, that classify tumors based on their gene expression patterns and other molecular features (Guinney *et al.* 2015). The subtyping could potentially contribute to evaluation of colorectal cancer prognosis and treatment response, as considered alongside other biomarkers (Guinney *et al.* 2015, Mooi *et al.* 2018). The characteristics of consensus molecular subtypes 1–4 are summarized in Table 5.

TABLE 5 Characteristics of consensus molecular subtypes[1].

Molecular subtype	**CMS1**[2] (MSI immune)	**CMS2** (canonical)	**CMS3** (metabolic)	**CMS4** (mesenchymal)
Incidence	14 %	37 %	13 %	23 %[3]
Location	proximal colon	distal colon to rectum	proximal colon	colorectum
Molecular pathway	hypermutated	CIN	CIN/hypermutated	CIN
MMR status	MSI	MSS	MSS/MSI	MSS
CIMP methylation	high		intermediate	
SCNA number	low	high	intermediate	high
Mutation profile	*BRAF*	*HNF4A*	*KRAS*	
Signaling pathways	RTK, MAPK	WNT, MYC	RTK, MAPK	
Immune infiltration	high	moderate	lower than CMS1, variable	variable
Prognosis	poor survival after relapse	better survival after relapse than others	better survival after relapse than others	worse overall and relapse-free survival
Immunotherapy response potential	high			poor
Other	young age, female gender, higher tumor grade	diagnosed at more advanced stages	metabolic dysregulation	angiogenesis, EMT activation, matrix remodelling, diagnosed at more advanced stages

[1]Classification and features adapted from Guinney *et al.* (2015) and Noack and Langer (2023).
[2]Abbreviations: CIMP, CpG island methylator phenotype; CIN, chromosomal instability; CMS, consensus molecular subtype; EMT, epithelial-mesenchymal transition; MMR, mismatch repair; MSI, microsatellite instability; MSS, microsatellite stable; SCNA, somatic copy number alteration.
[3]The rest 13% of colorectal cancers excluded from CMS classification due to mixed phenotype and/or intra-tumoral heterogeneity.

2.7.3 Treatment

Colonoscopy, computer tomography imaging, or magnetic resonance imaging are typically employed to confirm colorectal cancer diagnosis and to assess the presence of distant metastases. TNM staging, MMR status, and the number of lymph nodes are utilized to evaluate the risk of relapse (Argilés *et al.* 2020). The primary curative approach for operable colon and rectal cancers is surgery, entailing the removal of resection margins and adjacent lymph nodes (Argilés *et al.* 2020, Biller and Schrag 2021). Typically, patients with rectal cancer undergo preoperative treatment, commonly involving neoadjuvant radiotherapy or chemoradiotherapy. This treatment aims to enhance surgical outcomes by reducing the tumor size or extent and minimizing local recurrences and micrometastases (Kuipers *et al.* 2015). For non-operable metastatic colorectal cancers, systematic chemotherapy with or without immunotherapy is the primary therapeutic approach (Biller and Schrag 2021, Fabregas *et al.* 2022). In metastatic colorectal cancers, the molecular profile, including MMR status, *BRAF* mutation status, and *KRAS/NRAS* mutation status, significantly influences treatment selection and patient prognosis (Fabregas *et al.* 2022, Leowattana *et al.* 2023).

Immunotherapy represents a potential treatment option for certain patients with metastatic MMR-deficient/MSI-high colorectal cancer. Immunotherapy operates by modulating the host immune response to enhance its capability to target and eliminate tumor cells (Chen *et al.* 2024). Due to a limited number of tumor antigens, immunotherapies exhibit reduced efficacy for MMR-proficient/MSI-low tumors (Leowattana *et al.* 2023). Currently, three immunotherapies are approved by the Food and Drug Administration for colorectal cancer. These therapies are immune checkpoint inhibitors, which restore the anti-tumor activity of T cells through blocking the interaction between immune checkpoint molecules. Two immunotherapies, Pembrolizumab and Nivolumab, target PDCD1, while the third, Ipilimumab, targets cytotoxic T-Lymphocyte Antigen 4 (Biller and Schrag 2021, Chen *et al.* 2024). Although immunotherapies have demonstrated effective and durable responses in certain cancer types and patient populations, a majority of patients still fail to respond to therapy. Resistance to therapy constitutes a critical factor leading to treatment failure (Chen *et al.* 2024).

3 AIMS OF THE STUDY

i) To characterize the patterns of infiltration and prognostic value of immune cells in colorectal cancer (I–III).

ii) To analyse the spatial arrangement of immune cell subtypes and assess the prognostic significance of immune cells in spatial proximity of tumor cells (I–III).

iii) To assess the expression patterns and prognostic value of PDCD1 and CD274 immune checkpoints in T cells, macrophages, and tumor cells (II).

iv) To evaluate the expression levels and prognostic value of IDO and ARG1 amino acid metabolizing enzymes in myeloid cells and in tumor cells (III).

4 PATIENTS AND METHODS

4.1 Patients (I–III)

The studies (I–III) were based on a retrospectively collected colorectal cancer cohort of 1,343 patients. The patients were operated in Central Finland Central Hospital (Jyväskylä, Finland) between January 1, 2000 and December 31, 2015. The annual population of the area during this period averaged around 270,000 (Kellokumpu *et al.* 2021). The clinical data for the patients was retrieved from the digital patient database of Central Finland Central Hospital.

The median age of patients at the time of primary colorectal cancer surgery was 71 (IQR 63–79) years. All patients were followed from the primary colorectal cancer diagnosis until the end of November 2019. The mean follow-up time for censored patients (N=547) was 10.6 (IQR 7.0–13.7) years. During the study period, 30% of the patients experienced cancer-associated death, and 28% experienced non-cancer-related death. Estimated with the Kaplan-Meier method, the 5-year and 10-year cancer-specific survival rates were 73% and 68% and overall survival rates were 61% and 45%, respectively. During the study period (2000–2015), there was an increase in the frequency of neoadjuvant treatments administered to patients with rectal carcinoma. Additionally, the number of colon cancer surgeries increased among patients with severe co-morbidities (Kellokumpu *et al.* 2021). Furthermore, the introduction of novel monoclonal antibodies advanced the treatment of patients with metastatic colorectal cancers. Monoclonal antibodies targeting epidermal growth factor receptor (EGFR) were employed to impede or slow down cell growth in *KRAS/NRAS* wild-type tumors, while those targeting vascular endothelial growth factor receptor (VEGF) were utilized to disrupt blood vessel growth (Biller and Schrag 2021).

This study was conducted according to the guidelines of the Declaration of Helsinki and approved by the administration and Ethics Committee of Wellbeing Services County of Central Finland (Dnro13U/2011, 1/2016, 8/2020, and 2/2023), the National Supervisory Authority for Welfare and Health (Valvira), the Finnish Medicines Agency (Fimea), and the Central Finland Biobank (BB23–

0172). The need to obtain informed consent from the study patients was waived (Valvira Dnro 3916/06.01.03.01/2016, Dnro FIMEA/2023/001573, 4/2023).

4.2 Histopathological features (I–III)

Tumor stage, grade, and the presence of lymphovascular invasion were retrospectively analyzed from hematoxylin and eosin-stained tissue sections following the latest guidelines (World Health Organization 2019, AJCC 8th edition). The assessment of MMR status and *BRAF* mutation status were conducted using immunohistochemistry. MMR proficiency was confirmed in patients exhibiting positive expression of all four MMR proteins (MLH1, MSH2, MSH6, PMS2) within the nuclei of tumor cells. In contrast, MMR deficiency was defined as the absence of expression of one or several MMR proteins in tumor cells. Tumors with *BRAF* mutation were detected using an antibody that specifically targets the mutated BRAF^{V600E} protein, with positive immunoreactivity in tumor cells classifying them as *BRAF*-mutated tumors.

4.3 Study cohorts (I–III)

We excluded patients who had received any preoperative oncological treatments, including chemotherapy, radiotherapy, or chemoradiotherapy, or had died within 30 days after surgery for the primary tumor. Preoperative radiotherapy is mostly used before rectal cancer surgery as it has been shown to increase the likelihood of complete tumor removal and reduce local recurrences (Folkesson *et al.* 2005). However, it has also been associated with a reduction in certain immune cells, particularly T cells (Nagtegaal *et al.* 2002), and was therefore considered a potential confounding factor. Deaths within 30 days after primary tumor surgery were considered to be mostly related to surgical complications. Additionally, tumors with unsuccessful immunohistochemistry or inadequate tumor tissue were excluded, resulting in varying patient numbers across the final cohorts in studies I–III. The full cohort and final cohorts for each Study are represented in Table 6.

TABLE 6 Demographic and clinical characteristics of colorectal cancer cases.

Characteristic	N total	N (Study I)	N (Study II)	N (Study III)
All cases	1343 (100%)	983 (100%)	910 (100%)	833 (100%)
Gender				
female	628 (47%)	481 (49%)	464 (51%)	411 (49%)
male	715 (53%)	502 (51%)	446 (49%)	422 (51%)
Age (years)				
<65	400 (30%)	265 (27%)	247 (27%)	225 (27%)
65–75	457 (34%)	348 (35%)	331 (36%)	297 (36%)
>75	486 (36%)	370 (38%)	332 (36%)	311 (37%)
Year of operation				
2000–2005	451 (34%)	299 (30%)	280 (31%)	262 (31%)
2006–2010	414 (31%)	315 (32%)	283 (31%)	261 (31%)
2011–2015	478 (36%)	369 38%)	347 (38%)	310 (37%)
Tumor location				
proximal colon	536 (40%)	478 (49%)	445 (49%)	409 (49%)
distal colon	404 (30%)	359 (37%)	332 (36%)	299 (36%)
rectum	403 (30%)	146 (15%)	133 (15%)	125 (15%)
AJCC[1] stage				
I	250 (19%)	162 (16%)	151 (17%)	143 (17%)
II	489 (36%)	371 (38%)	342 (38%)	317 (38%)
III	429 (32%)	322 (33%)	301 (33%)	270 (32%)
IV	175 (13%)	128 (13%)	116 (13%)	103 (12%)
Tumor grade				
low-grade (well to moderately differentiated)	1118 (83%)	813 (83%)	760 (84%)	704 (85%)
high-grade (poorly differentiated)	225 (17%)	170 (17%)	150 (16%)	129 (15%)
Lymphovascular invasion				
no	1054 (78%)	772 (79%)	719 (79%)	654 (79%)
yes	289 (22%)	211 (21%)	191 (21%)	179 (21%)
MMR status				
MMR proficient	1170 (87%)	833 (85%)	772 (85%)	705 (85%)
MMR deficient	172 (13%)	150 (15%)	137 (15%)	128 (15%)
missing	1 (0.07%)	0 (0.00%)	0 (0.00%)	0 (0.00%)
BRAF status				
wild type	1152 (86%)	824 (84%)	763 (84%)	697 (84%)
mutant	188 (14%)	159 (16%)	147 (16%)	136 (16%)
missing	3 (0.22%)	0 (0.00%)	0 (0.00%)	0 (0.00%)
Preoperative oncological treatment				
no	1100 (82%)	983 (100%)	910 (100%)	833 (100%)
yes	243 (18%)	0 (0%)	0 (0%)	0 (0%)
30-day mortality				
no	1303 (97%)	983 (100%)	910 (100%)	833 (100%)
yes	40 (3%)	0 (0%)	0 (0%)	0 (0%)

[1]Abbreviations: AJCC, American Joint Committee on Cancer; MMR, mismatch repair.

4.4 Immune cell detection

4.4.1 Tissue specimens

The cohort consisted of 1,343 formalin-fixed, paraffin-embedded tissue specimens. In cases where several sequential tissue specimens were available for a patient, the most representative specimen, with the deepest invasion and/or highest amount of viable tumor tissue was selected.

4.4.2 Tissue microarray construction

The tissue microarray, first introduced by Kononen et al. 1998, is a high-throughput method, in which small cylindrical tissue biopsies from multiple different tumor specimens are transferred into one empty paraffin block. The tissue microarray technique enables the analysis of a large number of tissue specimens uniformly, faster, and more cost-efficiently compared to single whole tissue specimens (Kononen *et al.* 1998).

The tissue specimens (N=1,343) were sampled into 25 tissue microarray blocks for immunohistochemistry. Each tissue microarray was composed of 228 1-mm diameter tumor cores with two tonsil cores as staining control. From each tumor, two cores were taken from both the tumor center and the invasive margin, if possible. In minimum, one core was taken from both tumor compartments. Using hematoxylin and eosin-stained tissue slides, the core sites were selected to include histologically different sites of the tumor to capture tumor heterogeneity as comprehensively as possible. The cores from the invasive margin were selected from the sites of deepest invasion and were targeted to span 500 µm into non-neoplastic tissue and 500 µm into tumor tissue. Necrotic areas were avoided.

To test antibodies for immunohistochemistry, a separate tissue microarray block consisting of 1.5-mm diameter cores with tonsil tissue, non-neoplastic colon, and colorectal cancer tissue cores was constructed. The tumor tissue samples were chosen to represent a range of years from 2000 to 2015 and to include histologically diverse types of tumors.

4.4.3 Immunohistochemistry (I–III)

For immunohistochemistry, 3.5 µm thick tissue sections were cut into positively charged hydrophilic slides. All immunohistochemistry, except for $BRAF^{V600E}$ mutated protein, was performed using the BOND-III automated immunohistochemistry stainer (Leica Biosystems, Buffalo Grove, IL, USA). Heat-induced epitope retrieval was conducted with BOND Epitope Retrieval Solution 1 (citrate-based buffer, pH 6.0) or BOND Epitope Retrieval 2 (EDTA-based buffer, pH 9.0, Leica Biosystems). The epitope retrieval solution was selected separately for each antibody to enable optimal signal-to-noise ratio. Bound antibodies were detected with BOND Polymer Refine Detection system (Leica Biosystems), which employs 3,3'-Diaminobenzidine (DAB) as a chromogen and hematoxylin for

counterstaining. Immunohistochemistry for each marker was performed in a single batch to ensure uniform staining quality. Immunohistochemistry for $BRAF^{V600E}$ mutated protein was conducted using a BenchMark XT immunostainer (Ventana Medical Systems, Tucson, AZ, USA). The amplification was done with OptiView Amplification (Ventana). All monoclonal antibodies used for immunohistochemistry in studies I–III are listed in Table 7. To follow the recommendations of the expert panel and reduce ambiguity, the standardized nomenclature system for genes and gene products was used (Fujiyoshi *et al.* 2021).

TABLE 7 Antibodies and protocols used for immunohistochemistry.

Marker	Clone	Manufacturer	Target	Study
MLH1	ES05	Novocastra	MMR protein, MLH1	I–III
MSH2	FE11	Calbiochem	MMR protein, MSH2	I–III
MSH6	EP49	Epitomics	MMR protein, MSH6	I–III
PMS2	A16-4	BD-Pharmingen	MMR protein, PMS2	I–III
$BRAF^{V600E}$	VE1	Spring Bioscience	$BRAF^{V600E}$ mutated protein	I–III
CD3	LN10	Leica	T cell	I,II
CD8	SP16	Thermo Scientific	cytotoxic T cell	I
ITGAM (CD11b)	D6X1N	Cell Signaling	myeloid cell	III
CD14	D7A2T	Cell Signaling	monocytic cell	III
CD68	KP1	Biolegend	macrophage	II
CD86	E2G8P	Cell Signaling	M1-like macrophage	II
HLADR	TAL 1B5	Santa Cruz	M1-like macrophage, mature monocytic cell	II,III
CD163	10D6	Thermo Scientific	M2-like macrophage	II
MRC1 (CD206)	E2L9N	Cell Signaling	M2-like macrophage	II
CEACAM8 (CD66b)	G10F5	Biolegend	granulocyte	III
FCGR3 (CD16)	D1N9L	Cell Signaling	FCGR3 protein	III
CD33	SP266	Abcam	myeloid cell	III
TPSAB1 (tryptase)	AA1	Santa Cruz	mast cell	III
KRT	BS5	BioSite Histo	epithelial cell	II,III
PDCD1 (PD-1)	SP269	Abcam	PDCD1 protein	II
CD274 (PD-L1)	E1L3N	Cell Signaling	CD274 protein	II
ARG1	EPR6672(B)	Abcam	arginase	III
IDO	EPR20374	Abcam	indoleamine 2,3-dioxygenase	III

4.4.4 Multiplex immunohistochemistry (II, III)

Multiplex immunohistochemistry is a technique that allows for the simultaneous detection of multiple targets within a single tissue section, enabling more detailed cell phenotyping compared to conventional immunohistochemistry (Tan *et al.* 2020). In the present study, a cyclic chromogenic multiplex immunohistochemistry staining assay, together with computer-assisted image analysis, was applied to phenotype each cell in a tissue specimen with multiple markers. The staining was conducted using the same equipment and reagents as in conventional immunohistochemistry, with the exception that DAB chromogen was replaced with alcohol-soluble 3-Amino-9-Ethylcarbazole (AEC).

4.4.4.1 Staining procedure

The first staining cycle of the multiplex immunohistochemistry-panel followed the protocol of conventional immunohistochemistry. After the staining, the slides were temporarily mounted for scanning using VectaMount AQ Aqueous Mounting Medium (Vector Laboratories, Newark, CA, USA). The slides were digitized, after which they were soaked in water to detach the coverslips. Before the following staining cycle, the AEC chromogen was removed using 100% ethanol, and the antibodies were stripped by heating the slides. The multiplex immunohistochemistry staining procedure is described in Fig. 7.

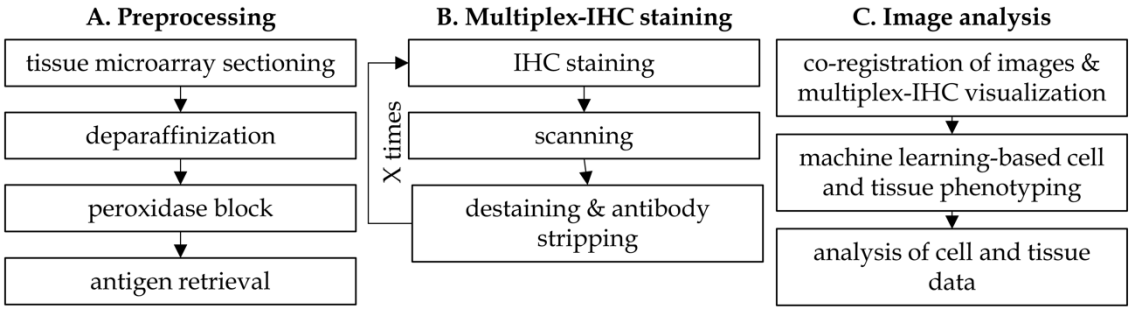

FIGURE 7 Procedure for multiplex immunohistochemistry staining and computer-assisted image analysis. Abbreviations: IHC, immunohistochemistry.

Although the staining can be repeated many times, it is notable that the risk for tissue sample detachment or damage heightens with increasing number of staining cycles. Repeated heating steps may also compromise the functionality of certain antibodies. Study II included a multiplex immunohistochemistry panel with 9 cycles, while Study III employed a panel with 10 cycles. To prevent the drying of tissue sections, slides were preserved in water at +4°C between staining cycles.

4.4.4.2 Optimizing the staining panel

All antibodies used in multiplex immunohistochemistry were first tested and optimized using conventional immunohistochemistry. The optimal staining order for antibodies in the panel was tested using a separate test tissue microarray specimen with tonsil, non-neoplastic colon, and colorectal cancer tissues. To ensure the functionality of the panel, the staining patterns were visually compared with those of conventional immunohistochemistry. To further validate the accuracy of multiplex immunohistochemistry staining panel, cell densities were manually calculated from respective tumor regions of immunohistochemistry and multiplex immunohistochemistry-stained slides (II).

4.4.4.3 Slide digitizing

Immunohistochemistry-stained tissue sections were mounted with a Tissue-Tek Glas Automated Glass Coverslipper (Sakura Finetek, Torrance, CA, USA) and digitized with NanoZoomer XR (Hamamatsu Photonics, Hamamatsu City,

Japan, resolution 0.45 µm/pixel) using a 20x magnification to enable computer-assisted image analyses.

4.4.4.4 Image preparation for image analyses

Tissue microarray cores were identified and separated into single core images using the *TMA dearrayer* function in QuPath open-source bioimage analysis software (Bankhead *et al.* 2017). Tumor cores that were detached, ruptured, necrotic, or contained minimal amount or no viable tumor tissue were excluded. Furthermore, for final analyses, only tumors that were successfully analyzed for at least one tumor core in both the tumor center and the invasive margin were included.

For multiplex immunohistochemistry panels, single core images of each staining cycle were co-registered into multi-channel images by aligning cell nuclei using the MultiStackReg macro in Fiji/ImageJ open-source software (Schindelin *et al.* 2012). Subsequently, these images were converted into pseudo-immunofluorescence images, with each channel represented by a unique colour (Fig. 8).

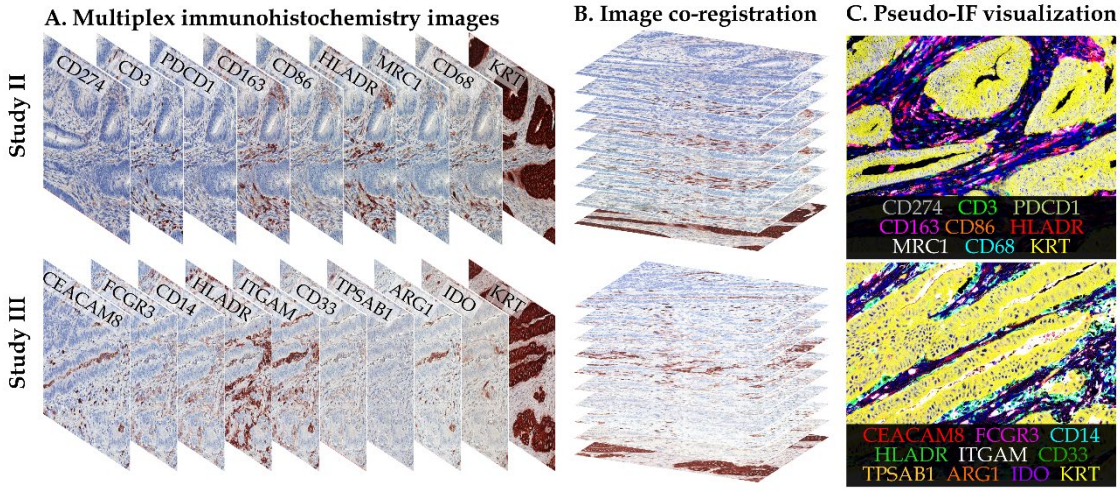

FIGURE 8 Co-registration and pseudo-immunofluorescence conversion of multiplex immunohistochemistry images in Studies II and III. Digitized multiple immunohistochemistry images from each staining cycle for one tumor (A), image co-registration into multi-channel image (B), and pseudo-immunofluorescence visualization (C). Abbreviations: IF, immunofluorescence.

4.5 Immune cell analyses

4.5.1 Computer-assisted digital image analyses (I–III)

Image analyses for multiplex immunohistochemistry images were conducted in QuPath, using supervised machine-learning based algorithms (Bankhead *et al.* 2017). QuPath was trained to classify cell types and tissue categories by manually

annotating cells or small regions in immunohistochemistry-stained slide images. The training was performed for a set of tumor regions selected from histologically variable tumor cores, which were assembled into two training images. One training image was utilized for cell classification, while another image was employed for tissue categorization.

Cells were detected using the *cell detection* function, with manual parameter adjustment to optimize the detection of cell nuclei. During cell detection, several features were calculated for each cell, including the area of nuclei, spatial localization of nuclei centroids in XY coordinates, and the mean staining intensities of each marker within each cell nuclei and cytoplasm (Bankhead *et al.* 2017). Additionally, Haralick (I) and Smoothed (I–III) features were then calculated to potentially enhance the classification of tissue compartments and cells, respectively. Haralick features measure grey-level intensities for each pixel across the tissue specimen to identify and analyse different tissue textures (Haralick *et al.* 1973), whereas Smoothed features compute weighted averages of specific cell parameters within a defined radius (Bankhead *et al.* 2017).

Training for cell classification was performed using the built-in random forest algorithm-based *object classifier* function, allowing cells to be efficiently trained into the main cell categories (*i.e.*, T cells, tumor cells, and other cells). The accuracy of the automated cell detection and classification in QuPath was validated by comparing cell densities obtained through manual cell counting with those derived from automated cell counting (I). In Study II, QuPath was trained to phenotype T cells, macrophages, tumor cells, and other cells. In Study III, cells were phenotyped into monocytic cells, granulocytic cells, mast cells, tumor cells, and other cells.

Tissue segments were classified using the built-in *pixel classifier* function, based on the random forest algorithm. Tissue segments were trained into tumor epithelial and stromal regions. Tumor core regions that were empty, ruptured, or necrotic, were excluded. Cell detection parameters along with cell and tissue classifications, were combined into a script, which was subsequently run for all representative tissue microarray cores in the cohort. The cell data yielded phenotypes, intensities of each marker, and cell coordinates for each cell. Tissue data included the areas of tumor epithelial and stromal regions along with counts of each cell type within each tissue microarray core. All image analyses were conducted blinded to any associated clinical data. Examples of cell phenotyping and tissue category segmentations in studies II and III are depicted in Fig. 9.

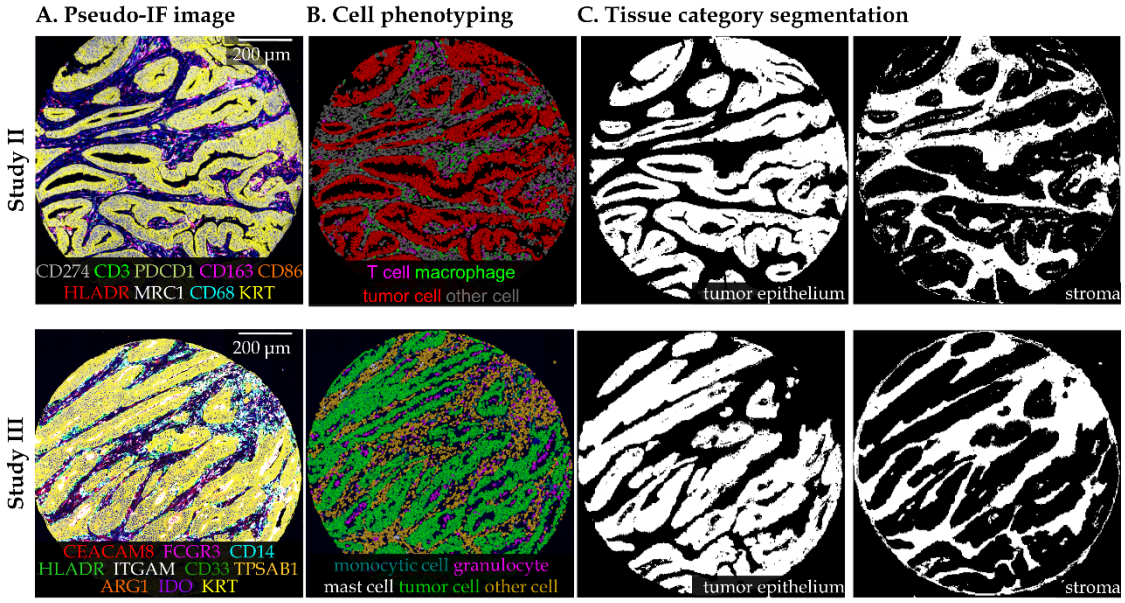

FIGURE 9 Cell phenotyping and tissue category segmentation using QuPath in Studies II and III. Pseudo-immunofluorescence image (A), machine learning-based cell segmentation and phenotyping (B), and mask images of the tissue category segmentation (C). Abbreviations: IF, immunofluorescence. Reproduced from publications II (Fig. 1e–g) and III (Fig. 1c). © Authors, CC BY.

4.5.2 Immune cell phenotyping (II, III)

Further cell and tissue data analyses, as well as statistical analyses, were performed in RStudio (RStudio Team 2020) using the R programming language (R Core Team 2020). For multiplex immunohistochemistry panels (II, III), which included markers for additional cell types not previously phenotyped in QuPath, the intensity information for each cell was utilized to classify the main cell types into more detailed subtypes. In Study II, macrophages were further phenotyped into M1- and M2-like macrophages. Additionally, CD274 expression was assessed in macrophages and their subtypes, as well as in tumor cells, while PDCD1 expression was evaluated in T cells. In Study III, Granulocytes were further classified based on their ARG1 and FCGR3 expression. Monocytes and tumor cells were further examined for IDO expression.

4.5.3 Spatial analyses (I–III)

Spatial information may provide deeper insights into cell-cell interactions within the tumor microenvironment compared to the overall immune cell infiltration (Tsujikawa *et al.* 2020). The spatial arrangement of immune cells was assessed using the Nearest Neighbor Distance (NND, II, III) or the G-cross function (I) in spatial point pattern analyses with the *spatstat* R package (Baddeley and Turner 2005).

4.5.3.1 Nearest Neighbor Distance analysis (II, III)

NND is the distance from a specific point to its nearest neighbor point of a specific type (Baddeley and Turner 2005). In studies II and III, NND was utilized for measuring the distance from each immune cell of a specific type to its closest tumor cell (Fig. 10). In further analyses, the average distances between specific immune cells to the closest tumor cells in each tumor were analyzed.

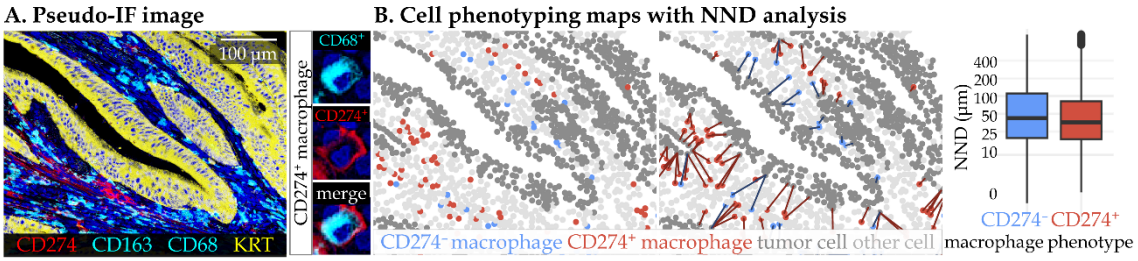

FIGURE 10 Spatial analysis using the Nearest Neighbor Distance analysis. Pseudo-immunofluorescence image illustrating CD274⁺ cells, macrophages, and tumor cells (A). Cell phenotyping maps with Nearest Neighbor Distance analysis from each CD274⁺ and CD274⁻ macrophage to the closest tumor cell and boxplots visualizing the distribution of Nearest Neighbor Distances (B). Abbreviations: IF, immunofluorescence; NND, Nearest Neighbor Distance.

4.5.3.2 G-cross function (I)

G-cross function is a tool for estimating the probability to find at least one cell of the certain type X within a certain radius from any cell of type Y (Baddeley and Turner 2005, Barua *et al.* 2018). G-cross function was utilized for analyzing the co-localization of T cells and tumor cells by evaluating the likelihood of at least one T cell to be located within 20 µm distance of any tumor cell (Fig. 11). Kaplan-Meier method was used for correcting edge effects due to the unobservable points in G-cross analysis window. The area under the curve of G-cross function represents T cell infiltration within the radius of 0–20 µm from tumor cells. The radius of 20 µm was chosen based on the suggestion that cells within this range could potentially engage in direct cell-cell interactions (Carstens *et al.* 2017).

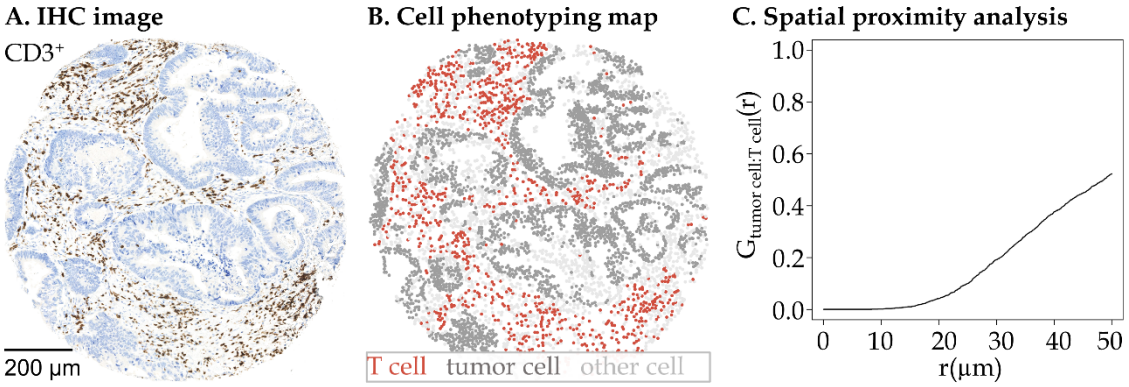

FIGURE 11 Spatial analysis using the G-cross function. CD3+ stained immunohistochemistry image (A), corresponding phenotyping map for T cells, tumor cells, and other cells (B), and spatial proximity analysis with G-cross ($G_{\text{tumor cell:Tcell}}$) as a function of radius (r) (C). Reproduced from publication I (Supplementary Fig. S6A). © Authors, CC BY.

4.5.4 Immune cell quantification

4.5.4.1 Immune cell density (I–III)

Immune cell infiltration was predominantly analyzed by calculating cell densities (cells/mm^2) separately in the tumor intraepithelial and stromal regions, as well as in the tumor center and the invasive margin. In case of several successfully analyzed tumor cores in the tumor center or in the invasive margin for one patient, the mean density was calculated. The densities were divided into ordinal quartiles (Q1–Q4, from low to high) for downstream analyses.

4.5.4.2 CD274 histoscore (II)

CD274 expressing tumor cells were assessed using the weighted histoscore method. Each tumor cell was categorized according to its CD274 expression intensity into negative, low, moderate, or high. Furthermore, the percentage of CD274$^+$ tumor cells was calculated separately in the tumor center and the invasive margin. The intensities and percentages were combined into histoscore as follows: histoscore = 1 x percentage of weakly stained cells + 2 x percentage of moderately stained cells + 3 x strongly stained cells (McCarty *et al.* 1986). In case of multiple tumor cores in the tumor center or the invasive margin for one patient, the mean histoscore was calculated.

4.5.4.3 T cell density and proximity score (I)

T cell infiltration within the tumor microenvironment was analyzed using T cell density score that was based on the principles of the Immunoscore® assay (Pagès *et al.* 2018). In T cell density score, the densities of all (CD3$^+$) T cells and cytotoxic (CD8$^+$) T cells were quantified both in the tumor center and the invasive margin. These four density values were then converted into percentiles (0–100%), from which the mean percentile was calculated. T cell density score classified the mean percentile into three categories of low (0–25%), intermediate (>25–70%), and high (>70–100%). The quantification of T cell density score is illustrated in Fig. 12.

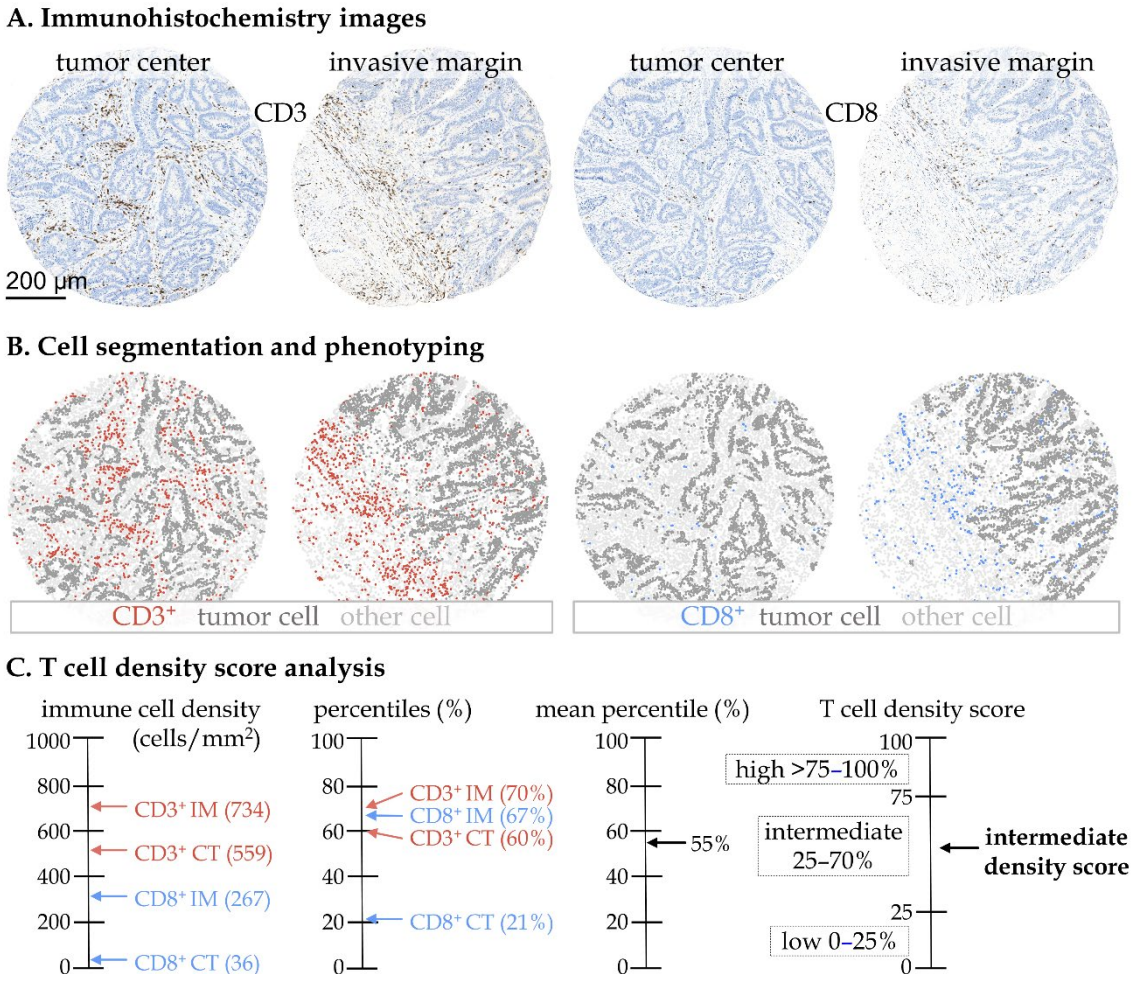

FIGURE 12 T cell density score analysis. Immunohistochemistry images for all T cells ($CD3^+$) and cytotoxic T cells ($CD8^+$) in one example tumor core from the tumor center and the invasive margin (A). Corresponding phenotyping maps for T cells, tumor cells, and other cells (B). Calculation chart for T cell density score (C).

In addition to assessing T cell densities, T cell proximity score was introduced the as a novel prognostic factor. This score utilized the G-cross [$G_{\text{tumor cell:Tcell}}$] function to determine the probability of T cells being located within 20 µm from any tumor cell. The quantification T cell proximity score based on the individual G-cross function values followed the principles of T cell density score. G-cross function values (range: 0–1) for $CD3^+$ and $CD8^+$ T cells in both the tumor center and the invasive margin were converted to percentiles (0–100%). The mean percentile, derived from the four percentile values (0–100%), was calculated and subsequently categorized into three categories of T cell proximity score: low (0–25%), intermediate (>25–70%), and high (>70–100%). The quantification of T cell proximity score is illustrated in Fig. 13.

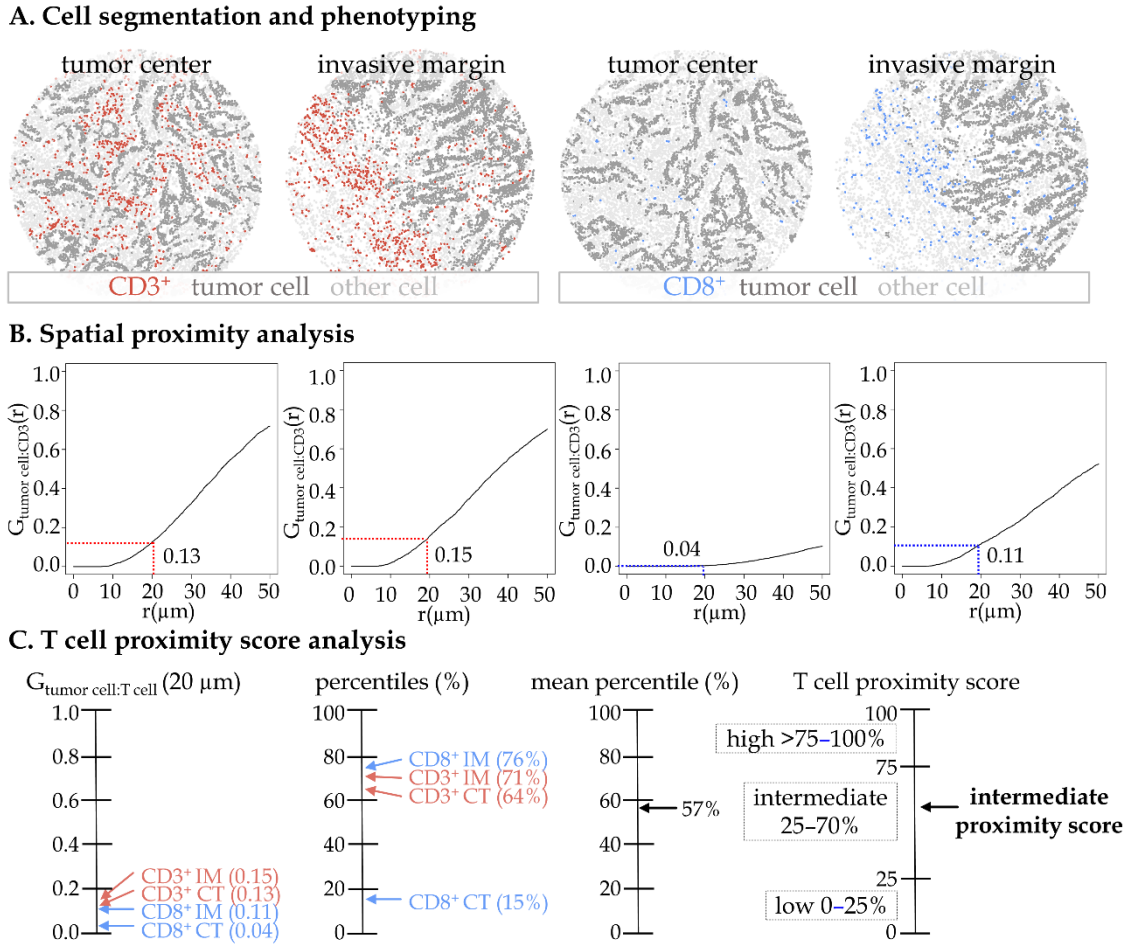

FIGURE 13 T cell proximity score analysis. Cell phenotyping maps for CD3⁺/CD8⁺ T cells, tumor cells, and other cells in one example tumor core from the tumor center and the invasive margin (A). Spatial proximity analysis with G-cross ($G_{tumor\ cell:Tcell}$) as a function of radius (r) (B). Calculation chart for T cell proximity score (C).

4.5.5 Single-cell RNA analyses (III)

In addition to immunohistochemistry-based analyses, an independent publicly available single-cell dataset for 62 tumors (Pelka *et al.* 2021) was utilized to analyse *IDO1* gene expression in colorectal cancer. *IDO1* messenger RNA expression and the activity of the tryptophan metabolism pathway, regulated by IDO, were analyzed in various cell populations, including immune cell subsets, stromal cells, and tumor cells. Moreover, gene enrichment analysis was performed on *IDO1*⁺ and *IDO1*⁻ monocytes to identify the biological processes associated with *IDO1* expression in monocytes. The analysis included Gene Ontology Biological process gene sets. These gene sets are related to a wide range of biological processes, each orchestrated by multiple molecular-level activities (Thomas 2017).

4.5.6 Statistical analyses (I–III)

The associations between two categorical variables were analyzed through crosstabulation with the Chi-square test to compare differences between groups (I–III). Continuous variables were presented as medians with interquartile ranges. The associations between continuous and categorical variables were tested using the Wilcoxon rank-sum test (for dichotomous variables) or with Kruskal-Wallis test (for variables with three or more categories) (II, III). Correlations between categorical data were examined with Spearman's correlation coefficients (II, III).

Cox proportion hazard regression models and Kaplan-Meier method were employed for survival analyses (I–III). Univariable and multivariable Cox proportion hazard regression models were used to estimate hazard ratio (HR) point estimates and 95% confidence intervals (CI) for cancer-specific and overall survival. Cancer-specific survival was defined as the time from primary tumor resection until colorectal cancer-related death or the end of follow-up. Overall survival was defined as the time from cancer diagnosis until death from any cause or the end of follow-up. Cancer-specific survival was set as the primary endpoint, and the follow-up was limited to 10 years following surgery for primary colorectal cancer, as Schoenfeld residual plots supported the proportionality of hazards during most of the follow-up period up to 10 years. The multivariable models were adjusted for pre-determined variables, including gender, age, year of operation, tumor location, tumor stage, tumor grade, lymphovascular invasion, MMR status, and *BRAF* mutation status. Kaplan-Meier method with the log-rank test was used to visualize colorectal-cancer specific survival. All *P* values were two-tailed, and statistical significance was set at $P \leq 0.005$ as recommended by an expert panel (Benjamin *et al.* 2018).

5 RESULTS

5.1 Immune cell infiltration patterns and the expression of immunosuppressive molecules

This study characterized T cells (I, II), monocytic cells (II, III), granulocytes (III) and mast cells (III). These immune cell types were further phenotyped into their subtypes and analyzed for the expression of immunosuppressive molecules. For most immune cell types, the densities tended to be higher in tumor stromal than intraepithelial regions and in the tumor center than the invasive margin. To gain insights into the interaction between the tumor microenvironment and the immune system, associations for several clinical and pathological features were analyzed. Higher densities of T cells (I, II), monocytic cells (III), macrophages (II), and granulocytes (III) were associated with high tumor grade, MMR deficiency, and *BRAF* mutation. In contrast, higher mast cell density (III) was associated with low tumor grade, MMR proficiency, and *BRAF* wild type status. Additionally, the densities of macrophages, monocytic cells, and granulocytes tended to be higher in the proximal colon compared to the distal colon or rectum. Higher densities of T cells, granulocytes, and mast cells were linked to low tumor stage. Granulocytes were more infiltrated in tumors without lymphovascular invasion.

T cells were further tested for the expression of PDCD1 and subdivided into cytotoxic T cells. Of T cells, 22% were positive for PDCD1 (II). Macrophages were subdivided into M1-like and M2-like subtypes and further tested for CD274 expression (II). CD274 was expressed on 20% of macrophages and more likely in M1-like than M2-like macrophages. Monocytic cells were subdivided according to their HLADR, FCGR3, and IDO expression being more likely $HLADR^+$ and $FCGR3^+$ than $HLADR^-$ or $FCGR3^-$ monocytic cells. Of monocytic cells, 4% expressed IDO (III). Granulocytes were further phenotyped into neutrophils with FCGR3 and tested for ARG1 expression (III). The majority of granulocytes were neutrophils and expressed ARG1 (81%). In addition to macrophages and monocytic cells, CD274 and IDO expression were found in some tumor cells.

The densities of CD274⁺ macrophages, PDCD1⁺ T cells, IDO⁺ monocytic cells, and ARG1⁺ granulocytes were assessed in relation to the clinicopathological characteristics. Higher densities of all these immune cell subsets were associated with lower tumor stage, MMR deficiency, and absence of lymphovascular invasion. Additionally, associations with high grade (all except for IDO⁺ monocytic cells), *BRAF* mutation (ARG1⁺ granulocytes and CD274⁺ macrophages), proximal colon location (CD274⁺ macrophages), and late operation year (IDO⁺ monocytic cells) were found.

In additional analyses, independent single-cell RNA data were utilized to further analyze the expression patterns of *IDO1* (III) (Fig. 14). The *IDO1* activity, as well as the activity of tryptophan metabolism, was found to be highest in dendritic cells and monocytes. Gene enrichment analysis for *IDO1*⁺ and *IDO1*⁻ monocytes revealed several IFNG-regulated immunostimulatory pathways to be enriched in *IDO1*⁺ monocytes. Furthermore, a strong association between high expression of *IDO1* and *IFNG*, and a higher T cell count, was observed as tumors were divided based on high and low monocytic cell *IDO1* expression.

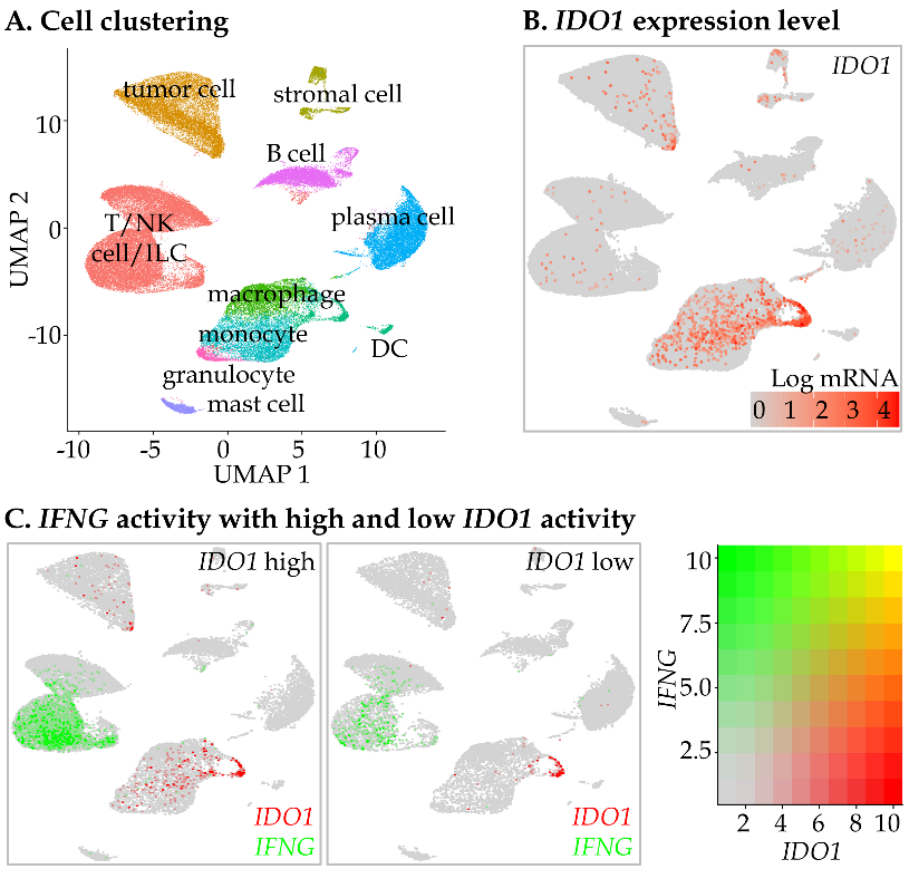

FIGURE 14 The distribution of *IDO1* expression and association with *IFNG* activity. Uniform Manifold Approximation and Projection representation for clustering cell communities (A). The expression level of *IDO1* in cell communities (B). *IFNG* activity in tumors with high and low *IDO1* activity (C). Abbreviations: DC, dendritic cell; ILC, innate lymphoid cell; NK, natural killer; UMAP, Uniform Manifold Approximation and Projection. Reproduced from publication III (Fig. 4A, B, and F). © Authors, CC BY.

5.2 The prognostic value of immune cell subtypes

In survival analyses, colorectal cancer-specific survival was used as the primary endpoint. The analyses for the main immune cell types are represented in Table 8. The cell densities were categorized into ordinal quartiles from low (Q1) to high (Q4).

TABLE 8 Univariable and multivariable Cox regression models for colorectal cancer-specific survival according to the main cell type densities in the tumor center and the invasive margin.

Cell type	Colorectal cancer-specific survival				Study
	Univariable HR[1] for Q4 [vs. Q1] (95% CI)	P_{trend}	**Multivariable HR for Q4 [vs. Q1] (95% CI)**	P_{trend}	
T cells					I,II
tumor center	0.31 (0.25-0.52)	<0.0001	0.52 (0.35-0.76)	0.0001	I
	0.38 (0.26–0.55)	<0.0001	0.67 (0.47–0.94)	0.0003	II
invasive margin	0.31 (0.21-0.45)	<0.0001	0.48 (0.32-0.71)	<0.0001	I
	0.39 (0.27–0.56)	<0.0001	0.58 (0.40–0.85)	0.0005	II
Monocytic cells					III
tumor center	0.92 (0.64–1.33)	0.54	0.92 (0.62–1.35)	0.45	
invasive margin	0.82 (0.57–1.19)	0.27	0.86 (0.58–1.28)	0.41	
Macrophages					II
tumor center	0.93 (0.65–1.32)	0.87	0.80 (0.56–1.16)	0.29	
invasive margin	0.99 (0.70–1.39)	0.54	0.93 (0.66–1.32)	0.46	
Granulocytes					III
tumor center	0.50 (0.33–0.73)	<0.0001	0.64 (0.42–0.97)	0.022	
invasive margin	0.48 (0.32–0.70)	<0.0001	0.79 (0.53–1.19)	0.13	
Mast cells					III
tumor center	0.69 (0.47–1.01)	0.086	0.68 (0.46–1.01)	0.098	
invasive margin	0.47 (0.32–0.69)	0.0002	0.60 (0.41–0.88)	0.0057	

[1]Abbreviations: CI, confidence interval, HR, hazard ratio.

Higher density of T cells (Table 8) and higher T cell density score were significantly associated with prolonged survival (I, II). The expression of PDCD1 in T cells did not significantly affect the prognostic value of T cells, as higher densities of both $PDCD1^+$ and $PDCD1^-$ T cells remained strongly associated with prolonged survival (II).

The overall densities of monocytic cells or macrophages were not associated with survival. However, higher densities of IDO^+ monocytic cells in both the tumor center and the invasive margin (III), as well as a higher density of $CD274^+$ macrophages in the invasive margin (II), were associated with prolonged survival independent of confounding factors. Furthermore, a higher density of M1-like macrophages in the tumor center was associated with improved survival in multivariable models, whereas a higher density of M2-like macrophages was a suggestive factor for poorer survival (II). $CD274^+$ M1-like macrophages had an

independent prognostic association with prolonged survival in both the tumor center and the invasive margin (II). The prognostic impacts of IDO (III) and PDCD1 (II) were further assessed in tumor cells, but no significant associations were found in multivariable models.

The prognostic associations of the densities of granulocytes, $FCGR3^+$ neutrophils, and $ARG1^+$ granulocytes were similar, showing an association with favorable prognosis in univariable analyses (III). These associations did not remain significant after adjusting for other confounding factors, but higher density of $ARG1^+FCGR3^+$ neutrophils in the tumor center was associated with prolonged survival also independent of the covariates. A higher density of mast cells was associated with better survival in the invasive margin in univariable analyses (III) (Table 8).

5.3 Spatial immune cells analyses for characterizing tumor-host interactions

5.3.1 Spatial arrangement of immune cells

Spatial localization of immune cells was analyzed using the G-cross function (I) and NND analysis (II, III). T cell proximity score utilized the G-cross function to quantify spatial co-localization of T cells and tumor cells (I). Among all tumors, 20% were classified as having a high proximity score, indicating a high probability of at least one $CD3^+/CD8^+$ T cell being co-localized with any tumor cell, while 55% of tumors were classified as intermediate and 25% as low for the proximity score.

NND analysis was employed to measure distances from each immune cell to its closest tumor cell (II, III). NNDs for multiple cell populations were calculated and visualized in Fig 14. T cells were, on average, located closer to tumor cells than macrophages. Among macrophages, M1-like macrophages were closer to tumor cells compared to M2-like macrophages. $CD274^+$ macrophages and $PDCD1^+$ T cells were closer to tumor cells than $CD274^-$ macrophages and $PDCD1^-$ T cells, respectively.

Among myeloid cell populations, granulocytes were found to be closer to tumor cells than monocytic cells. Furthermore, IDO^+ monocytic cells were closer to tumor cells than IDO^- monocytic cells, and $ARG1^-$ granulocytes located closer to tumor cells than $ARG1^+$ granulocytes (Fig. 15).

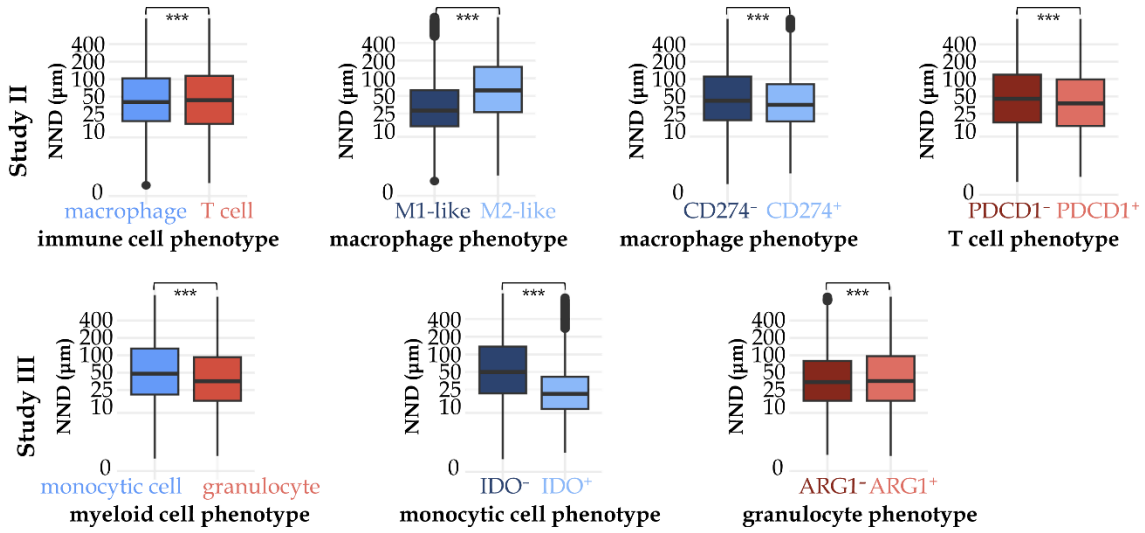

FIGURE 15 Nearest Neighbor Distance analyses for immune cell populations. The distribution of Nearest Neighbor Distances from each immune cell to its closest tumor cell are visualized. The significance between immune cell types was tested with Wilcoxon rank-sum test. ***P < 0.0001. Reproduced from publications II (Fig. 3a–b) and III (Fig. 3C). © Authors, CC BY.

5.3.2 Immune cell-tumor cell proximity

The prognostic value of T cell proximity to tumor cells was evaluated using T cell proximity score and NND analysis. Higher T cell proximity score was an independent prognostic factor in multivariable analyses for cancer-specific [HR for high (vs. low) 0.33, 95% CI 0.20–0.52, $P_{trend} < 0.0001$] survival (I). Furthermore, the prognostic significance of T cell proximity score was independent of T cell density score. However, NND analyses for T cell-tumor cell proximity did not show statistically significant prognostic impact (II). NND analysis was further applied to investigate the prognostic significance of cells expressing immunosuppressive molecules in tumor cell proximity. The spatial proximity of PDCD1⁺ T cells, CD274⁺ macrophages, IDO⁺ monocytes, or ARG1⁺ granulocytes with tumor cells did not demonstrate significance for cancer-specific survival. However, when analyzing the importance of proximity between PDCD1⁺ T cells and CD274⁺ macrophages, it was found that higher number of PDCD1⁺/CD274⁺ clusters, indicating a PDCD1⁺ T cell to be within a 20 µm distance from a CD274⁺ macrophage, served as an independent factor for prolonged survival (II).

6 DISCUSSION

The prognostication and treatment planning of colorectal cancer predominantly rely on TNM staging, which categorizes tumors based on size, extent, and invasion (Union for International Cancer Control 2017). Although TNM staging is a robust prognostic indicator, patient outcomes can vary even within the same stage, highlighting the need for additional biomarkers (Kannarkatt *et al.* 2017, Li *et al.* 2020). In the 21st century, understanding of the role of immune cells in cancer progression has deepened, leading to the development of immunotherapies (Chen *et al.* 2024). Strong immune cell infiltration in the tumor microenvironment, particularly high T cell density, has been recognized as beneficial for survival in colorectal cancer patients with stage I–III tumors, highlighting the potential of immune cell infiltration as a clinically relevant prognostic factor (Galon *et al.* 2006, Pagès *et al.* 2018, Alexander *et al.* 2020). However, immune infiltrate within the tumor microenvironment is highly heterogenous and can evolve over time, and its role and function remain incompletely characterized (Pagès *et al.* 2008, Philip and Schietinger 2022). This study aimed to increase the understanding of the tumor microenvironment by analyzing immune cell infiltration and the expression of immunoinhibitory molecules in a cohort of 1,343 colorectal cancer patients.

6.1 Characterization of the tumor microenvironment

Immunohistochemistry is a commonly used method for identifying cells or analyzing protein expression with antigen-specific antibodies in both routine diagnostics and research. However, phenotyping certain immune cells with a single marker is challenging due to their similar, non-specific surface antigens (Tan *et al.* 2020). In addition to conventional immunohistochemistry, this study utilized a cyclic chromogenic multiplex immunohistochemistry assay to phenotype cells based on multiple markers.

In addition to immunohistochemistry-based methods, multiple other approaches are utilized in characterizing the tumor microenvironment.

Multiplex immunofluorescence utilizes fluorophore-labeled antibodies to detect multiple targets (Rojas *et al.* 2022, Yan *et al.* 2024). Cytometry-based techniques, including flow cytometry, mass cytometry, and imaging mass cytometry, are used for detecting cells using fluorescent dye-labeled or metal-conjugated antibodies (Giesen *et al.* 2014, Adan *et al.* 2017, Yan *et al.* 2024). RNA sequencing techniques, such as bulk RNA sequencing, single-cell RNA sequencing, and spatial RNA sequencing, characterize gene expression profiles at the single-cell level and enable detailed characterization of cells and cellular interactions. Artificial Intelligence can be employed to analyze large amounts of biological data from the tumor microenvironment using machine learning and deep learning algorithms. However, of these methods, only multiplex immunofluorescence, imaging mass cytometry, and spatial RNA sequencing along with multiplex immunohistochemistry, enable the analysis of spatial localization of cells (Yan *et al.* 2024).

To analyse digitized immunohistochemistry-stained tissue specimens, machine learning-based image analysis tools in QuPath were used for categorizing and phenotyping cells and tissue compartments. In addition to QuPath, other open-source software platforms and tools are available for analyzing digitized tissue slides with machine-learning algorithms, including CellProlifer (McQuin *et al.* 2018) and HistoCAT (Schapiro *et al.* 2017). Additionally, several commercial platforms (*i.e.*, Halo and Oncotopix) are also available. Machine learning-based tools facilitate uniform analysis of a large number of samples, minimizing inter- or intra-observer variability and providing detailed information about each cell (Tan *et al.* 2020).

6.2 The significance of lymphoid and myeloid lineage immune cells

Immune cells have a critical role in tumor development and progression, and their significance in colorectal cancer has been increasingly recognized in recent decades (Guo *et al.* 2020). Typically, tumors with high immune cell infiltration exhibit an active anti-tumor immune response and favorable survival outcomes (Alexander *et al.* 2020). However, some immune cells may exert tumor-promoting or anti-inflammatory effects, and tumor cells can modulate certain immune cell types to support their own growth (Shankaran *et al.* 2001, Hanahan and Weinberg 2011).

This study examined the associations between immune cell infiltration and various clinicopathological features. Monocytic cells, macrophages, granulocytes, and T cells demonstrated higher densities in tumors with high grade, MMR deficiency, and *BRAF* mutation. Additionally, except for T cells, these cell types were more abundant in tumors located in the proximal colon. These associations align with the characteristics of MMR deficient tumors, commonly located in the proximal colon, exhibiting high grade, and harbouring

BRAF mutation (Kim and Kang 2014). The findings support the notion that MMR deficient tumors possess an elevated mutation burden, resulting in increased levels of neoantigens and a stronger immune response (Sammalkorpi *et al.* 2007, Zlobec and Lugli 2008).

Higher density of all T cells and cytotoxic T cells emerged as strong prognostic indicators, consistent with previous studies (Alexander *et al.* 2020, Idos *et al.* 2020). Immunoscore®, which quantifies T cell infiltration in the tumor center and the invasive margin, has been proposed as a new prognostic marker for colorectal cancer (Pagès *et al.* 2018). In this study, Immunoscore-based T cell density score proved to be a robust prognostic biomarker.

In addition to T cells, this study assessed the role of myeloid cells. Monocytic cells, macrophages, or mast cells did not exhibit prognostic effects, but granulocytes in the tumor center and the invasive margin and mast cells in the invasive margin were associated with favorable survival in univariable analyses. Further assessment of myeloid cell subtypes showed that M1-like macrophages, characterized by pro-inflammatory cells with high antigen presentation and cytotoxicity capabilities (Yadav *et al.* 2022), predicted prolonged survival independent of confounding factors, consistent with previous reports (Edin *et al.* 2012, Väyrynen *et al.* 2021).

Certain myeloid cell types display plasticity, indicating potential to exhibit both tumor growth-promoting or preventing effects (Fridlender *et al.* 2010, Italiani *et al.* 2014). Thus, the total infiltration of those myeloid cells may not exert strong prognostic effects in the tumor microenvironment. Additionally, myeloid cells lack specificity for tumor antigens (Murphy and Weaver 2017), suggesting that their infiltration may not directly correlate with the effectiveness of anti-tumor immune response. Moreover, in cancer, some myeloid cells may undergo incomplete maturation and develop into immunosuppressive MDSCs, which exhibit highly similar surface antigen structures to mature monocytic cells and granulocytes, making their phenotyping and differentiation from mature cells challenging (Bronte *et al.* 2016). Our findings from the survival analyses for myeloid cells underscore the importance of detailed immune cell phenotyping and characterization.

6.3 The role of immunosuppressive molecules

The present study assessed the prognostic impact of PDCD1 and CD274 immune checkpoint proteins, as well as IDO and ARG1 metabolic enzymes, all of which have been associated with immunosuppression due to their ability to downregulate T cell activation (Mondanelli *et al.* 2019, Pauken *et al.* 2021). Contrary to the expectation that high expression of immunosuppressive molecules could predict poor outcome in colorectal cancer, it was found that higher densities of IDO^+ monocytic cells and $CD274^+$ macrophages were significantly associated with better prognosis, independently of known prognostic indicators, such as stage, grade, MMR status, or *BRAF* mutation

status. Concordantly, some studies have previously reported associations between increased expression of IDO and CD274 in immune cells and better survival in colorectal cancer (Lee *et al.* 2017, Lee *et al.* 2018, Wyss *et al.* 2019). PDCD1 expression did not significantly affect the strong prognostic value of T cells, as both higher densities of $PDCD1^+$ and $PDCD1^-$ T cells showed an association with favorable survival. This suggests that the prognostic significance of T cells could be strong enough to not be affected by PDCD1 expression. The prognostic value of $ARG1^+$ granulocytes was similar to that of all granulocytes, both being suggestive markers for favorable survival. This similarity of the association could result from the majority of granulocytes expressing ARG1.

The findings indicating that higher expression levels of immunosuppressive molecules in immune cells tend to be associated with prolonged survival in colorectal cancer are paradoxical, but some explanations have been suggested. Their increased expression could be a response to an active anti-tumor immune reaction (Lazarus *et al.* 2018, Ahtiainen *et al.* 2019). Additionally, higher expression of immunosuppressive molecules could represent an intrinsic negative feedback mechanism of the immune system to downregulate excessive immune cell activity and prevent tissue damage (Pardoll 2012). Analyses of *IDO1* gene expression revealed correlations between *IDO1* and *IFNG* gene expression and higher T cell counts. IFNG, a proinflammatory cytokine primarily produced by T cells and natural killer cells, has been shown to correlate with favorable survival in colorectal cancer, but also to induce the expression of PDCD1, CD274 and IDO (Brandacher *et al.* 2006, Li *et al.* 2016, Mulder *et al.* 2021). These findings support the potential explanations of increased expression of immunosuppressive molecules as a response to active immune reactions, and further suggest that *IFNG* could be a key mediator for their expression. In this study, higher expression of immunosuppressive molecules tended to be associated with lower tumor stages, absence of lymphovascular invasion, and MMR deficiency. Since all these features are correlate with improved survival rates in colorectal cancer, the presence of immunosuppressive molecules might indicate a less aggressive tumor phenotype (Popat *et al.* 2005, Zlobec and Lugli 2008). Furthermore, it has been acknowledged that certain risk factors may lead to favorable disease outcomes. A molecular pathologic epidemiologic approach suggests that these relationships could be related to interpersonal or inherent disease heterogeneity, leading to variations in the genetic background of the patient or the molecular characteristics of the tumor (Nishihara *et al.* 2015). According to this approach, the incongruous associations between high expression of immunosuppressive molecules and improved prognosis could reflect the intricate balance between the immune system and individual molecular profiles.

6.4 Spatial localization of immune cells in the tumor microenvironment

A comprehensive characterization of spatial localization of immune cells is important for unravelling the dynamics of tumor-host interactions. Variations in immune cell infiltration and function across different tumor compartments have been observed (Galon *et al.* 2006, Fu *et al.* 2021), and patients with similar immune cell composition may exhibit differing prognoses (Galon *et al.* 2006, Schürch *et al.* 2020, Fu *et al.* 2021). For instance, tumor stromal T cell infiltration may be higher than intraepithelial infiltration (Halama *et al.* 2009), and intraepithelial cytotoxic T cells may exert more significant roles compared to those in other compartments (Naito *et al.* 1998, Chiba *et al.* 2004). Typically, immune cell infiltration is analyzed separately in the tumor center and the invasive margin. The invasive margin represents the interface where immune cells interact with the tumor, thus typically showing higher immune cell infiltration compared to the tumor center (Fu *et al.* 2021). To gain more detailed insight into tumor-host interactions within the tumor microenvironment, advanced spatial analysis methods have been employed. These methods encompass measuring distances between different cell types or calculating cell densities around specific cells, analyzing the spatial distribution of immunoregulatory molecules, and examining well-organized spatial patterns like tertiary lymphoid structures (Fu *et al.* 2021).

In this study, immune cell densities were separately analyzed in the tumor center and the invasive margin, as well as within the tumor intraepithelial and stromal regions. Additionally, detailed spatial analyses were conducted. Immune cell densities tended to be higher in the stromal than intraepithelial regions, and in the invasive margin than the tumor center. Moreover, the prognostic significance of certain cell types varied between the tumor compartments, although consistent findings across different cell types were lacking.

Spatial analyses further delineated differences in spatial distribution of immune cells in relation to tumor cells. Immune cells within tumor cell proximity are suggested to possess enhanced potential for direct cell-cell interactions, and subsequent anti-tumor activity (Carstens *et al.* 2017, Barua *et al.* 2018). Still, only higher density of T cells in tumor cell proximity, when analyzed using T cell proximity score, exhibited stronger prognostic value compared to total T cell density. For myeloid cell types, spatial proximity with tumor cells did not enhance or diminish prognostic value compared to total cell densities. It is notable that spatial proximity between cells is not necessarily an indication of actual cellular interactions, although their likelihood is increased (Fu *et al.* 2021).

6.5 Strengths and limitations

This study characterized the infiltration of multiple immune cell subtypes using multimarker analysis in a large study cohort. However, some limitations need to be considered. First, excluding patients with preoperative treatment due to their potential effects on immune infiltrate led to underrepresentation of rectal cancer. Second, standardizing methodologies and immune cell analyses could improve the reproducibility and comparability between studies (Alexander *et al.* 2020). For instance, a broad spectrum of antibodies with varying antigen-specificity and marker signal quality has been employed. Additionally, cell counting methods vary, including manual, semi-quantitative, or automated cell counting assays. Furthermore, criteria for setting thresholds for marker positivity, classifying cells into subtypes, and categorizing cells for further analyses fluctuate. In this study, antibody selection was based on their use in previous studies or in clinical routine pathology, and their functionality was tested using a test tissue microarray. Third, the analyses were conducted for tissue microarray specimens instead of whole tissue specimens, which has raised concern about their capability to adequately cover tumor heterogeneity (Voduc *et al.* 2008). However, sufficient coverage was ensured in this study by calculating core-to-core correlations for immune cell densities between the two cores in the tumor center and the invasive margin and has also been previously demonstrated in colorectal cancer (Hendriks *et al.* 2003, Jourdan *et al.* 2003) and other cancer types (Camp *et al.* 2000, Rosen *et al.* 2004). Fourth, the tissue sections captured only a single plane of the tissue, potentially providing limited information about the tumor architecture and the spatial distribution of cells (Lin *et al.* 2023). Fifth, in multiplex immunohistochemistry panels, multiple staining cycles resulted in some level of tissue microarray core loss or damage, leading to a reduced number of successfully analyzed tissue microarray cores and smaller number of tumors in the final cohorts. In addition, staining quality for certain antibodies decreased along the cycles, but this could be mostly addressed by the panel design and antibody ordering. However, multiplex-immunohistochemistry, compared to conventional immunohistochemistry, enabled the phenotyping of each cell with several markers simultaneously and conserved the tissue material. Sixth, cell detection and phenotyping and tissue compartmentalization, done using machine learning-based algorithms, were complicated by certain factors, and some compromise was needed. For instance, variabilities in cell morphologies and signal intensities tended to leave some cells split, merged, or undetected, affecting the number of analyzed cells. Histological variability between tumors and necrotic regions caused difficulties in tissue compartmentalization in some tumors. Furthermore, some technical errors during sample processing, such as tissue folding, artifacts, or improperly focused regions during slide scanning, complicated the analysis. An attempt was made to minimize these challenges by optimizing the staining protocol and antibody concentrations to acquire clear staining signals. Tumor areas for training batches were selected to encompass a

broad range of histological phenotypes. The results from the image analyses were confirmed by visually comparing the detected and phenotyped cells and tissue compartments in tissue microarray specimens with the immunohistochemistry-stained tissue microarrays. Multiplex immunohistochemistry combined with machine learning-based image analysis included a high amount of manual work, so wider implementation of the method would require further development and automation.

However, the study has numerous important strengths. The study included a large cohort of 1,343 colorectal cancer patients with comprehensive associated clinical, histological, and molecular data. The long follow-up time, being 10.6 years by mean for censored patients, enabled long course survival analyses. The methods applied in this study enabled analyzing the whole study cohort uniformly, enabling a detailed characterization of immune cells, tumor cells, and immunosuppressive molecules together with their spatial interactions and prognostic value. The study employed equipment utilized in routine pathology laboratory and open-source software for image processing (Fiji/ImageJ), image analysis (QuPath), and data analysis (RStudio), requiring no significant additional financial resources.

6.6 Clinical applications and future perspectives

This study offers detailed insight into immune cell infiltration and expression patterns of immunosuppressive molecules. The results contribute to the development and introduction of new prognostic biomarkers, supplementing those already in clinical use, to clarify colorectal cancer prognostication and treatment planning. Currently, no prognostic parameters based on assessing the tumor microenvironment are in clinical use. This study reinforced the potential utility of T cell infiltration as a prognostic factor, further suggesting T cells within tumor cell proximity, analyzed with T cell proximity score, to be a more robust biomarker.

Immunoinhibitory molecules, including PDCD1, CD274, IDO, and ARG1 suppress T cell activity and induce T cell exhaustion (Dong *et al.* 2002, Blackburn *et al.* 2009, Vinay *et al.* 2015, Ma *et al.* 2019, Chen *et al.* 2024), thus serving as potential predictive biomarkers for immunotherapy treatment responses and as targets for immunotherapy (Vinay *et al.* 2015). Currently, only two clinically approved checkpoint inhibitors targeting PDCD1 (Biller and Schrag 2021, Chen *et al.* 2024) have been established for metastatic colorectal cancer, with effective and durable responses achieved in only certain patients (Le *et al.* 2017). To develop more efficient immunotherapies, more detailed understanding of immune checkpoint molecules in colorectal cancer is required. Contradictory to our hypothesis, this study showed higher expression of IDO and CD274 in immune cells to be significantly associated with improved survival of colorectal cancer patients. These findings underline the complexity of the tumor microenvironment and highlights the need for additional studies characterizing

the role and expression of immunosuppressive molecules in different stages of cancer development.

The comprehensive data produced in this study could be utilized to further examine the colorectal cancer microenvironment. Both the findings and methods utilized in this study could be also used and applied to studying other solid cancer types. Although multiplex immunohistochemistry in its current form is not applicable for clinical use, it is a potential tool for providing detailed information, for instance, of the expression patterns of the immunosuppressive molecules in the tumor microenvironment. This information could be applied to evaluate the prognosis of colorectal cancer patients and the functionality of immunotherapies.

A deeper understanding of the immune landscape is necessary to create new prognostic and predictive biomarkers, evaluate the treatment response of cancer, and develop new effective immunotherapies. Standardized methodologies for immune cell detection and classification could increase the reproducibility and comparability between studies. Additionally, spatiotemporal immune cell analyses across different tumor stages could yield new insights into colorectal cancer development and cell-cell interactions. Analysing the interactions between immune cells and other components in the tumor microenvironment, such as fibroblasts, could also enhance the understanding of immune evasion by tumors and the effects of immunotherapy within the tumor microenvironment (Fu *et al.* 2021, Mun *et al.* 2022). While two-dimensional tissue sections enable comprehensive characterization of the tumor microenvironment, incorporating three-dimensional reconstruction could more accurately capture its full complexity, complementing and refining the findings of traditional two-dimensional methods (Lin *et al.* 2023).

7 CONCLUSIONS

This study analyzed the infiltration patterns and significance of various immune cell subtypes and the expression of immunoinhibitory molecules. Based on the results, following conclusions were made:

i) Multiplex immunohistochemistry and computer-based image analysis were shown to be accurate methods for phenotyping immune cell subtypes in the tumor microenvironment.

ii) Higher density of T cells, particularly in co-localization with tumor cells predicted favorable outcomes in colorectal cancer, suggesting T cell proximity score as a potential new prognostic parameter.

iii) Infiltration patterns of the overall populations of monocytic cells, macrophages, granulocytes, and mast cells, or their spatial proximity to tumor cells, did not show independent prognostic significance in colorectal cancer. Still their certain subtypes showed associations with survival, emphasizing the importance of detailed immune cell characterization.

iv) Increased infiltration of $CD274^+$ macrophages and IDO^+ monocytic cells had significant associations with improved survival, suggesting that the expression of immunoinhibitory molecules might be a compensatory response to active anti-tumor activity.

Acknowledgements

This study was carried out at the Department of Pathology of Hospital Nova of Central Finland during the years 2020–2024.

I express my deepest gratitude to Chief Physician Jan Böhm and Miia Siikaluoma for the opportunity to work at the Department of Pathology and for providing a welcoming and research-friendly environment. I also thank the entire staff of the Department for the friendship, cooperation, and guidance over the years.

First and foremost, I am grateful to my supervisors, Docent Juha Väyrynen, Docent Teijo Kuopio, and Professor Jari Ylänne, for enabling the research project. Juha, it was a great privilege to work under your guidance. I have learnt more than I ever imagined, and I am deeply impressed by your vast knowledge and enthusiasm for research. Teijo, thank you for igniting the spark in the world of histopathology and cancer research, as well as for the conversations in and out of the research context. Jari, sincere appreciation for the effort in finalizing the dissertation project and for trusting me the responsibility to teach in university courses.

I am thankful to the preliminary examiners, Professor Satu Mustjoki and Docent Tuomas Rauramaa, for valuable comments and dedication to my work. I want to thank Docent Anniina Färkkilä for accepting the invitation to act as my opponent.

This thesis would not have been completed without the research group and co-authors. My sincere gratitude to Maarit Ahtiainen, Professor Jukka-Pekka Mecklin, Jouni Härkönen, Marjukka Friman, and Jan Böhm at the Hospital Nova for valuable effort for the thesis project. Special thanks to Maarit for the support and for sharing all the moments with me already since the Master's thesis project. Jukka-Pekka, thank you for building the foundations for the whole colorectal cancer research in Jyväskylä. Jouni, I appreciate your friendship, dedication to research projects, and magic touch with bioinformatics and statistics. Marjukka and Jan, thank you for valuable efforts and expertise in the fields of immunohistochemistry and pathology.

I also want to acknowledge all other co-authors at the university hospitals of Oulu, Tampere, and Helsinki, and at the Harvard Medical School for the significant contribution to the original articles of the thesis. I warmly thank Kirsi Pylvänäinen for helping in navigating the jungle of hospital bureaucracy. I also owe thanks to follow-up members and collaborators Professor Lauri Aaltonen and Docent Kristiina Rajamäki for wise words, and for creating an open discussion atmosphere.

Above all, I would like to express my gratitude to my family. My parents, Eeva and Esa, I am grateful for the encouragement and full support during the thesis project and throughout my life. My siblings, Liisa and Timo, I appreciate you for being role models and always lending a helping hand. Finally, my husband, Henri, thank you for your love and patience, and for believing in me, even at moments when I did not.

I acknowledge the Cancer Foundation Finland, the State Research Funding, the Emil Aaltonen Foundation, the Orion Research Foundation, the Päivikki and Sakari Sohlberg Foundation, and the Science Commission of the Central Finland Central Hospital for funding the research.

YHTEENVETO (RÉSUMÉ IN FINNISH)

Immuunisolujen ja immuunivastetta hillitsevien tekijöiden merkitys paksu- ja peräsuolisyövän mikroympäristössä

Paksu- ja peräsuolisyöpä on maailmanlaajuisesti kolmanneksi yleisin syöpä ja toisiksi eniten syöpäkuolleisuutta aiheuttava tauti. Tämän vuoksi taudin vaiheen määrittäminen ja potilaan ennusteen arviointi on tärkeää hoidon suunnittelun määrittämiseksi. Syövän koon ja levinneisyyden arviointiin perustuva neliluokkainen TNM-luokitus on tärkein paksu- ja peräsuolisyövän ennusteen ja hoidon arvioinnissa käytetty menetelmä, mutta ei välttämättä yksinään riitä antamaan riittävän tarkkaa tietoa taudin kulusta. Viime vuosikymmeninä syövän mikroympäristössä olevilla immuunisoluilla on todettu olevan merkittävä vaikutus syövän kehittymisen, ennusteen ja hoitovasteen kannalta, mutta niiden merkitys tunnetaan vielä osin puutteellisesti.

Osa immuunijärjestelmän soluista kykenee tunnistamaan ja eliminoimaan syöpäsoluja sekä aktivoimaan muita immuunisoluja. Etenkin T-solujen vahva syövän kasvua rajoittava vaikutus on havaittu useissa tutkimuksissa. Joillakin immuunisoluilla on kuitenkin todettu olevan tulehdusreaktiota hillitsevä ja siten syövän kasvua edistävä vaikutus. Lisäksi syöpäsolut voivat edistää omaa kasvuaan heikentämällä immuunijärjestelmän toimintaa. Immuunivasteen tarkastuspisteet, kuten PDCD1 (*engl.* programmed death-1, PD-1) ja CD274 (*engl.* programmed death-ligand 1, PD-L1) ovat proteiineja, jotka rajoittavat T-solujen liiallista toimintaa. Useissa syövissä näiden PDCD1 ja CD274 proteiinien määrä on kuitenkin lisääntynyt, mikä estää T-solujen aktivoitumista ja kykyä eliminoida syöpäsoluja. Syöpäsolut voivat hillitä immuunivastetta myös säätelemällä solujen aminohappoaineenvaihduntaa. Aminohapot ovat proteiinien rakennusaineita ja siten välttämättömiä solun toiminnan kannalta. Indoleamiini 2,3-dioksigenaasi (IDO) ja arginaasi-1 (ARG1) ovat entsyymejä, jotka hajottavat etenkin T-solujen toiminnalle tärkeitä aminohappoja, tryptofaania ja arginiinia. ARG1 ja IDO entsyymien määrä syövässä on usein lisääntynyt, mikä voi johtaa T-solujen toiminnan heikkenemiseen ja siten kiihdyttää syövän kasvua.

Tämä tutkimus koostui kolmesta osatyöstä, joissa tunnistettiin kattavasti eri immuunisolutyyppejä ja kartoitettiin immuunivastetta heikentävien molekyylien ilmenemistä paksu- ja peräsuolisyövän mikroympäristössä hyödyntämällä immunohistokemiallisia värjäysmenetelmiä ja tietokoneavusteista kuva-analyysiä. Tavoitteena oli selvittää eri immuunisolutyyppien tiheyksien ja spatiaalisen sijoittumisen merkitystä paksu- ja peräsuolisyöpäpotilaan ennusteen kannalta. Immunohistokemiallisessa värjäyksessä solutyyppejä tunnistetaan vasta-aineiden ja värireaktion aikaansaavan kromogeenin avulla. Perinteisen immunohistokemian lisäksi tässä tutkimuksessa hyödynnettiin syklistä immunohistokemiallista monivärimenetelmää, jossa yhtä kudosleikettä värjättiin useasti peräkkäin eri vasta-aineilla. Monivärimenetelmällä jokainen solu voidaan tunnistaa usean eri vasta-aineen avulla, mikä mahdollistaa perinteistä immunohistokemiallista värjäystä tarkemman immuunisolujen luokittelun alatyyppeihin. Värjättyjen ku-

dosleikkeiden analysoimisessa hyödynnettiin tietokoneavusteista kuva-analyysiä, joka mahdollisti solutyyppien ja kudosalueiden yksityiskohtaisen tunnistamisen ja luokittelun.

Ensimmäisessä työssä kartoitettiin T-solutiheyden vaikutusta paksu- ja peräsuolisyövän ennusteeseen kahdella eri menetelmällä. *T cell density score*-menetelmällä analysoitiin T-solujen kokonaistiheyttä syövän mikroympäristössä kahdella eri alueella: syövän keskiosassa ja invaasioreunassa syövän ja terveen kudoksen rajapinnassa. Menetelmässä korkeampi T-solutiheys johti suurempaan *T cell density score*:n arvoon. Lisäksi työssä kehitettiin uusi *T cell proximity score*-menetelmä, jolla arvioitiin syöpäsolujen läheisyydessä olevien T-solujen tiheyttä. Sekä korkea *T cell density score* että *T cell proximity score* olivat vahvoja itsenäisiä ennustetekijöitä. Kuitenkin syöpäsolujen läheisyydessä olevien T-solujen tiheydellä oli hieman niiden kokonaistiheyttä suurempi merkitys.

Toisessa työssä tutkittiin M1- ja M2-tyypin makrofagien ja T-solujen tiheyksiä sekä PDCD1 ja CD274 proteiinien ilmenemistä moniväri-immunohistokemian avulla. Makrofagit ovat yksi paksu- ja peräsuolisyövän mikroympäristön yleisimmistä immuunisolutyypeistä, joista on tunnistettu kaksi alatyyppiä. M1-makrofageilla on kyky eliminoida syöpäsoluja ja aktivoida muita syövän kasvua rajoittavia immuunisoluja, kun taas M2-makrofageilla on todettu olevan syövän kasvua edistävä vaikutus. Työssä havaittiin, että PDCD1 ilmeni pääasiassa T-soluissa, kun taas CD274 ilmeni makrofageissa ja joissakin syöpäsoluissa. T-solujen korkea tiheys oli yhteydessä paksu- ja peräsuolisyöpäpotilaan parempaan ennusteeseen riippumatta PDCD1 proteiinin ilmenemisestä. Lisäksi korkealla $CD274^+$ makrofagien tiheydellä yhteys potilaiden parempaan ennusteeseen.

Kolmannessa työssä selvitettiin monosyyttien, granulosyyttien ja syöttösolujen tiheyksien sekä IDO ja ARG1 entsyymien ilmenemisen vaikutusta monivärimenetelmällä. Korkea IDO^+ monosyyttien tiheys oli merkittävä itsenäinen ennustetekijä. Myös korkeat granulosyyttien ja $ARG1^+$ granulosyyttien määrät olivat yhteydessä parempaan ennusteeseen, mutta nämä eivät olleet itsenäisiä ennustetekijöitä. Spatiaalianalyyseissä todettiin, ettei immuunisolujen sijainnilla syöpäsolujen suhteen ollut merkittävää vaikutusta ennusteen kannalta.

Tutkimuksessa kartoitettiin paksu- ja peräsuolisyövän mikroympäristöä värjäys- ja analysointimenetelmillä, jotka mahdollistivat suuren syöpäkudosaineiston analysoimisen yksityiskohtaisesti ja yhdenmukaisesti. Syövän mikroympäristön immuunisoluja on perinteisesti tutkittu tiheyteen perustuvilla analyysimenetelmillä, mutta tässä työssä tutkittiin lisäksi immuunisolujen spatiaalista sijoittumista. Kuten useissa aiemmissa tutkimuksissa, korkean T-solutiheyden todettiin olevan merkittävä ennustetekijä. Lisäksi syöpäsoluja lähellä olevien T-solujen merkitys vaikutti olevan etäämmällä olevia T-soluja suurempi, mikä voisi olla seurausta lähempänä olevien T-solujen suuremmasta mahdollisuudesta olla vuorovaikutuksessa syöpäsolujen kanssa ja siten saada aikaan tehokkaamman syövänvastaisen immuunireaktion. Vaikka korkealla CD274 ja IDO proteiinien ilmenemisellä on todettu olevan T-solujen aktiivisuutta hillitsevä ja siten potentiaalinen syövän kasvua edistävä vaikutus, tässä tutkimuksessa korkeat $CD274^+$ makrofagien ja IDO^+ monosyyttien tiheydet olivat yhteydessä paksu- ja

peräsuolisyövän parempaan ennusteeseen. Vaikka tulos on oletuksen vastainen, on esitetty, että vahva syövän kasvua rajoittava tulehdusreaktio voisi saada aikaan luontaisen vastareaktion. Siinä immuunireaktion liiallista toimintaa torjutaan lisäämällä immuunisolujen aktiivisuutta hillitsevien molekyylien ilmenemistä.

Immuunisolujen rooli paksu- ja peräsuolisyövässä tunnetaan vielä osittain puutteellisesti ja solujen tunnistamista hankaloittaa esimerkiksi niiden samankaltaisuus ja taipumus muuntautua ympäristöstä tulevien signaalien seurauksena. Tässä tutkimuksessa käytetyt immunohistokemiallinen monivärimenetelmä ja tietokoneavusteisen kuva-analyysi osoittautuivat toimiviksi menetelmiksi syövän mikroympäristön kartoittamiseen. Saadut tulokset edistävät syövän ja elimistön omien solujen välisten vuorovaikutussuhteiden ymmärtämistä. Tuloksia voidaan hyödyntää uusien paksu- ja peräsuolisyövän ennustetekijöiden määrittämisessä sekä syöpähoitojen kehittämisessä ja toimivuuden arvioimisessa.

REFERENCES

Adan A., Alizada G., Kiraz Y., Baran Y. & Nalbant A. 2017. Flow cytometry: basic principles and applications. *Crit. Rev. Biotechnol.* 37: 163–176.

Ahtiainen M., Wirta E.-V., Kuopio T., Seppälä T., Rantala J., Mecklin J.-P. & Böhm J. 2019. Combined prognostic value of CD274 (PD-L1)/PDCDI (PD-1) expression and immune cell infiltration in colorectal cancer as per mismatch repair status. *Mod. Pathol.* 32: 866–883.

Alexander P.G., McMillan D.C. & Park J.H. 2020. The local inflammatory response in colorectal cancer - type, location or density? A systematic review and meta-analysis. *Cancer Treat. Rev.* 83: 101949.

Angelova M., Charoentong P., Hackl H., Fischer M.L., Snajder R., Krogsdam A.M., Waldner M.J., Bindea G., Mlecnik B., Galon J. & Trajanoski Z. 2015. Characterization of the immunophenotypes and antigenomes of colorectal cancers reveals distinct tumor escape mechanisms and novel targets for immunotherapy. *Genome Biol.* 16: 64.

Arends M.J., Frayling I.M., Morreau H. & Tomlinson I. 2019. Other adenomatous polyposes: genetic tumour syndromes of the digestive system. In: *World Health Organization Classification of Tumours of the Digestive System*, IARC Press, pp. 529–531.

Argilés G., Tabernero J., Labianca R., Hochhauser D., Salazar R., Iveson T., Laurent-Puig P., Quirke P., Yoshino T., Taieb J., Martinelli E., Arnold D. & ESMO Guidelines Committee. Electronic address: clinicalguidelines@esmo.org. 2020. Localised colon cancer: ESMO clinical practice guidelines for diagnosis, treatment and follow-up. *Ann. Oncol. Off. J. Eur. Soc. Med. Oncol.* 31: 1291–1305.

Baddeley A. & Turner R. 2005. Spatstat : an R package for analyzing spatial point patterns. *J. Stat. Softw.* 12: 282–290.

Bankhead P., Loughrey M.B., Fernández J.A., Dombrowski Y., McArt D.G., Dunne P.D., McQuaid S., Gray R.T., Murray L.J., Coleman H.G., James J.A., Salto-Tellez M. & Hamilton P.W. 2017. QuPath: Open source software for digital pathology image analysis. *Sci. Rep.* 7: 16878.

Baran B., Mert Ozupek N., Yerli Tetik N., Acar E., Bekcioglu O. & Baskin Y. 2018. Difference between left-sided and right-sided colorectal cancer: a focused review of literature. *Gastroenterol. Res.* 11: 264–273.

Barua S., Fang P., Sharma A., Fujimoto J., Wistuba I., Rao A.U.K. & Lin S.H. 2018. Spatial interaction of tumor cells and regulatory T cells correlates with survival in non-small cell lung cancer. *Lung Cancer* 117: 73–79.

Bazira P.J. 2023. Anatomy of the caecum, appendix, and colon. *Surg.* 41: 1–6.

Beatty G.L. & Gladney W.L. 2015. Immune escape mechanisms as a guide for cancer immunotherapy. *Clin. Cancer Res.* 21: 687–692.

Benjamin D.J., Berger J.O., Johannesson M., Nosek B.A., Wagenmakers E.-J., Berk R., Bollen K.A., Brembs B., Brown L., Camerer C., Cesarini D., Chambers C.D., Clyde M., Cook T.D., Boeck P. De, Dienes Z., Dreber A., Easwaran K.,

Efferson C., Fehr E., Fidler F., Field A.P., Forster M., George E.I., Gonzalez R., Goodman S., Green E., Green D.P., Greenwald A.G., Hadfield J.D., Hedges L. V., Held L., Hua Ho T., Hoijtink H., Hruschka D.J., Imai K., Imbens G., Ioannidis J.P.A., Jeon M., Jones J.H., Kirchler M., Laibson D., List J., Little R., Lupia A., Machery E., Maxwell S.E., McCarthy M., Moore D.A., Morgan S.L., Munafó M., Nakagawa S., Nyhan B., Parker T.H., Pericchi L., Perugini M., Rouder J., Rousseau J., Savalei V., Schönbrodt F.D., Sellke T., Sinclair B., Tingley D., Zandt T. Van, Vazire S., Watts D.J., Winship C., Wolpert R.L., Xie Y., Young C., Zinman J. & Johnson V.E. 2018. Redefine statistical significance. *Nat. Hum. Behav.* 2: 6–10.

Berntsson J., Svensson M.C., Leandersson K., Nodin B., Micke P., Larsson A.H., Eberhard J. & Jirström K. 2017. The clinical impact of tumour-infiltrating lymphocytes in colorectal cancer differs by anatomical subsite: A cohort study. *Int. J. Cancer* 141: 1654–1666.

Bessa X., Ballesté B., Andreu M., Castells A., Bellosillo B., Balaguer F., Castellví-bel S., Paya A., Jover R., Alenda C., Titó L., Martinez-Villacampa M., Vilella A., Xicola R.M., Pons E. & Llor X. 2008. A prospective, multicenter, population-based study of BRAF mutational analysis for Lynch syndrome Screening. *Clin. Gastroenterol. Hepatol.* 6: 206–214.

Biller L.H. & Schrag D. 2021. Diagnosis and treatment of metastatic colorectal cancer: a review. *JAMA* 325: 669–685.

Bindea G., Mlecnik B., Tosolini M., Kirilovsky A., Waldner M., Obenauf A.C., Angell H., Fredriksen T., Lafontaine L., Berger A., Bruneval P., Fridman W.H., Becker C., Pagès F., Speicher M.R., Trajanoski Z. & Galon J. 2013. Spatiotemporal dynamics of intratumoral immune cells reveal the immune landscape in human cancer. *Immunity* 39: 782–795.

Bischoff S.C., Sellge G., Manns M.P. & Lorentz A. 2001. Interleukin-4 induces a switch of human intestinal mast cells from proinflammatory cells to Th2-type cells. *Int. Arch. Allergy Immunol.* 124: 151–154.

Bishnupuri K.S., Alvarado D.M., Khouri A.N., Shabsovich M., Chen B., Dieckgraefe B.K. & Ciorba M.A. 2019. IDO1 and kynurenine pathway metabolites activate PI3K-Akt signaling in the neoplastic colon epithelium to promote cancer cell proliferation and inhibit apoptosis. *Cancer Res.* 79: 1138–1150.

Blackburn S.D., Shin H., Haining W.N., Zou T., Workman C.J., Polley A., Betts M.R., Freeman G.J., Vignali D.A.A. & Wherry E.J. 2009. Coregulation of CD8+ T cell exhaustion by multiple inhibitory receptors during chronic viral infection. *Nat. Immunol.* 10: 29–37.

Borst J., Ahrends T., Bąbała N., Melief C.J.M. & Kastenmüller W. 2018. CD4+ T cell help in cancer immunology and immunotherapy. *Nat. Rev. Immunol.* 18: 635–647.

Boyle T., Keegel T., Bull F., Heyworth J. & Fritschi L. 2012. Physical activity and risks of proximal and distal colon cancers: a systematic review and meta-analysis. *J. Natl. Cancer Inst.* 104: 1548–1561.

Brandacher G., Perathoner A., Ladurner R., Schneeberger S., Obrist P., Winkler C., Werner E.R., Werner-Felmayer G., Weiss H.G., Göbel G., Margreiter R.,

Königsrainer A., Fuchs D. & Amberger A. 2006. Prognostic value of indoleamine 2,3-dioxygenase expression in colorectal cancer: effect on tumor-infiltrating T cells. *Clin. Cancer Res.* 12: 1144–1151.

Bray F., Laversanne M., Sung H., Ferlay J., Siegel R.L., Soerjomataram I. & Jemal A. 2024. Global cancer statistics 2022: GLOBOCAN estimates of incidence and mortality worldwide for 36 cancers in 185 countries. *CA. Cancer J. Clin.* 74: 229–263.

Bremnes R.M., Dønnem T., Al-Saad S., Al-Shibli K., Andersen S., Sirera R., Camps C., Marinez I. & Busund L.-T. 2011. The role of tumor stroma in cancer progression and prognosis: emphasis on carcinoma-associated fibroblasts and non-small cell lung cancer. *J. Thorac. Oncol.* 6: 209–217.

Brenner H., Stock C. & Hoffmeister M. 2014. Effect of screening sigmoidoscopy and screening colonoscopy on colorectal cancer incidence and mortality: systematic review and meta-analysis of randomised controlled trials and observational studies. *BMJ* 348: g2467.

Bronte V., Brandau S., Chen S.-H., Colombo M.P., Frey A.B., Greten T.F., Mandruzzato S., Murray P.J., Ochoa A., Ostrand-Rosenberg S., Rodriguez P.C., Sica A., Umansky V., Vonderheide R.H. & Gabrilovich D.I. 2016. Recommendations for myeloid-derived suppressor cell nomenclature and characterization standards. *Nat. Commun.* 7: 12150.

Caldwell R.W., Rodriguez P.C., Toque H.A., Narayanan S.P. & Caldwell R.B. 2018. Arginase: a multifaceted enzyme important in health and disease. *Physiol. Rev.* 98: 641–665.

Camp R.L., Charette L.A. & Rimm D.L. 2000. Validation of tissue microarray technology in breast carcinoma. *Lab. Invest.* 80: 1943–1949.

Campbell P.T., Jacobs E.T., Ulrich C.M., Figueiredo J.C., Poynter J.N., McLaughlin J.R., Haile R.W., Jacobs E.J., Newcomb P.A., Potter J.D., Marchand L. Le, Green R.C., Parfrey P., Younghusband H.B., Cotterchio M., Gallinger S., Jenkins M.A., Hopper J.L., Baron J.A., Thibodeau S.N., Lindor N.M., Limburg P.J., Martínez M.E. & Colon Cancer Family Registry. 2010. Case-control study of overweight, obesity, and colorectal cancer risk, overall and by tumor microsatellite instability status. *J. Natl. Cancer Inst.* 102: 391–400.

Cancer Genome Atlas Network. 2012. Comprehensive molecular characterization of human colon and rectal cancer. *Nature* 487: 330–337.

Cardamone C., Parente R., Feo G. De & Triggiani M. 2016. Mast cells as effector cells of innate immunity and regulators of adaptive immunity. *Immunol. Lett.* 178: 10–14.

Cardoso R., Guo F., Heisser T., Schutter H. De, Damme N. Van, Nilbert M.C., Tybjerg A.J., Bouvier A.-M., Bouvier V., Launoy G., Woronoff A.-S., Cariou M., Robaszkiewicz M., Delafosse P., Poncet F., Walsh P.M., Senore C., Rosso S., Lemmens V.E.P.P., Elferink M.A.G., Tomšič S., Žagar T., Lopez de Munain Marques A., Marcos-Gragera R., Puigdemont M., Galceran J., Carulla M., Sánchez-Gil A., Chirlaque M.-D., Hoffmeister M. & Brenner H. 2022. Proportion and stage distribution of screen-detected and non-screen-detected colorectal cancer in nine European countries: an international,

population-based study. *Lancet. Gastroenterol. Hepatol.* 7: 711–723.
Carmeliet P. & Jain R.K. 2000. Angiogenesis in cancer and other diseases. *Nature* 407: 249–257.
Carstens J.L., Correa de Sampaio P., Yang D., Barua S., Wang H., Rao A., Allison J.P., LeBleu V.S. & Kalluri R. 2017. Spatial computation of intratumoral T cells correlates with survival of patients with pancreatic cancer. *Nat. Commun.* 8: 15095.
Cenerenti M., Saillard M., Romero P. & Jandus C. 2022. The era of cytotoxic CD4 T cells. *Front. Immunol.* 13: 867189.
Chang C.I., Liao J.C. & Kuo L. 2001. Macrophage arginase promotes tumor cell growth and suppresses nitric oxide-mediated tumor cytotoxicity. *Cancer Res.* 61: 1100–1106.
Chen L. 2004. Co-inhibitory molecules of the B7-CD28 family in the control of T-cell immunity. *Nat. Rev. Immunol.* 4: 336–347.
Chen X., Chen L.-J., Peng X.-F., Deng L., Wang Y., Li J.-J., Guo D.-L. & Niu X.-H. 2024. Anti-PD-1/PD-L1 therapy for colorectal cancer: Clinical implications and future considerations. *Transl. Oncol.* 40: 101851.
Chen K., Collins G., Wang H. & Toh J.W.T. 2021a. Pathological features and prognostication in colorectal cancer. *Curr. Oncol.* 28: 5356–5383.
Chen Y., Zheng X. & Wu C. 2021b. The role of the tumor microenvironment and treatment strategies in colorectal cancer. *Front. Immunol.* 12: 792691.
Cheng Y., Ling Z. & Li L. 2020. The intestinal microbiota and colorectal cancer. *Front. Immunol.* 11: 615056.
Chiba T., Ohtani H., Mizoi T., Naito Y., Sato E., Nagura H., Ohuchi A., Ohuchi K., Shiiba K., Kurokawa Y. & Satomi S. 2004. Intraepithelial CD8+ T-cell-count becomes a prognostic factor after a longer follow-up period in human colorectal carcinoma: possible association with suppression of micrometastasis. *Br. J. Cancer* 91: 1711–1717.
Clinton S.K., Giovannucci E.L. & Hursting S.D. 2020. The world cancer research fund/American institute for cancer research third expert report on diet, nutrition, physical activity, and cancer: impact and future directions. *J. Nutr.* 150: 663–671.
Conlon K.C., Miljkovic M.D. & Waldmann T.A. 2019. Cytokines in the treatment of cancer. *J. Interferon Cytokine Res.* 39: 6–21.
Deng G., Bell I., Crawley S., Gum J., Terdiman J.P., Allen B.A., Truta B., Sleisenger M.H. & Kim Y.S. 2004. BRAF mutation is frequently present in sporadic colorectal cancer with methylated hMLH1, but not in hereditary nonpolyposis colorectal cancer. *Clin. Cancer Res.* 10: 191–195.
Dong H., Strome S.E., Salomao D.R., Tamura H., Hirano F., Flies D.B., Roche P.C., Lu J., Zhu G., Tamada K., Lennon V.A., Celis E. & Chen L. 2002. Tumor-associated B7-H1 promotes T-cell apoptosis: a potential mechanism of immune evasion. *Nat. Med.* 8: 793–800.
Driessens G., Kline J. & Gajewski T.F. 2009. Costimulatory and coinhibitory receptors in anti-tumor immunity. *Immunol. Rev.* 229: 126–144.
Dunn G.P., Old L.J. & Schreiber R.D. 2004. The immunobiology of cancer immunosurveillance and immunoediting. *Immunity* 21: 137–148.

Eaden J.A., Abrams K.R. & Mayberry J.F. 2001. The risk of colorectal cancer in ulcerative colitis: a meta-analysis. *Gut* 48: 526–535.

Edin S., Kaprio T., Hagström J., Larsson P., Mustonen H., Böckelman C., Strigård K., Gunnarsson U., Haglund C. & Palmqvist R. 2019. the prognostic importance of CD20+ B lymphocytes in colorectal cancer and the relation to other immune cell subsets. *Sci. Rep.* 9: 19997.

Edin S., Wikberg M.L., Dahlin A.M., Rutegård J., Öberg Å., Oldenborg P.-A. & Palmqvist R. 2012. The distribution of macrophages with a M1 or M2 phenotype in relation to prognosis and the molecular characteristics of colorectal cancer. *PLoS One* 7: e47045.

Fabregas J.C., Ramnaraign B. & George T.J. 2022. Clinical updates for colon cancer care in 2022. *Clin. Colorectal Cancer* 21: 198–203.

Fallarino F., Grohmann U., Vacca C., Bianchi R., Orabona C., Spreca A., Fioretti M.C. & Puccetti P. 2002. T cell apoptosis by tryptophan catabolism. *Cell Death Differ.* 9: 1069–1077.

Farber D.L., Yudanin N.A. & Restifo N.P. 2014. Human memory T cells: generation, compartmentalization and homeostasis. *Nat. Rev. Immunol.* 14: 24–35.

Fearon E.R. & Vogelstein B. 1990. A genetic model for colorectal tumorigenesis. *Cell* 61: 759–767.

Fedirko V., Tramacere I., Bagnardi V., Rota M., Scotti L., Islami F., Negri E., Straif K., Romieu I., Vecchia C. La, Boffetta P. & Jenab M. 2011. Alcohol drinking and colorectal cancer risk: an overall and dose-response meta-analysis of published studies. *Ann. Oncol. Off. J. Eur. Soc. Med. Oncol.* 22: 1958–1972.

Finnish Cancer Registry. 2023. Cancer statistics. Available online: https://cancerregistry.fi/statistics/cancer-statistics/ (accessed on 7 March 2024).

Finnish Cancer Registry. 2024. Colorectal cancer screening. Available online: https://cancerregistry.fi/screening/colorectal-cancer-screening/ (accessed on 7 March 2024).

Folkesson J., Birgisson H., Pahlman L., Cedermark B., Glimelius B. & Gunnarsson U. 2005. Swedish Rectal Cancer Trial: long lasting benefits from radiotherapy on survival and local recurrence rate. *J. Clin. Oncol.* 23: 5644–5650.

Frey D.M., Droeser R.A., Viehl C.T., Zlobec I., Lugli A., Zingg U., Oertli D., Kettelhack C., Terracciano L. & Tornillo L. 2010. High frequency of tumor-infiltrating FOXP3(+) regulatory T cells predicts improved survival in mismatch repair-proficient colorectal cancer patients. *Int. J. Cancer* 126: 2635–2643.

Fridlender Z.G., Sun J., Kim S., Kapoor V., Cheng G., Worthen G.S. & Albelda S.M. 2010. Polarization of TAN phenotype by TGFb: 'N1' versus 'N2' TAN. *Cancer Cell* 16: 183–194.

Fu T., Dai L.-J., Wu S.-Y., Xiao Y., Ma D., Jiang Y.-Z. & Shao Z.-M. 2021. Spatial architecture of the immune microenvironment orchestrates tumor immunity and therapeutic response. *J. Hematol. Oncol.* 14: 98.

Fu Q., Fu T.-M., Cruz A.C., Sengupta P., Thomas S.K., Wang S., Siegel R.M., Wu H. & Chou J.J. 2016. Structural basis and functional role of intramembrane

trimerization of the Fas/CD95 death receptor. *Mol. Cell* 61: 602–613.

Fuchs C.S., Giovannucci E.L., Colditz G.A., Hunter D.J., Speizer F.E. & Willett W.C. 1994. A prospective study of family history and the risk of colorectal cancer. *N. Engl. J. Med.* 331: 1669–1674.

Fujiyoshi K., Bruford E.A., Mroz P., Sims C.L., O'Leary T.J., Lo A.W.I., Chen N., Patel N.R., Patel K.P., Seliger B., Song M., Monzon F.A., Carter A.B., Gulley M.L., Mockus S.M., Phung T.L., Feilotter H., Williams H.E. & Ogino S. 2021. Opinion: Standardizing gene product nomenclature-a call to action. *Proc. Natl. Acad. Sci. U. S. A.* 118: 1–5.

Gabrilovich D.I., Chen H.L., Girgis K.R., Cunningham H.T., Meny G.M., Nadaf S., Kavanaugh D. & Carbone D.P. 1996. Production of vascular endothelial growth factor by human tumors inhibits the functional maturation of dendritic cells. *Nat. Med.* 2: 1096–1103.

Galon J., Costes A., Sanchez-Cabo F., Kirilovsky A., Mlecnik B., Lagorce-Pagès C., Tosolini M., Camus M., Berger A., Wind P., Zinzindohoué F., Bruneval P., Cugnenc P.-H., Trajanoski Z., Fridman W.-H. & Pagès F. 2006. Type, density, and location of immune cells within human colorectal tumors predict clinical outcome. *Science* 313: 1960–1964.

Galon J., Mlecnik B., Bindea G., Angell H.K., Berger A., Lagorce C., Lugli A., Zlobec I., Hartmann A., Bifulco C., Nagtegaal I.D., Palmqvist R., Masucci G. V., Botti G., Tatangelo F., Delrio P., Maio M., Laghi L., Grizzi F., Asslaber M., D'Arrigo C., Vidal-Vanaclocha F., Zavadova E., Chouchane L., Ohashi P.S., Hafezi-Bakhtiari S., Wouters B.G., Roehrl M., Nguyen L., Kawakami Y., Hazama S., Okuno K., Ogino S., Gibbs P., Waring P., Sato N., Torigoe T., Itoh K., Patel P.S., Shukla S.N., Wang Y., Kopetz S., Sinicrope F.A., Scripcariu V., Ascierto P.A., Marincola F.M., Fox B.A. & Pagès F. 2014. Towards the introduction of the 'Immunoscore' in the classification of malignant tumours. *J. Pathol.* 232: 199–209.

Garcia-Larsen V., Morton V., Norat T., Moreira A., Potts J.F., Reeves T. & Bakolis I. 2019. Dietary patterns derived from principal component analysis (PCA) and risk of colorectal cancer: a systematic review and meta-analysis. *Eur. J. Clin. Nutr.* 73: 366–386.

Giesen C., Wang H.A.O., Schapiro D., Zivanovic N., Jacobs A., Hattendorf B., Schüffler P.J., Grolimund D., Buhmann J.M., Brandt S., Varga Z., Wild P.J., Günther D. & Bodenmiller B. 2014. Highly multiplexed imaging of tumor tissues with subcellular resolution by mass cytometry. *Nat. Methods* 11: 417–422.

Giovanni M. De, Tam H., Valet C., Xu Y., Looney M.R. & Cyster J.G. 2022. GPR35 promotes neutrophil recruitment in response to serotonin metabolite 5-HIAA. *Cell* 185: 815-830.e19.

Giraldo N.A., Becht E., Remark R., Damotte D., Sautès-Fridman C. & Fridman W.H. 2014. The immune contexture of primary and metastatic human tumours. *Curr. Opin. Immunol.* 27: 8–15.

Glaire M.A., Domingo E., Sveen A., Bruun J., Nesbakken A., Nicholson G., Novelli M., Lawson K., Oukrif D., Kildal W., Danielsen H.E., Kerr R., Kerr D., Tomlinson I., Lothe R.A. & Church D.N. 2019. Tumour-infiltrating CD8+

lymphocytes and colorectal cancer recurrence by tumour and nodal stage. *Br. J. Cancer* 121: 474–482.

Gordy C. & He Y.-W. 2012. Endocytosis by target cells: an essential means for perforin- and granzyme-mediated killing. *Cell. Mol. Immunol.* 9: 5–6.

Guinney J., Dienstmann R., Wang X., Reyniès A. de, Schlicker A., Soneson C., Marisa L., Roepman P., Nyamundanda G., Angelino P., Bot B.M., Morris J.S., Simon I.M., Gerster S., Fessler E., Sousa E Melo F. De, Missiaglia E., Ramay H., Barras D., Homicsko K., Maru D., Manyam G.C., Broom B., Boige V., Perez-Villamil B., Laderas T., Salazar R., Gray J.W., Hanahan D., Tabernero J., Bernards R., Friend S.H., Laurent-Puig P., Medema J.P., Sadanandam A., Wessels L., Delorenzi M., Kopetz S., Vermeulen L. & Tejpar S. 2015. The consensus molecular subtypes of colorectal cancer. *Nat. Med.* 21: 1350–1356.

Guo L., Wang C., Qiu X., Pu X. & Chang P. 2020. Colorectal cancer immune infiltrates: significance in patient prognosis and immunotherapeutic efficacy. *Front. Immunol.* 11: 1052.

Halama N., Michel S., Kloor M., Zoernig I., Pommerencke T., Knebel Doeberitz M. von, Schirmacher P., Weitz J., Grabe N. & Jäger D. 2009. The localization and density of immune cells in primary tumors of human metastatic colorectal cancer shows an association with response to chemotherapy. *Cancer Immun.* 9: 1.

Halama N., Zoernig I., Spille A., Michel S., Kloor M., Grauling-Halama S., Westphal K., Schirmacher P., Jäger D. & Grabe N. 2010. Quantification of prognostic immune cell markers in colorectal cancer using whole slide imaging tumor maps. *Anal. Quant. Cytol. Histol.* 32: 333–340.

Half E., Bercovich D. & Rozen P. 2009. Familial adenomatous polyposis. *Orphanet J. Rare Dis.* 4: 22.

Hamilton S.R. & Sekine S. 2019. Conventional colorectal adenoma. In: *World Health Organization Classification of Tumours of the Digestive System*, IARC Press, pp. 170–173.

Hamzah J., Jugold M., Kiessling F., Rigby P., Manzur M., Marti H.H., Rabie T., Kaden S., Gröne H.-J., Hämmerling G.J., Arnold B. & Ganss R. 2008. Vascular normalization in Rgs5-deficient tumours promotes immune destruction. *Nature* 453: 410–414.

Hanahan D. 2022. Hallmarks of cancer: new dimensions. *Cancer Discov.* 12: 31–46.

Hanahan D. & Weinberg R.A. 2000. The hallmarks of cancer. *Cell* 100: 57–70.

Hanahan D. & Weinberg R.A. 2011. Hallmarks of cancer: the next generation. *Cell* 144: 646–674.

Haralick R.M., Dinstein I. & Shanmugam K. 1973. Textural features for image classification. *IEEE Trans. Syst. Man Cybern.* SMC-3: 610–621.

Hashimoto K., Kouno T., Ikawa T., Hayatsu N., Miyajima Y., Yabukami H., Terooatea T., Sasaki T., Suzuki T., Valentine M., Pascarella G., Okazaki Y., Suzuki H., Shin J.W., Minoda A., Taniuchi I., Okano H., Arai Y., Hirose N. & Carninci P. 2019. Single-cell transcriptomics reveals expansion of cytotoxic CD4 T cells in supercentenarians. *Proc. Natl. Acad. Sci. U. S. A.* 116: 24242–24251.

Hendriks Y., Franken P., Dierssen J.W., Leeuw W. De, Wijnen J., Dreef E., Tops C., Breuning M., Bröcker-Vriends A., Vasen H., Fodde R. & Morreau H. 2003. Conventional and tissue microarray immunohistochemical expression analysis of mismatch repair in hereditary colorectal tumors. *Am. J. Pathol.* 162: 469–477.

Hewitson P., Glasziou P., Watson E., Towler B. & Irwig L. 2008. Cochrane systematic review of colorectal cancer screening using the fecal occult blood test (Hemoccult): an update. *Am. J. Gastroenterol.* 103: 1541–1549.

Hilligan K.L. & Ronchese F. 2020. Antigen presentation by dendritic cells and their instruction of CD4+ T helper cell responses. *Cell. Mol. Immunol.* 17: 587–599.

Hornyák L., Dobos N., Koncz G., Karányi Z., Páll D., Szabó Z., Halmos G. & Székvölgyi L. 2018. The role of indoleamine-2,3-dioxygenase in cancer development, diagnostics, and therapy. *Front. Immunol.* 9: 151.

Idos G.E., Kwok J., Bonthala N., Kysh L., Gruber S.B. & Qu C. 2020. The prognostic implications of tumor infiltrating lymphocytes in colorectal cancer: a systematic review and meta-analysis. *Sci. Rep.* 10: 3360.

Italiani P., Mazza E.M.C., Lucchesi D., Cifola I., Gemelli C., Grande A., Battaglia C., Bicciato S. & Boraschi D. 2014. Transcriptomic profiling of the development of the inflammatory response in human monocytes in vitro. *PLoS One* 9: e87680.

Jaillon S., Ponzetta A., Mitri D. Di, Santoni A., Bonecchi R. & Mantovani A. 2020. Neutrophil diversity and plasticity in tumour progression and therapy. *Nat. Rev. Cancer* 20: 485–503.

Jasperson K.W., Tuohy T.M., Neklason D.W. & Burt R.W. 2010. Hereditary and familial colon cancer. *Gastroenterology* 138: 2044–2058.

Jenkins M.A., Hayashi S., O'Shea A.-M., Burgart L.J., Smyrk T.C., Shimizu D., Waring P.M., Ruszkiewicz A.R., Pollett A.F., Redston M., Barker M.A., Baron J.A., Casey G.R., Dowty J.G., Giles G.G., Limburg P., Newcomb P., Young J.P., Walsh M.D., Thibodeau S.N., Lindor N.M., Lemarchand L., Gallinger S., Haile R.W., Potter J.D., Hopper J.L., Jass J.R. & Colon Cancer Family Registry. 2007. Pathology features in Bethesda guidelines predict colorectal cancer microsatellite instability: a population-based study. *Gastroenterology* 133: 48–56.

Jenkinson C.P., Grody W.W. & Cederbaum S.D. 1996. Comparative properties of arginases. *Comp. Biochem. Physiol. B. Biochem. Mol. Biol.* 114: 107–132.

Jourdan F., Sebbagh N., Comperat E., Mourra N., Flahault A., Olschwang S., Duval A., Hamelin R. & Flejou J.-F. 2003. Tissue microarray technology: validation in colorectal carcinoma and analysis of p53, hMLH1, and hMSH2 immunohistochemical expression. *Virchows Arch.* 443: 115–121.

Kandoth C., McLellan M.D., Vandin F., Ye K., Niu B., Lu C., Xie M., Zhang Q., McMichael J.F., Wyczalkowski M.A., Leiserson M.D.M., Miller C.A., Welch J.S., Walter M.J., Wendl M.C., Ley T.J., Wilson R.K., Raphael B.J. & Ding L. 2013. Mutational landscape and significance across 12 major cancer types. *Nature* 502: 333–339.

Kannarkatt J., Joseph J., Kurniali P.C., Al-Janadi A. & Hrinczenko B. 2017.

Adjuvant chemotherapy for stage II colon cancer: a clinical dilemma. *J. Oncol. Pract.* 13: 233–241.

Kärre K., Ljunggren H.G., Piontek G. & Kiessling R. 1986. Selective rejection of H-2-deficient lymphoma variants suggests alternative immune defence strategy. *Nature* 319: 675–678.

Keir M.E., Liang S.C., Guleria I., Latchman Y.E., Qipo A., Albacker L.A., Koulmanda M., Freeman G.J., Sayegh M.H. & Sharpe A.H. 2006. Tissue expression of PD-L1 mediates peripheral T cell tolerance. *J. Exp. Med.* 203: 883–895.

Kellokumpu I., Kairaluoma M., Mecklin J.-P., Kellokumpu H., Väyrynen V., Wirta E.-V., Sihvo E., Kuopio T. & Seppälä T.T. 2021. Impact of age and comorbidity on multimodal management and survival from colorectal cancer: A population-based study. *J. Clin. Med.* 10: 1751.

Kierszenbaum A. & Tres L. 2020. Lower digestive segment. In: *Histology and Cell Biology: An introduction to Pathology*, Elsevier, pp. 544–575.

Kim J.H. & Kang G.H. 2014. Molecular and prognostic heterogeneity of microsatellite-unstable colorectal cancer. *World J. Gastroenterol.* 20: 4230–4243.

Kim S.-W., Roh J. & Park C.-S. 2016. Immunohistochemistry for pathologists: protocols, pitfalls, and tips. *J. Pathol. Transl. Med.* 50: 411–418.

Kononen J., Bubendorf L., Kallioniemi A., Bärlund M., Schraml P., Leighton S., Torhorst J., Mihatsch M.J., Sauter G. & Kallioniemi O.P. 1998. Tissue microarrays for high-throughput molecular profiling of tumor specimens. *Nat. Med.* 4: 844–847.

Kuipers E.J., Grady W.M., Lieberman D., Seufferlein T., Sung J.J., Boelens P.G., Velde C.J.H. van de & Watanabe T. 2015. Colorectal cancer. *Nat. Rev. Dis. Prim.* 1: 15065.

Kuwahara T., Hazama S., Suzuki N., Yoshida S., Tomochika S., Nakagami Y., Matsui H., Shindo Y., Kanekiyo S., Tokumitsu Y., Iida M., Tsunedomi R., Takeda S., Yoshino S., Okayama N., Suehiro Y., Yamasaki T., Fujita T., Kawakami Y., Ueno T. & Nagano H. 2019. Intratumoural-infiltrating CD4 + and FOXP3 + T cells as strong positive predictive markers for the prognosis of resectable colorectal cancer. *Br. J. Cancer* 121: 659–665.

la Chapelle A. de & Hampel H. 2010. Clinical relevance of microsatellite instability in colorectal cancer. *J. Clin. Oncol.* 28: 3380–3387.

Larsson S.C. & Wolk A. 2006. Meat consumption and risk of colorectal cancer: a meta-analysis of prospective studies. *Int. J. Cancer* 119: 2657–2664.

Lazarus J., Maj T., Smith J.J., Perusina Lanfranca M., Rao A., D'Angelica M.I., Delrosario L., Girgis A., Schukow C., Shia J., Kryczek I., Shi J., Wasserman I., Crawford H., Nathan H., Pasca Di Magliano M., Zou W. & Frankel T.L. 2018. Spatial and phenotypic immune profiling of metastatic colon cancer. *JCI Insight* 3: e121932.

Le D.T., Durham J.N., Smith K.N., Wang H., Bartlett B.R., Aulakh L.K., Lu S., Kemberling H., Wilt C., Luber B.S., Wong F., Azad N.S., Rucki A.A., Laheru D., Donehower R., Zaheer A., Fisher G.A., Crocenzi T.S., Lee J.J., Greten T.F., Duffy A.G., Ciombor K.K., Eyring A.D., Lam B.H., Joe A., Kang S.P.,

Holdhoff M., Danilova L., Cope L., Meyer C., Zhou S., Goldberg R.M., Armstrong D.K., Bever K.M., Fader A.N., Taube J., Housseau F., Spetzler D., Xiao N., Pardoll D.M., Papadopoulos N., Kinzler K.W., Eshleman J.R., Vogelstein B., Anders R.A. & Diaz L.A. 2017. Mismatch repair deficiency predicts response of solid tumors to PD-1 blockade. *Science* 357: 409–413.

Lee S.J., Jun S.-Y., Lee I.H., Kang B.W., Park S.Y., Kim H.J., Park J.S., Choi G.-S., Yoon G. & Kim J.G. 2018. CD274, LAG3, and IDO1 expressions in tumor-infiltrating immune cells as prognostic biomarker for patients with MSI-high colon cancer. *J. Cancer Res. Clin. Oncol.* 144: 1005–1014.

Lee K.S., Kwak Y., Ahn S., Shin E., Oh H.-K., Kim D.-W., Kang S.-B., Choe G., Kim W.H. & Lee H.S. 2017. Prognostic implication of CD274 (PD-L1) protein expression in tumor-infiltrating immune cells for microsatellite unstable and stable colorectal cancer. *Cancer Immunol. Immunother.* 66: 927–939.

Lee G.K., Park H.J., Macleod M., Chandler P., Munn D.H. & Mellor A.L. 2002. Tryptophan deprivation sensitizes activated T cells to apoptosis prior to cell division. *Immunology* 107: 452–460.

Leong S.P., Naxerova K., Keller L., Pantel K. & Witte M. 2022. Molecular mechanisms of cancer metastasis via the lymphatic versus the blood vessels. *Clin. Exp. Metastasis* 39: 159–179.

Leowattana W., Leowattana P. & Leowattana T. 2023. Systemic treatment for metastatic colorectal cancer. *World J. Gastroenterol.* 29: 1569–1588.

Leu S. -Y & Wang S. -R. 1992. Clinical significance of arginase in colorectal cancer. *Cancer* 70: 733–736.

Li H., Fu G., Wei W., Huang Y., Wang Z., Liang T., Tian S., Chen H. & Zhang W. 2020. Re-evaluation of the survival paradox between stage IIB/IIC and stage IIIA colon cancer. *Front. Oncol.* 10: 595107.

Li N., Zhu Q., Tian Y., Ahn K.J., Wang X., Cramer Z., Jou J., Folkert I.W., Yu P., Adams-Tzivelekidis S., Sehgal P., Mahmoud N.N., Aarons C.B., Roses R.E., Thomas-Tikhonenko A., Furth E.E., Stanger B.Z., Rustgi A., Haldar M., Katona B.W., Tan K. & Lengner C.J. 2023. Mapping and modeling human colorectal carcinoma interactions with the tumor microenvironment. *Nat. Commun.* 14: 7915.

Li Y., Liang L., Dai W., Cai G., Xu Y., Li X., Li Q. & Cai S. 2016. Prognostic impact of programed cell death-1 (PD-1) and PD-ligand 1 (PD-L1) expression in cancer cells and tumor infiltrating lymphocytes in colorectal cancer. *Mol. Cancer* 15: 55.

Lichtenstein P., Holm N. V, Verkasalo P.K., Iliadou A., Kaprio J., Koskenvuo M., Pukkala E., Skytthe A. & Hemminki K. 2000. Environmental and heritable factors in the causation of cancer--analyses of cohorts of twins from Sweden, Denmark, and Finland. *N. Engl. J. Med.* 343: 78–85.

Lin J.-R., Wang S., Coy S., Chen Y.-A., Yapp C., Tyler M., Nariya M.K., Heiser C.N., Lau K.S., Santagata S. & Sorger P.K. 2023. Multiplexed 3D atlas of state transitions and immune interaction in colorectal cancer. *Cell* 186: 363-381.e19.

Liu X., Li X., Wei H., Liu Y. & Li N. 2023. Mast cells in colorectal cancer tumour progression, angiogenesis, and lymphangiogenesis. *Front. Immunol.* 14:

1209056.

Luo D., Liu Q., Yu W., Ma Y., Zhu J., Lian P., Cai S., Li Q. & Li X. 2018. Prognostic value of distant metastasis sites and surgery in stage IV colorectal cancer: a population-based study. *Int. J. Colorectal Dis*. 33: 1241–1249.

Ma H., Brosens L.A.A., Offerhaus G.J.A., Giardiello F.M., Leng W.W.J. de & Montgomery E.A. 2018. Pathology and genetics of hereditary colorectal cancer. *Pathology* 50: 49–59.

Ma Z., Lian J., Yang M., Wuyang J., Zhao C., Chen W., Liu C., Zhao Q., Lou C., Han J. & Zhang Y. 2019. Overexpression of Arginase-1 is an indicator of poor prognosis in patients with colorectal cancer. *Pathol. Res. Pract.* 215: 152383.

Marhelava K., Pilch Z., Bajor M., Graczyk-Jarzynka A. & Zagozdzon R. 2019. Targeting negative and positive immune checkpoints with monoclonal antibodies in therapy of cancer. *Cancers (Basel)*. 11: 1–21.

McCarty K.S., Szabo E., Flowers J.L., Cox E.B., Leight G.S., Miller L., Konrath J., Soper J.T., Budwit D.A. & Creasman W.T. 1986. Use of a monoclonal anti-estrogen receptor antibody in the immunohistochemical evaluation of human tumors. *Cancer Res.* 46: 4244s-4248s.

McQuin C., Goodman A., Chernyshev V., Kamentsky L., Cimini B.A., Karhohs K.W., Doan M., Ding L., Rafelski S.M., Thirstrup D., Wiegraebe W., Singh S., Becker T., Caicedo J.C. & Carpenter A.E. 2018. CellProfiler 3.0: Next-generation image processing for biology. *PLoS Biol.* 16: e2005970.

Meireson A., Devos M. & Brochez L. 2020. IDO expression in cancer: different compartment, different functionality? *Front. Immunol.* 11: 531491.

Meitei H.T. & Lal G. 2023. T cell receptor signaling in the differentiation and plasticity of CD4+ T cells. *Cytokine Growth Factor Rev.* 69: 14–27.

Michielsen A.J., Hogan A.E., Marry J., Tosetto M., Cox F., Hyland J.M., Sheahan K.D., O'Donoghue D.P., Mulcahy H.E., Ryan E.J. & O'Sullivan J.N. 2011. Tumour tissue microenvironment can inhibit dendritic cell maturation in colorectal cancer. *PLoS One* 6: e27944.

Miller K.D., Nogueira L., Devasia T., Mariotto A.B., Yabroff K.R., Jemal A., Kramer J. & Siegel R.L. 2022. Cancer treatment and survivorship statistics, 2022. *CA. Cancer J. Clin.* 72: 409–436.

Mondanelli G., Iacono A., Allegrucci M., Puccetti P. & Grohmann U. 2019. Immunoregulatory interplay between arginine and tryptophan metabolism in health and disease. *Front. Immunol.* 10: 1565.

Mooi J.K., Wirapati P., Asher R., Lee C.K., Savas P., Price T.J., Townsend A., Hardingham J., Buchanan D., Williams D., Tejpar S., Mariadason J.M. & Tebbutt N.C. 2018. The prognostic impact of consensus molecular subtypes (CMS) and its predictive effects for bevacizumab benefit in metastatic colorectal cancer: molecular analysis of the AGITG MAX clinical trial. *Ann. Oncol. Off. J. Eur. Soc. Med. Oncol.* 29: 2240–2246.

Morath A. & Schamel W.W. 2020. Aβ and γδ T cell receptors: similar but different. *J. Leukoc. Biol.* 107: 1045–1055.

Mulder K., Patel A.A., Kong W.T., Piot C., Halitzki E., Dunsmore G., Khalilnezhad S., Irac S.E., Dubuisson A., Chevrier M., Zhang X.M., Tam J.K.C., Lim T.K.H., Wong R.M.M., Pai R., Khalil A.I.S., Chow P.K.H., Wu

S.Z., Al-Eryani G., Roden D., Swarbrick A., Chan J.K.Y., Albani S., Derosa L., Zitvogel L., Sharma A., Chen J., Silvin A., Bertoletti A., Blériot C., Dutertre C.-A. & Ginhoux F. 2021. Cross-tissue single-cell landscape of human monocytes and macrophages in health and disease. *Immunity* 54: 1883-1900.e5.

Mun J.-Y., Leem S.-H., Lee J.H. & Kim H.S. 2022. Dual relationship between stromal cells and immune cells in the tumor microenvironment. *Front. Immunol.* 13: 864739.

Munder M., Mollinedo F., Calafat J., Canchado J., Gil-Lamaignere C., Fuentes J.M., Luckner C., Doschko G., Soler G., Eichmann K., Müller F.-M., Ho A.D., Goerner M. & Modolell M. 2005. Arginase I is constitutively expressed in human granulocytes and participates in fungicidal activity. *Blood* 105: 2549–2556.

Murphy K. & Weaver C. 2017. Basic concepts in immunobiology. In: *Janeway's Immunobiology*, Garland Science, pp. 1–36.

Murray P.J. 2017. Macrophage polarization. *Annu. Rev. Physiol.* 79: 541–566.

Nagasaka T., Koi M., Kloor M., Gebert J., Vilkin A., Nishida N., Shin S.K., Sasamoto H., Tanaka N., Matsubara N., Boland C.R. & Goel A. 2008. Mutations in both KRAS and BRAF may contribute to the methylator phenotype in colon cancer. *Gastroenterology* 134: 1950–1960, 1960.e1.

Nagtegaal I.D., Arends M.J. & Salto-Tellez M. 2019. Colorectal adenocarcinoma: tumours of the colon and rectum. In: *World Health Organization Classification of Tumours of the Digestive System*, IARC Press, pp. 177–187.

Nagtegaal I.D., Marijnen C.A.M., Kranenbarg E.K., Mulder-Stapel A., Hermans J., Velde C.J.H. van de, Krieken J.H.J.M. van & Pathology Review Committee. 2002. Short-term preoperative radiotherapy interferes with the determination of pathological parameters in rectal cancer. *J. Pathol.* 197: 20–27.

Naito Y., Saito K., Shiiba K., Ohuchi A., Saigenji K., Nagura H. & Ohtani H. 1998. CD8+ T cells infiltrated within cancer cell nests as a prognostic factor in human colorectal cancer. *Cancer Res.* 58: 3491–3494.

Nelson B.H. 2010. CD20+ B cells: the other tumor-infiltrating lymphocytes. *J. Immunol.* 185: 4977–4982.

Ness S., Lin S. & Gordon J.R. 2021. Regulatory dendritic cells, T cell tolerance, and dendritic cell therapy for immunologic disease. *Front. Immunol.* 12: 633436.

Nguyen L.H., Goel A. & Chung D.C. 2020. Pathways of colorectal carcinogenesis. *Gastroenterology* 158: 291–302.

Nielsen S.R. & Schmid M.C. 2017. Macrophages as key drivers of cancer progression and metastasis. *Mediators Inflamm*. 2017: 9624760.

Nishihara R., VanderWeele T.J., Shibuya K., Mittleman M.A., Wang M., Field A.E., Giovannucci E., Lochhead P. & Ogino S. 2015. Molecular pathological epidemiology gives clues to paradoxical findings. *Eur. J. Epidemiol.* 30: 1129–1135.

Niu F., Yu Y., Li Z., Ren Y., Li Z., Ye Q., Liu P., Ji C., Qian L. & Xiong Y. 2022. Arginase: An emerging and promising therapeutic target for cancer

treatment. *Biomed. Pharmacother.* 149: 112840.

Noack P. & Langer R. 2023. Molecular pathology of colorectal cancer. *Memo - Mag. Eur. Med. Oncol.* 16: 116–121.

Ogino S., Chan A.T., Fuchs C.S. & Giovannucci E. 2011. Molecular pathological epidemiology of colorectal neoplasia: an emerging transdisciplinary and interdisciplinary field. *Gut* 60: 397–411.

Ogino S., Nosho K., Kirkner G.J., Kawasaki T., Meyerhardt J.A., Loda M., Giovannucci E.L. & Fuchs C.S. 2009. CpG island methylator phenotype, microsatellite instability, BRAF mutation and clinical outcome in colon cancer. *Gut* 58: 90–96.

Pagès F., Galon J. & Fridman W.H. 2008. The essential role of the in situ immune reaction in human colorectal cancer. *J. Leukoc. Biol.* 84: 981–987.

Pagès F., Mlecnik B., Marliot F., Bindea G., Ou F.-S., Bifulco C., Lugli A., Zlobec I., Rau T.T., Berger M.D., Nagtegaal I.D., Vink-Börger E., Hartmann A., Geppert C., Kolwelter J., Merkel S., Grützmann R., Eynde M. Van den, Jouret-Mourin A., Kartheuser A., Léonard D., Remue C., Wang J.Y., Bavi P., Roehrl M.H.A., Ohashi P.S., Nguyen L.T., Han S., MacGregor H.L., Hafezi-Bakhtiari S., Wouters B.G., Masucci G. V., Andersson E.K., Zavadova E., Vocka M., Spacek J., Petruzelka L., Konopasek B., Dundr P., Skalova H., Nemejcova K., Botti G., Tatangelo F., Delrio P., Ciliberto G., Maio M., Laghi L., Grizzi F., Fredriksen T., Buttard B., Angelova M., Vasaturo A., Maby P., Church S.E., Angell H.K., Lafontaine L., Bruni D., Sissy C. El, Haicheur N., Kirilovsky A., Berger A., Lagorce C., Meyers J.P., Paustian C., Feng Z., Ballesteros-Merino C., Dijkstra J., Water C. van de, Lent-van Vliet S. van, Knijn N., Muşină A.-M., Scripcariu D.-V., Popivanova B., Xu M., Fujita T., Hazama S., Suzuki N., Nagano H., Okuno K., Torigoe T., Sato N., Furuhata T., Takemasa I., Itoh K., Patel P.S., Vora H.H., Shah B., Patel J.B., Rajvik K.N., Pandya S.J., Shukla S.N., Wang Y., Zhang G., Kawakami Y., Marincola F.M., Ascierto P.A., Sargent D.J., Fox B.A., et al. 2018. International validation of the consensus Immunoscore for the classification of colon cancer: a prognostic and accuracy study. *Lancet (London, England)* 391: 2128–2139.

Pai R., Mäkinen M.J. & Rosty C. 2019. Colorectal serrated lesions and polyps. In: *World Health Organization Classification of Tumours of the Digestive System*, IARC Press, pp. 163–169.

Pardoll D.M. 2012. The blockade of immune checkpoints in cancer immunotherapy. *Nat. Rev. Cancer* 12: 252–264.

Pauken K.E., Torchia J.A., Chaudhri A., Sharpe A.H. & Freeman G.J. 2021. Emerging concepts in PD-1 checkpoint biology. *Semin. Immunol.* 52: 101480.

Pelka K., Hofree M., Chen J.H., Sarkizova S., Pirl J.D., Jorgji V., Bejnood A., Dionne D., Ge W.H., Xu K.H., Chao S.X., Zollinger D.R., Lieb D.J., Reeves J.W., Fuhrman C.A., Hoang M.L., Delorey T., Nguyen L.T., Waldman J., Klapholz M., Wakiro I., Cohen O., Albers J., Smillie C.S., Cuoco M.S., Wu J., Su M.-J., Yeung J., Vijaykumar B., Magnuson A.M., Asinovski N., Moll T., Goder-Reiser M.N., Applebaum A.S., Brais L.K., DelloStritto L.K., Denning S.L., Phillips S.T., Hill E.K., Meehan J.K., Frederick D.T., Sharova T., Kanodia A., Todres E.Z., Jané-Valbuena J., Biton M., Izar B., Lambden C.D., Clancy

T.E., Bleday R., Melnitchouk N., Irani J., Kunitake H., Berger D.L., Srivastava A., Hornick J.L., Ogino S., Rotem A., Vigneau S., Johnson B.E., Corcoran R.B., Sharpe A.H., Kuchroo V.K., Ng K., Giannakis M., Nieman L.T., Boland G.M., Aguirre A.J., Anderson A.C., Rozenblatt-Rosen O., Regev A. & Hacohen N. 2021. Spatially organized multicellular immune hubs in human colorectal cancer. *Cell* 184: 4734-4752.e20.

Peltomäki P. 2014. Epigenetic mechanisms in the pathogenesis of Lynch syndrome. *Clin. Genet.* 85: 403–412.

Peltomäki P., Nyström M., Mecklin J.-P. & Seppälä T.T. 2023. Lynch syndrome genetics and clinical implications. *Gastroenterology* 164: 783–799.

Philip M. & Schietinger A. 2022. CD8+ T cell differentiation and dysfunction in cancer. *Nat. Rev. Immunol.* 22: 209–223.

Pino M.S. & Chung D.C. 2010. The chromosomal instability pathway in colon cancer. *Gastroenterology* 138: 2059–2072.

Ponz de Leon M. & Gregorio C. Di. 2001. Pathology of colorectal cancer. *Dig. Liver Dis.* 33: 372–388.

Popat S., Hubner R. & Houlston R.S. 2005. Systematic review of microsatellite instability and colorectal cancer prognosis. *J. Clin. Oncol.* 23: 609–618.

Powell S.M., Zilz N., Beazer-Barclay Y., Bryan T.M., Hamilton S.R., Thibodeau S.N., Vogelstein B. & Kinzler K.W. 1992. APC mutations occur early during colorectal tumorigenesis. *Nature* 359: 235–237.

Prager I. & Watzl C. 2019. Mechanisms of natural killer cell-mediated cellular cytotoxicity. *J. Leukoc. Biol.* 105: 1319–1329.

Quezada S.A., Simpson T.R., Peggs K.S., Merghoub T., Vider J., Fan X., Blasberg R., Yagita H., Muranski P., Antony P.A., Restifo N.P. & Allison J.P. 2010. Tumor-reactive CD4(+) T cells develop cytotoxic activity and eradicate large established melanoma after transfer into lymphopenic hosts. *J. Exp. Med.* 207: 637–650.

R Core Team. 2020. R: A language and environment for statistical computing, R Foundation for Statistical Computing, Vienna, Austria. URL http://www.R-project.org/.

Rajagopalan H., Bardelli A., Lengauer C., Kinzler K.W., Vogelstein B. & Velculescu V.E. 2002. Tumorigenesis: RAF/RAS oncogenes and mismatch-repair status. *Nature* 418: 934.

Raskov H., Orhan A., Christensen J.P. & Gögenur I. 2021. Cytotoxic CD8+ T cells in cancer and cancer immunotherapy. *Br. J. Cancer* 124: 359–367.

Reid F.S.W., Egoroff N., Pockney P.G. & Smith S.R. 2021. A systematic scoping review on natural killer cell function in colorectal cancer. *Cancer Immunol. Immunother.* 70: 597–606.

Renehan A.G., Tyson M., Egger M., Heller R.F. & Zwahlen M. 2008. Body-mass index and incidence of cancer: a systematic review and meta-analysis of prospective observational studies. *Lancet (London, England)* 371: 569–578.

Rodriguez P.C., Ernstoff M.S., Hernandez C., Atkins M., Zabaleta J., Sierra R. & Ochoa A.C. 2009. Arginase I-producing myeloid-derived suppressor cells in renal cell carcinoma are a subpopulation of activated granulocytes. *Cancer Res.* 69: 1553–1560.

Rodriguez P.C., Quiceno D.G. & Ochoa A.C. 2007. L-arginine availability regulates T-lymphocyte cell-cycle progression. *Blood* 109: 1568–1573.

Rojas F., Hernandez S., Lazcano R., Laberiano-Fernandez C. & Parra E.R. 2022. Multiplex immunofluorescence and the digital image analysis workflow for evaluation of the tumor immune environment in translational research. *Front. Oncol.* 12: 889886.

Rosen D.G., Huang X., Deavers M.T., Malpica A., Silva E.G. & Liu J. 2004. Validation of tissue microarray technology in ovarian carcinoma. *Mod. Pathol.* 17: 790–797.

RStudio Team. 2020. RStudio: integrated development for R. RStudio, PBC, Boston, MA. URL http://www.posit.co/.

Sahai E., Astsaturov I., Cukierman E., DeNardo D.G., Egeblad M., Evans R.M., Fearon D., Greten F.R., Hingorani S.R., Hunter T., Hynes R.O., Jain R.K., Janowitz T., Jorgensen C., Kimmelman A.C., Kolonin M.G., Maki R.G., Powers R.S., Puré E., Ramirez D.C., Scherz-Shouval R., Sherman M.H., Stewart S., Tlsty T.D., Tuveson D.A., Watt F.M., Weaver V., Weeraratna A.T. & Werb Z. 2020. A framework for advancing our understanding of cancer-associated fibroblasts. *Nat. Rev. Cancer* 20: 174–186.

Salama P., Phillips M., Grieu F., Morris M., Zeps N., Joseph D., Platell C. & Iacopetta B. 2009. Tumor-infiltrating FOXP3+ T regulatory cells show strong prognostic significance in colorectal cancer. *J. Clin. Oncol.* 27: 186–192.

Samad A.K.A., Taylor R.S., Marshall T. & Chapman M.A.S. 2005. A meta-analysis of the association of physical activity with reduced risk of colorectal cancer. *Colorectal Dis.* 7: 204–213.

Sammalkorpi H., Alhopuro P., Lehtonen R., Tuimala J., Mecklin J.-P., Järvinen H.J., Jiricny J., Karhu A. & Aaltonen L.A. 2007. Background mutation frequency in microsatellite-unstable colorectal cancer. *Cancer Res.* 67: 5691–5698.

Saraiva M.R., Rosa I. & Claro I. 2023. Early-onset colorectal cancer: a review of current knowledge. *World J. Gastroenterol.* 29: 1289–1303.

Sargent D.J., Conley B.A., Allegra C. & Collette L. 2005. Clinical trial designs for predictive marker validation in cancer treatment trials. *J. Clin. Oncol.* 23: 2020–2027.

Schapiro D., Jackson H.W., Raghuraman S., Fischer J.R., Zanotelli V.R.T., Schulz D., Giesen C., Catena R., Varga Z. & Bodenmiller B. 2017. HistoCAT: analysis of cell phenotypes and interactions in multiplex image cytometry data. *Nat. Methods* 14: 873–876.

Schindelin J., Arganda-Carreras I., Frise E., Kaynig V., Longair M., Pietzsch T., Preibisch S., Rueden C., Saalfeld S., Schmid B., Tinevez J.-Y., White D.J., Hartenstein V., Eliceiri K., Tomancak P. & Cardona A. 2012. Fiji: an open-source platform for biological-image analysis. *Nat. Methods* 9: 676–682.

Schüler T., Qin Z., Ibe S., Noben-Trauth N. & Blankenstein T. 1999. T helper cell type 1-associated and cytotoxic T lymphocyte-mediated tumor immunity is impaired in interleukin 4-deficient mice. *J. Exp. Med.* 189: 803–810.

Schürch C.M., Bhate S.S., Barlow G.L., Phillips D.J., Noti L., Zlobec I., Chu P., Black S., Demeter J., McIlwain D.R., Kinoshita S., Samusik N., Goltsev Y. &

Nolan G.P. 2020. Coordinated cellular neighborhoods orchestrate antitumoral immunity at the colorectal cancer invasive front. *Cell* 182: 1341-1359.e19.

Seppä K., Tanskanen T., Heikkinen S., Malila N. & Pitkäniemi J. 2023. Syöpä 2021. Tilastoraportti Suomen syöpätilanteesta. Helsinki.

Shankaran V., Ikeda H., Bruce A.T., White J.M., Swanson P.E., Old L.J. & Schreiber R.D. 2001. IFNgamma and lymphocytes prevent primary tumour development and shape tumour immunogenicity. *Nature* 410: 1107–1111.

Shaukat A. & Levin T.R. 2022. Current and future colorectal cancer screening strategies. *Nat. Rev. Gastroenterol. Hepatol.* 19: 521–531.

Simon K. 2016. Colorectal cancer development and advances in screening. *Clin. Interv. Aging* 11: 967–976.

Sinicrope F.A., Rego R.L., Ansell S.M., Knutson K.L., Foster N.R. & Sargent D.J. 2009. Intraepithelial effector (CD3+)/regulatory (FoxP3+) T-cell ratio predicts a clinical outcome of human colon carcinoma. *Gastroenterology* 137: 1270–1279.

Slattery M.L., Anderson K., Curtin K., Ma K.N., Schaffer D. & Samowitz W. 2001. Dietary intake and microsatellite instability in colon tumors. *Int. J. Cancer* 93: 601–607.

Spence A., Klementowicz J.E., Bluestone J.A. & Tang Q. 2015. Targeting Treg signaling for the treatment of autoimmune diseases. *Curr. Opin. Immunol.* 37: 11–20.

Suzuki T. 2020. Regulation of the intestinal barrier by nutrients: The role of tight junctions. *Anim. Sci. J.* 91: e13357.

Tan W.C.C., Nerurkar S.N., Cai H.Y., Ng H.H.M., Wu D., Wee Y.T.F., Lim J.C.T., Yeong J. & Lim T.K.H. 2020. Overview of multiplex immunohistochemistry/immunofluorescence techniques in the era of cancer immunotherapy. *Cancer Commun. (London, England)* 40: 135–153.

Theoharides T.C., Alysandratos K.-D., Angelidou A., Delivanis D.-A., Sismanopoulos N., Zhang B., Asadi S., Vasiadi M., Weng Z., Miniati A. & Kalogeromitros D. 2012. Mast cells and inflammation. *Biochim. Biophys. Acta* 1822: 21–33.

Thomas P.D. 2017. The gene ontology and the meaning of biological function. *Methods Mol. Biol.* 1446: 15–24.

Tosolini M., Kirilovsky A., Mlecnik B., Fredriksen T., Mauger S., Bindea G., Berger A., Bruneval P., Fridman W.H., Pagès F. & Galon J. 2011. Clinical impact of different classes of infiltrating T cytotoxic and helper cells (Th1, Th2, Treg, Th17) in patients with colorectal cancer. *Cancer Res.* 71: 1263–1271.

Tsujikawa T., Mitsuda J., Ogi H., Miyagawa-Hayashino A., Konishi E., Itoh K. & Hirano S. 2020. Prognostic significance of spatial immune profiles in human solid cancers. *Cancer Sci.* 111: 3426–3434.

Union for International Cancer Control. 2017. Colon and rectum. In: *TNM Classification of Malignant Tumours*, Wiley-Blackwell, pp. 73–76.

Vasen H.F.A., Blanco I., Aktan-Collan K., Gopie J.P., Alonso A., Aretz S., Bernstein I., Bertario L., Burn J., Capella G., Colas C., Engel C., Frayling I.M., Genuardi M., Heinimann K., Hes F.J., Hodgson S. V., Karagiannis J.A.,

Lalloo F., Lindblom A., Mecklin J.-P., Møller P., Myrhoj T., Nagengast F.M., Parc Y., Ponz de Leon M., Renkonen-Sinisalo L., Sampson J.R., Stormorken A., Sijmons R.H., Tejpar S., Thomas H.J.W., Rahner N., Wijnen J.T., Järvinen H.J., Möslein G. & Mallorca group. 2013. Revised guidelines for the clinical management of Lynch syndrome (HNPCC): recommendations by a group of European experts. *Gut* 62: 812–823.

Väyrynen J.P., Haruki K., Väyrynen S.A., Lau M.C., Dias Costa A., Borowsky J., Zhao M., Ugai T., Kishikawa J., Akimoto N., Zhong R., Shi S., Chang T.-W., Fujiyoshi K., Arima K., Twombly T.S., Silva A. Da, Song M., Wu K., Zhang X., Chan A.T., Nishihara R., Fuchs C.S., Meyerhardt J.A., Giannakis M., Ogino S. & Nowak J.A. 2021. Prognostic significance of myeloid immune cells and their spatial distribution in the colorectal cancer microenvironment. *J. Immunother. Cancer* 9: e002297.

Vignali D.A.A., Collison L.W. & Workman C.J. 2008. How regulatory T cells work. *Nat. Rev. Immunol.* 8: 523–532.

Vinay D.S., Ryan E.P., Pawelec G., Talib W.H., Stagg J., Elkord E., Lichtor T., Decker W.K., Whelan R.L., Kumara H.M.C.S., Signori E., Honoki K., Georgakilas A.G., Amin A., Helferich W.G., Boosani C.S., Guha G., Ciriolo M.R., Chen S., Mohammed S.I., Azmi A.S., Keith W.N., Bilsland A., Bhakta D., Halicka D., Fujii H., Aquilano K., Ashraf S.S., Nowsheen S., Yang X., Choi B.K. & Kwon B.S. 2015. Immune evasion in cancer: Mechanistic basis and therapeutic strategies. *Semin. Cancer Biol.* 35 Suppl: S185–S198.

Visser K.E. de, Eichten A. & Coussens L.M. 2006. Paradoxical roles of the immune system during cancer development. *Nat. Rev. Cancer* 6: 24–37.

Voduc D., Kenney C. & Nielsen T.O. 2008. Tissue microarrays in clinical oncology. *Semin. Radiat. Oncol.* 18: 89–97.

Waldner M.J. & Neurath M.F. 2009. Colitis-associated cancer: the role of T cells in tumor development. *Semin. Immunopathol.* 31: 249–256.

Walker J.A. & McKenzie A.N.J. 2018. TH2 cell development and function. *Nat. Rev. Immunol.* 18: 121–133.

Walter V., Jansen L., Hoffmeister M. & Brenner H. 2014. Smoking and survival of colorectal cancer patients: systematic review and meta-analysis. *Ann. Oncol. Off. J. Eur. Soc. Med. Oncol.* 25: 1517–1525.

Wherry E.J. 2011. T cell exhaustion. *Nat. Immunol.* 12: 492–499.

Wilcox R.A. 2016. A three-signal model of T-cell lymphoma pathogenesis. *Am. J. Hematol.* 91: 113–122.

Wyss J., Dislich B., Koelzer V.H., Galván J.A., Dawson H., Hädrich M., Inderbitzin D., Lugli A., Zlobec I. & Berger M.D. 2019. Stromal PD-1/PD-L1 expression predicts outcome in colon cancer patients. *Clin. Colorectal Cancer* 18: e20–e38.

Yadav S., Dwivedi A. & Tripathi A. 2022. Biology of macrophage fate decision: implication in inflammatory disorders. *Cell Biol. Int.* 46: 1539–1556.

Yahaya M.A.F., Lila M.A.M., Ismail S., Zainol M. & Afizan N.A.R.N.M. 2019. Tumour-associated macrophages (TAMs) in colon cancer and how to reeducate them. *J. Immunol. Res.* 2019: 2368249.

Yamauchi M., Lochhead P., Morikawa T., Huttenhower C., Chan A.T.,

Giovannucci E., Fuchs C. & Ogino S. 2012. Colorectal cancer: a tale of two sides or a continuum? *Gut* 61: 794–797.

Yan H., Ju X., Huang A. & Yuan J. 2024. Advancements in technology for characterizing the tumor immune microenvironment. *Int. J. Biol. Sci.* 20: 2151–2167.

Yang R., Gao N., Chang Q., Meng X. & Wang W. 2019. The role of IDO, IL-10, and TGF-β in the HCV-associated chronic hepatitis, liver cirrhosis, and hepatocellular carcinoma. *J. Med. Virol.* 91: 265–271.

Ye Z., Yue L., Shi J., Shao M. & Wu T. 2019. Role of IDO and TDO in cancers and related diseases and the therapeutic implications. *J. Cancer* 10: 2771–2782.

Zamarron B.F. & Chen W. 2011. Dual roles of immune cells and their factors in cancer development and progression. *Int. J. Biol. Sci.* 7: 651–658.

Zea A.H., Rodriguez P.C., Atkins M.B., Hernandez C., Signoretti S., Zabaleta J., McDermott D., Quiceno D., Youmans A., O'Neill A., Mier J. & Ochoa A.C. 2005. Arginase-producing myeloid suppressor cells in renal cell carcinoma patients: a mechanism of tumor evasion. *Cancer Res.* 65: 3044–3048.

Zea A.H., Rodriguez P.C., Culotta K.S., Hernandez C.P., DeSalvo J., Ochoa J.B., Park H.J., Zabaleta J. & Ochoa A.C. 2004. L-Arginine modulates CD3ζ expression and T cell function in activated human T lymphocytes. *Cell. Immunol.* 232: 21–31.

Zhang J., Zou S. & Fang L. 2023. Metabolic reprogramming in colorectal cancer: regulatory networks and therapy. *Cell Biosci.* 13: 25.

Zitti B. & Bryceson Y.T. 2018. Natural killer cells in inflammation and autoimmunity. *Cytokine Growth Factor Rev.* 42: 37–46.

Zlobec I. & Lugli A. 2008. Prognostic and predictive factors in colorectal cancer. *Postgrad. Med. J.* 84: 403–411.

Zumerle S., Molon B. & Viola A. 2017. Membrane rafts in T cell activation: a spotlight on CD28 costimulation. *Front. Immunol.* 8: 1467.

ORIGINAL PUBLICATIONS

I

PROGNOSTIC SIGNIFICANCE OF SPATIAL AND DENSITY ANALYSIS OF T LYMPHOCYTES IN COLORECTAL CANCER

by

Elomaa H, Ahtiainen M, Väyrynen SA, Ogino S, Nowak JA, Friman M, Helminen O, Wirta EV, Seppälä T, Böhm J, Mäkinen MJ, Mecklin JP, Kuopio T, Väyrynen JP.
2022

British Journal of Cancer 127: 514–523.

https://doi.org/10.1038/s41416-022-01822-6

British Journal of Cancer www.nature.com/bjc

ARTICLE OPEN

Check for updates

Clinical Studies

Prognostic significance of spatial and density analysis of T lymphocytes in colorectal cancer

Hanna Elomaa[1,2], Maarit Ahtiainen[3], Sara A. Väyrynen[4], Shuji Ogino[5,6,7,8], Jonathan A. Nowak[5], Marjukka Friman[3], Olli Helminen[9], Erkki-Ville Wirta[10], Toni T. Seppälä[11,12], Jan Böhm[3], Markus J. Mäkinen[13], Jukka-Pekka Mecklin[2,14], Teijo Kuopio[1,3] and Juha P. Väyrynen[13]✉

BACKGROUND: Although high T cell density is a strong favourable prognostic factor in colorectal cancer, the significance of the spatial distribution of T cells is incompletely understood. We aimed to evaluate the prognostic significance of tumour cell-T cell co-localisation and T cell densities.

METHODS: We analysed CD3 and CD8 immunohistochemistry in a study cohort of 983 colorectal cancer patients and a validation cohort ($N = 246$). Individual immune and tumour cells were identified to calculate T cell densities (to derive T cell density score) and G-cross function values, estimating the likelihood of tumour cells being co-located with T cells within 20 µm radius (to derive T cell proximity score).

RESULTS: High T cell proximity score associated with longer cancer-specific survival in both the study cohort [adjusted HR for high (vs. low) 0.33, 95% CI 0.20–0.52, $P_{trend} < 0.0001$] and the validation cohort [adjusted HR for high (vs. low) 0.15, 95% CI 0.05–0.45, $P_{trend} < 0.0001$] and its prognostic value was independent of T cell density score.

CONCLUSIONS: The spatial point pattern analysis of tumour cell-T cell co-localisation could provide detailed information on colorectal cancer prognosis, supporting the value of spatial measurement of T cell infiltrates as a novel, robust tumour-immune biomarker.

British Journal of Cancer; https://doi.org/10.1038/s41416-022-01822-6

BACKGROUND

Colorectal cancer is the third most common cancer, covering around 10% of all new cancer cases worldwide [1]. The tumour microenvironment is composed of neoplastic tumour cells and non-neoplastic cells, such as host immune cells, interacting through cell–cell contacts and inflammatory mediators [2]. The assessment of colorectal cancer prognosis and treatment is mainly based on evaluating neoplastic tumour cells and tumour spread rather than analysing the host immune response [3]. The most widely used clinical staging system is the American Joint Committee on Cancer/International Union Against Cancer (AJCC/UICC) TNM classification, which includes the extent of the primary tumour (T), presence of lymph node metastasis (N) and spread to distant organs (M), while World Health Organization (WHO) histologic grading categorises tumours according to their differentiation [4]. However, these methods do not entirely capture the characteristics of colorectal tumours and their prognoses.

Immunoscore® is a T cell scoring system based on computer-assisted quantification of $CD3^+$ and $CD8^+$ cell densities in the tumour centre and the invasive margin [5, 6]. T cell density varies within a single tumour and between different tumours. The density is generally higher in the invasive margin than in the centre of the tumour. In mismatch repair (MMR)-deficient colorectal cancers, T cell densities are also usually higher than in MMR proficient tumours [7, 8]. High Immunoscore® has been associated with better prognosis and has been internationally validated as an independent prognostic parameter in a cohort of more than 2600 disease stage I–III colorectal cancer cases [6]. However, most studies evaluating immune cell infiltrates in colorectal cancer have

[1]Department of Biological and Environmental Science, University of Jyväskylä, Jyväskylä, Finland. [2]Department of Education and Research, Central Finland Health Care District, Jyväskylä, Finland. [3]Department of Pathology, Central Finland Health Care District, Jyväskylä, Finland. [4]Department of Internal Medicine, Oulu University Hospital, Oulu, Finland. [5]Program in MPE Molecular Pathological Epidemiology, Department of Pathology, Brigham and Women's Hospital and Harvard Medical School, Boston, MA, USA. [6]Department of Epidemiology, Harvard T.H. Chan School of Public Health, Boston, MA, USA. [7]Broad Institute of MIT and Harvard, Cambridge, MA, USA. [8]Cancer Immunology and Cancer Epidemiology Programs, Dana-Farber Harvard Cancer Center, Boston, MA, USA. [9]Surgery Research Unit, Cancer and Translational Medicine Research Unit, Medical Research Center Oulu, Oulu University Hospital, and University of Oulu, Oulu, Finland. [10]Department of Gastroenterology and Alimentary Tract Surgery, Tampere University Hospital, Tampere, Finland. [11]Department of Gastrointestinal Surgery, Helsinki University Hospital, Helsinki, Finland. [12]Applied Tumor Genomics Research Program, University of Helsinki, Helsinki, Finland. [13]Cancer and Translational Medicine Research Unit, Medical Research Center Oulu, Oulu University Hospital, and University of Oulu, Oulu, Finland. [14]Faculty of Sport and Health Sciences, University of Jyväskylä, Jyväskylä, Finland. ✉email: juha.vayrynen@oulu.fi

Received: 7 January 2022 Revised: 31 March 2022 Accepted: 4 April 2022
Published online: 21 April 2022

Published on Behalf of CRUK

been limited to density-based analyses [9] and the significance of the co-localisation between tumour cells and T cells is not well-established.

In this study, we used immunohistochemistry and digital image analysis to identify $CD3^+$ and $CD8^+$ cells and tumour cells in 1229 colorectal cancer samples, including a study cohort of 983 patients and an independent validation cohort of 246 cases. We present the T cell proximity score as a novel prognostic parameter based on the evaluation of co-localisation of tumour cells with T cells. Our primary aim was to evaluate the prognostic value of the T cell proximity score and compare it to that of the T cell density score (based on the principles of Immunoscore®). We hypothesised that a high T cell proximity score (high likelihood of tumour cells being co-located with T cells) might be associated with favourable outcome. As secondary aims, we investigated the associations of T cell proximity score with tumour and patient characteristics and the prognostic significance of spatial T cell proximity measurements separately in the tumour centre and the invasive margin, in MMR proficient and MMR deficient tumour subgroups as well as in low and high disease stage tumours.

METHODS

Patients

We identified 1343 patients who underwent resection for colorectal cancer at Central Finland Central Hospital between January 1, 2000 and December 31, 2015 and had adequate tumour samples available. The samples were retrospectively collected from the pathology registry of Central Finland Central Hospital, which covers all colorectal cancers diagnosed in Central Finland (the population of the area-averaged around 270,000 during the study period) [10]. Associated clinical data were collected from clinical patient records by study physicians. We excluded patients who died within 30 days after surgery ($N = 40$) or received any preoperative oncological treatments (radiotherapy, chemotherapy or chemoradiotherapy) ($N = 243$) due to their potential influences on tumour characteristics [11]. The final cohort with adequate samples in tissue microarrays and successful quantification of $CD3^+$ and $CD8^+$ cells included 983 patients. The median follow-up time for censored was 9.3 years (IQR 6.8–13.3 years). The main clinicopathologic features of the cases are shown in Table 1. Histological tumour parameters were re-evaluated by the study pathologist (J.P.V.), including tumour differentiation and lymphovascular invasion, using hematoxylin and eosin (H&E) stained whole slides. All the histological analyses were performed blinded to the clinical data.

Tissue microarrays

For tissue microarray construction, we selected one representative formalin-fixed paraffin-embedded tumour sample with the deepest cancer invasion for each patient. The arrays were constructed using a TMA Master II tissue microarrayer (3DHistech Ltd., Budapest, Hungary), and they included two 1 mm-diameter cores from representative areas of the tumour centre and the invasive margin (total: four cores). The core sites were annotated to best represent overall tumour morphology while avoiding necrosis. The invasive margin cores were targeted to span 500 µm into the healthy tissue and 500 µm into the tumour. In total, the cohort included 25 tissue microarray blocks, each containing two tonsil cores as staining controls. Tissue microarray blocks were tempered overnight at 60 °C and cut at 3.5 µm thickness.

Immunohistochemistry

The samples were screened for DNA mismatch repair (MMR) deficiency with MLH1, MSH2, MSH6 and PMS2 immunohistochemistry and for *BRAF* V600E mutation status with immunohistochemistry [12]. Immunohistochemistry for T cells and MMR genes were performed by BOND-III automated IHC stainer (Leica Biosystems, Buffalo Grove, IL, USA) with monoclonal antibodies and protocols shown in Table S1. All antibodies were in clinical use in the pathology laboratory of Central Finland Central Hospital, and appropriate staining was also confirmed by examining positive and negative controls. After bake, dewax and peroxide block, slides were processed with heat-induced antigen retrieval with EDTA-based buffer, pH 9.0 (BOND Epitope retrieval solution 2, Leica Biosystems, AR9640) at 100 °C. Antigen retrieval time was 30 min for MLH1, MSH2, MSH6 and PMS2 and 20 min for CD3 and CD8. Primary antibodies were incubated for 30 min. Visualisation was performed according to the manufacturer's instructions using a BOND Polymer Refine Detection kit (Leica Biosystems, DS9800) with a horseradish peroxidase-conjugated secondary antibody (<25 µg/ml), 3.3-diaminobenzidine chromogen and hematoxylin (0.1%) counterstain. Stained slides were coverslipped with a Tissue-Tek Glas Automated Glass Coverslipper (Sakura) and digitalised with a NanoZoomer-XR (Hamamatsu Photonics, Hamamatsu City, Japan) slide scanner with a ×20 objective.

Immunohistochemistry to evaluate *BRAF* V600E mutation status was conducted using a BenchMark XT immunostainer (Ventana Medical Systems, Tucson, AZ) and a BRAF V600E mutation-specific mouse monoclonal antibody (clone: VE1, Spring Bioscience, Pleasonton, CA, US, dilution: 1:400). The amplification was done with OptiView Amplification (Ventana [13]).

Image analysis

T cell analyses were conducted with supervised machine learning approaches built-in QuPath (version 0.2.3), an open-source bioimage analysis software [14], using previously validated algorithms [15]. The software was trained to recognise tissue and cell types by manually annotating representative areas/cells. The identification of tissue from the background was done with the random forests *pixel classifier*. Cells were detected and classified into tumour cells, T cells, and other cells using the random forests *object classifier*. T cells were recognised by CD3 or CD8 expression and tumour cells were identified through their morphology. The remaining cells were classified as other. The workflow for image analysis is shown in Fig. S1. We confirmed the validity of the automated cell classifier by reviewing the classification result images. We further quantified the accuracy of the classifier by manually annotating each cell in 50 tumour regions (25 stained for CD3 and 25 stained for CD8; size 200 × 200 µm) and comparing the cell densities observed in these regions with those obtained with the automated classifier using the Spearman's rank correlation test.

All tissue microarray cores were reviewed, and those with folding or detaching during processing, minimal amount or absence of tumour, or high amount of necrosis were excluded from the analyses. For the final analyses, we included only cases that at least one representative successfully analysed the tumour core from the tumour centre and the invasive margin for both CD3 and CD8. For each tissue microarray core, we calculated $CD3^+$ and $CD8^+$ cell densities by dividing the cell counts by the tumour core area in mm^2. For tumours with multiple successfully analysed tumour centre cores or invasive margin cores, we calculated mean cell densities. As a result, each tumour had one density value for (1) $CD3^+$ cells in the tumour centre, (2) $CD3^+$ cells in the invasive margin, (3) $CD8^+$ cells in the tumour centre and (4) $CD8^+$ cells in the invasive margin.

To calculate the T cell density score, we followed the main principles of the Immunoscore assay [6]. The densities of $CD3^+$ cells in the tumour centre, $CD3^+$ cells in the invasive margin, $CD8^+$ cells in the tumour centre and $CD8^+$ cells in the invasive margin were converted to percentiles (0–100), which resulted in four separate percentile values for each tumour. T cell density score was determined by calculating the mean of the four percentiles and categorising it to low (0–25), intermediate (>25–70) or high (>70–100). The workflow for T cell density score analysis is shown in Fig. 1.

In this study, we introduced the T cell proximity score as a new prognostic parameter based on tumour cell-T cell co-localisation. We estimated the empirical G-cross [$G_{tumour:T\ cell}$ (r)] function for each sample, evaluating the likelihood of any tumour cell in the sample having at least one T cell at a specific radius r. The function is formed by measuring the distances from each tumour cell centroid to the closest immune cell centroid. Thus, higher G-cross function values result from a higher percentage of tumour cells harbouring T cells in their proximity and indicate greater co-localisation of tumour cells with T cells. We chose to examine the function values at 20 µm radius to identify T cell populations likely capable of effective, direct, cell-to-cell interaction with tumour cells, consistent with previous reports [15–18]. We applied the Kaplan–Meier correction for edge effects. T cell proximity score was calculated using a similar approach as in T cell density score. We calculated G-cross [$G_{tumour:T\ cell}$ (20 µm)] function values for $CD3^+$ and $CD8^+$ cells in the tumour centre and in the invasive margin and converted these four values into percentiles. To determine the T cell proximity score for each tumour, we calculated the mean of the four percentiles and categorised it into low (0–25), intermediate (>25–70) or high (>70–100). In sensitivity analysis, we tested the T cell proximity score at G-cross function radii of 10, 30, 40, 50, 100 and 500 µm. The workflow for the proximity score analysis for two example cores of the same tumour is shown in Fig. 1. Figure S2

Table 1. Demographic and clinicopathologic characteristics of colorectal cancer cases according to T cell proximity score.

		T cell proximity score			
Characteristic	**Total *N***	**Low**	**Intermediate**	**High**	***P***
All cases	983 (100%)	194 (20%)	545 (55%)	244 (25%)	
Sex					0.65
Female	481 (49%)	96 (49%)	260 (48%)	125 (51%)	
Male	502 (51%)	98 (51%)	285 (52%)	119 (49%)	
Age (years)					0.17
<65	265 (27%)	57 (29%)	142 (26%)	66 (27%)	
65–75	348 (35%)	58 (30%)	211 (39%)	79 (32%)	
>75	370 (38%)	79 (41%)	192 (35%)	99 (41%)	
Year of operation					0.26
2000–2005	299 (30%)	60 (31%)	153 (28%)	86 (35%)	
2006–2010	315 (32%)	65 (34%)	183 (34%)	67 (28%)	
2011–2015	369 38%)	69 (36%)	209 (38%)	91 (37%)	
Tumour location					0.0003
Proximal colon	478 (49%)	82 (42%)	249 (46%)	147 (60%)	
Distal colon	359 (40%)	83 (43%)	214 (39%)	62 (25%)	
Rectum	146 (15%)	29 (15%)	82 (15%)	35 (14 %)	
AJCC disease stage					<0.0001
I	162 (16%)	19 (10%)	84 (15%)	59 (24%)	
II	371 (38%)	62 (32%)	193 (35%)	116 (48%)	
III	322 (33%)	80 (41%)	186 (34%)	56 (23%)	
IV	128 (13%)	33 (17%)	82 (15%)	13 (5.3%)	
Tumour grade					0.061
Low-grade (well to moderately differentiated)	813 (83%)	166 (86%)	457 (84%)	190 (78%)	
High-grade (poorly differentiated)	170 (17%)	28 (14%)	88 (16%)	54 (22%)	
Lymphovascular invasion					<0.0001
No	772 (79%)	132 (68%)	423 (78%)	217 (89%)	
Yes	211 (21%)	62 (32%)	122 (22%)	17 (11%)	
MMR status					<0.0001
MMR proficient	833 (85%)	184 (95%)	485 (89%)	164 (67%)	
MMR deficient	150 (15%)	10 (5.2%)	60 (11%)	80 (33%)	
BRAF status					<0.0001
Wild-type	824 (84%)	177 (91%)	469 (86%)	178 (73%)	
Mutant	159 (16%)	17 (8.8%)	76 (14 %)	66 (27%)	

AJCC American Joint Committee on Cancer, *MMR* mismatch repair.

represents the respective analysis for the two remaining cores of the example tumour.

Validation cohort

For validation, we retrospectively analysed an independent, previously described colorectal cancer cohort operated at Oulu University Hospital from 2006 to 2014 [19]. Patients with preoperative treatment and unsuccessful $CD3^+$ or $CD8^+$ cell analysis were excluded, and the final data included 246 patients. The median follow-up time for censored cases was 6.2 years (IQR 5.0–7.6 years). Analyses were conducted for one to four 3 mm-diameter TMA cores per patient [19]. Antibodies and staining protocols are shown in Table S2. The densities and G-cross function values were compared with those obtained in the study cohort to convert them into percentiles.

Statistical analyses

Statistical analyses were performed using RStudio (version 1.3.1093) and R statistical programming (version 4.0.5, R Core Team) with packages *gmodels* (2.18.1), *spatstat* (2.1-0), *survival* (3.2-7), *survminer* (0.4.9) and *tidyverse* (1.3.0).

Categorical data were analysed by cross-tabulation of T cell scores and other variables and using Chi-square test to evaluate the statistical significance. Kaplan–Meier method was used for visualising the cumulative survival probabilities, and the comparison between categories was done with the Log-rank test. As our primary analyses, we utilised univariable and multivariable Cox proportion hazard regression to estimate mortality hazard ratio (HR) point estimates and their 95% confidence intervals (CIs). Cancer-specific survival was evaluated as the primary endpoint, and it was defined as the time from surgery to cancer death. Overall survival was evaluated as the secondary endpoint, and it was defined as the time between colorectal cancer surgery and death. We limited the follow-up to 10 years, considering that most colorectal cancer deaths occur within that period. Schoenfeld residual plots supported the proportionality of hazards during most of the follow-up period up to 10 years. Multivariable models included the following pre-determined indicator variables (with the reference category listed first): sex (male, female), age (<65, 65–75, >75), year of operation (2000–2005, 2006–2010, 2011–2015), tumour location (proximal colon, distal colon, rectum), disease stage (I–II, III, IV), tumour grade (well/moderately differentiated, poorly differentiated), lymphovascular invasion (negative, positive), MMR status (proficient, deficient), *BRAF* status (wild-type, mutant). Cases with missing data (validation cohort only) were included in the majority

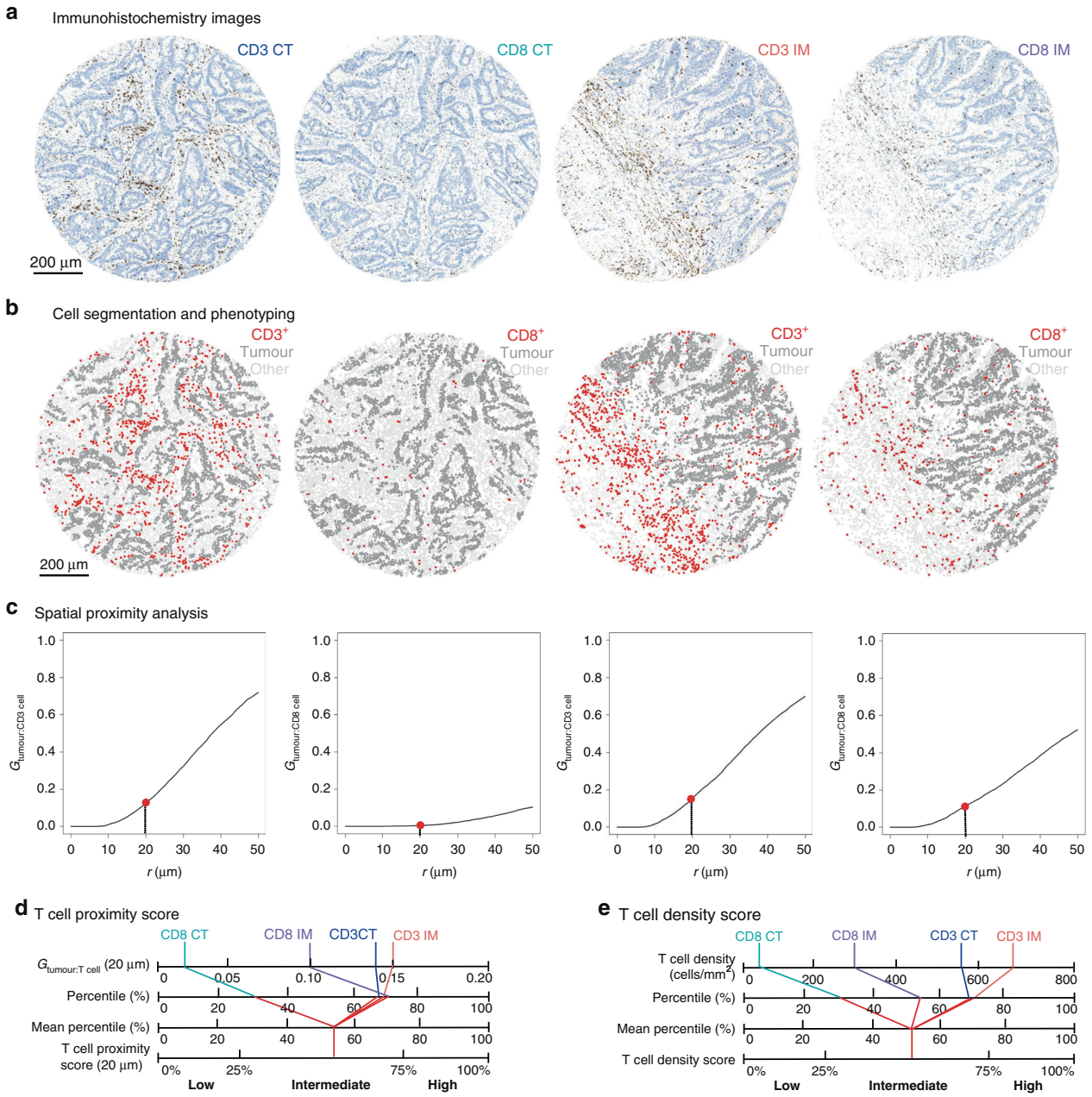

Fig. 1 T cell proximity and density score analyses in colorectal cancer. The figure shows analysis steps for one example tumour core from the tumour centre (CT) and the invasive margin (IM). Tumour cores stained with CD3 and CD8 (**a**) and corresponding phenotyping maps for T cells, tumour cells and other cells (**b**). G-cross ($G_{tumour:T\ cell}$) function curves, representing the likelihood of any tumour cell in the sample being co-located with at least one $CD3^+$/$CD8^+$ T cell within a radius r (**c**). Calculation charts for T cell proximity score (**d**) and for T cell density score (**e**). Respective example images for two remaining cores of the same sample are shown in Fig. S2.

category of a given categorical covariate to limit the degrees of freedom. The following covariates had missing values in the validation cohort: disease stage (0.4% missing), differentiation (0.4% missing), lymphovascular invasion (1.2% missing), MMR status (0.4% missing). Excluding those missing cases in each covariate did not substantially alter results. We used a stringent alpha level of 0.005 according to the recommendation of an expert panel [20].

RESULTS

Patient characteristics

We analysed T cell infiltrates in tumour samples of 983 colorectal cancer patients. Of the patients, 481 (49%) were women and the median age at the time of surgery was 72 years (range 36–100 years). The most prevalent site for the primary tumour was the proximal colon (cecum to transverse colon) with 478 (49%) cases. MMR deficiency was detected in 150 (15%) tumours (Table 1).

Cell analysis of tissue microarray cores

We successfully analysed a total of 2,351,513 $CD3^+$ cells from 3632 tissue microarray cores and 1,105,424 $CD8^+$ cells from 3608 tissue microarray cores. The average number of analysed cores was 3.7 per patient for both CD3 and CD8. Core-to-core correlations for G-cross ($G_{tumour:T\ cell}$) function values at 20 µm radius were 0.69 for

$CD3^+$ cells in the tumour centre 0.70 for $CD3^+$ cells in the invasive margin, 0.69 for $CD8^+$ cells in the tumour centre and 0.70 for $CD8^+$ cells for the invasive margin (Fig. S3), being slightly higher than the respective core-to-core correlations for T cell densities (Fig. S4).

We tested the accuracy of machine-learning-based image analysis by manually annotating all cells (T cells, tumour cells and other cells) in 50 tumour images and then applying the optimised automated classifier to these images. The total number of detected cells was 11,312 in manual counting and 12,097 in automated cell counting. The Spearman's rank correlations coefficient between automated and manual cell densities was 0.94 for T cells, 0.87 for tumour cells and 0.86 for other cells, indicating that the classifier had reached good accuracy (Fig. S5).

T cell proximity and density score

T cell proximity score was calculated based on tumour cell-T cell co-localisation measurements, using $G_{tumour:T\ cell}$ function values at 20 µm (Fig. 1). Examples of tissue microarray cores with distinct T cell infiltration patterns and corresponding G-cross function curves are shown in Fig. S6. Of the patients, 545 (55%) cases were classified as intermediate for the proximity score, whereas low covered 20% and high covered 25% of the cases. High T cell proximity score was strongly associated with proximal tumour location ($P = 0.0003$), low disease stage, absence of lymphovascular invasion, MMR deficiency and *BRAF* mutation (all $P < 0.0001$; Table 1).

T cell density score was calculated based on the mean $CD3^+$ and $CD8^+$ cell densities in the tumour centre and the invasive margin according to the principles of Immunoscore® (Fig. 1). Like the proximity score, high density score was associated with proximal tumour location ($P = 0.003$), low disease stage ($P = 0.0002$), absence of lymphovascular invasion ($P = 0.0004$), MMR deficiency ($P < 0.0001$) and *BRAF* mutation ($P = 0.001$; Table S3).

Survival analyses

In total, there were 574 (58%) deaths including 278 (28%) colorectal cancer deaths. The 5-year and 10-year cancer-specific survival rates were 74% and 69% and overall survival rates were 61% and 46%, respectively.

Our primary aim was to evaluate the prognostic significance of the T cell proximity score and compare it to that of the T cell density score. High proximity and density scores predicted improved outcomes compared to low scores. The 10-year cancer-specific survival for patients with high and low proximity scores were 88% and 48%, respectively (Fig. 2, Table 2). High T cell proximity and density scores were associated with better cancer-specific and overall survival both in univariable and multivariable analyses. In cancer-specific survival analysis, the multivariable HR for high (vs. low) T cell proximity score was 0.33 (95% CI 0.20–0.52, $P_{trend} < 0.0001$) and for high (vs. low) density score 0.47 (95% CI 0.31–0.73, $P_{trend} = 0.0007$) (Table 2, Table S4).

To directly compare the prognostic value of T cell proximity and density scores for cancer-specific survival, we included these variables in the same multivariable Cox regression model for reciprocal adjustment (Table 3). This analysis indicated that the prognostic significance of the proximity score ($P_{trend} = 0.001$) was independent of the density score ($P_{trend} = 0.75$).

Of the proximity score high cases ($N = 244$), 179 (73%) cases were high and 65 (27%) were intermediate for the density score. Of the proximity score low cases ($N = 196$), 121 (62%) were low and 75 (38%) were intermediate for the density score. We categorised the tumours into four subgroups to evaluate the combined prognostic effect of the proximity and density scores (Fig. S7, Table S5). This analysis further indicated that a high T cell proximity score was associated with better survival regardless of the density score.

In secondary analyses, we evaluated the survival associations of the four components ($CD3^+$ and $CD8^+$ cells in the tumour centre and the invasive margin) of T cell proximity [($G_{tumour:T\ cell}$) at a 20 µm radius] and density scores as ordinal quartile categories (Table 4, Fig. S8). In this analysis, higher values in all four components of both T cell proximity and T cell density score, except $CD8^+$ cell density in the tumour centre, were statistically significantly associated with longer cancer-specific survival (all $P_{trend} < 0.005$). The HR point estimates suggested stronger survival associations for the measurements based on the invasive margin, as compared to the tumour centre, and for the G-cross proximity estimates, as compared to the densities.

For sensitivity analysis, modified T cell proximity scores were derived from $G_{tumour:T\ cell}$ function values at different radii (10–50, 100 and 500 µm) (Table S6). Univariable and multivariable Cox regression models for cancer-specific survival indicated strong prognostic associations for the proximity scores at 10–50 µm and 100 µm radii (all $P_{trend} < 0.0001$), but not at 500 µm radius ($P_{trend} = 0.22$). These results support the significance of tumour cell-T cell co-localisation within radii of 10–100 µm.

To further evaluate factors potentially influencing the prognostic significance of the T cell proximity score, we investigated the prognostic effect of the proximity score in MMR proficient and deficient tumour subgroups, as well as in different disease stages. The association between a higher T cell proximity score and longer cancer-specific survival did not significantly differ by MMR status ($P_{interaction} = 0.69$) (Table S7), while a higher T cell proximity score was associated with longer cancer-specific survival in stages I–III but not in stage IV ($P_{interaction} < 0.0001$) (Fig. S9, Tables S8, S9).

Validation cohort

We analysed an independent validation cohort of 246 patients. The clinicopathologic features for the validation cohort ($N = 246$) are shown in Table S10. High T cell proximity score was associated with low disease stage ($P < 0.0001$), absence of lymphovascular invasion ($P = 0.0002$), MMR deficiency ($P < 0.0001$) and *BRAF* mutation ($P = 0.0002$).

In total, there were 80 (33%) deaths including 58 (24%) colorectal cancer deaths. In this cohort, T cell proximity score was associated with longer cancer-specific survival [multivariable HR for high (vs. low) 0.15, 95% CI 0.05–0.45, $P_{trend} < 0.0001$; Table S11]. As in the main cohort, the prognostic association of the proximity score was independent of the density score (Table S12).

DISCUSSION

We investigated the spatial distribution and density of $CD3^+$ and $CD8^+$ cells in a large, population-based cohort of 983 colorectal cancer patients and an independent validation cohort of 246 colorectal cancer cases. T cell density is a well-established favourable prognostic parameter in colorectal cancer [9], but relatively few studies [15–18, 21–24] have investigated the role of the spatial organisation of immune cell infiltrates in cancer. G-cross function has been previously used for analyzing the spatial interactions of T cells and tumour cells in primary tumours [15, 17] and in liver metastases [22] of colorectal cancer, in non-small cell lung cancer [16] and in pancreatic cancer [18]. In this study, we utilised CD3 and CD8 immunohistochemistry and quantified G-cross ($G_{tumour:T\ cell}$) function values at 20 µm radius at the invasive margin and tumour centre and established T cell proximity score as a new, reproducible system for analyzing the co-localisation of tumour cells with T cells. Our main finding was that a high T cell proximity score was associated with favourable outcomes independent of potential confounding factors such as disease stage and MMR status, as well as T cell density score. We envision that the method would be applicable to the analysis of a variety of other solid tumours and could be used as a quantitative

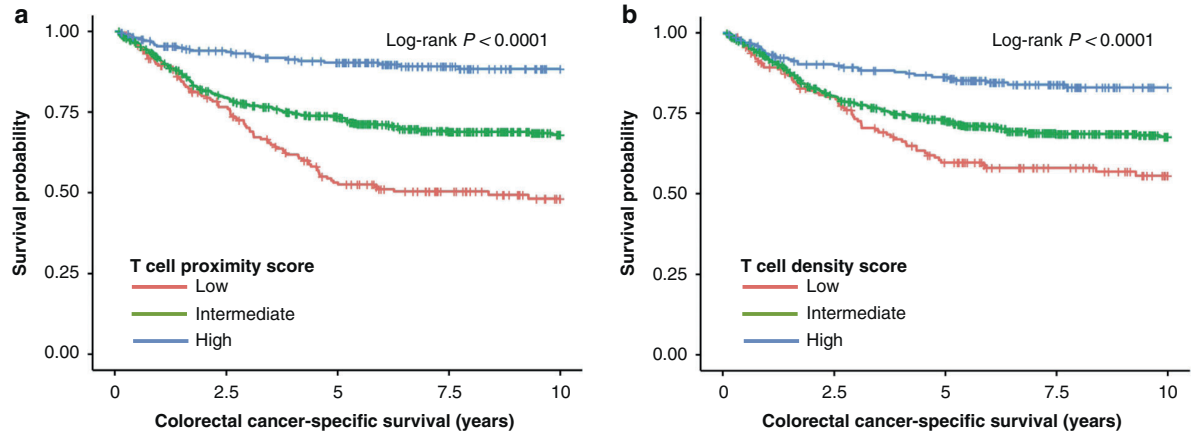

	Years, number at risk				
	0	2.5	5	7.5	10
Low	194	133	84	57	33
Intermediate	545	402	326	223	138
High	244	205	185	121	88

	Years, number at risk				
	0	2.5	5	7.5	10
Low	163	119	80	56	35
Intermediate	596	437	352	236	151
High	224	184	163	109	73

Fig. 2 Kaplan-Meier estimates of colorectal cancer-specific survival. Kaplan–Meier cancer-specific survival curves for T cell proximity score (**a**) and T cell density score (**b**). Log-rank test was used to estimate the statistical significance.

Table 2. Univariable and multivariable Cox regression models for cancer-specific survival and overall survival according to T cell proximity score and T cell density score.

		Colorectal cancer-specific survival			Overall survival		
	No. of cases	No. of events	Univariable HR (95% CI)	Multivariable HR (95% CI)	No. of events	Univariable HR (95% CI)	Multivariable HR (95% CI)
T cell proximity score							
Low	194	88	1 (referent)	1 (referent)	127	1 (referent)	1 (referent)
Intermediate	545	157	0.57 (0.44–0.75)	0.72 (0.55–0.94	269	0.66 (0.53–0.81)	0.74 (0.59–0.91)
High	244	25	0.18 (0.12–0.29)	0.33 (0.20–0.52)	98	0.47 (0.36–0.61)	0.57 (0.43–0.76)
P_{trend}			<0.0001	<0.0001		<0.0001	0.0001
T cell density score							
Low	163	64	1 (referent)	1 (referent)	98	1 (referent)	1 (referent)
Intermediate	596	172	0.69 (0.52–0.93)	0.74 (0.55–0.99)	302	0.78 (0.62–0.99)	0.78 (0.62–0.99)
High	224	34	0.34 (0.22–0.51)	0.47 (0.31–0.73)	94	0.59 (0.44–0.78)	0.62 (0.46–0.84)
P_{trend}			<0.0001	0.0007		0.0002	0.002

Multivariable Cox proportional hazards regression models were adjusted for sex, age (<65, 65–75, >75), year of operation (2000–2005, 2006–2010, 2011–2015), tumour location (proximal colon, distal colon, rectum), disease stage (I–II, III, IV), tumour grade (well/moderately differentiated, poorly differentiated), lymphovascular invasion (negative, positive), MMR status (proficient, deficient), *BRAF* status (wild-type, mutant).
P_{trend} values were calculated by using the three ordinal categories of T cell proximity score and T cell density score as continuous variables in univariable and multivariable Cox proportional hazard regression models.
CI confidence interval, *HR* hazard ratio.

tumour-immune biomarker, evaluating not only the density but also the spatial patterns of T cell infiltrates in the tumour.

Our findings were consistent with a recent study in colorectal cancer, where the co-localisation of tumour cells with $CD3^+$ T cells within 20 µm radius was a stronger prognostic factor than total T cell density in the tumour microenvironment [17]. Moreover, previous studies have demonstrated that strong engagement and mixing of $CD8^+$ cytotoxic T cells with tumour cells in colorectal cancer liver metastases are associated with favourable outcomes [21, 22]. In our study of primary colorectal cancer, the prognostic value of the spatial measurements for $CD3^+$ cells was as significant as those for $CD8^+$ cells both in the tumour centre and in the invasive margin. The present study represents a comprehensive analysis of tumour cell-T cell co-localisation in two large colorectal cancer cohorts, with detailed clinicopathologic characterisation [17].

T cell proximity score, introduced in this study, specifically evaluates the co-localisation of tumour cells with T cells within 20 µm radius, ignoring T cells located further from tumour cells. In our analyses, the proximity score had a higher prognostic value

Table 3. Comparison of prognostic power of T cell proximity score and T cell density score using Cox regression models for cancer-specific survival.

	No. of cases	No. of events	Model 1 (univariable) HR (95% CI)	Model 2 (multivariable) HR (95% CI)	Model 3 (multivariable) HR (95% CI)
T cell proximity score					
Low	194	88	1 (referent)	1 (referent)	1 (referent)
Intermediate	545	157	0.57 (0.44–0.75)	0.52 (0.38–0.73)	0.75 (0.54–1.04)
High	244	25	0.18 (0.12–0.29)	0.15 (0.08–0.27)	0.32 (0.17–0.60)
P_{trend}			<0.0001	<0.0001	0.001
T cell density score					
Low	163	64	1 (referent)	1 (referent)	1 (referent)
Intermediate	596	172	0.69 (0.52–0.93)	1.15 (0.81–1.65)	0.91 (0.64–1.30)
High	224	34	0.34 (0.22–0.51)	1.33 (0.75–2.34)	1.01 (0.56–1.81)
P_{trend}			<0.0001	0.35	0.75

Model 2: Cox proportional hazards regression model including T cell proximity score and T cell density score.
Model 3: Cox proportional hazards regression model based on Model 2 that was additionally adjusted for sex, age (<65, 65–75, >75), year of operation (2000–2005, 2006–2010, 2011–2015), tumour location (proximal colon, distal colon, rectum), disease stage (I–II, III, IV), tumour grade (well/moderately differentiated, poorly differentiated), lymphovascular invasion (negative, positive), MMR status (proficient, deficient), *BRAF* status (wild-type, mutant).
P_{trend} values were calculated by using the three ordinal categories of T cell proximity score and T cell density score as continuous variables in univariable and multivariable Cox proportional hazard regression models.
CI confidence interval, *HR* hazard ratio.

than the density score. We hypothesise that this may be related to the proximity score focusing on T cells with the potential for direct cell–cell interactions with tumour cells, such as cytotoxicity [15, 16, 18, 24]. It is conceivable that distant T cells may have a reduced possibility for anti-tumoural activity compared with T cells in close tumour proximity. Moreover, a high stromal percentage predicts an unfavourable prognosis in colorectal cancer, while a low stromal percentage is associated with favourable outcomes [25, 26]. Considering that the majority of immune cells in the colorectal cancer microenvironment are located in tumour stromal rather than intraepithelial regions [15, 27, 28], the tumours with low stroma percentage might have low overall T cell densities as a result of low stromal content rather than a weak anti-tumour-immune response, while spatial point pattern analysis may still classify these tumours into higher T cell proximity score categories if T cells are located close to tumour cells. All four components of the proximity score ($CD3^+$ and $CD8^+$ cells in tumour centre and in invasive margin) had strong prognostic significance as separate variables. In addition, our sensitivity analyses showed that high G-cross ($G_{tumour:T\ cell}$) function values were associated with better prognosis within a range of radii between 10–50 µm and 100 µm, but not at 500 µm. These findings further highlight the robustness of the analysis, not dependent on a single, specific radius or component, and supports the potential of T cell proximity score as a relevant prognostic factor in colorectal cancer.

We identified the cell types with a machine-learning-based cell classifier using the QuPath software. We confirmed the adequacy of the classifier by manually viewing all result images and tested the accuracy of our cell classifier by comparing the densities of manually annotated cells and automatedly classified cells, supporting high concordance for all three cell types (T cells, tumour cells, and other cells). The machine-learning-based cell analysis for immunohistochemically stained tumour tissue samples using QuPath has also been validated in previous studies with high accuracy [15, 29, 30].

Some limitations should be considered. First, we used tissue microarrays, which may not totally represent the immunological milieu in the whole tumour [31, 32]. However, we successfully analysed on average 3.7 tumour cores for each patient, which should demonstrate relatively good concordance with the whole tumour [31]. We also observed reasonably good core-to-core correlation for both G-cross and density measurements, suggesting that T cell infiltrates can be evaluated using our tissue microarrays with reasonable accuracy. Moreover, measurement errors related to tissue microarrays would likely have a nearly random distribution, driving our findings towards the null hypothesis. Tissue microarrays also enabled staining of all samples at the same time, so the staining quality was uniform between the specimens. Second, the information on cancer treatment was lacking. Nevertheless, treatments have likely been principally based on the disease stage and MMR status rather than immune infiltrate, and we adjusted the multivariable survival models for several factors, including disease stage and MMR status. Third, we excluded all patients with preoperative treatment from analyses, which led to the under-representation of rectal cancers in these cohorts. The prognostic significance of the T cell proximity score should be interpedently evaluated in rectal cancer patients who have received neoadjuvant treatments. Fourth, although T cells play a critical role in anti-tumoural immunity, this study lacks the prognostic information of other immune cells in the tumour microenvironment. Fifth, most patients were non-Hispanic White, and the prognostic significance of the T cell proximity score should be confirmed in different populations.

There were several strengths in the study. This study included a large, thoroughly analysed study cohort [12, 33–36], as well as an independent validation cohort, which can forward the generalisability of the findings. The histological parameters were evaluated uniformly in accordance with the latest guidelines and the tumours were screened for two key molecular prognostic parameters (MMR status and *BRAF* mutation status). The machine learning assessment of immune cell infiltrates enabled uniform analysis throughout cases and spatial point pattern analyses based on positions of single cells [15]. This facilitated more detailed analyses of tumour cell-immune cell co-localisation than possible using traditional methods.

In conclusion, this study showed that the T cell proximity score, derived from G-cross measurements of co-localisation of tumour cells with T cells, was strongly associated with the survival of colorectal cancer patients, representing a new, quantitative prognostic parameter for colorectal cancer. Our results highlight the importance of the spatial context in the analysis of immune cell infiltrates in cancer and could be utilised to develop improved tumour-immune biomarkers for precision medicine.

Table 4. Univariable and multivariable Cox regression models for cancer-specific and overall survival according to G-cross ($G_{tumour:T\ cell}$) proximity function values at 20 µm radius and T cell densities.

		Colorectal cancer-specific survival			Overall survival		
	No. of cases	No. of events	Univariable HR (95% CI)	Multivariable HR (95% CI)	No. of events	Univariable HR (95% CI)	Multivariable HR (95% CI)
$CD3^+$ cell proximity							
Tumour center							
Q1	246	100	1 (referent)	1 (referent)	152	1 (referent)	1 (referent)
Q2	246	82	0.75 (0.56–1.00)	0.88 (0.65–1.18)	135	0.81 (0.64–1.02)	0.86 (0.68–1.08)
Q3	246	55	0.48 (0.34–0.67)	0.65 (0.46–0.91)	114	0.64 (0.50–0.81)	0.75 (0.58–0.96)
Q4	245	33	0.26 (0.18–0.39)	0.45 (0.30–0.68)	93	0.47 (0.36–0.61)	0.57 (0.43–0.75)
P_{trend}			<0.0001	<0.0001		<0.0001	<0.0001
Invasive margin							
Q1	246	106	1 (referent)	1 (referent)	158	1 (referent)	1 (referent)
Q2	246	91	0.84 (0.63–1.11)	0.93 (0.70–1.24)	137	0.84 (0.67–1.06)	0.88 (0.70–1.11)
Q3	246	45	0.35 (0.25–0.50)	0.61 (0.42–0.88)	94	0.48 (0.37–0.62)	0.66 (0.50–0.86)
Q4	245	28	0.22 (0.15–0.34)	0.35 (0.22–0.55)	105	0.53 (0.42–0.68)	0.62 (0.47–0.81)
P_{trend}			<0.0001	<0.0001		<0.0001	<0.0001
$CD8^+$ cell proximity							
Tumour center							
Q1	246	95	1 (referent)	1 (referent)	146	1 (referent)	1 (referent)
Q2	246	82	0.85 (0.63–1.15)	1.08 (0.80–1.46)	135	0.91 (0.72–1.14)	1.04 (0.82-1.32)
Q3	246	57	0.54 (0.39–0.75)	0.77 (0.55–1.08)	110	0.65 (0.51–0.84	0.81 (0.63–1.04)
Q4	245	36	0.33 (0.22–0.48)	0.59 (0.39–0.89)	103	0.58 (0.45–0.74)	0.75 (0.57–0.98)
P_{trend}			<0.0001	0.006		<0.0001	0.012
Invasive margin							
Q1	246	110	1 (referent)	1 (referent)	151	1 (referent)	1 (referent)
Q2	246	80	0.70 (0.53–0.94)	0.70 (0.52–0.94)	135	0.85 (0.67–1.07)	0.90 (0.71–1.14)
Q3	246	49	0.38 (0.27–0.53)	0.57 (0.40–0.82)	99	0.54 (0.42–0.70)	0.71 (0.55–0.93)
Q4	245	31	0.24 (0.16–0.35)	0.38 (0.25–0.58)	109	0.59 (0.46–0.75)	0.70 (0.53–0.91)
P_{trend}			<0.0001	<0.0001		<0.0001	0.003
$CD3^+$ cell density							
Tumour center							
Q1	246	92	1 (referent)	1 (referent)	151	1 (referent)	1 (referent)
Q2	246	85	0.88 (0.66–1.19)	1.17 (0.86–1.59)	135	0.85 (0.67–1.07)	1.14 (0.89–1.45)
Q3	246	54	0.50 (0.36–0.70)	0.71 (0.50–1.00)	105	0.58 (0.45–0.75)	0.79 (0.61–1.02)
Q4	245	39	0.31 (0.25–0.52)	0.52 (0.35–0.76)	103	0.56 (0.43–0.71)	0.67 (0.52–0.87)
P_{trend}			<0.0001	0.0001		<0.0001	0.0003
Invasive margin							
Q1	246	98	1 (referent)	1 (referent)	152	1 (referent)	1 (referent)
Q2	246	81	0.78 (0.58–1.05)	0.92 (0.68–1.24)	127	0.78 (0.61–0.98)	0.89 (0.70–1.13)
Q3	246	55	0.50 (0.36–0.69)	0.66 (0.47–0.93)	114	0.65 (0.51–0.83)	0.75 (0.58–0.96)
Q4	245	36	0.31 (0.21–0.45)	0.48 (0.32–0.71)	101	0.54 (0.42–0.69)	0.61 (0.47–0.80)
P_{trend}			<0.0001	<0.0001		<0.0001	0.0002
$CD8^+$ cell density							
Tumour center							
Q1	246	90	1 (referent)	1 (referent)	145	1 (referent)	1 (referent)
Q2	246	78	0.84 (0.62–1.13)	0.97 (0.71–1.31)	128	0.85 (0.67–1.08)	0.95 (0.74–1.20)
Q3	246	57	0.59 (0.42–0.82)	0.74 (0.52–1.04)	117	0.73 (0.57–0.93)	0.83 (0.65–1.06)
Q4	245	45	0.44 (0.31–0.63)	0.65 (0.45–0.95)	104	0.61 (0.48–0.79)	0.73 (0.56–0.95)
P_{trend}			<0.0001	0.010		<0.0001	0.011
Invasive margin							
Q1	246	105	1 (referent)	1 (referent)	155	1 (referent)	1 (referent)

Table 4. continued

		Colorectal cancer-specific survival			Overall survival		
	No. of cases	No. of events	Univariable HR (95% CI)	Multivariable HR (95% CI)	No. of events	Univariable HR (95% CI)	Multivariable HR (95% CI)
Q2	246	62	0.51 (0.37–0.69)	0.73 (0.53–1.02)	112	0.60 (0.47–0.76)	0.76 (0.59–0.97)
Q3	246	61	0.51 (0.37–0.70)	0.65 (0.47–0.90)	114	0.64 (0.50–0.81)	0.72 (0.56–0.93)
Q4	245	42	0.34 (0.24–0.49)	0.53 (0.37–0.78)	113	0.61 (0.48–0.78)	0.72 (0.56–0.94)
P_{trend}			<0.0001	0.0004		0.0003	0.013

Analyses were done separately for $CD3^+$ and $CD8^+$ cells in tumour center and in invasive margin by using ordinal quartile categories (Q1–Q4, from low to high).
Multivariable Cox proportional hazards regression models were adjusted for sex, age (<65, 65–75, >75), year of operation (2000–2005, 2006–2010, 2011–2015), tumour location (proximal colon, distal colon, rectum), disease stage (I–II, III, IV), tumour grade (well/moderately differentiated, poorly differentiated), lymphovascular invasion (negative, positive), MMR status (proficient, deficient), *BRAF* status (wild-type, mutant).
P_{trend} values were calculated by using the four ordinal categories of G-cross ($G_{tumour:T\ cell}$) proximity function values at 20 µm radius and T cell densities as continuous variables in univariable and multivariable Cox proportional hazard regression models.
CI confidence interval, *HR* hazard ratio.

DATA AVAILABILITY

The datasets generated and/or analysed during this study are not publicly available. The sharing of data will require approval from relevant ethics committees and/or biobanks. Further information including the procedures to obtain and access data of Finnish Biobanks are described at https://finbb.fi/en/fingenious-service.

REFERENCES

1. Sung H, Ferlay J, Siegel RL, Laversanne M, Soerjomataram I, Jemal A, et al. Global Cancer Statistics 2020: GLOBOCAN estimates of incidence and mortality worldwide for 36 cancers in 185 countries. CA Cancer J Clin. 2021;71:209–49.
2. Waldman AD, Fritz JM, Lenardo MJ. A guide to cancer immunotherapy: from T cell basic science to clinical practice. Nat Rev Immunol. 2020;20:651–68.
3. Bruni D, Angell HK, Galon J. The immune contexture and Immunoscore in cancer prognosis and therapeutic efficacy. Nat Rev Cancer. 2020;20:662–80.
4. Argilés G, Tabernero J, Labianca R, Hochhauser D, Salazar R, Iveson T, et al. Localised colon cancer: ESMO Clinical Practice Guidelines for diagnosis, treatment and follow-up. Ann Oncol. 2020;31:1291–305.
5. Galon J, Mlecnik B, Bindea G, Angell HK, Berger A, Lagorce C, et al. Towards the introduction of the "Immunoscore" in the classification of malignant tumours. J Pathol. 2014;232:199–209.
6. Pagès F, Mlecnik B, Marliot F, Bindea G, Ou F-S, Bifulco C, et al. International validation of the consensus Immunoscore for the classification of colon cancer: a prognostic and accuracy study. Lancet (Lond, Engl). 2018;391:2128–39.
7. Dienstmann R, Vermeulen L, Guinney J, Kopetz S, Tejpar S, Tabernero J. Consensus molecular subtypes and the evolution of precision medicine in colorectal cancer. Nat Rev Cancer. 2017;17:79–92.
8. Dahlin AM, Henriksson ML, Van Guelpen B, Stenling R, Oberg A, Rutegård J, et al. Colorectal cancer prognosis depends on T-cell infiltration and molecular characteristics of the tumor. Mod Pathol. 2011;24:671–82.
9. Alexander PG, McMillan DC, Park JH. The local inflammatory response in colorectal cancer—type, location or density? A systematic review and meta-analysis. Cancer Treat Rev. 2020;83:101949.
10. Väyrynen V, Wirta E-V, Seppälä T, Sihvo E, Mecklin J-P, Vasala K, et al. Incidence and management of patients with colorectal cancer and synchronous and metachronous colorectal metastases: a population-based study. BJS Open. 2020;4:685–92.
11. Nagtegaal ID, Marijnen CAM, Kranenbarg EK, Mulder-Stapel A, Hermans J, van de Velde CJH, et al. Short-term preoperative radiotherapy interferes with the determination of pathological parameters in rectal cancer. J Pathol. 2002;197:20–7.
12. Seppälä TT, Böhm JP, Friman M, Lahtinen L, Väyrynen VMJ, Liipo TKE, et al. Combination of microsatellite instability and BRAF mutation status for subtyping colorectal cancer. Br J Cancer. 2015;112:1966–75.
13. Thiel A, Heinonen M, Kantonen J, Gylling A, Lahtinen L, Korhonen M, et al. BRAF mutation in sporadic colorectal cancer and Lynch syndrome. Virchows Arch. 2013;463:613–21.
14. Bankhead P, Loughrey MB, Fernández JA, Dombrowski Y, McArt DG, Dunne PD, et al. QuPath: Open source software for digital pathology image analysis. Sci Rep. 2017;7:16878.
15. Väyrynen JP, Lau MC, Haruki K, Väyrynen SA, Dias Costa A, Borowsky J, et al. Prognostic significance of immune cell populations identified by machine learning in colorectal cancer using routine hematoxylin and eosin-stained sections. Clin Cancer Res. 2020;26:4326–38.
16. Barua S, Fang P, Sharma A, Fujimoto J, Wistuba I, Rao AUK, et al. Spatial interaction of tumor cells and regulatory T cells correlates with survival in non-small cell lung cancer. Lung Cancer. 2018;117:73–9.
17. Väyrynen JP, Haruki K, Lau MC, Väyrynen SA, Ugai T, Akimoto N, et al. Spatial organization and prognostic significance of NK and NKT-like cells via multimarker analysis of the colorectal cancer microenvironment. Cancer Immunol Res. 2021;10:215–28.
18. Carstens JL, Correa de Sampaio P, Yang D, Barua S, Wang H, Rao A, et al. Spatial computation of intratumoral T cells correlates with survival of patients with pancreatic cancer. Nat Commun. 2017;8:15095.
19. Väyrynen JP, Tuomisto A, Väyrynen SA, Klintrup K, Karhu T, Mäkelä J, et al. Preoperative anemia in colorectal cancer: relationships with tumor characteristics, systemic inflammation, and survival. Sci Rep. 2018;8:1–11.
20. Benjamin DJ, Berger JO, Johannesson M, Nosek BA, Wagenmakers E-J, Berk R, et al. Redefine statistical significance. Nat Hum Behav. 2018;2:6–10.
21. Lazarus J, Maj T, Smith JJ, Perusina Lanfranca M, Rao A, D'Angelica MI, et al. Spatial and phenotypic immune profiling of metastatic colon cancer. JCI insight. 2018;3:e121932.
22. Lazarus J, Oneka MD, Barua S, Maj T, Lanfranca MP, Delrosario L, et al. Mathematical modeling of the metastatic colorectal cancer microenvironment defines the importance of cytotoxic lymphocyte infiltration and presence of PD-L1 on antigen presenting cells. Ann Surg Oncol. 2019;26:2821–30.
23. Berthel A, Zoernig I, Valous NA, Kahlert C, Klupp F, Ulrich A, et al. Detailed resolution analysis reveals spatial T cell heterogeneity in the invasive margin of colorectal cancer liver metastases associated with improved survival. Oncoimmunology. 2017;6:e1286436.
24. Wang M, Huang Y-K, Kong JC, Sun Y, Tantalo DG, Yeang HXA, et al. High-dimensional analyses reveal a distinct role of T-cell subsets in the immune microenvironment of gastric cancer. Clin Transl Immunol. 2020;9:e1127.
25. van Pelt GW, Kjær-Frifeldt S, van Krieken JHJM, Al Dieri R, Morreau H, Tollenaar RAEM, et al. Scoring the tumor-stroma ratio in colon cancer: procedure and recommendations. Virchows Arch. 2018;473:405–12.
26. Eriksen AC, Sørensen FB, Lindebjerg J, Hager H, dePont Christensen R, Kjær-Frifeldt S, et al. The prognostic value of tumour stroma ratio and tumour budding in stage II colon cancer. A nationwide population-based study. Int J Colorectal Dis. 2018;33:1115–24.
27. Väyrynen JP, Haruki K, Väyrynen SA, Lau MC, Dias Costa A, Borowsky J, et al. Prognostic significance of myeloid immune cells and their spatial distribution in the colorectal cancer microenvironment. J Immunother Cancer. 2021;9:e002297.
28. Yoo S-Y, Park HE, Kim JH, Wen X, Jeong S, Cho N-Y, et al. Whole-slide image analysis reveals quantitative landscape of tumor-immune microenvironment in colorectal cancers. Clin Cancer Res. 2020;26:870–81.
29. Loughrey MB, Bankhead P, Coleman HG, Hagan RS, Craig S, McCorry AMB, et al. Validation of the systematic scoring of immunohistochemically stained tumour tissue microarrays using QuPath digital image analysis. Histopathology. 2018;73:327–38.
30. Bankhead P, Fernández JA, McArt DG, Boyle DP, Li G, Loughrey MB, et al. Integrated tumor identification and automated scoring minimizes pathologist involvement and provides new insights to key biomarkers in breast cancer. Lab Invest. 2018;98:15–26.

31. Voduc D, Kenney C, Nielsen TO. Tissue microarrays in clinical oncology. Semin Radiat Oncol. 2008;18:89–97.
32. Giltnane JM, Rimm DL. Technology insight: identification of biomarkers with tissue microarray technology. Nat Clin Pract Oncol. 2004;1:104–11.
33. Ahtiainen M, Wirta E-V, Kuopio T, Seppälä T, Rantala J, Mecklin J-P, et al. Combined prognostic value of CD274 (PD-L1)/PDCDl (PD-1) expression and immune cell infiltration in colorectal cancer as per mismatch repair status. Mod Pathol. 2019;32:866–83.
34. Porkka N, Lahtinen L, Ahtiainen M, Böhm JP, Kuopio T, Eldfors S, et al. Epidemiological, clinical and molecular characterization of Lynch-like syndrome: a population-based study. Int J Cancer. 2019;145:87–98.
35. Wirta E-V, Seppälä T, Friman M, Väyrynen J, Ahtiainen M, Kautiainen H, et al. Immunoscore in mismatch repair-proficient and -deficient colon cancer. J Pathol Clin Res. 2017;3:203–13.
36. Kellokumpu I, Kairaluoma M, Mecklin J-P, Kellokumpu H, Väyrynen V, Wirta E-V, et al. Impact of age and comorbidity on multimodal management and survival from colorectal cancer: a population-based study. J Clin Med. 2021;10:1751.

AUTHOR CONTRIBUTIONS

Conceptualisation: HE, SO, JAN, JB, TK, JPV. Data curation: HE, MA, OH, E-VW, TTS, JB, MJM, JPM, JPV. Funding acquisition: MJM, JPM, JPV. Investigation: HE, MA, SAV, MF, OH, E-VW, TTS, JB, MJM, JPM, JPV. Methodology: HE, SAV, SO, JAN, MF, JPV. Formal analysis: HE, JPV. Resources: MJM, JB, JPM, TK, JPV. Supervision: TK, JPV. Visualisation: HE, SAV, JPV. Writing—original draft: HE, JPV. Writing—review and editing: All authors.

FUNDING

This study was funded by Cancer Foundation Finland (59-5619 to JPV). SO's effort was supported in part by a U.S. National Institutes of Health grant (R35 CA197735). The funders had no role in study design, data collection and analysis, decision to publish or preparation of the manuscript. Open Access funding provided by University of Oulu including Oulu University Hospital.

COMPETING INTERESTS

JAN reports grants from NanoString, Akoya Biosciences and Illumina outside the submitted work. TTS is the CEO and co-owner of Healthfund Finland Oy and reports interview honoraria from Boehringer Ingelheim Finland. The remaining authors declare no competing interests.

ETHICS APPROVAL AND CONSENT TO PARTICIPATE

The study was conducted according to the guidelines of the Declaration of Helsinki and approved by the hospital administration and the ethics board (Dnro13U/2011, 1/2016 and 8/2020) and the National Supervisory Authority for Welfare and Health (Valvira). The need to obtain informed consent from the study patients was waived (Valvira Dnro 3916/06.01.03.01/2016). The validation study was conducted under permissions form the Ethics Committee of Oulu University Hospital (25/2002, 42/2005, 122/2009, 37/2020) and Biobank Borealis (BB-2017_1012).

CONSENT FOR PUBLICATION

Not applicable.

ADDITIONAL INFORMATION

Supplementary information The online version contains supplementary material available at https://doi.org/10.1038/s41416-022-01822-6.

Correspondence and requests for materials should be addressed to Juha P. Väyrynen.

Reprints and permission information is available at http://www.nature.com/reprints

Publisher's note Springer Nature remains neutral with regard to jurisdictional claims in published maps and institutional affiliations.

II

SPATIALLY RESOLVED MULTIMARKER EVALUATION OF CD274 (PD-L1)/PDCD1 (PD-1) IMMUNE CHECKPOINT EXPRESSION AND MACROPHAGE POLARISATION IN COLORECTAL CANCER

by

Elomaa H, Ahtiainen M, Väyrynen SA, Ogino S, Nowak JA, Lau MC, Helminen O, Wirta EV, Seppälä TT, Böhm J, Mecklin JP, Kuopio T, Väyrynen JP. 2023.

British Journal of Cancer 128: 2104–2115

https://doi.org/10.1038/s41416-023-02238-6

British Journal of Cancer www.nature.com/bjc

ARTICLE OPEN

Check for updates

Molecular Diagnostics

Spatially resolved multimarker evaluation of CD274 (PD-L1)/PDCD1 (PD-1) immune checkpoint expression and macrophage polarisation in colorectal cancer

Hanna Elomaa[1,2], Maarit Ahtiainen[3], Sara A. Väyrynen[4], Shuji Ogino[5,6,7,8], Jonathan A. Nowak[5], Mai Chan Lau[9], Olli Helminen[10], Erkki-Ville Wirta[11,12], Toni T. Seppälä[12,13,14], Jan Böhm[3], Jukka-Pekka Mecklin[2,15], Teijo Kuopio[1,3] and Juha P. Väyrynen[3,10]✉

BACKGROUND: The CD274 (PD-L1)/PDCD1 (PD-1) immune checkpoint interaction may promote cancer progression, but the expression patterns and prognostic significance of PD-L1 and PD-1 in the colorectal cancer microenvironment are inadequately characterised.
METHODS: We used a custom 9-plex immunohistochemistry assay to quantify the expression patterns of PD-L1 and PD-1 in macrophages, T cells, and tumour cells in 910 colorectal cancer patients. We evaluated cancer-specific mortality according to immune cell subset densities using multivariable Cox regression models.
RESULTS: Compared to PD-L1$^-$ macrophages, PD-L1$^+$ macrophages were more likely M1-polarised than M2-polarised and located closer to tumour cells. PD-L1$^+$ macrophage density in the invasive margin associated with longer cancer-specific survival [$P_{trend} = 0.0004$, HR for the highest vs. lowest quartile, 0.52; 95% CI: 0.34–0.78]. T cell densities associated with longer cancer-specific survival regardless of PD-1 expression ($P_{trend} < 0.005$ for both PD-1$^+$ and PD-1$^-$ subsets). Higher densities of PD-1$^+$ T cell/PD-L1$^+$ macrophage clusters associated with longer cancer-specific survival ($P_{trend} < 0.005$).
CONCLUSIONS: PD-L1$^+$ macrophages show distinct polarisation profiles (more M1-like), spatial features (greater co-localisation with tumour cells and PD-1$^+$ T cells), and associations with favourable clinical outcome. Our comprehensive multimarker assessment could enhance the understanding of immune checkpoints in the tumour microenvironment and promote the development of improved immunotherapies.

British Journal of Cancer; https://doi.org/10.1038/s41416-023-02238-6

BACKGROUND

Colorectal cancer is the second leading cause of cancer death worldwide with over 900,000 deaths in 2020 [1]. The assessment of cancer prognosis and treatment is mainly based on the tumour extent and tumour morphology, but the rapidly increasing knowledge on the significance of tumour immune contexture has led to the development of improved immune-related prognostic markers and effective anticancer immunotherapies [2]. In addition to the quantity of immune cells, the activity of immunoregulatory signalling pathways, such as the co-inhibitory pathway of programmed death ligand 1 (PD-L1, CD274) and its receptor programmed death 1 (PD-1, PDCD1), may affect cancer progression. Hereinafter, CD274 and PDCD1 are referred as PD-L1 and PD-1 due to the ubiquity of these "colloquial" protein names. PD-L1 is mainly expressed in macrophages [3], whereas PD-1 is mainly expressed in T cells [4]. The expression of PD-L1 and PD-1 is often upregulated in cancer and their interaction may lead to immunosuppression through T cell exhaustion, thus promoting tumour growth [4]. However, the prognostic significance of immune checkpoint protein expression in many tumour types, including colorectal cancer, has remained controversial [5].

Macrophages are inflammatory cells which have shown to associate with cancer progression [6]. They are commonly

[1]Department of Biological and Environmental Science, University of Jyväskylä, Jyväskylä, Finland. [2]Department of Education and Research, Hospital Nova of Central Finland, Well Being Services County of Central Finland, Jyväskylä, Finland. [3]Department of Pathology, Hospital Nova of Central Finland, Well Being Services County of Central Finland, Jyväskylä, Finland. [4]Department of Internal Medicine, Oulu University Hospital, Oulu, Finland. [5]Program in Molecular Pathological Epidemiology, Department of Pathology, Brigham and Women's Hospital and Harvard Medical School, Boston, MA, USA. [6]Department of Epidemiology, Harvard T.H. Chan School of Public Health, Boston, MA, USA. [7]Broad Institute of MIT and Harvard, Cambridge, MA, USA. [8]Cancer Immunology and Cancer Epidemiology Programs, Dana-Farber Harvard Cancer Center, Boston, MA, USA. [9]Institute of Molecular Cell Biology, Agency of Science, Technology and Research (A*STAR), Singapore, Singapore. [10]Translational Medicine Research Unit, Medical Research Center Oulu, Oulu University Hospital, and University of Oulu, Oulu, Finland. [11]Department of Gastroenterology and Alimentary Tract Surgery, Tampere University Hospital, Tampere, Finland. [12]Faculty of Medicine and Health Technology, Tampere University and Tays Cancer Center, Tampere University Hospital, Tampere, Finland. [13]Department of Gastrointestinal Surgery, Helsinki University Central Hospital, University of Helsinki, Helsinki, Finland. [14]Applied Tumor Genomics, Research Program Unit, University of Helsinki, Helsinki, Finland. [15]Faculty of Sport and Health Sciences, University of Jyväskylä, Jyväskylä, Finland. ✉email: juha.vayrynen@oulu.fi

Received: 11 October 2022 Revised: 14 March 2023 Accepted: 15 March 2023
Published online: 31 March 2023

categorised into classically activated, M1-polarised, and alternatively activated, M2-polarised macrophages, which differ by their surface antigens, cytokine secretion profiles, and physiological functions. However, instead of two completely distinct subtypes, macrophages are considered to form a continuum of phenotypes that may gradually change their polarisation towards M1-like or M2-like and simultaneously express phenotypic markers for both subtypes. In the tumour microenvironment, M1-like macrophages are thought to have pro-inflammatory effect and be more prevalent in early-stage cancer, whereas the proportion of anti-inflammatory M2-like macrophages increases along cancer progression [6]. Higher M1/M2-like macrophage ratio has been thought to associate with improved cancer-specific survival [7]. The expression patterns of immune checkpoints in macrophages and their clinical value are poorly established in colorectal cancer.

In this study, we used multiplex immunohistochemistry and machine learning-based image analysis to comprehensively characterise PD-L1 and PD-1 immune checkpoint expression in M1-like and M2-like macrophages, T cells, and tumour cells in a large, population-based colorectal cancer cohort of 910 patients. Our primary aim was to (i) evaluate the expression patterns and prognostic significance of PD-L1 and PD-1 in immune cells and tumour cells. As secondary aims, we (ii) clarified the associations between immune checkpoint expression and tumour characteristics, and (iii) investigated the infiltration patterns and prognostic role of M1-like and M2-like polarised macrophages. We hypothesised low expression of PD-L1 and PD-1 immune checkpoints and higher density of M1-like macrophages to associate with favourable colorectal cancer outcome.

METHODS

Study population

The study was based on a cohort of 1343 colorectal cancer patients, who underwent a resection for primary colon or rectum carcinoma between January 1, 2000 and December 31, 2015 in Central Finland Central Hospital. The population of the area was on average 270,000 during the study period [8]. The clinical, histopathological, and follow-up data were retrospectively collected from the pathology registry and clinical records of Central Finland Central Hospital. All tumours were screened for DNA mismatch repair (MMR) deficiency and *BRAF* V600E mutation status with immunohistochemistry [9]. Histological tumour parameters, including tumour differentiation and lymphovascular invasion, were re-evaluated from hematoxylin and eosin-stained whole slides by the study pathologist (J.P.V.). All histological data were analysed blinded to clinical data. We excluded patients who died within 30 days after surgery ($N = 40$) or received any preoperative oncological treatments (radiotherapy, chemotherapy, or chemoradiotherapy) ($N = 243$) due to their potential influences on tumour characteristics or immune response [10]. After applying further exclusion criteria of unsuccessful multiplex immunohistochemistry staining or inadequate tumour tissue of both the tumour centre and the invasive margin in tissue microarrays ($N = 150$), the final cohort comprised samples of 910 colorectal cancer patients.

Multiplex immunohistochemistry

Tissue microarrays were constructed by selecting four 1-mm diameter cores from each tumour [9]. We designed a 9-plex immunohistochemistry panel to identify macrophages with CD68 and CD163, T cells with CD3, and tumour cells with KRT (keratin). PD-L1 and PD-1 immune checkpoint molecules and four macrophage polarisation markers (CD86, CD163, HLA-DR, MRC1) were included in the assay.

The multiplex immunohistochemistry staining was done with Bond-III automated IHC stainer (Leica Biosystems, Buffalo Grove, IL, USA) and Bond Refine Detection kit (DS9800, Leica Biosystems). We used sections of 3.5 µm. Candidate antibodies and suitable dilutions were optimised using conventional immunohistochemistry with 3,3′-Diaminobenzidine (DAB) chromogen in a test tissue microarray consisting of normal colorectal mucosa, colorectal cancer tissue, and tonsil tissue. These antibodies were then combined into a multiplex immunohistochemistry assay. The correspondence of staining patterns of multiplex and conventional immunohistochemistry were visually confirmed in serial sections of a test microarray, and the correspondence was further quantified by manually annotating cells in 10 respective regions (size 200 × 200 µm) of multiplex and conventional immunohistochemistry (Supplementary Fig. S1). The multiplex staining was conducted using a previously validated, cyclic method that uses 3-Amino-9-Ethylcarbazole (AEC) as the chromogen [11]. The workflow for the staining is shown in Supplementary Fig. S2 and the selected monoclonal antibodies along with their dilutions and antigen retrieval conditions are listed in Supplementary Table S1. We used AEC$^+$ high sensitivity substrate (K3469, Dako, Glostrup, Denmark) as the chromogen. After each cycle, the slides were mounted with VectaMount AQ Aqueous Mounting Medium (H-5501, Vector Laboratories, Newark, CA, USA), scanned with 20× objective of NanoZoomer XR (Hamamatsu Photonics, Hamamatsu City, Japan, resolution 0.45 µm/pixel), de-stained with ethanol, and heated to remove the primary and secondary antibodies.

Image analysis

The digitised images of multiplex immunohistochemistry slides were processed with QuPath (version 0.2.3) [12]. Tissue microarray cores were recognised with *TMA dearrayer* function and separated into single core images. We excluded cores which were folded, included minimal amount of tumour, were necrotic, or comprised less than 50% of the 1-mm diameter core area after all staining cycles. The single core images of all 9 staining cycles were stacked into one 10-channel pseudo-immunofluorescence image (with hematoxylin as the 10th channel) by aligning cell nuclei using the MultiStackReg macro (downloaded from http://bradbusse.net/downloads.html) in ImageJ/Fiji open-source software [13]. This macro enabled the co-registration of the images despite potential minor shifts in tissue during the staining cycles. The conversion of single images into a 10-plex pseudo-immunofluorescence image is illustrated in Fig. 1a–d. The staining intensities were consistent across tissue microarrays (Supplementary Fig. S3), indicating that the assay had performed uniformly.

The pseudo-immunofluorescence images were analysed with QuPath, utilising previously validated [14], supervised machine learning algorithms. We identified cells with *cell detection* function and calculated additional smoothed object features to improve subsequent cell phenotyping. Cells were phenotyped into T cells, macrophages, tumour cells, and other cells using the *object classifier* function built in QuPath, based on the random forests algorithm. For training, example cells were annotated as follows: (1) all CD3 expressing cells were phenotyped as T cells; (2) cells expressing CD68 [15] and/or CD163 [7] were identified as macrophages in line with a prior study [16]; (3) KRT expressing cells were phenotyped as tumour cells; and (4) cells negative for CD3, CD68, CD163 and KRT were classified as other cells. Cell data yielded phenotypes, marker intensities, and coordinates for each cell. To classify tissue categories, QuPath was trained to identify tissue segments of tumour epithelium and stroma using the built-in *pixel classifier* function. Necrotic regions, empty white space without any tissue, and regions of partial core loss (the hematoxylin staining from the first staining cycle not corresponding with the hematoxylin staining form the last staining cycle) were excluded. The workflow for cell and tissue analyses is described in Supplementary Fig. S4 and the example images from cell segmentation and tissue categorisation in QuPath are represented in Fig. 1e–h.

Immune cell phenotyping and classification

Cell level data were further processed with RStudio (version 1.3.1093) and R statistical programming (version 4.0.3, R Core Team).

Macrophages were classified according to PD-L1 expression and M1/M2 polarisation state. To categorise macrophages according to their polarisation, we calculated a polarisation index for each macrophage consistent with a prior study [16]. First, we converted the intensities of all four macrophage markers into percentiles across all macrophages and calculated a polarisation index by reducing the intensities of M2-like macrophage markers from the intensities of M1-like macrophage markers [formula: (CD86 + HLA-DR) − (CD163 + MRC1); with marker names denoting intensity percentiles]. Using this formula, macrophages with higher polarisation index values were considered more M1-polarised, while those with lower values were considered more M2-polarised. For downstream analyses, the index values were divided into ordinal quartile categories (Q1–Q4) across all macrophages in 910 colorectal cancer cases. As in a prior study [16], macrophages in the lowest group (Q1) were classified as M1-like macrophages and those in the highest group (Q4) were classified as M2-like macrophages. Macrophages in the middle groups (Q2–Q3), covering 50% of the cells, were left unclassified to limit this analysis to the

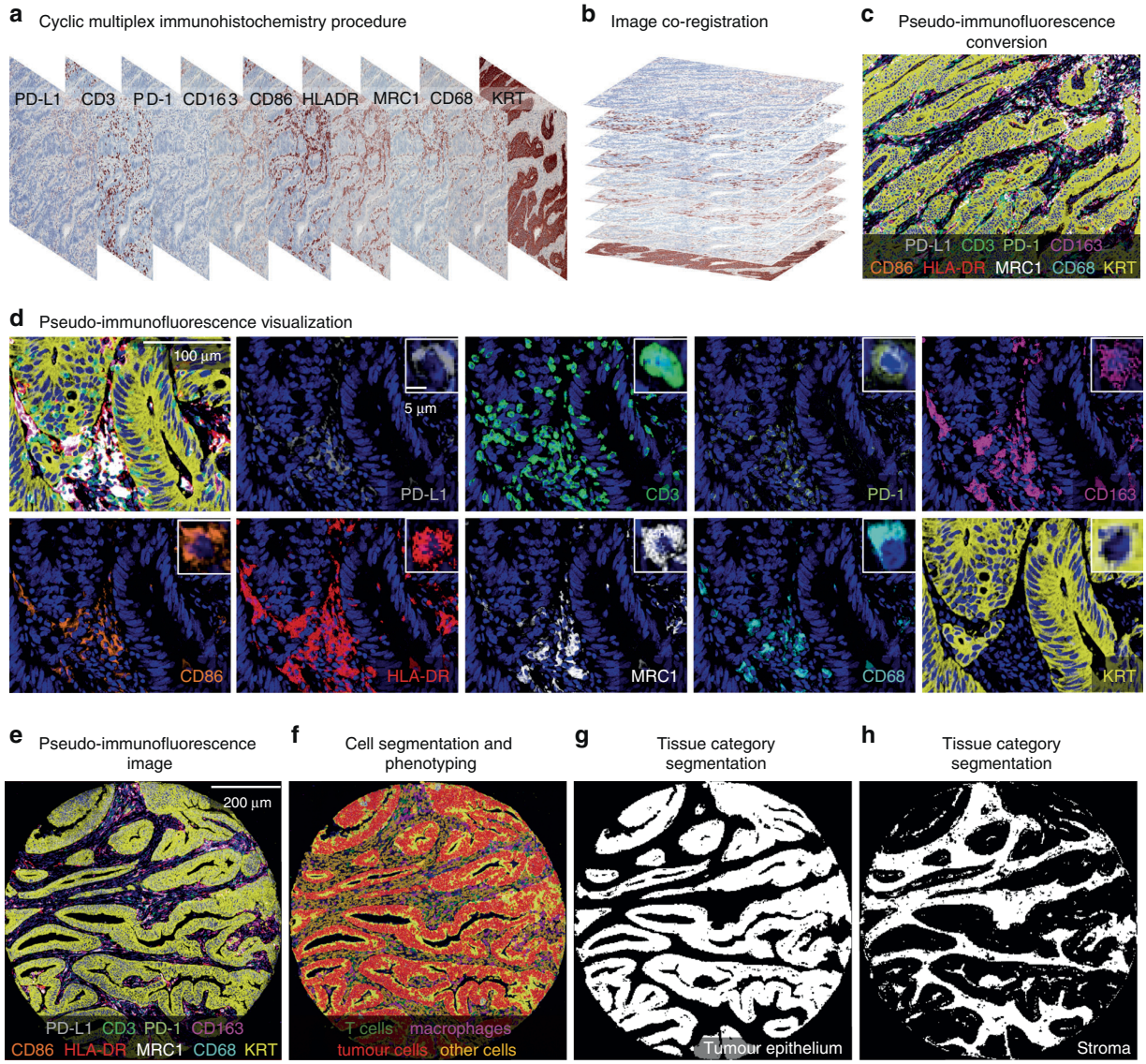

Fig. 1 Multiplex immunohistochemistry panel and image analysis. a Digitised multiplex immunohistochemistry image from each staining cycle for one tumour. **b**, **c** Image co-registration based on aligning the hematoxylin layers to merge individual images into one 10-channel pseudo-immunofluorescence image. **d** example images showing the expression patterns of each marker merged and separately. **e**–**h** pseudo-immunofluorescence image (**e**), machine learning-based cell segmentation and phenotyping into T cells, macrophages, tumour cells, and other cells (**f**), and mask images of the categorisation of tissue into tumour epithelium and stroma (**g**, **h**).

most strongly polarised M1-like and M2-like macrophages. For downstream survival analyses, we calculated the densities of various macrophage subsets in the tumour centre and the invasive margin and categorised the densities into ordinal quartile categories (Q1–Q4). For variables including over 25% zero densities, all zero values were categorised into the lowest group Q1. The remaining values were divided equally into groups Q2–Q4. Ordinal quartile categories were also similarly defined for other immune cell variables.

In addition to macrophages, PD-L1 expression was evaluated in tumour epithelial cells, based on the weighted histoscore method. For each cell, we classified the staining intensity (negative, weak, intermediate, or high), and for each case, we calculated the percentage (0–100%) of tumour cells within each category separately in the tumour centre and the invasive margin. In cases with multiple tissue microarray cores from one region, we calculated the mean values. Finally, PD-L1 histoscore was calculated as follows: PD-L1 histoscore = [(1 × percentage of weakly stained cells) +(2 × percentage of moderately stained cells)+(3 × percentage of strongly stained cells)]. The possible range for values was from 0 (all cells negative) to 300 (all cells strongly positive) [17]. For survival analyses, we calculated the mean histoscore for each tumour and categorised the tumours into negative or positive using a cut-off value of ≥5 for the positivity.

T cells were further subdivided into PD-1 positive or negative based on a fixed cut-off value for their cytoplasmic PD-1 staining intensity (40 intensity units).

To analyse spatial interactions between immune and tumour cells, we used the *spatstat* (2.2–0) package to calculate nearest neighbour distances (NNDs), which measure the distance from a specific point (e.g., macrophage) to its closest neighbour point of specific category (e.g., tumour cell). For visualisation, scaled intensities of macrophage polarisation markers as a function of NND from tumour cells were plotted with *ggplot2* (3.3.3) package using generalised additive model smoothing [formula y ~ s(x)]. For further spatial analyses, we calculated the density of PD-1^+/PD-$L1^+$ clusters defined as PD-1^+ T cell located within 20-µm distance from the closest PD-$L1^+$ macrophage. The radius was selected in order to identify cells with capability for direct cell-cell interaction consistent with prior reports [9, 18].

Statistical analysis

Statistical analyses were performed in RStudio using packages *corrplot* (0.90), *forestplot* (2.0.1), *ggpubr* (0.4.0), *gmodels* (2.18.1), *spatstat* (2.1–0), *survival* (3.2–7), *survminer* (0.4.9), and *tidyverse* (1.3.1).

We used the Wilcoxon rank-sum test for dichotomous variables and the Kruskal–Wallis test for variables with three or more categories to evaluate the associations of continuous immune cell density variables with patient characteristics. The associations of categorical immune cell density variables with patient characteristics were tested with crosstabulation and the Chi-square test to evaluate the statistical significance. We examined the correlations between immune cell densities by calculating Spearman's correlation coefficients.

As our main analysis, we used univariable and multivariable Cox proportion hazard regression models to measure hazard ratio (HR) point estimates and 95% confidence intervals (CIs) for cancer-specific and overall survival. Cancer-specific survival was considered as the primary survival endpoint, and it was defined as the time from surgery to colorectal cancer death or the end of follow-up. Overall survival was defined as the duration from surgery to death of any cause or the end of follow-up. The total number of deaths was 525 (58%) including 250 (31%) cancer-specific deaths. The median follow-up time for censored cases was 10.1 years (IQR 6.6–13.1). We limited the follow-up to 10 years, considering that most colorectal cancer deaths occur within that period. Schoenfeld residual plots supported the proportionality of hazards during most of the follow-up period up to 10 years. Multivariable models included the following predetermined indicator variables (with the reference category listed first): sex (male, female), age (<65, 65–75, >75), year of operation (2000–2005, 2006–2010, 2011–2015), tumour location (proximal colon, distal colon, rectum), American Joint Committee on Cancer (AJCC) stage (I–II, III, IV), tumour grade (well/moderately differentiated, poorly differentiated), lymphovascular invasion (negative, positive), MMR status (proficient, deficient), *BRAF* status (wild-type, mutant). Kaplan–Meier method was used to visualise the estimates of cancer-specific survival, and the statistical significance was tested with the Log-rank test. A P value less than 0.005 was considered statistically significant, in accordance with the recommendation of an expert panel [19].

RESULTS

Image analysis

We analysed 3190 tissue microarray cores from 910 colorectal cancer patients (mean 3.5 per patient, SD 0.69; tumour centre: mean 1.8, SD 0.39; invasive margin: mean 1.7, SD 0.51). The supervised machine learning algorithms yielded data for 21,503,560 cells including 9,136,506 tumour cells, 1,788,538 macrophages, and 1,582,095 T cells. Macrophages were further phenotyped into PD-L1$^+$ and PD-L1$^-$ and M1- and M2-like subpopulations. T cells were phenotyped into PD-1$^+$ and PD-1$^-$ subpopulations. The median immune cell densities in the tumour centre and the invasive margin were 512 and 808 cells/mm^2 for all macrophages, 33 and 64 cells/mm^2 for PD-L1$^+$ macrophages and 390 and 591 cells/mm^2 for T cells, respectively. Core-to-core correlations for immune cell densities were good or moderate in both the tumour centre and the invasive margin (Supplementary Fig. S5).

PD-L1 expression patterns

PD-L1 expression was detected mainly in macrophages. Of macrophages, 20% were positive and 80% were negative for PD-L1. In macrophage subsets defined by four polarisation markers, PD-L1 expression was enriched in M1-like macrophages. Of PD-L1$^+$ macrophages, 33% were M1-like, 16% were M2-like, and the remaining 51% were less strongly polarised mixed phenotype macrophages. Correspondingly, PD-L1$^+$ macrophage density and M1-like macrophage density showed a moderate positive correlation (R = 0.54), while the correlation between the densities of PD-L1$^+$ macrophages and M2-like macrophages was weak (R = 0.24) (Supplementary Fig. S6). Conversely, PD-L1$^-$ macrophage densities showed a stronger correlation with M2-like macrophage densities (R = 0.67) than M1-like macrophage densities (R = 0.29). Median densities for both PD-L1$^+$ and PD-L1$^-$ macrophages were higher in tumour stromal (110/mm^2 for PD-L1$^+$ and 991/mm^2 for PD-L1$^-$) than intraepithelial regions (11.5/mm^2 for PD-L1$^+$ and 119/mm^2 for PD-L1$^-$).

The clinicopathological characteristics according to PD-L1$^+$ and PD-L1$^-$ macrophage densities are shown in Table 1. Higher density of PD-L1$^+$ macrophages associated with proximal tumour location ($P = 0.0012$), low stage, poor tumour differentiation, absent lymphovascular invasion, MMR deficiency, and *BRAF* mutation (all $P < 0.0001$). Higher density of PD-L1$^-$ macrophages associated with high stage ($P = 0.0049$). The associations of macrophage polarisation with clinicopathological characteristics are visualised in Supplementary Fig. S7.

In addition to macrophages, we investigated the PD-L1 expression in tumour cells using the histoscore method. Most of the tumours were negative for PD-L1 or showed very weak expression (histoscore < 5), and only 66 (7%) of the tumours were classified as PD-L1 positive (histoscore ≥ 5). Similar to high PD-L1$^+$ macrophage density, PD-L1 positivity in tumour cells associated with proximal tumour location, poor differentiation, MMR deficiency and *BRAF* mutation (all $P < 0.0001$), but there were no associations with stage or lymphovascular invasion (Supplementary Table S2).

PD-1 expression patterns

We evaluated PD-1 expression in T cells. Of all detected T cells, 22% were positive for PD-1. Higher T cell density associated with low stage [$P = 0.00025$ (tumour centre), $P < 0.0001$ (invasive margin)], high tumour grade ($P < 0.0001$, $P = 0.0032$), MMR deficiency (both $P < 0.0001$) and *BRAF* mutation ($P < 0.0001$, $P = 0.062$). The findings were mainly similar for PD-1$^+$ and PD-1$^-$ T cells (Supplementary Fig. S8). The density of PD-L1$^+$ macrophages positively correlated with the densities of both PD-1$^+$ T cells (R = 0.64) and PD-1$^-$ T cells (R = 0.50) (Supplementary Fig. S6).

Survival analyses

We first examined the prognostic role of total (CD68$^+$/CD163$^+$) macrophage population, which did not reach statistical significance either in the tumour centre or the invasive margin in univariable (Supplementary Fig. S9, Table 2) or multivariable analyses (Table 2) (all $P > 0.005$). When macrophages were classified according to their PD-L1 expression, higher density of PD-L1$^+$ macrophages associated with improved cancer-specific survival in both the tumour centre and the invasive margin in univariable analyses (Fig. 2a, Table 2). The prognostic value remained significant in the invasive margin in multivariable analysis ($P_{trend} = 0.0004$, HR for Q4 vs. Q1 0.52, 95% CI 0.34–0.78) (Table 2). The full multivariable Cox regression models for PD-L1$^+$ and PD-L1$^-$ macrophage densities are shown in Supplementary Table S3. When tumour epithelial and stromal compartments were examined separately, higher PD-L1$^+$ macrophage density associated with longer cancer-specific survival in both tumour intraepithelial and stromal compartments of the tumour centre and the invasive margin in univariable analyses (all $P_{trend} < 0.005$) (Supplementary Fig. S10, Supplementary Table S4). These associations remained significant in the invasive margin in multivariable analyses (Supplementary Table S4). Higher density of PD-L1$^-$ macrophages in the invasive margin tended to associate with poor survival but did not reach statistical significance in either univariable or multivariable analysis ($P_{trend} > 0.005$) (Table 2). PD-L1 expression in tumour cells did not significantly associate with survival (Supplementary Table S5). We further evaluated the prognostic significance of PD-L1$^+$ and PD-L1$^-$ macrophage densities in relation to MMR status and stage. The survival associations of PD-L1$^+$ or PD-L1$^-$ macrophage densities did not significantly differ by MMR status (Supplementary Table S6) or stage (Supplementary Tables S7, S8) in univariable or multivariable analysis (all $P_{interaction} > 0.005$).

Higher T cell density associated with better cancer-specific survival regardless of PD-1 expression in both univariable (Fig. 2b, Table 3) and multivariable analyses (Table 3). In multivariable

Table 1. Demographic and clinical characteristics of colorectal cancer cases according to PD-L1$^+$ and PD-L1$^-$ macrophage densities.

Characteristic	Total *N*	Overall cell density (cells/mm^2) Median (25–75th percentiles)			
		PD-L1$^+$ macrophages	*P*	PD-L1$^-$ macrophages	*P*
All cases	910 (100%)	59 (16–170)		560 (380–780)	
Sex			0.50		0.47
Male	464 (51%)	60 (17–160)		570 (390–790)	
Female	446 (49%)	59 (15–190)		560 (370–770)	
Age (years)			0.18		0.95
<65	247 (27%)	54 (15–160)		580 (360–790)	
65–75	331 (36%)	58 (15–150)		560 (390–750)	
>75	332 (36%)	74 (18–230)		550 (370–800)	
Tumour location			0.0012		0.19
Proximal colon	445 (49%)	74 (20–220)		580 (420–790)	
Distal colon	332 (36%)	51 (12–140)		530 (360–750)	
Rectum	133 (15%)	38 (15–160)		560 (360–750)	
AJCC stage			<0.0001		0.0049
I	151 (17%)	84 (19–210)		500 (340–670)	
II	342 (38%)	84 (26–210)		540 (390–790)	
III	301 (33%)	47 (11–130)		590 (420–800)	
IV	116 (13%)	26 (6.6–100)		650 (370–890)	
Tumour grade			<0.0001		0.73
Low-grade (well to moderately differentiated)	760 (84%)	55 (15–160)		560 (370–780)	
High-grade (poorly differentiated)	150 (16%)	104 (24–310)		570 (410–760)	
Lymphovascular invasion			<0.0001		0.20
No	719 (79%)	70 (21–190)		550 (380–770)	
Yes	191 (21%)	32 (6.5–100)		600 (380–820)	
MMR status			<0.0001		0.20
MMR proficient	772 (85%)	48 (12–150)		550 (370–780)	
MMR deficient	137 (15%)	190 (60–350)		590 (460–770)	
BRAF status			<0.0001		0.046
Wild-type	763 (84%)	52 (14–160)		550 (370–770)	
Mutant	147 (16%)	98 (37–290)		590 (440–790)	

AJCC American Joint Committee on Cancer, *MMR* mismatch repair.

analyses, the HR for high PD-1$^+$ T cell density in the tumour centre (Q4 vs. Q1) was 0.46 (95% CI: 0.30–0.71), while the HR for high PD-1$^-$ T cell density (Q4 vs. Q1) was 0.48 (95% CI: 0.32–0.70) and the HR for high T cell density (Q4 vs. Q1) was 0.49 (95% CI: 0.33–0.73). Full multivariable Cox regression models with all variables are shown in Supplementary Table S9.

Considering potential interactions between PD-1 and PD-L1, we next evaluated the prognostic value of PD-1$^+$ T cell density in tumour groups defined by PD-L1$^+$ macrophage densities or tumour cell PD-L1 expression. These analyses indicated that the survival associations of PD-1$^+$ T cells did not statistically significantly differ according to the density of PD-L1$^+$ macrophages or PD-L1 expression in tumour cells in univariable (Supplementary Fig. S11, Supplementary Tables S10, S11) or multivariable analyses (Supplementary Tables S10, S11) (all $P_{interaction} > 0.005$).

In secondary analyses, we investigated the prognostic significance of M1-like and M2-like macrophage densities. Higher M1-like macrophage density associated with longer cancer-specific survival in both the tumour centre and the invasive margin in univariable analyses (Supplementary Fig. S9, Supplementary Table S12). The prognostic value remained significant in the tumour centre in multivariable analyses [$P_{trend} = 0.0004$, HR for high (Q4 vs. Q1) 0.54, 95% CI: 0.38–0.78] (Supplementary Table S12). Higher M2-like macrophage density in the tumour centre associated with longer cancer-specific survival and higher M1:M2-like macrophage density ratio in the tumour centre and the invasive margin associated with worse cancer-specific survival in univariable analyses (Supplementary Fig. S9, Supplementary Table S12) but did not reach statistical significance in multivariable analysis ($P_{trend} > 0.005$). To evaluate the prognostic value of PD-L1 expression in differently polarised macrophage subpopulations, we calculated macrophage densities based on subpopulations defined by both PD-L1 expression and polarisation state (Supplementary Table S13). We found that higher PD-L1$^+$ M1-like macrophage density in both the tumour centre and the invasive margin predicted longer cancer-specific survival in univariable and multivariable models (multivariable $P_{trend} = 0.0005$ and $P_{trend} = 0.0008$, respectively), while the densities of PD-L1$^-$ M1-like macrophages, PD-L1$^+$ M2-like macrophages, or PD-L1$^-$ M2-like macrophages did not significantly associate with the survival in multivariable models (all $P_{trend} > 0.005$). These results indicate that higher densities of PD-L1$^+$ and M1-like macrophages associate with favourable prognosis, which is further highlighted when PD-L1 expression and polarisation are examined simultaneously.

Table 2. Univariable and multivariable Cox regression models for colorectal cancer-specific and overall survival according to the total, PD-L1$^+$, and PD-L1$^-$ macrophage densities in the tumour centre and the invasive margin.

	No. of cases	Colorectal cancer-specific survival			Overall survival		
		No. of events	Univariable HR (95% CI)	Multivariable HR (95% CI)	No. of events	Univariable HR (95% CI)	Multivariable HR (95% CI)
Tumour centre							
Macrophage density							
Q1	228	64	1 (referent)	1 (referent)	116	1 (referent)	1 (referent)
Q2	228	56	0.85 (0.59–1.21)	0.81 (0.56–1.18)	109	0.93 (0.71–1.21)	0.92 (0.70–1.20)
Q3	227	63	0.97 (0.69–1.38)	0.84 (0.59–1.20)	107	0.93 (0.72–1.21)	0.84 (0.64–1.10)
Q4	227	59	0.93 (0.65–1.32)	0.80 (0.56–1.16)	117	1.03 (0.80–1.33)	0.84 (0.65–1.10)
P_{trend}			0.87	0.29		0.81	0.17
PD-L1$^+$ macrophage density							
Q1	228	83	1 (referent)	1 (referent)	134	1 (referent)	1 (referent)
Q2	228	61	0.68 (0.49–0.94)	0.81 (0.57–1.13)	106	0.72 (0.56–0.93)	0.82 (0.64–1.07)
Q3	227	54	0.59 (0.42–0.83)	0.75 (0.53–1.06)	102	0.68 (0.53–0.88)	0.73 (0.56–0.95)
Q4	227	44	0.47 (0.33–0.69)	0.63 (0.43–0.93)	107	0.70 (0.54–0.90)	0.72 (0.55–0.94)
P_{trend}			<0.0001	0.015		0.0050	0.011
PD-L1$^-$ macrophage density							
Q1	228	59	1 (referent)	1 (referent)	110	1 (referent)	1 (referent)
Q2	228	52	0.86 (0.59–1.25)	0.75 (0.51–1.09)	111	1.01 (0.77–1.31)	0.93 (0.71–1.22)
Q3	227	58	0.97 (0.68–1.39)	0.88 (0.61–1.27)	108	0.99 (0.73–1.29)	0.93 (0.71–1.21)
Q4	227	73	1.31 (0.93–1.85)	0.85 (0.60–1.21)	120	1.18 (0.91–1.53)	0.88 (0.67–1.14)
P_{trend}			0.085	0.62		0.25	0.35
Invasive margin							
Macrophage density							
Q1	228	67	1 (referent)	1 (referent)	113	1 (referent)	1 (referent)
Q2	228	62	0.94 (0.66–1.32)	1.16 (0.81–1.66)	118	1.07 (0.83–1.39)	1.19 (0.91–1.56)
Q3	227	47	0.67 (0.46–0.97)	0.92 (0.62–1.36)	100	0.84 (0.64–1.09)	0.98 (0.74–1.28)
Q4	227	66	0.99 (0.70–1.39)	0.93 (0.66–1.32)	118	1.05 (0.81–1.36)	0.98 (0.76–1.28)
P_{trend}			0.54	0.46		0.83	0.57
PD-L1$^+$ macrophage density							
Q1	228	92	1 (referent)	1 (referent)	136	1 (referent)	1 (referent)
Q2	228	71	0.75 (0.55–1.02)	1.07 (0.78–1.48)	116	0.82 (0.64–1.06)	1.02 (0.79–1.32)
Q3	227	43	0.43 (0.30–0.61)	0.68 (0.47–0.99)	97	0.64 (0.50–0.83)	0.85 (0.65–1.12)
Q4	227	36	0.34 (0.23–0.50)	0.52 (0.34–0.78)	100	0.62 (0.48–0.80)	0.69 (0.52–0.91)
P_{trend}			<0.0001	0.0004		<0.0001	0.0053
PD-L1$^-$ macrophage density							
Q1	228	55	1 (referent)	1 (referent)	113	1 (referent)	1 (referent)
Q2	228	58	1.08 (0.74–1.56)	1.33 (0.91–1.94)	108	0.98 (0.75–1.28)	1.08 (0.83–1.42)
Q3	227	50	0.88 (0.60–1.29)	1.02 (0.69–1.50)	101	0.86 (0.66–1.13)	0.95 (0.72–1.25)
Q4	227	79	1.53 (1.08–2.16)	1.36 (0.96–1.92)	127	1.21 (0.94–1.56)	1.13 (0.88–1.46)
P_{trend}			0.038	0.21		0.27	0.52

The densities were divided into ordinal quartile categories from low (Q1) to high (Q4).
Multivariable Cox proportional hazards regression models were adjusted for sex (male, female), age (<65, 65–75, >75), year of operation (2000–2005, 2006–2010, 2011–2015), tumour location (proximal colon, distal colon, rectum), stage (I–II, III, IV), tumour grade (well/moderately differentiated, poorly differentiated), lymphovascular invasion (negative, positive), MMR status (proficient, deficient), and *BRAF* status (wild-type, mutant).
P_{trend} values were calculated by using the four categories of immune cell densities as continuous variables in univariable and multivariable Cox proportional hazard regression models.
CI confidence interval, *HR* hazard ratio.

Spatial analyses

We characterised the spatial arrangement of immune cells by measuring the average distances from immune cells to the nearest tumour cell with NND analysis. Macrophages were located 4.6% closer to tumour cells than T cells on average. Of macrophages, PD-L1$^+$ macrophages were located 24% closer to tumour cells than PD-L1$^-$ macrophages ($P < 0.0001$) and M1-like macrophages were 48% closer to tumour cells than M2-like macrophages ($P < 0.0001$) (Fig. 3a). To further visualise these findings, we plotted scaled intensities of macrophage polarisation

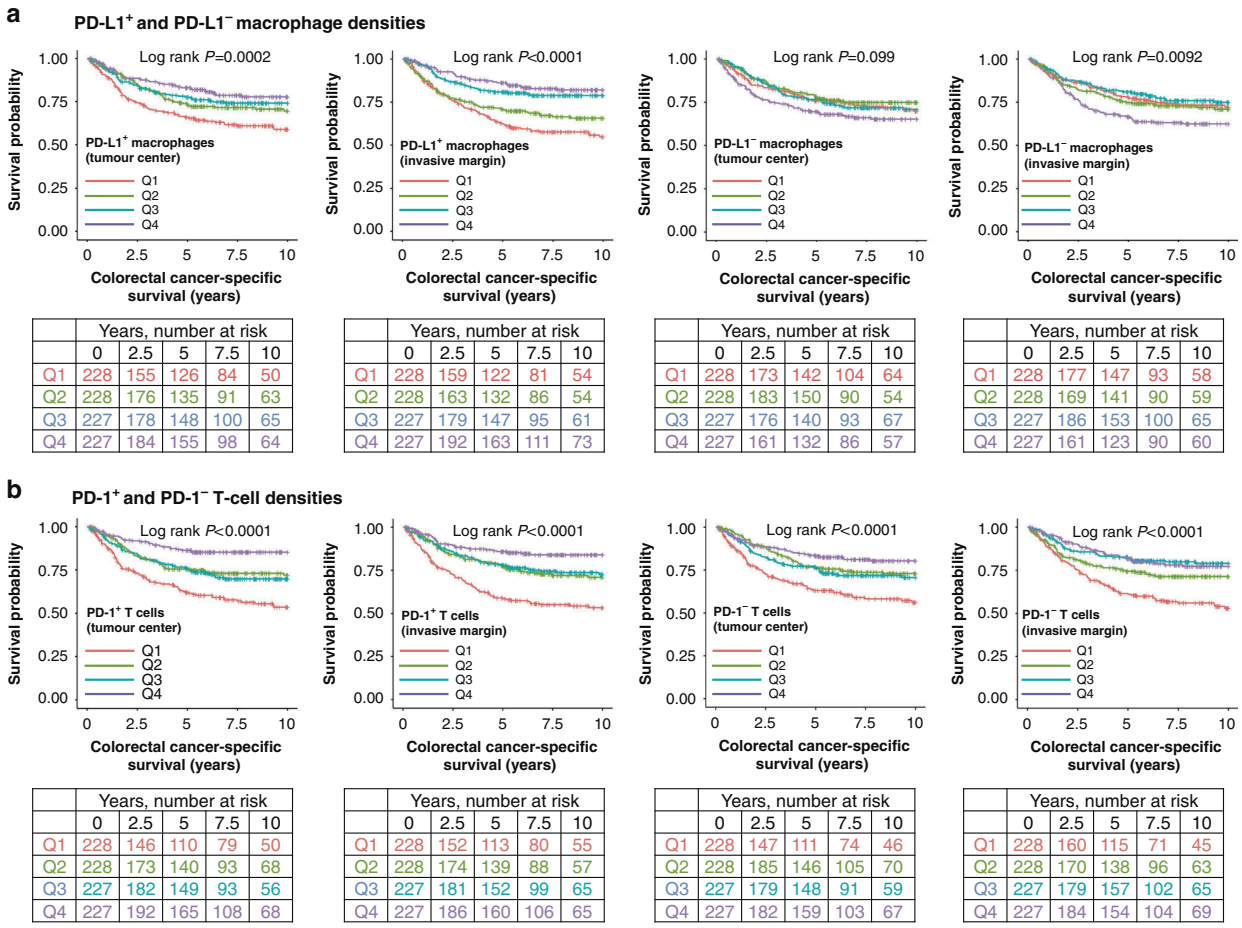

Fig. 2 Kaplan–Meier survival analysis. Cancer-specific survival curves for the PD-L1$^+$ and PD-L1$^-$ macrophage (**a**) and PD-1$^+$ and PD-1$^-$ T cell (**b**) densities in the tumour centre and the invasive margin. The densities were divided into ordinal quartiles from low (Q1) to high (Q4). Statistical significance was determined with Log-rank test.

markers and PD-L1 as a function of NND from tumour cells using generalised additive model smoothing (Fig. 3a). This plot showed that M2-like macrophage markers (MRC1 and CD163) had lower scaled intensities at tumour cell proximity than other macrophage markers. The Kaplan–Meier curves showed that the spatial proximity of macrophages (total, PD-L1$^+$, or PD-L1$^-$) or T cells (total, PD-1$^+$, or PD-1$^-$) with tumour cells, as measured with mean NNDs from immune cell to the closest tumour cell, did not significantly associate with cancer-specific survival ($P > 0.005$) (Supplementary Fig. S12).

For T cells, we measured NNDs to the closest tumour cell and to the closest PD-L1$^+$ macrophage to evaluate the possibility for PD-1−PD-L1 interactions. We found that PD-1$^+$ T cells were located closer to both tumour cells (difference 13%, $P < 0.0001$) and PD-L1$^+$ macrophages (difference 35%, $P < 0.0001$) than PD-1$^-$ T cells (Fig. 3b). To evaluate the prognostic value of PD-1$^+$ T cells co-localised with PD-L1$^+$ macrophages, we calculated the density of PD-1$^+$/PD-L1$^+$ clusters. The mean cluster densities in the tumour centre and the invasive margin were 34 clusters/mm^2 and 47 clusters/mm^2, respectively. Higher density of PD-1$^+$/PD-L1$^+$ clusters associated with longer cancer-specific survival in both the tumour centre and the invasive margin in univariable and multivariable analyses (Fig. 3c). The prognostic value was slightly stronger in the invasive margin, in which the multivariable HR for high cluster density (Q4 vs. Q1) was 0.39 (95% CI 0.25–0.60, $P_{trend} < 0.0001$).

DISCUSSION

In the present study, we used multiplex immunohistochemistry combined with digital image analysis and quantitative density and spatial analysis to comprehensively characterise the expression of PD-L1 (CD274) and PD-1 (PDCD1) immune checkpoints in the colorectal cancer microenvironment. This analysis, conducted in a large, population-based cohort of 910 colorectal cancer patients expands the knowledge on immune checkpoint expression patterns, their prognostic value, and associations with T cell and macrophage infiltration and may help to develop cancer therapies.

The expression of PD-L1 and PD-1 is often elevated in cancer and their interaction may repress the cytotoxic activity of T cells and thus promote tumour immune escape [4]. However, the prognostic value of PD-L1 is incompletely established in colorectal cancer and prior studies have reached contradictory conclusions [20]. We found that PD-L1 expression was more frequently present in macrophages than in tumour cells. Although PD-L1 is commonly thought to have immunosuppressive effect, we found that higher density of PD-L1$^+$ macrophages in the invasive margin associated with longer colorectal cancer-specific survival independent of stage, grade, and MMR status. Our finding is concordant with some prior studies which have reported association between high PD-L1 expression in immune cells and better survival [21–23] and adds to these findings by more accurately defining phenotypes of the immune cells expressing PD-L1. In our study, PD-L1 expression in tumour cells did not associate with prognosis.

Table 3. Univariable and multivariable Cox regression models for cancer-specific and overall survival according to the densities of total, PD-1$^+$, and PD-1$^-$ T cells in the tumour centre and the invasive margin.

	No. of cases	Colorectal cancer-specific survival			Overall survival		
		No. of events	Univariable HR (95% CI)	Multivariable HR (95% CI)	No. of events	Univariable HR (95% CI)	Multivariable HR (95% CI)
Tumour centre							
T cell density							
Q1	228	88	1 (referent)	1 (referent)	146	1 (referent)	1 (referent)
Q2	228	58	0.55 (0.40–0.77)	0.72 (0.51–1.01)	103	0.58 (0.45–0.74)	0.68 (0.53–0.88)
Q3	227	56	0.54 (0.39–0.76)	0.67 (0.47–0.94)	100	0.57 (0.44–0.74)	0.62 (0.48–0.80)
Q4	227	40	0.38 (0.26–0.55)	0.49 (0.33–0.73)	100	0.56 (0.43–0.72)	0.59 (0.45–0.77)
P_{trend}			<0.0001	0.0003		<0.0001	<0.0001
PD-1$^+$ T cell density							
Q1	228	91	1 (referent)	1 (referent)	147	1 (referent)	1 (referent)
Q2	228	57	0.55 (0.39–0.76)	0.82 (0.58–1.16)	103	0.60 (0.47–0.77)	0.78 (0.60–1.01)
Q3	227	63	0.59 (0.43–0.82)	0.75 (0.54–1.04)	109	0.63 (0.49–0.81)	0.68 (0.53–0.87)
Q4	227	31	0.28 (0.18–0.42)	0.46 (0.30–0.71)	90	0.49 (0.38–0.64)	0.57 (0.43–0.76)
P_{trend}			<0.0001	0.0006		<0.0001	<0.0001
PD-1$^-$ T cell density							
Q1	228	86	1 (referent)	1 (referent)	145	1 (referent)	1 (referent)
Q2	228	55	0.54 (0.38–0.76)	0.68 (0.48–0.96)	103	0.58 (0.45–0.75)	0.69 (0.54–0.90)
Q3	227	61	0.61 (0.44–0.85)	0.67 (0.48–0.94)	106	0.63 (0.49–0.81)	0.61 (0.47–0.79)
Q4	227	40	0.39 (0.27–0.57)	0.48 (0.32–0.70)	95	0.54 (0.42–0.70)	0.55 (0.42–0.71)
P_{trend}			<0.0001	0.0002		<0.0001	<0.0001
Invasive margin							
T cell density							
Q1	228	94	1 (referent)	1 (referent)	146	1 (referent)	1 (referent)
Q2	228	67	0.66 (0.48–0.90)	0.83 (0.60–1.14)	103	0.71 (0.56–0.91)	0.80 (0.62–1.03)
Q3	227	38	0.34 (0.23–0.49)	0.53 (0.36–0.78)	100	0.51 (0.39–0.66)	0.65 (0.50–0.86)
Q4	227	43	0.39 (0.27–0.56)	0.58 (0.40–0.85)	100	0.58 (0.45–0.75)	0.64 (0.48–0.83)
P_{trend}			<0.0001	0.0005		<0.0001	0.0003
PD-1$^+$ T cell density							
Q1	228	97	1 (referent)	1 (referent)	141	1 (referent)	1 (referent)
Q2	228	57	0.52 (0.38–0.72)	0.81 (0.58–1.14)	112	0.71 (0.55–0.90)	0.90 (0.70–1.17)
Q3	227	55	0.49 (0.35–0.68)	0.83 (0.58–1.17)	101	0.61 (0.47–0.79)	0.82 (0.63–1.08)
Q4	227	33	0.29 (0.19–0.43)	0.52 (0.34–0.79)	95	0.56 (0.43–0.72)	0.70 (0.53–0.93)
P_{trend}			<0.0001	0.0043		<0.0001	0.011
PD-1$^-$ T cell density							
Q1	228	94	1 (referent)	1 (referent)	144	1 (referent)	1 (referent)
Q2	228	60	0.60 (0.43–0.82)	0.80 (0.58–1.12)	105	0.66 (0.51–0.85)	0.77 (0.59–0.99)
Q3	227	43	0.40 (0.28–0.58)	0.62 (0.43–0.90)	101	0.60 (0.46–0.77)	0.75 (0.57–0.97)
Q4	227	45	0.42 (0.29–0.60)	0.61 (0.42–0.88)	99	0.58 (0.45–0.76)	0.65 (0.50–0.85)
P_{trend}			<0.0001	0.0027		<0.0001	0.0021

The densities were divided into ordinal quartile categories from low (Q1) to high (Q4).
Multivariable Cox proportional hazards regression models were adjusted for sex (male, female), age (<65, 65–75, >75), year of operation (2000–2005, 2006–2010, 2011–2015), tumour location (proximal colon, distal colon, rectum), stage (I–II, III, IV), tumour grade (well/moderately differentiated, poorly differentiated), lymphovascular invasion (negative, positive), MMR status (proficient, deficient), and *BRAF* status (wild-type, mutant).
P_{trend} values were calculated by using the four categories of immune cell densities as continuous variables in univariable and multivariable Cox proportional hazard regression models.
CI confidence interval, *HR* hazard ratio.

Prior colorectal cancer studies have reported inconsistent deductions of the prognostic value of PD-L1$^+$ expression in tumour cells [22–27]. Divergent results may be due to the small percentage of PD-L1 positive tumours and variability in antibody selection, quantification methods, or setting cut-off value for the positivity.

The detection and phenotyping of macrophages are challenging because of their plasticity and the lack of specific or standardised immunohistochemical markers for various subpopulations [7]. We used multiplex immunohistochemistry instead of conventional single-plex chromogenic staining, enabling us to

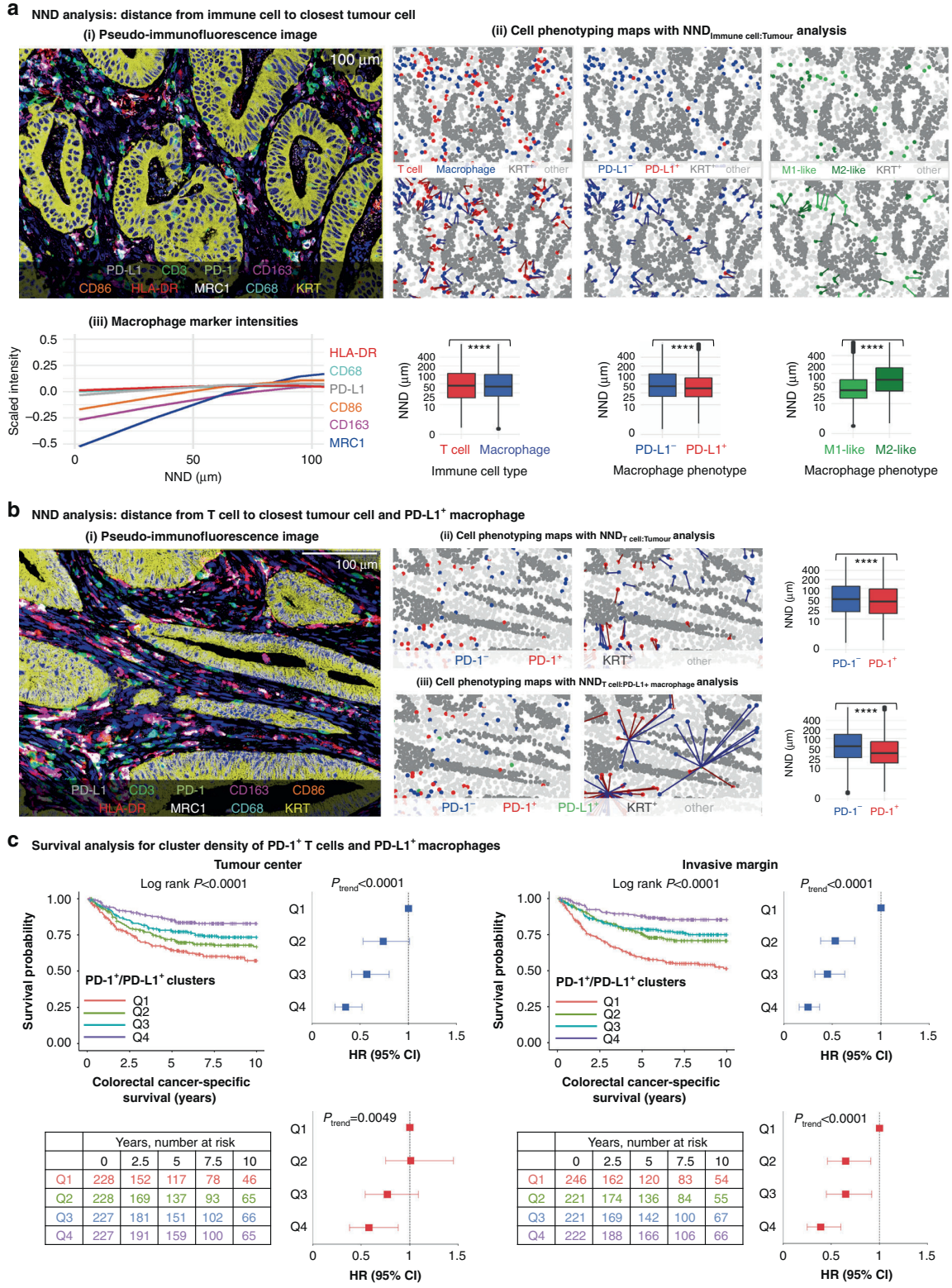

phenotype cells with multimarker combinations and to analyse spatial relationships between cells. To separate M1-like and M2-like polarisation states, we utilised two markers for both phenotypes, in line with two previous studies [16, 28], and only included the extremes of the polarisation spectrum in our main analyses. We found that higher density of M1-like macrophages in the tumour centre associated with longer cancer-specific survival, which is in line with some previous studies [29–31], while M2-like macrophages tended to associate with shorter survival, but not significantly in multivariable models.

Fig. 3 Spatial analysis of immune cells using the nearest neighbour distance (NND) function and the cancer-specific survival analysis for PD-1/PD-L1 cluster density. a pseudo-immunofluorescence image from a tumour site showing all nine markers (i). Cell phenotyping maps with nearest neighbour distance analysis from each immune cell to the closest tumour cell and boxplots visualising the distribution of nearest neighbour distances across all tumour images ($N = 3{,}190$). The statistical significance was tested with Wilcoxon rank-sum test. ****$P < 0.0001$ (ii). The expression levels of various phenotypic markers in macrophages according to the distance to the closest tumour cell. The plots are based on 1,582,095 T cells and 1,788,538 macrophages (iii). **b** pseudo-immunofluorescence image from a tumour site showing all nine markers (i). Cell phenotyping maps and nearest neighbour distance analyses from each PD-1$^+$ and PD-1$^-$ T cell to the closest tumour cell (ii) and to the closest PD-L1$^+$ macrophage (iii). Boxplots visualise the distribution of nearest neighbour distances across all tumour images ($N = 3{,}190$). The significance was tested with Wilcoxon rank-sum test. ****$P < 0.0001$. **c** Kaplan–Meier survival curves and Cox proportion hazards regression models for cancer-specific survival for PD-1$^+$ T cell/PD-L1$^+$ macrophage cluster densities in 910 patients in the tumour centre and the invasive margin. One cluster is composed of one PD-1$^+$ T cell with at least one PD-L1$^+$ macrophage within a 20 µm radius. The cluster densities were divided into ordinal quartiles from low (Q1) to high (Q4). Statistical significance for Kaplan–Meier survival estimates were determined with Log-rank test. Univariable (blue) and multivariable (red) Cox proportional hazards regression models are represented as forest plots with HRs along with their 95% CIs as whiskers. Multivariable Cox proportional hazards regression models were adjusted for sex (male, female), age (<65, 65–75, >75), year of operation (2000–2005, 2006–2010, 2011–2015), tumour location (proximal colon, distal colon, rectum), stage (I–II, III, IV), tumour grade (well/moderately differentiated, poorly differentiated), lymphovascular invasion (negative, positive), MMR status (proficient, deficient), and *BRAF* status (wild-type, mutant).

In analyses combining PD-L1 expression and polarisation status of macrophages, PD-L1$^+$ macrophages were more likely M1-polarised than M2-polarised, which could partly explain their comparable spatial arrangement and prognostic value. The associations of macrophage polarisation phenotypes with PD-L1 expression are not well-characterised, but may be affected by the cytokine environment [32]. In particular, IFNG can induce M1-like macrophage polarisation and PD-L1 expression in macrophages [33, 34]. However, other studies have found that certain cytokines, such as IL6 and IL10, increase PD-L1 expression but drive macrophage polarisation towards an M2-phenotype [33, 35, 36]. Our analyses suggested that the prognostic value of macrophages was influenced by both the polarisation phenotype (M1-like vs. M2-like) and PD-L1 expression, with PD-L1$^+$ M1-like phenotype showing the strongest association with a favourable outcome.

Some recent studies have reported the co-localisation of immune cells with tumour cells to be strongly prognostic [16, 37–39]. Interestingly, macrophage subtypes frequently located in closer proximity to tumour cells (PD-L1$^+$ and M1-like macrophages) also showed the strongest associations with favourable clinical outcome. Shorter average distance of M1-like than M2-like macrophages from the closest tumour cell has been reported also in prior studies of gastric [28], lung [29] and pancreatic [16] cancers. Based on these findings, we hypothesise that the greater co-localisation between macrophages and tumour cells could increase the probability of cell contacts, thus allowing enhanced anti-tumoral macrophage function.

Our study addressed the prognostic significance of T cell subsets defined by PD-1 expression. We found that higher densities of both PD-1$^+$ and PD-1$^-$ T cells showed strong associations with favourable survival, and their HR point estimates were very close to that of the overall T cell population. This supports the strong prognostic significance of T cells in general [40], and indicates that it appears to be independent of PD-1 expression by T cells. Our findings were in line with some prior studies in colorectal cancer that have reported associations between higher PD-1$^+$ cell densities and longer survival [22, 24, 25].

To evaluate the possibility of PD-1/PD-L1 interactions occurring in the tumour microenvironment, we assessed the correlations between the densities of immune checkpoint expressing (PD-1$^+$ and PD-L1$^+$) cells, as well as their co-localisation. In line with prior reports [21, 22, 24], we found a moderate correlation between PD-L1$^+$ macrophage and T cell densities. Furthermore, this correlation was higher for PD-1$^+$ T cells than for PD-1$^-$ T cells. A prior study [25] reported that mismatch repair deficient colorectal tumours with high PD-1 expression associated with worse recurrence-free survival if PD-L1 expression was high, while high expression of PD-1 associated with prolonged survival if PD-L1 expression was low. In our cohort, such findings were not identified, as higher PD-1$^+$ T cell densities associated with favourable outcome regardless of PD-L1 expression in tumour cells or PD-L1$^+$ macrophage densities. Furthermore, higher density of PD-1$^+$ T cell/PD-L1$^+$ macrophage clusters strongly associated with longer cancer-specific survival.

In contrast to our hypotheses, higher densities of PD-L1$^+$ macrophages and PD-1$^+$ T cells individually, as well as higher density of PD-1$^+$ T cell/PD-L1$^+$ macrophage clusters associated with favourable prognostic impact. It has been well known that certain cancer risk factors (such as obesity and Lynch syndrome genetic mutations) may associate with better clinical outcomes among patients with a given cancer type. Those apparent paradoxical findings can be explained by interpersonal heterogeneity of cancer [41]. Our findings may be explained by the strong induction of these immune checkpoints as a compensatory response to generally elevated anti-tumour inflammatory reaction in immunologically hot tumours [22, 38]. Favourable outcome of high immune checkpoint expression could also be related to IFNG, which is secreted mainly by activated infiltrating T cells and NK cells. High IFNG expression is correlated with both PD-L1 and PD-1 expression and associates with better colorectal cancer prognosis [24]. Furthermore, gut microbiota e.g., *Fusobacterium nucleatum*, might associate with T cell count, PD-1 and PD-L1 expression, and colorectal cancer prognosis [42].

To our knowledge, this is the first study examining the PD-L1/PD-1 expression along with macrophage polarisation using multimarker analysis. However, the findings of this study should be interpreted with some caution. First, the analyses were conducted using tissue microarrays, which may not fully represent the immune infiltration in the whole tumour area [43]. To increase the validity of our results, we analysed multiple cores from each tumour (average: 3.5 cores) and the cores were selected from different sites representing average immune cell infiltrates. Reasonably good core-to-core correlations indicated that the number of analysed tissue microarray cores was adequate. By using tissue microarrays, we could examine 910 tumours cost-efficiently and select only representative tumour areas to be stained and analysed. Second, PD-L1 staining patterns may differ between antibody clones. We decided to use a well-validated clone (E1L3N) that is frequently applied for clinical use in evaluating PD-L1 status in lung cancer [44]. However, the optimal antibody for colorectal cancer is yet to be determined. Third, macrophage phenotyping requires several markers and there are no single consensus markers for M1/M2 polarisation states. We used two polarisation markers for both M1 and M2 subpopulations and determined the polarisation states in line with prior reports [16, 45]. Fourth, the cell detection algorithm of QuPath (image analysis software that was utilised) is not able to segment cell membrane, and we used cytoplasmic staining intensities for markers that are expressed in either cell cytoplasm or cell membrane. Fifth, most of the patients were non-Hispanic

white, and we excluded patients with preoperative treatment, which led to underrepresentation of rectal cancers. Therefore, the applicability of the results for patients of different ethnicities and with preoperative treatments needs to be confirmed by independent studies. Furthermore, the patients were operated along a period of 16 years, during which the cancer treatments have developed. To mitigate possible bias related to this, we included year of operation as a covariate in multivariable survival models. Sixth, the information on extramural venous invasion and perineural invasion were not available, although they are strong prognostic indicators in colorectal cancer. Seventh, although multiplex immunohistochemistry analysis enabled detailed immune cell characterisation, the method is laborious and would need further automation and validation to be applied as a biomarker in clinical setting.

This study has important strengths. Our study included a large, comprehensively analysed [9, 22, 46–49] population-based cohort evaluated in accordance with the latest guidelines. All tumours were also screened for MMR status and *BRAF* mutation status representing two key molecular features of colorectal cancer. Multiplex immunohistochemistry staining together with machine learning-based image analysis enabled accurate phenotyping of each cell with multimarker combination in a single batch, facilitating the consistency and reproducibility of the analysis. Flow cytometry and RNA sequencing methods are other commonly used myeloid cell phenotyping methods but, unlike multiplex immunohistochemistry, they do not provide the spatial information of the cells.

In conclusion, this study shows that higher density of PD-L1 expressing macrophages and their spatial proximity with PD-1 expressing T cells associate with prolonged survival of colorectal cancer patients. Our results highlight the utility of detailed multimarker analysis in understanding the role of PD-L1 and PD-1 expression in cancer immune escape and developing improved immunotherapies.

DATA AVAILABILITY

The datasets generated and/or analysed during this study are not publicly available. The sharing of data will require approval from relevant ethics committees and/or biobanks. Further information including the procedures to obtain and access data of Finnish Biobanks are described at https://finbb.fi/en/fingenious-service.

REFERENCES

1. Sung H, Ferlay J, Siegel RL, Laversanne M, Soerjomataram I, Jemal A, et al. Global cancer statistics 2020: GLOBOCAN estimates of incidence and mortality worldwide for 36 cancers in 185 countries. CA Cancer J Clin. 2021;71:209–49.
2. Fridman WH, Zitvogel L, Sautès-Fridman C, Kroemer G. The immune contexture in cancer prognosis and treatment. Nat Rev Clin Oncol. 2017;14:717–34.
3. Llosa NJ, Cruise M, Tam A, Wicks EC, Hechenbleikner EM, Taube JM, et al. The vigorous immune microenvironment of microsatellite instable colon cancer is balanced by multiple counter-inhibitory checkpoints. Cancer Discov. 2015;5:43–51.
4. Pauken KE, Torchia JA, Chaudhri A, Sharpe AH, Freeman GJ. Emerging concepts in PD-1 checkpoint biology. Semin Immunol. 2021;52:101480.
5. Ni X, Sun X, Wang D, Chen Y, Zhang Y, Li W, et al. The clinicopathological and prognostic value of programmed death-ligand 1 in colorectal cancer: a meta-analysis. Clin Transl Oncol. 2019;21:674–86.
6. Boutilier AJ, Elsawa SF. Macrophage polarization states in the tumor microenvironment. Int J Mol Sci. 2021;22:6995.
7. Jayasingam SD, Citartan M, Thang TH, Mat Zin AA, Ang KC, Ch'ng ES. Evaluating the polarization of tumor-associated macrophages into M1 and M2 phenotypes in human cancer tissue: technicalities and challenges in routine clinical practice. Front Oncol. 2019;9:1512.
8. Väyrynen V, Wirta E-V, Seppälä T, Sihvo E, Mecklin J-P, Vasala K, et al. Incidence and management of patients with colorectal cancer and synchronous and metachronous colorectal metastases: a population-based study. BJS Open. 2020;4:685–92.
9. Elomaa H, Ahtiainen M, Väyrynen SA, Ogino S, Nowak JA, Friman M, et al. Prognostic significance of spatial and density analysis of T lymphocytes in colorectal cancer. Br J Cancer. 2022;127:514–23.
10. Nagtegaal ID, Marijnen CAM, Kranenbarg EK, Mulder-Stapel A, Hermans J, van de Velde CJH, et al. Short-term preoperative radiotherapy interferes with the determination of pathological parameters in rectal cancer. J Pathol. 2002;197:20–7.
11. Banik G, Betts CB, Liudahl SM, Sivagnanam S, Kawashima R, Cotechini T, et al. High-dimensional multiplexed immunohistochemical characterization of immune contexture in human cancers. Methods Enzymol. 2020;635:1–20.
12. Bankhead P, Loughrey MB, Fernández JA, Dombrowski Y, McArt DG, Dunne PD, et al. QuPath: open source software for digital pathology image analysis. Sci Rep. 2017;7:16878.
13. Schindelin J, Arganda-Carreras I, Frise E, Kaynig V, Longair M, Pietzsch T, et al. Fiji: an open-source platform for biological-image analysis. Nat Methods. 2012;9:676–82.
14. Väyrynen JP, Lau MC, Haruki K, Väyrynen SA, Dias Costa A, Borowsky J, et al. Prognostic significance of immune cell populations identified by machine learning in colorectal cancer using routine hematoxylin and eosin-stained sections. Clin Cancer Res. 2020;26:4326–38.
15. Chistiakov DA, Killingsworth MC, Myasoedova VA, Orekhov AN, Bobryshev YV. CD68/macrosialin: not just a histochemical marker. Lab Invest. 2017;97:4–13.
16. Väyrynen SA, Zhang J, Yuan C, Väyrynen JP, Dias Costa A, Williams H, et al. Composition, spatial characteristics, and prognostic significance of myeloid cell infiltration in pancreatic cancer. Clin Cancer Res. 2021;27:1069–81.
17. Jensen K, Krusenstjerna-Hafstrøm R, Lohse J, Petersen KH, Derand H. A novel quantitative immunohistochemistry method for precise protein measurements directly in formalin-fixed, paraffin-embedded specimens: analytical performance measuring HER2. Mod Pathol. 2017;30:180–93.
18. Carstens JL, Correa de Sampaio P, Yang D, Barua S, Wang H, Rao A, et al. Spatial computation of intratumoral T cells correlates with survival of patients with pancreatic cancer. Nat Commun. 2017;8:15095.
19. Benjamin DJ, Berger JO, Johannesson M, Nosek BA, Wagenmakers E-J, Berk R, et al. Redefine statistical significance. Nat Hum Behav. 2018;2:6–10.
20. Alexander PG, McMillan DC, Park JH. A meta-analysis of CD274 (PD-L1) assessment and prognosis in colorectal cancer and its role in predicting response to anti-PD-1 therapy. Crit Rev Oncol Hematol. 2021;157:103147.
21. Lee KS, Kwak Y, Ahn S, Shin E, Oh H-K, Kim D-W, et al. Prognostic implication of CD274 (PD-L1) protein expression in tumor-infiltrating immune cells for microsatellite unstable and stable colorectal cancer. Cancer Immunol Immunother. 2017;66:927–39.
22. Ahtiainen M, Wirta E-V, Kuopio T, Seppälä T, Rantala J, Mecklin J-P, et al. Combined prognostic value of CD274 (PD-L1)/PDCDI (PD-1) expression and immune cell infiltration in colorectal cancer as per mismatch repair status. Mod Pathol. 2019;32:866–83.
23. Wyss J, Dislich B, Koelzer VH, Galván JA, Dawson H, Hädrich M, et al. Stromal PD-1/PD-L1 expression predicts outcome in colon cancer patients. Clin Colorectal Cancer. 2019;18:e20–38.
24. Li Y, Liang L, Dai W, Cai G, Xu Y, Li X, et al. Prognostic impact of programed cell death-1 (PD-1) and PD-ligand 1 (PD-L1) expression in cancer cells and tumor infiltrating lymphocytes in colorectal cancer. Mol Cancer. 2016;15:55.
25. Lee LH, Cavalcanti MS, Segal NH, Hechtman JF, Weiser MR, Smith JJ, et al. Patterns and prognostic relevance of PD-1 and PD-L1 expression in colorectal carcinoma. Mod Pathol. 2016;29:1433–42.
26. Masugi Y, Nishihara R, Yang J, Mima K, da Silva A, Shi Y, et al. Tumour CD274 (PD-L1) expression and T cells in colorectal cancer. Gut. 2017;66:1463–73.
27. Droeser RA, Hirt C, Viehl CT, Frey DM, Nebiker C, Huber X, et al. Clinical impact of programmed cell death ligand 1 expression in colorectal cancer. Eur J Cancer. 2013;49:2233–42.
28. Huang Y-K, Wang M, Sun Y, Di Costanzo N, Mitchell C, Achuthan A, et al. Macrophage spatial heterogeneity in gastric cancer defined by multiplex immunohistochemistry. Nat Commun. 2019;10:3928.
29. Zheng X, Weigert A, Reu S, Guenther S, Mansouri S, Bassaly B, et al. Spatial density and distribution of tumor-associated macrophages predict survival in non-small cell lung carcinoma. Cancer Res. 2020;80:4414–25.
30. Edin S, Wikberg ML, Dahlin AM, Rutegård J, Öberg Å, Oldenborg P-A, et al. The distribution of macrophages with a M1 or M2 phenotype in relation to prognosis and the molecular characteristics of colorectal cancer. PLoS One. 2012;7:e47045.
31. Väyrynen JP, Haruki K, Väyrynen SA, Lau MC, Dias Costa A, Borowsky J, et al. Prognostic significance of myeloid immune cells and their spatial distribution in the colorectal cancer microenvironment. J Immunother Cancer. 2021;9:e002297.
32. Cai H, Zhang Y, Wang J, Gu J. Defects in macrophage reprogramming in cancer therapy: the negative impact of PD-L1/PD-1. Front Immunol. 2021;12:690869.
33. Najafi M, Hashemi Goradel N, Farhood B, Salehi E, Nashtaei MS, Khanlarkhani N, et al. Macrophage polarity in cancer: a review. J Cell Biochem. 2019;120:2756–65.
34. Duffield AS, Ascierto ML, Anders RA, Taube JM, Meeker AK, Chen S, et al. Th17 immune microenvironment in Epstein-Barr virus-negative Hodgkin lymphoma: implications for immunotherapy. Blood Adv. 2017;1:1324–34.

35. Zhang W, Liu Y, Yan Z, Yang H, Sun W, Yao Y, et al. IL-6 promotes PD-L1 expression in monocytes and macrophages by decreasing protein tyrosine phosphatase receptor type O expression in human hepatocellular carcinoma. J Immunother Cancer. 2020;8:1–14.
36. Chen S, Crabill GA, Pritchard TS, McMiller TL, Wei P, Pardoll DM, et al. Mechanisms regulating PD-L1 expression on tumor and immune cells. J Immunother Cancer. 2019;7:305.
37. Väyrynen JP, Haruki K, Lau MC, Väyrynen SA, Ugai T, Akimoto N, et al. Spatial organization and prognostic significance of NK and NKT-like cells via multimarker analysis of the colorectal cancer microenvironment. Cancer Immunol Res. 2022;10:215–27.
38. Lazarus J, Maj T, Smith JJ, Perusina Lanfranca M, Rao A, D'Angelica MI, et al. Spatial and phenotypic immune profiling of metastatic colon cancer. JCI Insight. 2018;3:e121932.
39. Lazarus J, Oneka MD, Barua S, Maj T, Lanfranca MP, Delrosario L, et al. Mathematical modeling of the metastatic colorectal cancer microenvironment defines the importance of cytotoxic lymphocyte infiltration and presence of PD-L1 on antigen presenting cells. Ann Surg Oncol. 2019;26:2821–30.
40. Alexander PG, McMillan DC, Park JH. The local inflammatory response in colorectal cancer - Type, location or density? A systematic review and meta-analysis. Cancer Treat Rev. 2020;83:101949.
41. Nishihara R, VanderWeele TJ, Shibuya K, Mittleman MA, Wang M, Field AE, et al. Molecular pathological epidemiology gives clues to paradoxical findings. Eur J Epidemiol. 2015;30:1129–35.
42. Gao Y, Bi D, Xie R, Li M, Guo J, Liu H, et al. Fusobacterium nucleatum enhances the efficacy of PD-L1 blockade in colorectal cancer. Signal Transduct Target Ther. 2021;6:398.
43. Giltnane JM, Rimm DL. Technology insight: identification of biomarkers with tissue microarray technology. Nat Clin Pract Oncol. 2004;1:104–11.
44. Munari E, Zamboni G, Lunardi G, Marconi M, Brunelli M, Martignoni G, et al. PD-L1 expression in non-small cell lung cancer: evaluation of the diagnostic accuracy of a laboratory-developed test using clone E1L3N in comparison with 22C3 and SP263 assays. Hum Pathol. 2019;90:54–9.
45. Väyrynen JP, Haruki K, Lau MC, Väyrynen SA, Zhong R, Dias Costa A, et al. The prognostic role of macrophage polarization in the colorectal cancer microenvironment. Cancer Immunol Res. 2021;9:8–19.
46. Seppälä TT, Böhm JP, Friman M, Lahtinen L, Väyrynen VMJ, Liipo TKE, et al. Combination of microsatellite instability and BRAF mutation status for subtyping colorectal cancer. Br J Cancer. 2015;112:1966–75.
47. Porkka N, Lahtinen L, Ahtiainen M, Böhm JP, Kuopio T, Eldfors S, et al. Epidemiological, clinical and molecular characterization of Lynch-like syndrome: A population-based study. Int J Cancer. 2019;145:87–98.
48. Wirta E-V, Seppälä T, Friman M, Väyrynen J, Ahtiainen M, Kautiainen H, et al. Immunoscore in mismatch repair-proficient and -deficient colon cancer. J Pathol Clin Res. 2017;3:203–13.
49. Kellokumpu I, Kairaluoma M, Mecklin J-P, Kellokumpu H, Väyrynen V, Wirta E-V, et al. Impact of age and comorbidity on multimodal management and survival from colorectal cancer: a population-based study. J Clin Med. 2021;10:1751.

AUTHOR CONTRIBUTIONS

Conceptualisation: HE, SAV, SO, JAN, JB, TK, JPV. Data curation: HE, MA, OH, E-VW, TTS, JB, JPM, JPV. Funding acquisition: HE, JPM, JPV. Investigation: HE, MA, SAV, OH, E-VW, TTS, JB, JPM, TK, JPV. Methodology: HE, SAV, SO, JAN, MCL, JPV. Formal analysis: HE, JPV. Resources: JB, JPM, TK, JPV. Supervision: TK, JPV. Visualisation: HE, SAV, MCL, JPV. Writing – original draft: HE, JPV. Writing – review & editing: All authors.

FUNDING

This study was funded by Cancer Foundation Finland (59-5619 to J.P. Väyrynen) and Emil Aaltonen Foundation (220022K to H. Elomaa). The funders had no role in study design, data collection and analysis, decision to publish, or preparation of the manuscript. Open Access funding provided by University of Oulu including Oulu University Hospital.

COMPETING INTERESTS

JAN reports grants from NanoString, Akoya Biosciences and Illumina outside the submitted work. TTS is the CEO and co-owner of Healthfund Finland Oy and reports interview honoraria from Boehringer Ingelheim Finland and Amgen Finland. The other authors declare that they have no conflicts of interest.

ETHICS APPROVAL AND CONSENT TO PARTICIPATE

The study was conducted according to the guidelines of the Declaration of Helsinki and approved by the hospital administration and the ethics board (Dnro13U/2011, 1/2016 and 8/2020) and the National Supervisory Authority for Welfare and Health (Valvira). The need to obtain informed consent from the study patients was waived (Valvira Dnro 3916/06.01.03.01/2016).

ADDITIONAL INFORMATION

Supplementary information The online version contains supplementary material available at https://doi.org/10.1038/s41416-023-02238-6.

Correspondence and requests for materials should be addressed to Juha P. Väyrynen.

Reprints and permission information is available at http://www.nature.com/reprints

Publisher's note Springer Nature remains neutral with regard to jurisdictional claims in published maps and institutional affiliations.

III

QUANTITATIVE MULTIPLEXED ANALYSIS OF INDOLEAMINE 2,3-DIOXYGENASE (IDO) AND ARGINASE-1 (ARG1) EXPRESSION AND MYELOID CELL INFILTRATION IN COLORECTAL CANCER

by

Elomaa H, Härkönen J, Väyrynen SA, Ahtiainen M, Ogino S, Nowak JA, Lau MC, Helminen O, Wirta EV, Seppälä TT, Böhm J, Mecklin JP, Kuopio T, Väyrynen JP. 2024.

Modern pathology 37: 100450

https://doi.org/10.1016/j.modpat.2024.100450

Mod Pathol 37 (2024) 100450

MODERN PATHOLOGY

USCAP UNITED STATES AND CANADIAN ACADEMY OF PATHOLOGY
Creating a Better Pathologist

Journal homepage: https://modernpathology.org/

Research Article

Quantitative Multiplexed Analysis of Indoleamine 2,3-Dioxygenase (IDO) and Arginase-1 (ARG1) Expression and Myeloid Cell Infiltration in Colorectal Cancer

Hanna Elomaa[a,b], Jouni Härkönen[c,d], Sara A. Väyrynen[e], Maarit Ahtiainen[c], Shuji Ogino[f,g,h,i], Jonathan A. Nowak[f], Mai Chan Lau[j,k], Olli Helminen[l], Erkki-Ville Wirta[m,n], Toni T. Seppälä[n,o,p,q], Jan Böhm[c], Jukka-Pekka Mecklin[b,r], Teijo Kuopio[a,c], Juha P. Väyrynen[l,*]

[a] *Department of Biological and Environmental Science, University of Jyväskylä, Jyväskylä, Finland;* [b] *Department of Education and Research, Hospital Nova of Central Finland, Well Being Services County of Central Finland, Jyväskylä, Finland;* [c] *Department of Pathology, Hospital Nova of Central Finland, Well Being Services County of Central Finland, Jyväskylä, Finland;* [d] *Faculty of Health Sciences, A.I. Virtanen Institute for Molecular Sciences, University of Eastern Finland, Kuopio, Finland;* [e] *Department of Internal Medicine, Oulu University Hospital, Oulu, Finland;* [f] *Program in Molecular Pathological Epidemiology, Department of Pathology, Brigham and Women's Hospital and Harvard Medical School, Boston, Massachusetts;* [g] *Department of Epidemiology, Harvard T.H. Chan School of Public Health, Boston, Massachusetts;* [h] *Broad Institute of MIT and Harvard, Cambridge, Massachusetts;* [i] *Cancer Immunology and Cancer Epidemiology Programs, Dana-Farber Harvard Cancer Center, Boston, Massachusetts;* [j] *Bioinformatics Institute (BII), Agency of Science, Technology and Research (A*STAR), Singapore, Singapore;* [k] *Singapore Immunology Network (SIgN), Agency of Science, Technology and Research (A*STAR), Singapore, Singapore;* [l] *Translational Medicine Research Unit, Medical Research Center Oulu, Oulu University Hospital, University of Oulu, Oulu, Finland;* [m] *Department of Gastroenterology and Alimentary Tract Surgery, Tampere University Hospital, Tampere, Finland;* [n] *Faculty of Medicine and Health Technology, Tampere University and Tays Cancer Center, Tampere University Hospital, Tampere, Finland;* [o] *Department of Gastrointestinal Surgery, Helsinki University Central Hospital, University of Helsinki, Helsinki, Finland;* [p] *Applied Tumor Genomics, Research Program Unit, University of Helsinki, Helsinki, Finland;* [q] *Abdominal Center, Helsinki University Hospital, Helsinki, Finland;* [r] *Faculty of Sport and Health Sciences, University of Jyväskylä, Jyväskylä, Finland*

ARTICLE INFO

Article history:
Received 19 October 2023
Revised 12 January 2024
Accepted 4 February 2024
Available online 16 February 2024

Keywords:
bioimage analysis
colorectal carcinoma
multiplex immunohistochemistry
prognostic factors
spatial analysis
tumor immunology

ABSTRACT

Indoleamine 2,3-dioxygenase (IDO) and arginase-1 (ARG1) are amino acid–metabolizing enzymes, frequently highly expressed in cancer. Their expression may deplete essential amino acids, lead to immunosuppression, and promote cancer growth. Still, their expression patterns, prognostic significance, and spatial localization in the colorectal cancer microenvironment are incompletely understood. Using a custom 10-plex immunohistochemistry assay and supervised machine learning–based digital image analysis, we characterized IDO and ARG1 expression in monocytic cells, granulocytes, mast cells, and tumor cells in 833 colorectal cancer patients. We evaluated the prognostic value and spatial arrangement of IDO- and ARG1-expressing myeloid and tumor cells. IDO was mainly expressed not only by monocytic cells but also by some tumor cells, whereas ARG1 was predominantly expressed by granulocytes. Higher density of IDO^+ monocytic cells was an independent prognostic factor for improved cancer-specific survival both in the tumor center ($P_{trend} = .0002$; hazard ratio [HR] for the highest ordinal category Q4 [vs Q1], 0.51; 95% CI, 0.33-0.79) and the invasive margin ($P_{trend} = .0015$). Higher density of granulocytes was associated with prolonged cancer-specific survival in univariable models, and higher $FCGR3^+ARG1^+$ neutrophil density in the tumor center also in multivariable analysis ($P_{trend} = .0020$). Granulocytes were, on average, located closer to tumor cells than monocytic cells. Furthermore, IDO^+ monocytic cells and $ARG1^-$ granulocytes were closer than IDO^- monocytic cells and $ARG1^+$ granulocytes, respectively. The mRNA expression of the *IDO1* gene was assessed in myeloid and tumor cells using publicly available single-cell RNA sequencing data for 62 colorectal cancers. *IDO1* was

* Corresponding author.
E-mail address: juha.vayrynen@oulu.fi (J.P. Väyrynen).

https://doi.org/10.1016/j.modpat.2024.100450

mainly expressed in monocytes and dendritic cells, and high *IDO1* activity in monocytes was associated with enriched immunostimulatory pathways. Our findings provided in-depth information about the infiltration patterns and prognostic value of cells expressing IDO and/or ARG1 in the colorectal cancer microenvironment, highlighting the significance of host immune response in tumor progression.

Introduction

Amino acid metabolism is often altered in cancer, and colorectal cancer is frequently associated with upregulated expression of amino acid–metabolizing enzymes indoleamine 2,3-dioxygenase (IDO) and arginase-1 (ARG1).[1,2] Tryptophan is an essential amino acid, which promotes T cell activation and proliferation. IDO plays an important role in the catabolism of tryptophan into kynurenine, leading to diminished tryptophan levels and potentially contributing to T cell suppression.[3] L-arginine is a semiessential amino acid, promoting the production of memory T cells and T cell survival. ARG1 is involved in the catabolism of L-arginine to L-ornithine and urea.[4] Increased expression of ARG1 may deplete L-arginine levels and thus lead to immunosuppression and cancer progression.[5] Some studies have found high expression of IDO and ARG1 to be associated with lower T cell activity, immune tolerance, metastasis, and poor clinical outcome in various tumors,[6,7] including colorectal cancer.[2,8,9] Thus, IDO and ARG1 are potential targets for cancer immunotherapy.

IDO is expressed by several cells in the tumor microenvironment, including monocytic cells, tumor cells, and endothelial cells,[3] whereas ARG1 is highly expressed by granulocytes.[10] The patterns of myeloid immune cell infiltration and IDO and ARG1 expression are heterogeneous between tumors, and their prognostic roles in colorectal cancer are still incompletely understood. Phenotyping myeloid cell subtypes using standard immunohistochemistry is challenging because of lack of single specific surface antigens,[11] but recent advances in multiplex immunohistochemistry have enabled detailed, spatially resolved analysis of multiple antigens at single-cell resolution.

In this study, we quantified the expression of IDO and ARG1 in monocytic cells, granulocytes, mast cells, and tumor cells in 833 colorectal cancers using a custom multiplexed immunohistochemistry assay and machine learning–based image analysis. We aimed to (1) characterize the expression patterns and prognostic value of IDO and ARG1 in the colorectal cancer microenvironment, (2) analyze the infiltration patterns and prognostic significance of myeloid cell subtypes, and (3) investigate the spatial proximity between IDO- and ARG1-expressing myeloid cells and tumor cells. We hypothesized that higher densities of IDO^+ and $ARG1^+$ myeloid cells and higher expression of IDO in tumor cells would be associated with shorter colorectal cancer-specific survival.

Material and Methods

Study Population

This study was based on an earlier described[12,13] cohort composing 1343 retrospectively collected primary tumor samples of colorectal cancer patients who underwent surgery during 2000-2015 in Central Finland Central Hospital, Jyväskylä, Finland. The study benefited from samples/data from Central Finland Biobank, Jyväskylä, Finland. In accordance with our previous studies,[12,13] we excluded patients who died within 30 days after surgery ($N = 40$) or had received preoperative radiotherapy, chemotherapy, or chemoradiotherapy ($N = 243$). After further excluding tumors with inadequate tumor tissue or unsuccessful multiplex immunohistochemistry staining either in the tumor center or in the invasive margin ($N = 346$), the final cohort included samples of 833 colorectal cancer patients (Table 1). These patients included two patients with known Lynch syndrome. All tumors were previously screened for mismatch repair (MMR) deficiency and *BRAF* V600E mutation with immunohistochemistry.[13] Furthermore, the densities of $CD3^+$ and $CD8^+$ T cells were previously analyzed using immunohistochemistry and machine learning–based image analysis.[13]

Multiplex Immunohistochemistry

Multiplex immunohistochemistry was conducted using tissue microarrays designed to contain 4 (2 tumor centers and 2 invasive margins) 1-mm diameter cores from each tumor.[13] We built a 10-plex immunohistochemistry assay to characterize IDO and ARG1 expression and myeloid cell infiltration in the colorectal cancer microenvironment. The panel included a myeloid cell marker (ITGAM [CD11b]) and markers for monocytic cells (CD14), granulocytes (CEACAM8 [CD66b]), mast cells (TPSAB1 [mast cell tryptase]), and tumor cells (KRT [keratin]). Additionally, IDO, ARG1, FCGR3 (CD16), HLADR, and CD33 were included. We follow the standardized nomenclature system for protein names recommended by the expert panel.[14]

The potential primary antibodies were screened based on their clinical use in the pathology laboratory of Hospital Nova (Jyväskylä, Finland) or their previous utilization in published literature. The characteristics and optimal dilutions of the antibodies were first tested using standard immunohistochemistry in a tissue microarray containing several cores from tonsils, normal colon mucosa, and colorectal adenocarcinomas. The cyclic 10-plex immunohistochemistry assay was then optimized, and the validity of the assay was confirmed by comparing the staining patterns of multiplex immunohistochemistry with those of standard single-plex immunohistochemistry (Supplementary Fig. S1).

The multiplex immunohistochemistry staining protocol, reagents, and the primary antibodies along with their dilutions and epitope retrieval conditions are shown in Supplementary Figure S2. All markers were sequentially stained with Bond-III automated immunohistochemistry stainer using a Bond Refine Detection kit (DS9800, Leica Biosystems), with 3,3'-diaminobenzidine replaced with 3-amino-9-ethylcarbazole. The tissue microarray specimens were cut at 3.5-μm thickness and stained in one batch to ensure uniform staining across all tissue microarrays (Supplementary Fig. S3). After each staining cycle, the slides were mounted with water-soluble mounting medium and

Table 1
Demographic and clinical characteristics of colorectal cancer cases according to the overall density of IDO^+ monocytic cells

Characteristic	Total *N*	IDO^+ monocytic cell density				
		Q1	Q2	Q3	Q4	*P*
All cases	833 (100%)	209 (25%)	208 (25%)	208 (25%)	208 (25%)	
Sex						.35
Female	411 (49%)	94 (45%)	103 (50%)	102 (49%)	112 (54%)	
Male	422 (51%)	115 (55%)	105 (50%)	106 (51%)	96 (46%)	
Age (y)						.12
<65	225 (27%)	68 (33%)	57 (27%)	53 (26%)	47 (23%)	
65-75	297 (36%)	71 (34%)	81 (39%)	77 (37%)	68 (33%)	
>75	311 (37%)	70 (34%)	70 (34%)	78 (38%)	93 (45%)	
Year of operation						< .0001
2000-2005	262 (31%)	62 (30%)	64 (31%)	65 (31%)	71 (34%)	
2006-2010	261 (31%)	89 (43%)	74 (36%)	53 (26%)	45 (22%)	
2011-2015	310 (37%)	58 (28%)	70 (34%)	90 (43%)	92 (44%)	
Tumor location						.072
Proximal colon	409 (49%)	91 (44%)	112 (54%)	92 (44%)	114 (55%)	
Distal colon	299 (36%)	86 (41%)	69 (33%)	84 (40%)	60 (29%)	
Rectum	125 (15%)	32 (15%)	27 (13%)	32 (15%)	34 (16%)	
AJCC stages						< .0001
I	143 (17%)	16 (8%)	41 (20%)	41 (20%)	45 (22%)	
II	317 (38%)	66 (32%)	65 (31%)	93 (45%)	93 (45%)	
III	270 (32%)	90 (43%)	64 (31%)	56 (27%)	60 (29%)	
IV	103 (12%)	37 (18%)	38 (18%)	18 (9%)	10 (5%)	
Tumor grade						.019
Low-grade (well to moderately differentiated)	704 (85%)	182 (87%)	177 (85%)	183 (88%)	162 (78%)	
High-grade (poorly differentiated)	129 (15%)	27 (13%)	31 (15%)	25 (12%)	46 (22%)	
Lymphovascular invasion						.0003
No	654 (79%)	144 (69%)	161 (77%)	174 (84%)	175 (84%)	
Yes	179 (21%)	65 (31%)	47 (23%)	34 (16%)	33 (16%)	
MMR status						< .0001
MMR proficient	705 (85%)	196 (94%)	184 (89%)	167 (80%)	158 (76%)	
MMR deficient	128 (15%)	13 (6%)	24 (12%)	41 (20%)	50 (24%)	
BRAF status						.12
Wild type	697 (84%)	181 (87%)	180 (87%)	171 (82%)	165 (79%)	
Mutant	136 (16%)	28 (13%)	28 (14%)	37 (18%)	43 (21%)	

AJCC, American Joint Committee on Cancer; MMR, mismatch repair.

scanned using an automated slide scanner equipped with a 20× objective. Destaining with ethanol and heat-mediated antibody stripping was performed before the sequential staining cycle, using the previously described method.[13]

Machine Learning-Based Cell and Tissue Phenotyping

Tissue microarray cores were recognized and separated into single-core images using the *TMA dearrayer* function in QuPath (0.2.3) image analysis software.[15] We removed all unrepresentative core images, which were fully or partly (less than 50% of the entire core area after all staining cycles present) detached or included a minimal amount of tumor tissue. Only representative cores with successful staining in all 10 staining cycles were included for further analyses. The single-core images were merged into 12-channel pseudoimmunofluorescence multiplex images (hematoxylin channels as the 1st and 12th, 10 multiplex immunohistochemistry staining channels as the 2nd to 11th) using the MultiStackReg macro (downloaded from: http://bradbusse.net/downloads.html) in Fiji/ImageJ software.[16] The hematoxylin channels were used for aligning nuclei of all core images. We followed previously used[13] principles for tissue microarray core selection criteria and for aligning single-core images into pseudoimmunofluorescence multiplex images. An example of the conversion of multiplex immunohistochemistry images into a 12-channel pseudoimmunofluorescence image is illustrated in Figure 1A, B.

Tissue compartments and cells were detected and phenotyped using previously validated[17] supervised machine learning–based algorithms in QuPath. The image analysis was performed blinded to the clinical data and following the main steps of a previous study.[12] We classified tissue compartments into tumor epithelium, stroma, and other (ignored from the analysis) using the built-in *pixel classifier* function. Cells were detected using the *cell detection* function and phenotyped into 5 main categories using the *object classifier* function: monocytic cells ($CD14^+CEACAM8^-TBSAB1^-KRT^-$), granulocytes ($CD14^-CEACAM8^+TBSAB1^-KRT^-$), mast cells ($CD14^-CEACAM8^-TBSAB1^+KRT^-$), tumor cells ($CD14^-CEACAM8^-TBSAB1^-KRT^+$), and other cells ($CD14^-CEACAM8^-TBSAB1^-KRT^-$) (Fig. 1C).

Further cell data processing, quantification, and statistical analyses were conducted in RStudio (1.3.1093) and R statistical programming (4.0.3, R Core Team) with packages *circlize* (0.4.15), *corrplot* (0.92), *ComplexHeatmap* (2.16.0), *ggplot2* (3.4.2), *ggpubr* (0.6.0), *gmodels* (2.18.1.1), *spatstat* (3.0-5), *survival* (3.5-5), *survminer* (0.4.9), and *tidyverse* (2.0.0). We categorized cells according to their cytoplasmic staining intensities of FCGR3 (Fc gamma receptor 3A, CD16), HLADR, IDO, and ARG1 by setting fixed cutoff values. We calculated cell densities (cells/mm^2) within the region of interest. The mean density was calculated when multiple cores were successfully analyzed from the same tumor region. IDO

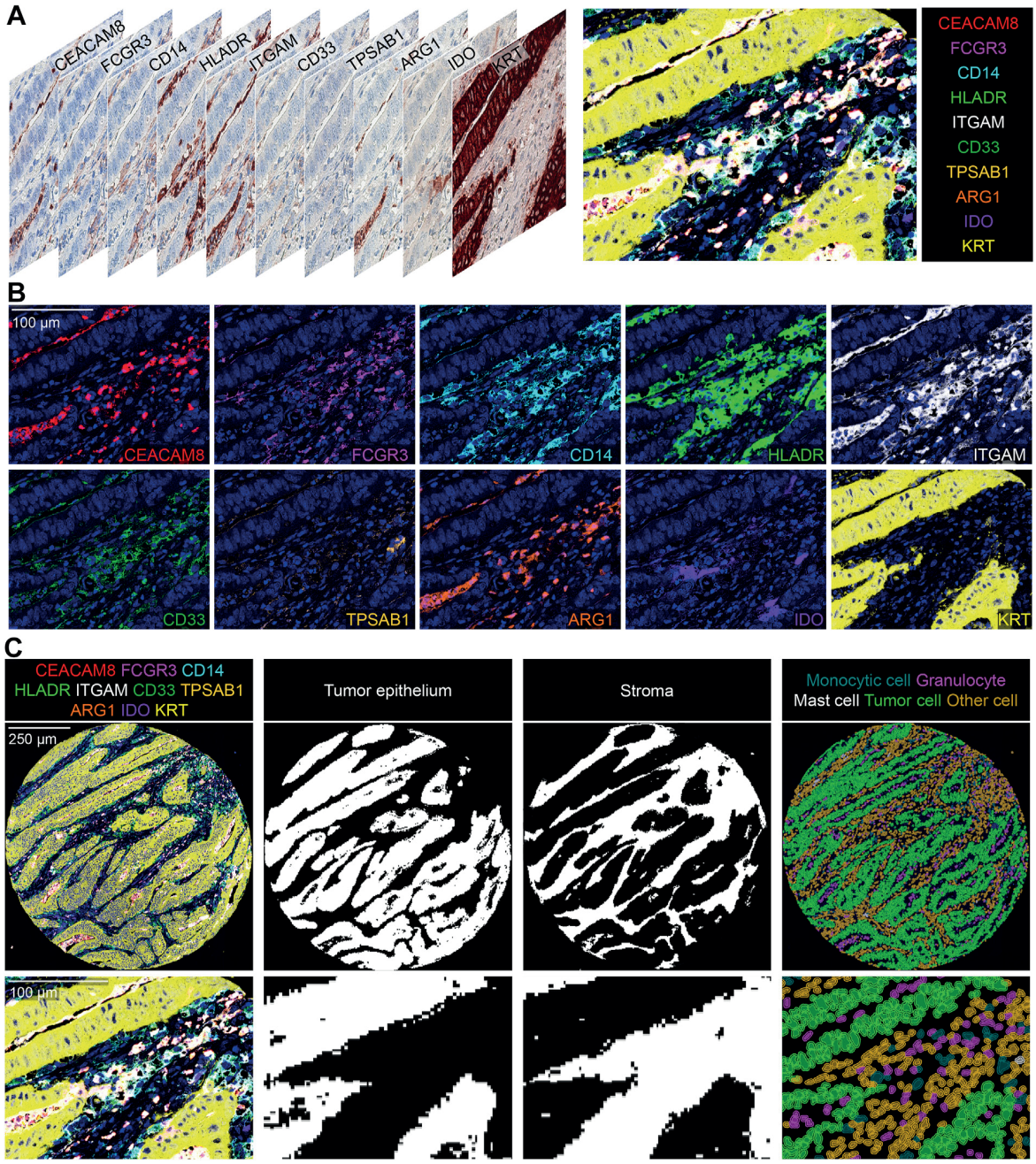

Figure 1.
Multiplex immunohistochemistry assay and machine learning–based image analysis. (A) Digitized multiplex immunohistochemistry images from each staining cycle were co-registered and converted into 10-plex pseudo-immunofluorescence images. (B) Each channel of a 10-plex pseudo-immunohistochemistry image represented separately. (C) Machine learning–based image analysis for detecting and classifying tissue compartments and cells in QuPath. Tissue compartments were classified into tumor epithelium and stroma. Cells were classified into monocytic cells, granulocytes, mast cells, tumor cells, and other cells.

expression in tumor cells was assessed by calculating the percentage of IDO^+ tumor cells relative to all tumor cells. Myeloid cell densities and IDO^+ tumor cell percentage were categorized into ordinal quartiles (Q1-Q4). In cell density variables with over 25% of zero cell densities, all zero densities were categorized as Q1, and the remaining values were divided equally into Q2 to Q4. All tumors with less than 1% of IDO^+ tumor cells were categorized as negative. To analyze spatial proximity between immune cells and tumor cells, we calculated nearest neighbor distances (NNDs). NND measures the distance from a specific point (eg, immune cell) to its closest neighbor point of a specific category (eg, tumor cell).

Statistical Analysis

The associations between categorical cell density variables and patient characteristics were tested using crosstabulation and the χ^2 test. The associations between continuous cell density variables

and patient characteristics were assessed with the Wilcoxon rank-sum test (comparing 2 classes) or the Kruskal-Wallis test (comparing more than 2 classes). Correlations between cell densities were assessed using Spearman's rank correlation test.

The survival outcomes were analyzed with univariable and multivariable Cox proportional hazard models for cancer-specific and overall survival, with cancer-specific survival as the primary survival endpoint. We limited the follow-up to 10 years, as Schoenfeld residual plots supported the proportionality of hazards during most of the follow-up period up to 10 years. The selection of variables for multivariable models was based on previous studies in this patient cohort[12,13] and included (reference category listed first) sex (male or female), age (<65, 65-75, and >75 years), year of operation (2000-2005, 2006-2010, and 2011-2015), tumor location (proximal colon, distal colon, and rectum), American Joint Committee on Cancer stages (I-II, III, and IV), tumor grade (well/moderately differentiated or poorly differentiated), lymphovascular invasion (negative or positive), MMR status (proficient or deficient), and *BRAF* status (wild type or mutant). Kaplan-Meier curves were used to visualize survival, and log-rank test was used to evaluate the statistical significance. In accordance with our previous studies,[12,13] P values < .005 were considered statistically significant based on the recommendation of an expert panel.[18]

Single-Cell RNA Transcriptomic Analysis for IDO1 Expression

We also assessed *IDO1* expression using publicly available single-cell data for 62 tumors. Single-cell RNA-seq counts and metadata were downloaded from Gene Expression Omnibus (GEO, GSID: GSE178341) and Broad Institute Single Cell Portal (https://singlecell.broadinstitute.org/single_cell, dataset c295). Single-cell data processing was conducted with *scCustomize* (1.1.3), *hdf5r* (1.3.8), and *Seurat* (1.3.8) R-packages. Only tumor samples were included in the analysis. Outlier cells were filtered by excluding those with more than 200 and less than 2500 features, as well as those with over 10% mitochondrial reads. Data were log-normalized and scaled with standard *Seurat* functions. Cell populations from the original publication[19] were used. For visual representation of the data, principal component analysis and uniform manifold approximation and projection were run with top 2500 variable features and 15 dimensions, respectively. *IDO1*-positive cells were classified as cells expressing over 1.5 log-normalized mRNA. Pathway analysis between *IDO1*$^+$ and *IDO1*$^-$ monocytes was computed with *fGSEA* (1.22) package for the differentially expressed genes assessed with *Seurat* function *FindMarkers* with *GO Biological Process* gene sets. To assess for differences in cellular interactions between different monocyte compositions, we computed *CellChat* (1.6.1) secretory interactions for the patients harboring either low or high fractions of IDO1+ monocytes (lower and higher quantiles, respectively).[20] Single-cell data visualization was conducted with *Seurat* and *CellChat* packages.

Results

Myeloid Cell Phenotypes and Density Analyses

We successfully analyzed 2813 tissue microarray cores for tumors of 833 colorectal cancer patients (mean, 3.4 per patient; SD, 0.71; tumor center, 1.8; SD, 0.43; and invasive margin, 1.6; SD, 0.52). Core-to-core correlations for myeloid cell densities were moderate to high both in the tumor center (R = 0.42-0.58) and in the invasive margin (R = 0.48-0.68) (Supplementary Fig. S4). We identified 24,310,185 cells across all tissue microarrays, of which 6.4% were monocytic cells, 3.9% were granulocytes, 1.4% were mast cells, and 42% were tumor cells.

We further classified monocytic cells according to HLADR and FCGR3 expression into mature CD14$^+$HLADR$^+$ and immature CD14$^+$HLADR$^-$ monocytic cells and into CD14$^+$FCGR3$^+$ and CD14$^+$FCGR3$^-$ monocytic cells. Granulocytes were further classified according to FCGR3 expression into FCGR3$^+$ neutrophils (CEACAM8$^+$FCGR3$^+$) and FCGR3$^-$ other granulocytes (CEACAM8$^+$FCGR3$^-$). The majority of CD14$^+$ monocytic cells were mature (HLADR$^+$, 84%) and more likely FCGR3$^+$ (65%) than FCGR3$^-$ (35%). Of CEACAM8$^+$ granulocytes, the majority (84%) were identified as FCGR3$^+$ neutrophils.

We evaluated the associations between myeloid cell densities and clinicopathologic features. Higher densities of monocytic cells and granulocytes were associated with proximal tumor location, high tumor grade, MMR deficiency, and *BRAF* mutation, whereas higher mast cell density was associated with low tumor grade, MMR proficiency, and absence of *BRAF* mutation. Both higher densities of granulocytes and mast cells were associated with low stage and absence of lymphovascular invasion (all P < .005, Supplementary Fig. S5). The correlations between densities of different myeloid cell subtypes were low to moderate (Supplementary Fig. S6).

IDO and ARG1 Expression Patterns

We next examined IDO and ARG1 expression patterns. IDO was mainly expressed by monocytic cells (4.1% of all monocytic cells), and the expression was enriched in mature monocytic cells (4.8% of HLADR$^+$ monocytic cells and 0.64% of HLADR$^-$ monocytic cells). Accordingly, IDO$^+$ monocytic cell density was more highly correlated with HLADR$^+$ and FCGR3$^+$ (R = 0.52 and R = 0.34) monocytic cells than with HLADR$^-$ and FCGR3$^-$ (R = 0.13 and R = 0.04) monocytic cells, respectively (Supplementary Fig. S6). In addition to monocytic cells, a small number of tumor cells (2.7%) expressed IDO. There was a strong positive correlation between IDO$^+$ monocytic cell density and IDO$^+$ tumor cell percentage (R = 0.62) (Supplementary Fig. S6). ARG1 was primarily expressed by granulocytes, of which 81% were ARG1$^+$. Furthermore, ARG1 was more likely expressed by FCGR3$^+$ neutrophils than FCGR3$^-$ granulocytes (87% and 13%, respectively). Accordingly, the densities of ARG1$^+$ and FCGR3$^+$ neutrophils were closely correlated (R = 0.90) (Supplementary Fig. S6). The correlations of IDO$^+$ monocytic cell and ARG1$^+$ granulocyte densities with CD3$^+$ and CD8$^+$ T cell densities were further examined in 807 tumors that were successfully analyzed for these immune cell types in both the tumor center and the invasive margin. IDO$^+$ monocytic cell densities were moderately correlated with T cell densities in both tumor compartments, whereas ARG1$^+$ granulocyte densities showed lower correlation with T cell densities (Supplementary Fig. S7).

We analyzed the associations of clinicopathological characteristics with the density of IDO$^+$ monocytic cells (Table 1), IDO$^+$ tumor cell percentage (Supplementary Table S1), and the density of ARG1$^+$ granulocytes (Supplementary Table S2). Higher densities of IDO$^+$ monocytic cells and ARG1$^+$ granulocytes and higher IDO$^+$ tumor cell percentage were associated with low stage, absence of lymphovascular invasion, and MMR deficiency. Higher density of granulocytes and higher IDO$^+$ tumor cell percentage were associated with high tumor grade and *BRAF* mutation. Furthermore, higher density of IDO$^+$ monocytic cells was associated with operation in 2011-2015, and higher IDO$^+$ tumor cell

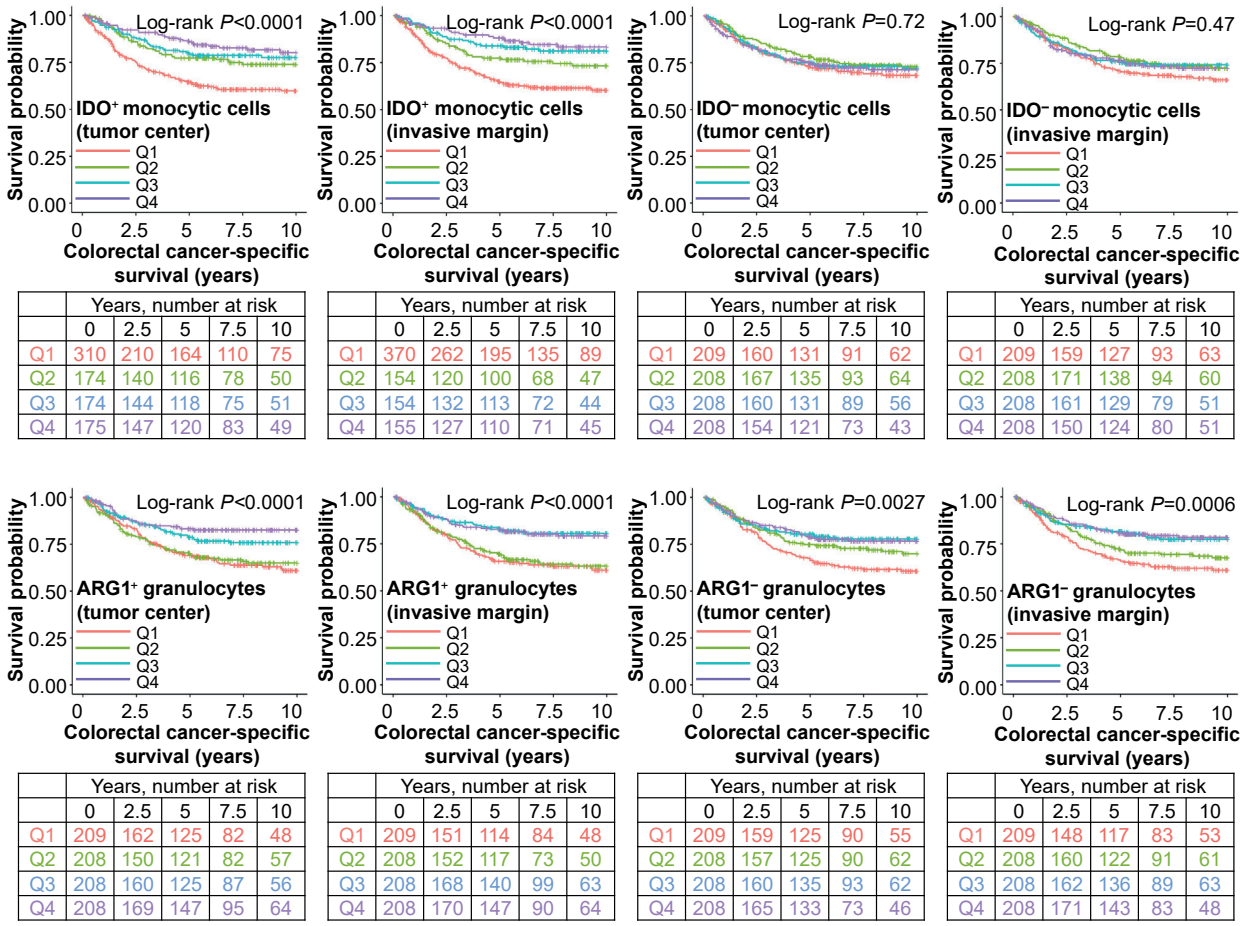

	Years, number at risk				
	0	2.5	5	7.5	10
Q1	310	210	164	110	75
Q2	174	140	116	78	50
Q3	174	144	118	75	51
Q4	175	147	120	83	49

	Years, number at risk				
	0	2.5	5	7.5	10
Q1	370	262	195	135	89
Q2	154	120	100	68	47
Q3	154	132	113	72	44
Q4	155	127	110	71	45

	Years, number at risk				
	0	2.5	5	7.5	10
Q1	209	160	131	91	62
Q2	208	167	135	93	64
Q3	208	160	131	89	56
Q4	208	154	121	73	43

	Years, number at risk				
	0	2.5	5	7.5	10
Q1	209	159	127	93	63
Q2	208	171	138	94	60
Q3	208	161	129	79	51
Q4	208	150	124	80	51

	Years, number at risk				
	0	2.5	5	7.5	10
Q1	209	162	125	82	48
Q2	208	150	121	82	57
Q3	208	160	125	87	56
Q4	208	169	147	95	64

	Years, number at risk				
	0	2.5	5	7.5	10
Q1	209	151	114	84	48
Q2	208	152	117	73	50
Q3	208	168	140	99	63
Q4	208	170	147	90	64

	Years, number at risk				
	0	2.5	5	7.5	10
Q1	209	159	125	90	55
Q2	208	157	125	90	62
Q3	208	160	135	93	62
Q4	208	165	133	73	46

	Years, number at risk				
	0	2.5	5	7.5	10
Q1	209	148	117	83	53
Q2	208	160	122	91	61
Q3	208	162	136	89	63
Q4	208	171	143	83	48

Figure 2.
Kaplan-Meier cancer-specific survival curves for the IDO$^+$ and IDO$^-$ monocytic cell and ARG1$^+$ and ARG1$^-$ granulocyte densities in the tumor center and in the invasive margin. The densities were divided into ordinal categories from low (Q1) to high (Q4). Statistical significance was determined with log-rank test.

percentage was associated with tumor location in the proximal colon. The associations between clinicopathologic features and IDO$^+$ and IDO$^-$ monocytic cells, as well as ARG1$^+$ and ARG1$^-$ granulocytes, in the tumor center and the invasive margin are shown in Supplementary Figure S8.

Survival Analyses

We examined the prognostic value of IDO and ARG1 expression, along with monocytic cell, granulocyte, and mast cell populations defined with various marker combinations. The total number of deaths was 477 (57%), including 224 (27%) cancer-specific deaths. The median follow-up time for censored cases was 10.1 years (IQR, 6.6-13.0). The overall density of monocytic cells did not associate with survival in univariable (Supplementary Fig. S9; Table S3) or multivariable (Supplementary Table S3) models. However, higher density of IDO$^+$ monocytic cells was associated with favorable cancer-specific and overall survival both in univariable (Fig. 2; Table 2) and multivariable analyses (Table 2) (cancer-specific survival, tumor center: P_{trend} = .0002; multivariable hazard ratio [HR] for Q4 [vs Q1], 0.51; 95% CI, 0.33-0.79; invasive margin: P_{trend}=0.0015; multivariable HR for Q4 [vs Q1], 0.51; 95% CI, 0.31-0.83). Full multivariable Cox regression models for IDO$^+$ and IDO$^-$ monocytic cells with all variables are shown in Supplementary Table S4. When tumor epithelial and stromal compartments were examined separately, the point estimate was stronger in the stroma (Supplementary Table S5).

To gain insights into the prognostic significance of more detailed monocytic cell populations, we assessed the prognostic impact of HLADR (Supplementary Table S6) and FCGR3 (Supplementary Table S7) expression in all monocytic cells and IDO$^+$ monocytic cells. The positive prognostic value of IDO$^+$ monocytic cells remained in the mature (HLADR$^+$) but not in the immature (HLADR$^-$) subset, whereas the survival associations were quite similar for FCGR3$^+$ and FCGR3$^-$ monocytic cell subpopulations.

In addition to monocytic cells, the prognostic significance of IDO expression in tumor cells was assessed. Higher IDO$^+$ tumor cell percentage was associated with longer survival in univariable models both in the tumor center and in the invasive margin, but these associations did not remain significant in multivariable models (Supplementary Fig. S10).

Higher density of granulocytes associated with favorable cancer-specific survival in univariable analyses in both the tumor center and the invasive margin (Supplementary Fig. S9; Table S3), but not in multivariable models (Supplementary Table S3). Comparable results were observed for ARG1$^+$ (Fig. 2; Supplementary

Table 2
Univariable and multivariable Cox regression models for cancer-specific and overall survival according to densities of IDO^+ and IDO^- monocytic cells in the tumor center and the invasive margin

	No. of cases	Colorectal cancer-specific survival			Overall survival		
		No. of events	Univariable HR (95% CI)	Multivariable HR (95% CI)	No. of events	Univariable HR (95% CI)	Multivariable HR (95% CI)
Tumor center							
IDO^+ monocytic cell density	833	216			406		
Q1	303	109	1 (referent)	1 (referent)	175	1 (referent)	1 (referent)
Q2	177	42	0.56 (0.40-0.81)	0.58 (0.40-0.84)	76	0.63 (0.48-0.82)	0.68 (0.51-0.89)
Q3	176	36	0.49 (0.34-0.71)	0.53 (0.36-0.78)	76	0.64 (0.49-0.83)	0.60 (0.45-0.79)
Q4	177	29	0.38 (0.25-0.58)	0.51 (0.33-0.79)	79	0.64 (0.49-0.84)	0.69 (0.52-0.91)
P_{trend}			<0.0001	0.0002		0.0003	0.0012
IDO^- monocytic cell density	833	216			406		
Q1	209	60	1 (referent)	1 (referent)	109	1 (referent)	1 (referent)
Q2	208	50	0.81 (0.55-1.18)	0.92 (0.63-1.35)	93	0.83 (0.63-1.10)	0.91 (0.69-1.21)
Q3	208	53	0.88 (0.61-1.28)	0.87 (0.59-1.26)	96	0.90 (0.68-1.18)	0.87 (0.65-1.15)
Q4	208	53	0.93 (0.74-1.34)	0.96 (0.65-1.42)	108	1.08 (0.83-1.41)	0.97 (0.73-1.28)
P_{trend}			0.78	0.73		0.50	0.73
Invasive margin							
IDO^+ monocytic cell density	833	216			406		
Q1	364	130	1 (referent)	1 (referent)	204	1 (referent)	1 (referent)
Q2	156	37	0.60 (0.42-0.87)	0.77 (0.53-1.12)	70	0.72 (0.55-0.94)	0.79 (0.60-1.04)
Q3	156	27	0.41 (0.27-0.63)	0.62 (0.40-0.96)	66	0.63 (0.48-0.84)	0.70 (0.53-0.94)
Q4	157	22	0.34 (0.22-0.54)	0.51 (0.31-0.83)	66	0.65 (0.49-0.86)	0.66 (0.49-0.90)
P_{trend}			<0.0001	0.0015		0.0002	0.0024
IDO^- monocytic cell density	833	216			406		
Q1	209	64	1 (referent)	1 (referent)	102	1 (referent)	1 (referent)
Q2	208	51	0.77 (0.53-1.11)	1.07 (0.73-1.56)	97	0.92 (0.70-1.22)	1.11 (0.84-1.49)
Q3	208	50	0.79 (0.55-1.15)	1.05 (0.72-1.55)	105	1.07 (0.82-1.41)	1.17 (0.88-0.56)
Q4	208	51	0.83 (0.57-1.20)	0.87 (0.59-1.28)	102	1.07 (0.81-1.41)	1.00 (0.75-1.33)
P_{trend}			0.35	0.51		0.42	0.93

The densities were divided into ordinal quartile categories from low (Q1) to high (Q4). Multivariable Cox proportional hazards regression models were adjusted for sex (male, female), age (<65, 65-75, and >75 years), year of operation (2000-2005, 2006-2010, and 2011-2015), tumor location (proximal colon, distal colon, and rectum), stages (I-II, III, and IV), tumor grade (well/moderately differentiated and poorly differentiated), lymphovascular invasion (negative or positive), MMR status (proficient or deficient), and *BRAF* status (wild type or mutant). P_{trend} values were calculated by using the 4 categories of immune cell densities as continuous variables in univariable and multivariable Cox proportional hazard regression models.

Table S8) and $FCGR3^+$ subpopulations (Supplementary Table S9). However, higher density of $ARG1^+FCGR3^+$ neutrophils in the tumor center was also significantly associated with longer cancer-specific survival in multivariable analysis (P_{trend} = .0020; HR, 0.49; 95% CI, 0.31-0.76; Supplementary Table S9). Higher mast cell density in the invasive margin was associated with longer cancer-specific survival in univariable analyses (Supplementary Fig. S9; Table S3), but not in multivariable models (Supplementary Table S3).

In secondary analyses, we examined the survival association of IDO^+ monocytic cells and $ARG1^+$ granulocytes in the strata of MMR status and stage. The survival association of IDO^+ monocytic cell density did not statistically significantly differ by MMR status ($P_{interaction}$ > .08) (Supplementary Table S10) or stage ($P_{interaction}$ > .17) (Supplementary Table S11). The survival association of $ARG1^+$ granulocyte density did not statistically significantly differ by MMR status ($P_{interaction}$ > .57) (Supplementary Table S12), but $ARG1^+$ granulocytes appeared to predict survival in stages I to III tumors and not in stage IV tumors ($P_{interaction}$ = .047 for multivariable cancer-specific survival models (Supplementary Table S13).

To assess the potential effect of the number of tissue microarray cores analyzed, we conducted survival analyses for the densities of IDO^+ monocytic cells and $ARG1^+$ granulocytic cells stratified by the number of analyzed cores (2-3 vs 4) (Supplementary Tables S14 and S15). The prognostic value did not statistically significantly differ by the number of analyzed tumor cores ($P_{interaction}$ > .24 for IDO^+ monocytic cells, $P_{interaction}$ > .32 for $ARG1^+$ granulocytes).

Spatial Analyses

We measured spatial arrangement of myeloid cells relative to tumor cells by using the NND analysis and found that granulocytes were significantly closer to tumor cells than monocytic cells and mast cells. Furthermore, $ARG1^-$ granulocytes were closer to tumor cells than $ARG1^+$ granulocytes, and IDO^+ monocytic cells were closer than IDO^- monocytic cells. However, the average NNDs from IDO^+ monocytic cells or $ARG1^+$ granulocytes to tumor cells did not associate with colorectal cancer-specific survival (Fig. 3).

Single-Cell RNA Transcriptomic Analysis for IDO1 Expression

To further characterize the factors potentially contributing to the association between higher IDO expression and better outcome, we analyzed *IDO1* expression in single-cell RNA transcriptomic data. Using previously determined cell communities (Fig. 4A),[19] we measured the expression of *IDO1* mRNA across the immune cells, tumor cells, and stromal cells. As IDO is a key regulator of tryptophan catabolism, we measured the activity of

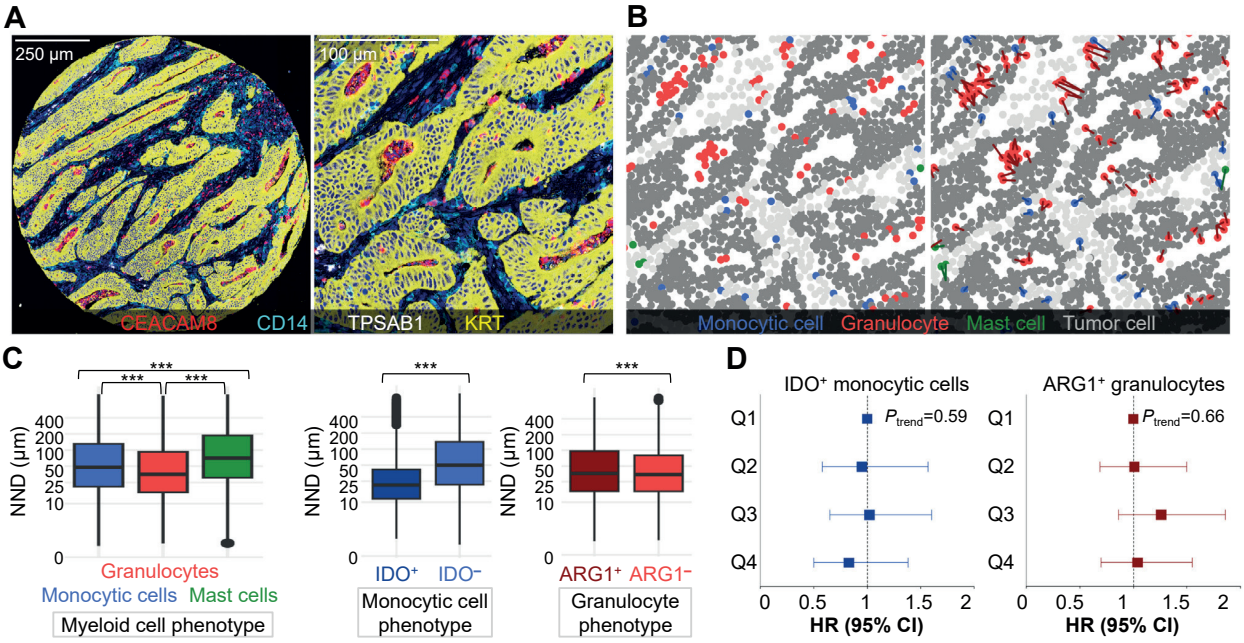

Figure 3.
Nearest neighbor distance (NND) analysis for myeloid cells and tumor cells. (A) Example multiplex-immunohistochemistry image representing granulocytes (CEACAM8$^+$), monocytic cells (CD14$^+$), mast cells (TPSAB1$^+$), and tumor cells (KRT$^+$) in one tumor core and in close-up view. (B) Cell phenotyping maps and NNDs calculated from each myeloid cell to the closest tumor cell. (C) Boxplots representing the average distribution of NNDs across all tumor images ($N = 2813$). The statistical significance was tested with Wilcoxon rank-sum test. *** $P < .0001$. (D) Forest plots visualizing colorectal cancer-specific survival according to average NNDs for 2 specific immune cell types in each tumor. NNDs were divided into ordinal quartiles from short (Q1) to long (Q4) NND. We only included tumors with at least one specific immune cell ($N = 626$ for IDO$^+$ monocytic cells and $N = 821$ for ARG1$^+$ granulocytes). Multivariable Cox proportional hazards regression models were represented with hazard ratios (HRs) and 95% CI as whiskers. The models were adjusted for sex (male and female), age (<65, 65–75, and >75 years), year of operation (2000-2005, 2006-2010, and 2011-2015), tumor location (proximal colon, distal colon, and rectum), stages (I-II, III, and IV), tumor grade (well/moderately differentiated and poorly differentiated), lymphovascular invasion (negative or positive), MMR status (proficient or deficient), and *BRAF* status (wild type or mutant).

the tryptophan metabolism pathway (GO:0006568). The activities of *IDO1* (Fig. 4B) and tryptophan metabolism (Fig. 4C) were highest in monocytes and dendritic cells. Next, we calculated the median percentage of *IDO1*$^+$ cells within each cell community. *IDO1*$^+$ fraction was the highest on dendritic cells, as almost 30% of all patients' dendritic cells, by median, were *IDO1*$^+$ (Fig. 4D). To find the enriched cell processes, we conducted a gene set enrichment analysis for *IDO1*$^+$ (vs *IDO1*$^-$) monocytes. We found that several IFNG-regulated immunostimulatory pathways were positively enriched in *IDO1*$^+$ monocytes (Fig. 4E). Thus, we further studied the association between *IDO1* and *IFNG* by dividing tumors based on high and low monocytic cell *IDO1* expression. *IFNG* was strongly expressed in T cells within tumors exhibiting high *IDO1* activity in monocytes. In tumors with low monocytic *IDO1* activity, lymphocyte *IFNG* expression was lower, and the population of T cells was diminished (Fig. 4F). To investigate the impact of high *IDO1* expression on cellular interactions, we compared the number of interactions between tumors with higher and lower *IDO1* expressions. High *IDO1* expression was associated with stronger interactions between most immune cells, although interactions between granulocytes and other cell types were diminished (Fig. 4G).

Discussion

In the present study, we used a detailed immunohistochemical multimarker technique and machine learning–based image analysis to comprehensively characterize IDO and ARG1 expression patterns and myeloid immune cell infiltration in the colorectal cancer microenvironment of 833 tumors. We also used publicly available single-cell mRNA data for 62 colorectal cancer patients to further assess functional pathways associated with *IDO1* expression. These analyses improve our understanding of the spatial distribution and implications of IDO and ARG1 within the colorectal cancer microenvironment and offer potential insights into tumor immunology, treatment development, and biomarker discovery.

We found that IDO was mainly expressed by monocytic cells and tumor cells, whereas ARG1 was expressed by granulocytes. Although the overall density of monocytic cells was not prognostic, higher infiltration of IDO$^+$ monocytic cells both in the tumor center and the invasive margin was associated with improved cancer-specific survival, independent of potential confounding factors such as MMR status and stage. Higher percentage of IDO$^+$ tumor cells was also associated with longer survival but only in univariable models. Our findings were in line with previous studies in colorectal[21,22] and other solid cancers[23-25] reporting the association between high IDO expression and prolonged survival. In contrast, some studies have reported an association between increased IDO expression and poor survival in colorectal cancer[8,26] and some other solid cancers.[7] The diversity of the analysis methods may account for this discrepancy, and to our knowledge, no previous studies have specifically evaluated CD14$^+$IDO$^+$ monocytic cells, which is impossible using conventional single-color immunohistochemistry.

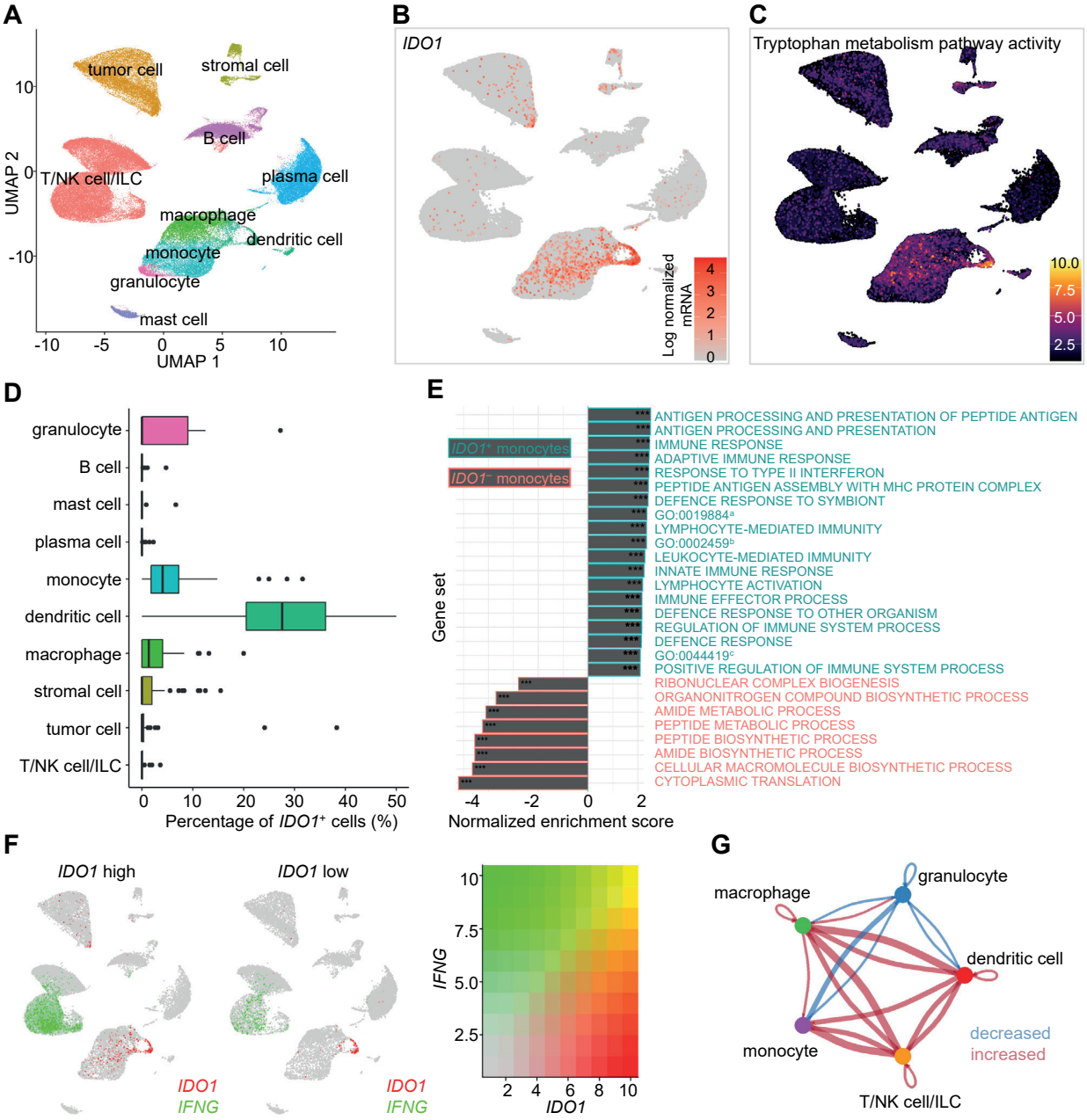

Figure 4.

The distribution of *IDO1* expression in immune cell subtypes and tumor cells. (A) Uniform manifold approximation and projection (UMAP) representation for cell communities clustering in 62 tumors. (B) The expression level of *IDO1* in cell communities. (C) The activity of tryptophan metabolism pathway in cell communities. (D) Boxplots representing the percentage of *IDO1* active cells in cell populations ($N = 62$ tumors). (E) Bar plot of the pathway enrichment analysis shows pathways activated in *IDO1*$^+$ monocytes in green and those activated in *IDO1*$^-$ monocytes in red. ***$P < .0001$. [a]ANTIGEN PROCESSING AND PRESENTATION OF EXOGENOUS ANTIGEN. [b]ADAPTIVE IMMUNE RESPONSE BASED ON SOMATIC RECOMBINATION OF IMMUNE RECEPTORS BUILT FROM LEUCINE-RICH REPEAT DOMAINS. [c]BIOLOGICAL PROCESS INVOLVED IN INTERSPECIES INTERACTION BETWEEN ORGANISMS. (F) *IFNG* activity in tumors with high and low *IDO1* activity. (G) The number of cellular interactions between immune cells in *IDO1* high tumors. The width of the edges represents the number of communications. Red color indicates increased number of communications and blue decreased number of communications in *IDO1* high tumors compared to *IDO1* low tumors. ILC, innate lymphoid cell; NK, natural killer; UMAP, Uniform manifold approximation and projection.

Higher granulocyte density in the tumor center and the invasive margin was a favorable prognostic factor in univariable analyses, supported by several previous studies in colorectal cancer.[17,27-31] However, conflicting findings of the association between higher granulocyte density and worse colorectal cancer survival have also been reported.[32] Our study benefited from the multimarker approach, which enabled us to define granulocyte subpopulations based on simultaneous expression of CEACAM8, FCGR3, and ARG1. The majority of granulocytes were FCGR3$^+$ neutrophils and also expressed ARG1. Higher density of CEACAM8$^+$FCGR3$^+$ARG1$^+$ neutrophils in the tumor center was significantly associated with prolonged cancer-specific survival also in multivariable analysis. As we further assessed the prognostic value of ARG1$^+$ granulocytes in strata of the stage, the

independent survival association remained only in the lower stages (I-III) tumors. These findings suggest that neutrophils, many of which express ARG1$^+$, may lose their beneficial antitumor effect during the progression of colorectal cancer.

The association between higher IDO and ARG1 expression and longer cancer-specific survival is paradoxical, as IDO and ARG1 are thought to be immunosuppressive enzymes.[33] The factors accounting for this association are not obvious, but our findings and previous literature provide some potential explanations. It has been hypothesized that increased expression of IDO and ARG1 could be a compensatory, intrinsic negative feedback reaction to the generally strengthened antitumor immune response in the tumor microenvironment.[22,34-36] In accordance with this hypothesis, we found that immunostimulatory pathways were enriched in *IDO1*$^+$ monocytes. IFNG is a molecule contributing to several proinflammatory processes and has been suggested to induce IDO expression.[8,36,37] Our single-cell RNA analysis also supported an association between *IDO1* and *IFNG* expression, as cases with higher monocyte-derived *IDO1* expression were associated with higher numbers of T cells and with higher expression of *IFNG* on T cells compared with those with lower *IDO1* expression. A positive correlation between IDO$^+$ monocytic cells and T cells was also observed in the main cohort and has been reported in several previous studies.[22,36,38] Furthermore, it is known that certain cancer risk factors may paradoxically be linked with favorable survival among cancer patients, which is explained by the interpersonal heterogeneity of cancer.[39] In this study, we found that higher density of IDO$^+$ monocytic cells, higher percentage of IDO$^+$ tumor cells, and higher density of ARG1$^+$ granulocytes were associated with low stage and absence of lymphovascular invasion, which are known to be strong favorable prognostic indicators in colorectal cancer.[40] Therefore, higher expression of these immunosuppressive molecules could be a marker of a less aggressive tumor phenotype. Indeed, some cell types, such as ARG1$^+$ granulocytes, had a considerably weaker prognostic association after adjustment for other clinicopathologic features. However, IDO$^+$ monocytic cells remained significant in multivariable Cox regression models for cancer-specific survival after adjusting for a group of known prognostic indicators such as disease stage, tumor grade, lymphovascular invasion, MMR status, and *BRAF* status, supporting their independent prognostic value.

To our knowledge, this is the first study examining the myeloid cell infiltration along with IDO and ARG1 immunoregulatory enzymes in colorectal cancer using multiplex immunohistochemistry. However, some important limitations need to be considered. First, there are no standardized and fully specific markers for phenotyping myeloid cells, which complicates the interpretation of findings between different studies. However, we selected well-validated antibodies that were in clinical use at our pathology laboratory or utilized in previous studies. Second, we used tissue microarrays instead of whole tissue slides, which may not fully represent the whole tumor immune milieu.[41] However, we analyzed tumor cores taken from both the tumor center and the invasive margin and reached moderate-to-high core-to-core correlations. This suggested tissue microarray–based methods to be suitable for evaluating these immune cell infiltrates. Third, we used a cyclic staining assay, where the loss of tumor cores was higher than in standard immunohistochemical staining. Still, the size of our study cohort remained large, and the tissue microarray-based multiplex-immunohistochemistry analysis enabled us to analyze all samples cost-efficiently in one batch. Fourth, most patients are non-Hispanic white. Thus, our findings need to be confirmed in patients with non-White Caucasian ethnicities. Independent validation study is also required to confirm whether IDO1$^+$ monocytic cell densities could be used as a clinically relevant prognostic marker in colorectal cancer. Fifth, data on recurrence-free survival were not available for this study. Nevertheless, a long follow-up period enabled the assessment of long-term survival impact, based on cancer-specific and overall survival outcomes. Sixth, the patients underwent surgery over a 16-year period, during which cancer treatments have evolved, potentially influencing disease outcome and clinicopathologic features of the patients included in the cohort. To minimize potential bias, we included the year of operation as a covariate in the multivariable survival models.

This study has notable strengths. It included a large cohort of 833 colorectal cancers, with a comprehensive database from multiple previous studies,[12,13,34,42-45] and an independent single-cell RNA transcriptomic dataset with 62 colorectal cancers. We only included patients without neoadjuvant treatment to eliminate the possible bias related to its effects on the immune microenvironment, which however led to the underrepresentation of rectal cancers. Multiplex-immunohistochemistry analysis combined with machine learning-based image analysis enabled detailed phenotyping of cells using several markers and the study of spatial relationships between cell types, which cannot be done using conventional immunohistochemistry.[11]

In conclusion, our study provided detailed information about IDO and ARG1 expression patterns and myeloid cell infiltration in the colorectal cancer microenvironment. We found that the density of IDO-expressing monocytic cells was an independent favorable prognostic factor, and at the single-cell level, *IDO1* expression was strongly associated with *IFNG*-regulated immunostimulatory pathways. Our results provide insight into the complexity of colorectal cancer immunity and suggest that comprehensive characterization is necessary to dissect its effects on patient outcomes.

Author Contributions

H.E., S.A.V., S.O., J.A.N., J.B., T.K., and J.P.V. designed study concept; J.B., J.P.M., T.K., and J.P.V. provided resources; H.E., J.H., M.A., O.H., E.V.W., T.T.S., J.B., J.P.M., and J.P.V. were responsible for data curation; T.K. and J.P.V. supervised this study; H.E. and J.P.V. conducted formal analysis and acquired the funding; H.E., J.H., S.A.V., M.A., O.H., E.V.W., T.T.S., J.B., J.P.M., T.K., and J.P.V. conducted investigation; H.E., J.H., S.A.V., M.C.L., and J.P.V. visualized the data; H.E., J.H., S.A.V., .S.O., J.A.N., M.C.L., and J.P.V. contributed to the methodology; H.E., J.H., and J.P.V. wrote the original draft. All authors edited and approved the manuscript.

Data Availability

Single-cell RNA-seq counts and metadata were publicly available at GEO (GSE178341) and at Broad Institute Single Cell Portal (https://singlecell.broadinstitute.org/single_cell, dataset c295). Other data generated and/or analyzed during this study are not publicly available. The sharing of data will require approval from relevant ethics committees and/or biobanks. Further information including the procedures to obtain and access data of Finnish Biobanks are described at https://finbb.fi/en/fingenious-service.

Funding

This study was funded by Cancer Foundation Finland (59-5619 to J.P.V. and to H.E.), Emil Aaltonen Foundation (220022K to H.E.), Orion Research Foundation sr (to H.E.), Päivikki and Sakari

Sohlberg Foundation (to H.E.), Sigrid Jusélius Foundation (230229 to J.P.V.), and the State Research Funding (to J.P.V. and to H.E.). T.T.S. was supported by research grants from Jane and Aatos Erkko Foundation, Sigrid Jusélius Foundation, Finnish Medical Foundation, Emil Aaltonen Foundation, Cancer Foundation Finland, Relander Foundation, and the State Research Funding. The funders had no role in study design, data collection and analysis, decision to publish, or preparation of the manuscript.

Declaration of Competing Interest

J.A. Nowak reports grant funding from Natera and consulting fees from Leica Biosystems. T.T. Seppälä reports a consultation fee from Amgen Finland and being a co-owner and CEO of Healthfund Finland Ltd, and the Clinical Advisory Board of LS Cancer Diag Ltd. The other authors declare no potential conflicts of interest.

Ethics Approval and Consent to Participate

The study was conducted according to the guidelines of the Declaration of Helsinki and approved by the hospital administration and the ethics board (Dnro13U/2011, 1/2016, 8/2020, and 2/2023), the Finnish Medicines Agency (Fimea), and the Central Finland Biobank (BB23-0172). The need to obtain informed consent from the study patients was waived (Dnro FIMEA/2023/001573, 4/2023).

Supplementary Material

The online version contains supplementary material available at https://doi.org/10.1016/j.modpat.2024.100450

References

1. Zhang J, Zou S, Fang L. Metabolic reprogramming in colorectal cancer: regulatory networks and therapy. *Cell Biosci*. 2023;13(1):25. https://doi.org/10.1186/s13578-023-00977-w
2. Ma Z, Lian J, Yang M, et al. Overexpression of Arginase-1 is an indicator of poor prognosis in patients with colorectal cancer. *Pathol Res Pract*. 2019;215(6):152383. https://doi.org/10.1016/j.prp.2019.03.012
3. Meireson A, Devos M, Brochez L. IDO Expression in cancer: different compartment, different functionality? *Front Immunol*. 2020;11:531491. https://doi.org/10.3389/fimmu.2020.531491
4. Bronte V, Zanovello P. Regulation of immune responses by L-arginine metabolism. *Nat Rev Immunol*. 2005;5(8):641–654. https://doi.org/10.1038/nri1668
5. Wei Z, Liu X, Cheng C, Yu W, Yi P. Metabolism of amino acids in cancer. *Front cell Dev Biol*. 2020;8:603837. https://doi.org/10.3389/fcell.2020.603837
6. Grzywa TM, Sosnowska A, Matryba P, et al. Myeloid cell-derived arginase in cancer immune response. *Front Immunol*. 2020;11(8):938. https://doi.org/10.3389/fimmu.2020.00938
7. Wang S, Wu J, Shen H, Wang J. The prognostic value of IDO expression in solid tumors: a systematic review and meta-analysis. *BMC Cancer*. 2020;20(1):471. https://doi.org/10.1186/s12885-020-06956-5
8. Brandacher G, Perathoner A, Ladurner R, et al. Prognostic value of indoleamine 2,3-dioxygenase expression in colorectal cancer: effect on tumor-infiltrating T cells. *Clin Cancer Res*. 2006;12(4):1144–1151. https://doi.org/10.1158/1078-0432.CCR-05-1966
9. Ma WJ, Wang X, Yan WT, et al. Indoleamine-2,3-dioxygenase 1/cyclooxygenase 2 expression prediction for adverse prognosis in colorectal cancer. *World J Gastroenterol*. 2018;24(20):2181–2190. https://doi.org/10.3748/wjg.v24.i20.2181
10. Munder M, Mollinedo F, Calafat J, et al. Arginase I is constitutively expressed in human granulocytes and participates in fungicidal activity. *Blood*. 2005;105(6):2549–2556. https://doi.org/10.1182/blood-2004-07-2521
11. Elliott LA, Doherty GA, Sheahan K, Ryan EJ. Human tumor-infiltrating myeloid cells: phenotypic and functional diversity. *Front Immunol*. 2017;8:86. https://doi.org/10.3389/fimmu.2017.00086
12. Elomaa H, Ahtiainen M, Väyrynen SA, et al. Spatially resolved multimarker evaluation of CD274 (PD-L1)/PDCD1 (PD-1) immune checkpoint expression and macrophage polarisation in colorectal cancer. *Br J Cancer*. 2023;128(11):2104–2115. https://doi.org/10.1038/s41416-023-02238-6
13. Elomaa H, Ahtiainen M, Väyrynen SA, et al. Prognostic significance of spatial and density analysis of T lymphocytes in colorectal cancer. *Br J Cancer*. 2022;127(3):514–523. https://doi.org/10.1038/s41416-022-01822-6
14. Fujiyoshi K, Bruford EA, Mroz P, et al. Opinion: standardizing gene product nomenclature-a call to action. *Proc Natl Acad Sci USA*. 2021;118(3):1–5. https://doi.org/10.1073/pnas.2025207118
15. Bankhead P, Loughrey MB, Fernández JA, et al. QuPath: open source software for digital pathology image analysis. *Sci Rep*. 2017;7(1):16878. https://doi.org/10.1038/s41598-017-17204-5
16. Schindelin J, Arganda-Carreras I, Frise E, et al. Fiji: an open-source platform for biological-image analysis. *Nat Methods*. 2012;9(7):676–682. https://doi.org/10.1038/nmeth.2019
17. Väyrynen JP, Lau MC, Haruki K, et al. Prognostic significance of immune cell populations identified by machine learning in colorectal cancer using routine hematoxylin and eosin-stained sections. *Clin Cancer Res*. 2020;26(16):4326–4338. https://doi.org/10.1158/1078-0432.CCR-20-0071
18. Benjamin DJ, Berger JO, Johannesson M, et al. Redefine statistical significance. *Nat Hum Behav*. 2018;2(1):6–10. https://doi.org/10.1038/s41562-017-0189-z
19. Pelka K, Hofree M, Chen JH, et al. Spatially organized multicellular immune hubs in human colorectal cancer. *Cell*. 2021;184(18):4734–4752.e20. https://doi.org/10.1016/j.cell.2021.08.003
20. Jin S, Guerrero-Juarez CF, Zhang L, et al. Inference and analysis of cell-cell communication using CellChat. *Nat Commun*. 2021;12(1):1088. https://doi.org/10.1038/s41467-021-21246-9
21. Lee SJ, Jun SY, Lee IH, et al. CD274, LAG3, and IDO1 expressions in tumor-infiltrating immune cells as prognostic biomarker for patients with MSI-high colon cancer. *J Cancer Res Clin Oncol*. 2018;144(6):1005–1014. https://doi.org/10.1007/s00432-018-2620-x
22. Schollbach J, Kircher S, Wiegering A, et al. Prognostic value of tumour-infiltrating CD8+ lymphocytes in rectal cancer after neoadjuvant chemoradiation: is indoleamine-2,3-dioxygenase (IDO1) a friend or foe? *Cancer Immunol Immunother*. 2019;68(4):563–575. https://doi.org/10.1007/s00262-019-02306-y
23. Ma W, Duan H, Zhang R, et al. High expression of indoleamine 2, 3-dioxygenase in adenosquamous lung carcinoma correlates with favorable patient outcome. *J Cancer*. 2019;10(1):267–276. https://doi.org/10.7150/jca.27507
24. Ishio T, Goto S, Tahara K, Tone S, Kawano K, Kitano S. Immunoactivative role of indoleamine 2,3-dioxygenase in human hepatocellular carcinoma. *J Gastroenterol Hepatol*. 2004;19(3):319–326. https://doi.org/10.1111/j.1440-1746.2003.03259.x
25. Jacquemier J, Bertucci F, Finetti P, et al. High expression of indoleamine 2,3-dioxygenase in the tumour is associated with medullary features and favourable outcome in basal-like breast carcinoma. *Int J cancer*. 2012;130(1):96–104. https://doi.org/10.1002/ijc.25979
26. Ferdinande L, Decaestecker C, Verset L, et al. Clinicopathological significance of indoleamine 2,3-dioxygenase 1 expression in colorectal cancer. *Br J Cancer*. 2012;106(1):141–147. https://doi.org/10.1038/bjc.2011.513
27. Väyrynen JP, Haruki K, Väyrynen SA, et al. Prognostic significance of myeloid immune cells and their spatial distribution in the colorectal cancer microenvironment. *J Immunother cancer*. 2021;9(4):e002297. https://doi.org/10.1136/jitc-2020-002297
28. Governa V, Trella E, Mele V, et al. The interplay between neutrophils and CD8+ T cells improves survival in human colorectal cancer. *Clin Cancer Res*. 2017;23(14):3847–3858. https://doi.org/10.1158/1078-0432.CCR-16-2047
29. Galdiero MR, Bianchi P, Grizzi F, et al. Occurrence and significance of tumor-associated neutrophils in patients with colorectal cancer. *Int J cancer*. 2016;139(2):446–456. https://doi.org/10.1002/ijc.30076
30. Berry RS, Xiong MJ, Greenbaum A, et al. High levels of tumor-associated neutrophils are associated with improved overall survival in patients with stage II colorectal cancer. *PLoS One*. 2017;12(12):e0188799. https://doi.org/10.1371/journal.pone.0188799
31. Droeser RA, Hirt C, Eppenberger-Castori S, et al. High myeloperoxidase positive cell infiltration in colorectal cancer is an independent favorable prognostic factor. *PLoS One*. 2013;8(5):e64814. https://doi.org/10.1371/journal.pone.0064814
32. Wikberg ML, Ling A, Li X, Å Öberg, Edin S, Palmqvist R. Neutrophil infiltration is a favorable prognostic factor in early stages of colon cancer. *Hum Pathol*. 2017;68(2017):193–202. https://doi.org/10.1016/j.humpath.2017.08.028
33. Mondanelli G, Iacono A, Allegrucci M, Puccetti P, Grohmann U. Immunoregulatory interplay between arginine and tryptophan metabolism in health and disease. *Front Immunol*. 2019;10:1565. https://doi.org/10.3389/fimmu.2019.01565
34. Ahtiainen M, Wirta EV, Kuopio T, et al. Combined prognostic value of CD274 (PD-L1)/PDCDI (PD-1) expression and immune cell infiltration in colorectal cancer as per mismatch repair status. *Mod Pathol*. 2019;32(6):866–883. https://doi.org/10.1038/s41379-019-0219-7

35. Lazarus J, Oneka MD, Barua S, et al. Mathematical modeling of the metastatic colorectal cancer microenvironment defines the importance of cytotoxic lymphocyte infiltration and presence of PD-L1 on antigen presenting cells. *Ann Surg Oncol*. 2019;26(9):2821−2830. https://doi.org/10.1245/s10434-019-07508-3
36. Spranger S, Spaapen RM, Zha Y, et al. Up-regulation of PD-L1, IDO, and T(regs) in the melanoma tumor microenvironment is driven by CD8(+) T cells. *Sci Transl Med*. 2013;5(200):200ra116. https://doi.org/10.1126/scitranslmed.3006504
37. Schalper KA, Carvajal-Hausdorf D, McLaughlin J, et al. Differential expression and significance of PD-L1, IDO-1, and B7-H4 in human lung cancer. *Clin Cancer Res*. 2017;23(2):370−378. https://doi.org/10.1158/1078-0432.CCR-16-0150
38. Zhang ML, Kem M, Mooradian MJ, et al. Differential expression of PD-L1 and IDO1 in association with the immune microenvironment in resected lung adenocarcinomas. *Mod Pathol*. 2019;32(4):511−523. https://doi.org/10.1038/s41379-018-0160-1
39. Nishihara R, VanderWeele TJ, Shibuya K, et al. Molecular pathological epidemiology gives clues to paradoxical findings. *Eur J Epidemiol*. 2015;30(10):1129−1135. https://doi.org/10.1007/s10654-015-0088-4
40. Zlobec I, Lugli A. Prognostic and predictive factors in colorectal cancer. *Postgrad Med J*. 2008;84(994):403−411. https://doi.org/10.1136/jcp.2007.054858
41. Giltnane JM, Rimm DL. Technology insight: identification of biomarkers with tissue microarray technology. *Nat Clin Pract Oncol*. 2004;1(2):104−111. https://doi.org/10.1038/ncponc0046
42. Seppälä TT, Böhm JP, Friman M, et al. Combination of microsatellite instability and BRAF mutation status for subtyping colorectal cancer. *Br J Cancer*. 2015;112(12):1966−1975. https://doi.org/10.1038/bjc.2015.160
43. Porkka N, Lahtinen L, Ahtiainen M, et al. Epidemiological, clinical and molecular characterization of Lynch-like syndrome: a population-based study. *Int J cancer*. 2019;145(1):87−98. https://doi.org/10.1002/ijc.32085
44. Wirta EV, Seppälä T, Friman M, et al. Immunoscore in mismatch repair-proficient and -deficient colon cancer. *J Pathol Clin Res*. 2017;3(3):203−213. https://doi.org/10.1002/cjp2.71
45. Kellokumpu I, Kairaluoma M, Mecklin JP, et al. Impact of age and comorbidity on multimodal management and survival from colorectal cancer: a population-based study. *J Clin Med*. 2021;10(8):1751. https://doi.org/10.3390/jcm10081751